

https://dspace.org/

The consolidation and transformation of an ultra-ferritic stainless steel by hot isostatic pressing

Kian, Michael Christopher Wong.

1998

https://hdl.handle.net/10539/26148

Downloaded from a DSpace repository. https://dspace.org/

MSc Dissertation:

The consolidation and transformation of an ultra-ferritic stainless steel by Hot Isostatic Pressing

Michael Christopher Wong Kian

A dissertation submitted to the Faculty of Engineering, University of the Witwatersrand, Johannesburg, in fulfilment of the requirements for the degree of Master of Science in Engineering.

Johannesburg, 1998.

DECLARATION

I declare that this dissertation is my own, unaided work. It is being submitted for the degree of Master of Science in Engineering at the University of the Witwatersrand, Johannesburg. It has not been submitted before for any degree or examination at any other university.

Signed: MKar

Date: 12 October 1998

DEDICATION AND ACKNOWLEDGEMENTS

This dissertation is dedicated to my family for their enthusiastic support throughout my studies.

I am deeply indebted to:

Dr Lesley Cornish for her cheerful supervision, thoughtful guidance and thoroughly constructive advice.

Dr Mike Cortie for his outstanding knowledge of diverse technical subjects and many helpful and essential suggestions.

David Knight for assistance in powder manufacture, heat treatment, photography and numerous other matters.

Leon Langenhoven who toiled enthusiastically throughout the potentiodynamic corrosion testing.

Maclean Sibanda for recommendations involving diffusion theory.

The staff of the Electron Microscopy Unit at the University of the Witwatersrand.

Ultra High Pressure Units (Pty) Ltd* and Mintek** for supporting the project and providing the use of their facilities.

* P.O.Box 561, Springs, 1560, South Africa

** Physical Metallurgy Division, Private Bag X3105, Randburg, South Africa

ABSTRACT

Ferritic stainless steels possess a number of properties which render them superior to austenitic stainless steels in certain applications. The ferritic stainless steels are highly resistant to stress-corrosion cracking and are generally of lower cost. Previous work had shown that the corrosion properties of the ferritic steels were optimised at a chromium content of forty percent. Extensive research had already characterised the mechanical and corrosion behaviour of the Fe-40Cr alloy in the cast and wrought form. This investigation involves the development of the material by powder metallurgy processing. Particular emphasis is placed on a proprietary powder production technique as well as on powder consolidation by Hot Isostatic Pressing. The effect of Ni, Mo, Ru, Nb, Al and Fe additions and well as various techniques of introducing these additions are examined. The unique effect of powder metallurgy manufacture on microstructure and the kinetics of sigma phase formation is highlighted. Corrosion tests in various concentrations of sulphuric acid and an industrial field trial were performed. It was found that combined Ni and Mo contents exceeding four percent resulted in severe embrittlement due to widespread formation of sigma phase during the HIP process. The use of powder metallurgy techniques was also found to enhance the kinetics of sigma phase formation in a particular alloy when compared to the as-cast state. Direct additions of Fe powder were successful in inhibiting embrittlement, possibly due to a mechanism of Fe diffusion into Cr-rich regions. This lowered of the Cr content in these regions, thereby reducing the tendency for sigma precipitation. Corrosion tests indicate satisfactory resistance for the Fe-40Cr-2Ni-2Mo alloys in 70 weight percent sulphuric acid at 50°C . Alloys with 0.2 percent Ru additions were found to be especially resistant, due to the role of Ru as a cathodic modifier. The method of mixing and diffusion bonding metallic powders of varying composition was found to be feasible and certain novel combinations of Ni and Fe-rich alloys exhibited satisfactory corrosion resistance. A mathematical diffusion model was found to provide an order of magnitude approximation of the time required for homogenisation in a certain mixture of powders.

CONTENTS

	Page
1. INTRODUCTION	1
2. LITERATURE SURVEY	3
2.1. General stainless steel overview	3
2.2. The embrittlement of ferritic stainless steels	6
2.2.1. High temperature embrittlement	7
2.2.2.475°C embrittlement	8
2.3. Sigma phase embrittlement	9
2.4. Background to the 40 percent chromium alloys	10
2.5. The kinetics of sigma phase formation in Fe-40Cr alloys	17
2.6. The effect of alloying additions to Fe-40Cr	24
2.7. An economic assessment of the Fe-40Cr alloy	25
2.8. Powder metallurgy	26
2.8.1. Production of stainless steel powders	27
2.9. Hot Isostatic Pressing	28
2.9.1. Diffusion bonding	31
2.9.2. Industrial HIP	32
2.9.3. The theoretical basis of powder consolidation during HIPping	32
2.10. Milling	33
2.11. Duplex powders	37
2.12. Corrosion	38
2.12.1. Mixed potential theory	41
2.12.2. Passivity	42
2.12.3. Galvanic coupling	44
2.12.4. Corrosion tests	47
2.12.4.1. The linear polarisation method	47
2.12.4.2. Tafel extrapolation	49
2.12.5. Corrosion of the Fe-40Cr alloys	50
2.12.6. Sigma phase and corrosion resistance	57
2.13. The mathematics of diffusion	61
2.13.1. The Kirkendall Effect	63
2.13.2. The infinite diffusion couple	64
2.13.3. The mathematics of homogenisation	65
2.13.4. Arunsingh's homogenisation model	66
2.13.5. Heckel's homogenisation model	68
2.13.6. Larsson's homogenisation model	73
2.14. Summary	76

CONTENTS (Continued)

	Page
3. EXPERIMENTAL PROCEDURE	77
3.1. Alloys produced from a single powder: Introduction	77
3.2. Alloy description	80
3.3. Powder production	82
3.4. Hot Isostatic Pressing	84
3.5. Heat treatment and metallographic examination	86
3.6. Heat treatment comparison between cast and HIPped VFA622	86
3.7. Examination of hardness versus time at 750°C	87
3.8. Extra communition of VFA543(24h)-(SP001012)	88
3.9. Experimental procedure for potentiodynamic corrosion tests	89
3.10. Experimental procedure for field trials	90
3.11. Duplex powders	92
3.12. Inhibition of sigma phase formation by mechanical mixing	92
3.12.1. Mechanical mixing with 2%Al (SP001005)	92
3.13. The addition of extra Fe to VFA543 and VFA622 by hand mixing	94
3.14. The manufacture of a synthetic duplex alloy	96
3.14.1. Experimental procedure - duplex powders	96
3.15. Hardness and micro-hardness tests	97
3.16. Experimental procedure: SEM examination	98
3.16.1. Elemental scans	98
3.17. Experimental procedure for potentiodynamic corrosion tests on duplex materials	99
4. RESULTS	100
4.1. Powder manufacture:	100
4.1.1. Single powders	100
4.1.2. Carbon and oxygen analysis of VFA622	100
4.1.3. Duplex powders	101
4.1.3.1. Mechanical mixing with Al (SP001005)	101
4.1.3.2. Mechanical blending with added Fe (SP001008)	104
4.2. Hardness vs time at 750°C for VFA647 and VFA654	106
4.3. Metallography results	108
4.3.1. Microstructures of the Fe-38Cr-4Mo-2Ni alloys (As-HIPped)	109
4.3.2. Microstructures of the 2Ni-4Mo-38Cr-Fe alloys (Solution annealed)	110

CONTENTS (continued)

Page

RESULTS (continued)

4.3.3. The 2Ni-2Mo alloys 117
4.3 4. Metallographic results of VFA622 121
4.3.5. Comparison of HIPped and cast material VFA622. 122
4.3.6. Extra mi .ed VFA543 (SP001012) 125
4.3.7. Analysis of milling media 125
4.3.8. Microstructures of alloys made from duplex powders. 129
4.3.9. The addition of extra Fe to VFA543 and VFA622 by hand mixing 132
4.3.10. Microstructures of duplex powders 134
4.4. Summary of hardness results. 145
4.5. Elemental scans 149
4.6. Corrosion results in 10% sulphuric acid. 156
4.7. Corrosion results in 70% sulphuric acid at 50°C. 166
4.8. Field trials 173

5. DISCUSSION 174
5.1. Powder production 174
5.2. Powder particles 176
5.3. The effect of time at 750°C on hardness 176
5.4. Mechanical mixing of Al (SP001005) 178
5.5. Mechanical mixing with extra Fe (SP001008) 181
5.6. Metallographic examination of alloys from single powders 183
5.7. Fe-40Cr-4Mo-2Ni alloys 187
5.7.1. Microstructure of VFA543 (2Ni-4Mo-0.4Nb-40Cr)-As-HIPped 189
5.7.2. Microstructure of VFA543 (2Ni-4Mo-0.4Nb-40Cr)-heat treated 189
5.8. 38 or 40Cr alloys with 2Mo-2Ni 190
5.9. The extra-communited powder VFA543 (SP001012) 191
5.9.1. Microstructure of extra-communited VFA543 (SP001012)-As-HIPped 192
5.9.2. Microstructure of extra-communited VFA543 (SP001012)-heat treated. 193
5.10.1. Microstructure of Fe (SP001008), - As-HIPped 194
5.10.2. Microstructure of Fe (SP001008), - heat treated 197
5.11. Extra Fe alloys (hand mixed) 197

CONTENTS (continued)

Page

DISCUSSION (continued)

5.12. Microstructure of duplex alloys 200
5.12.1. 20% 316L+80% VFA622 200
5.12.2. 50% 316L+50% VFA622 201
5.12.3. 80% 316L + 20% VFA622 201
5.12.4. 50% Hastelloy C + 50% Prem V 204
5.13. Elemental scans 206
5.13.1. Alloys with pure Fe additions: SP001008 (as-HIP) and VFA622+Fe 206
5.14. Duplex powders with 316L additions 208
5.15. 50% Hastelloy C + 50% Prem V 209
5.16. The effect of HIPping on the kinetics of sigma formation 210
5.17. Corrosion behaviour (Fe-39Cr-2Ni-2Mo alloys) 213
5.18. Corrosion behaviour (alloys with Fe additions) 216
5.18.1. (SP001008 and VFA622+Fe) 216
5.19. Corrosion of alloys from duplex powders in 10 wt% H_2SO_4 219
5.20. Summary of corrosion resistance of duplex powders 221
5.21. Springlock field trials 222
5.22. Composition and manufacturing guidelines 223
5.23. Mathematical model comparison 225
5.23.1. The infinite diffusion couple 227
5.23.2. Arunsingh's model 228
5.23.3. Heckel's model 228
5.23.4. Larsson's model 229

6. CONCLUSIONS 232

7. COMMERCIAL PROSPECTS AND FUTURE WORK 234

8. REFERENCES 235

9. APPENDIX 241

LIST OF FIGURES

Page

2. LITERATURE SURVEY

Figure 2.1: Cr-Fe phase diagram.[9] 5

Figure 2.2: The effect of SHT (solution heat treatment) temperature on the room temperature Charpy toughness of Fe-40%Cr alloys[25]. 14

Figure 2.3: Mechanical properties of the warm-worked Fe-40Cr-2Ni-2Mo alloy as a function of SHT time at 1100°C[25]. 14

Figure 2.4: The effect of SHT temperature on the tensile properties of cold-worked Fe-40Cr-2Ni-2Mo[25]. 15

Figure 2.5: Corrosion rate (mm per annum) of several alloys in 10% H_2SO_4 at 30°C[25]. 15

Figure 2.6: Potentiodynamic curves (against the standard calomel electrode) for the corrosion of four superferritic alloys in 10% H_2SO_4[25]. 16

Figure 2.7: The effect of cathodic modification of Fe-40Cr with Ru in 0.5M H_2SO_4[25]. 16

Figure 2.8: The effect of thermo-mechanical processing on sigma phase formation on alloy T15 at 750°C[21]. 18

Figure 2.9: The rate of sigma phase formation in a 6Ni-40Cr-Fe as-cast alloy at 750°C[21]. 18

Figure 2.10: The rate of sigma phase formation in hot rolled 4Mo-39Cr-Fe at various temperatures[21]. 19

Figure 2.11: The rate of sigma formation in warm rolled (300°C) alloys K(4Mo-29Cr-Fe) and S(39Cr-Fe)[21]. 19

Figure 2.12: The rate of sigma phase formation in as-cast 2Ni-2Mo-39Cr-Fe at various temperatures[21]. 20

Figure 2.13 The rate of sigma formation at 750°C in the as-cast alloys containing 2%Mo and 2%Ni, with different stabilisers[21]. 20

Figure 2.14 The rate of sigma phase formation at 650°C in the as-cast alloys containing 2%Mo and 2%Ni, with different stabilisers.[21] 21

Figure 2.15 Formation of sigma phase in hot rolled alloys P (Al+Nb stabilised), N (Al+Zr stabilised) and Z (Al stabilised) at 750°C.[21] 21

Figure 2.16 Formation of sigma phase in hot rolled 2%Mo and 2%Ni containing alloys V (unstabilised) and W (0.05% nitrogen) at 750°C.[21] 22

Figure 2.17 The effect of prior mechanical work on the formation of sigma phase in 2Ni-2Mo-40Cr-Fe.[25] 22

Figure 2.18. Time-temperature-transformation diagrams for the formation of sigma in as-cast unstabilised (V), Nb stabilised (G), Ti stabilised (B) alloys.[21] 23

Figure 2.19: Cost-life comparisons in boiling 10% (by mass) sulphuric acid[29] 25

Figure 2.20: The principle of HIPping.[34] 29

LIST OF FIGURES (continued)

Page

LITERATURE SURVEY (continued)

Figure 2.21: Comparison of material properties: as-cast and cast+HIPped. The material is Al-7 wt% Si alloy L99.[34] 30

Figure 2.22: Illustrative comparison of material properties: as-cast and cast+HIPped.[34] 30

Figure 2.23: Tumbler used for milling metal powders.[33] 33

Figure 2.24: Representation of communition by ball milling. The large circles represent the balls, whilst the particles around them represent the powder.[33] 34

Figure 2.25: Narrow particle size distribution caused by tendency of small particles to weld and large particles to fracture.[33] 35

Figure 2.26: Cold welding of particles during ball milling. 36

Figure 2.27: Overvoltage versus current density.[1] 40

Figure 2.28: Electrode kinetic behaviour of Zn in acid solution[1] 41

Figure 2.29: Behaviour of non-passive metal. 42

Figure 2.30: Typical anodic dissolution behaviour of an active-passive metal.[1] 42

Figure 2.31: The effect of temperature and acid concentration on passivation.[1] 43

Figure 2.32: Galvanic couple between two corroding metals.[1] 44

Figure 2.33: Requirements for cathodic modification[1] 46

Figure 2.34: Linear region in cathodic and anodic polarisation curves.[47] 47

Figure 2.35: Applied current cathodic polarisation curve of a corroding metal showing Tafel extrapolation[1]. 49

Figure 2.36: Potential-time curves for Fe-40Cr-Ru alloys displaying spontaneous passivation in 0 5M acids at 25°C [ ] 51

Figure 2.37: General corrosion rates of Fe-40Cr alloys and commercial stainless steels in 10% H_2SO_4 at 30°C [ ] 52

Figure 2.38: General corrosion rates of Fe- 40Cr alloys and commercial stainless steels in 10% H_2SO_4 +100ppm KSCN at 40°C[3]. 53

Figure 2.39: Pitting potentials of 40Cr-Fe alloys and commercial stainless steels in 3%NaCl at 60°C.[3] 53

Figure 2.40: Potentiodynamic responses of Fe-40%Cr-Ru alloys in 10% H_2SO_4 at 25°C. [51] 54

Figure 2.41: Potentiodynamic responses of Fe-30%Cr-Ru alloys in 10% H_2SO_4 at 25°C[51]. 55

Figure 2.42: Open circuit corrosion potential variations with time of Fe-30%Cr-Ru alloys in 10% H_2SO_4 at 25°C. [51] 55

Figure 2.43: Open circuit corrosion potential variations with time of Fe-40%Cr-Ru alloys in 10% H_2SO4 at 25°C.[51] 56

Figure 2.44: Breakdown potential (E_{bd}) and critical current density (i_c) as a function of ageing time (i.e.increasing sigma content).[52] 57

LIST OF FIGURES (continued)

Page

LITERATURE SURVEY (continued)

Figure 2.45: Critical crevice corrosion temperature (CCT) and impact value as a function of ageing time (i.e. increasing sigma content).[52] 58

Figure 2.46: Potentiodynamic responses for SAF2205 duplex stainless steel with various sigma phase contents at 10%H_2SO_4 at 25°C.[53] 59

Figure 2.47: Anodic pitting polarisation curves of duplex alloy SAF2205 with various sigma phase contents exposed to 3.5%NaCl solution at 25°C.[53] 60

Figure 2.48: Basis for derivation of Fick's first law.[55] 61

Figure 2.49: Diffusion couple used by Kirkendall.[58] 63

Figure 2.50: Normalised concentration profile produced by diffusion in an infinite diffusion couple.[55] 64

Figure 2.51: Arunsingh's model.[62] 66

Figure 2.52: Heckel's model.[64] 68

Figure 2.53: Homogenisation behaviour of planar, cylindrical and spherical models in terms of the degree of interdiffusion F, as a function of normalised homogenisation time, for various mean compositions $\overline{C}$.[64] 69

Figure 2.54: Normalised degree of interdiffusion F as a function of D, t, l_o, n and Y.[64] 70

Figure 2.55: Comparison of experimental F data on Ni-0.20Cu compacts with model predictions.[59] 71

Figure 2.56: Comparison of data from two alloy systems (Ni-Cu) and (Cu-Ni) with model predictions.[64] 71

Figure 2.57: Larsson's model of homogenisation.[66] 73

Figure 2.58: Concentration profiles along radius of sphere after various homogenisation times. Relative starting surface concentrations were: (a)10, (b)4, (c)∞, (d)2.[66] 74

Figure 2.59: Comparison between predicted homogenisation behaviour based on the equation of Lavender and Jones and Larrson's study. Numbers on the curves show surface concentrations at $\frac{Dt}{a^2}$=0.[66] 75

3.EXPERIMENTAL PROCEDURE

Figure 3.1: Particle size distribution of VFA543 (as received) 85

Figure 3.2: Experimental springlock used in industrial field trial 91

LIST OF FIGURES (continued)

Page

4.RESULTS

Figure 4.1:Micrograph of FeCr powder particles. 100
Figure 4.2: Malvern analysis of VFA543. 101
Figure 4.3: Malvern analysis of SP001005. 102
Figure 4.4: FeCr-Al agglomerates after ball milling. 103
Figure 4.5: Detail of FeCr-Al agglomerate. 103
Figure 4.6: Particle size distribution of Fe powder. 104
Figure 4.7: Particle size distribution of SP001008 (Extra Fe). 105
Figure 4.8: Hardness vs time at 750°C. 107
Figure 4.9: VFA543, as-HIPped, unetched (100X). 109
Figure 4.10: DS-1, (1100°C), KOH electrolytic etch, (200X) 110
Figure 4.11: DS-1, (1100°C), KOH electrolytic etch, (500X). 110
Figure 4.12: DS-C, (annealed 1100°C), (200X). 111
Figure 4.13: DS-C, (annealed 1100°C), (500X). 111
Figure 4.14: VFA417, (annealed 1100°, HCl etch, (200X). 112
Figure 4.15: VFA417, (annealed 1100°, HCl etch,)(500X). 112
Figure 4.16: VFA419, (annealed 1100°C), HCl etch, (200X). 113
Figure 4.17: VFA419, (annealed 1100°C), HCl etch, (500X). 113
Figure 4.18: VFA420, (annealed 1100°C), HCl etch, (200X). 114
Figure 4.19: VFA420, (annealed 1100°C), HCl etch, (500X). 114
Figure 4.20: VFA423, (annealed 1100°C), HCl etch, (200X). 115
Figure 4.21: VFA423, (annealed 1100°C), HCl etch, (500X). 115
Figure 4.22: VFA543, (annealed 1100°C), HCl etch, (500X). 116
Figure 4.23: PremAlloy V, (as-HIPped), HCl etch, (100X). 117
Figure 4.24: PremAlloy V, (annealed 1100°C), (100X). 117
Figure 4.25: PremAlloy V, (annealed 1100°C), (200X). 118
Figure 4.26: PremAlloy V, (annealed 1100°C), (500X). 119
Figure 4.27: VFA487, (as-HIPped), HCl etch, (100X). 120
Figure 4.28:VFA 487, (annealed 1100°C), HCl etch, (200X). 120
Figure 4.29: VFA622, (HIPped + annealed 1100°C), (200X). 121
Figure 4.30: VFA622, (HIPped + annealed 1100°C), (500X). 121
Figure 4.31: VFA622 , (Cast and HIPped), (200X). 122
Figure 4.32: VFA622 , (Cast and HIPped), (500X). 122
Figure 4.33: VFA622 , (HIPped+solution annealed), (500X). 123
Figure 4.34: VFA622 , (HIPped twice only), (200X). 123
Figure 4.35: VFA622 , (HIPped twice only), (500X). 124
Figure 4.36: Microstructure of steel milling media (500X). 125
Figure 4.37: Frequency and cumulative particle size distribution of (Extra milled VFA543-SP001012). 126
Figure 4.38:SP001012, (As-HIPped), HCl etch, (100X). 127
Figure 4.39:SP001012, (As-HIPped), HCl etch, (500X). 127
Figure 4.40:SP001012, (As-HIPped), (200X). 128
Figure 4.41: SP001012, (annealed 1100°C), HCl etch, (500X). 128

LIST OF FIGURES (continued)

Page

RESULTS (continued)

Figure 4.42: Micr. structure SP001008, (As-HIPped), 200X. 129
Figure 4.43: Microstructure SP001008 (As-HIPped) 500X 130
Figure 4.44: SP001008 (HIPped + solution annealed), (200X). 131
Figure 4.45: SP001008 (solution annealed 1100°C) 500X. 131
Figure 4.46: VFA622+Fe (as-HIPped), HCl etchant, (200X) 132
Figure 4.47: VFA622+Fe (1100°C anneal), (200X). 133
Figure 4.48: VFA622+Fe (1100°C anneal), (500X). 133
Figure 4.49: (20% 316L+80% VFA622), As-HIP (200X) 134
Figure 4.50: (20% 316L+80% VFA622), As-HIP (500X). 134
Figure 4.51: (20% 316L+80% VFA622) 1100°C,(500X). 135
Figure 4.52: (50% 316L+50% VFA622), As-HIP,(200X). 135
Figure 4.53: (50% 316L+50% VFA622), 1100°C(200X). 136
Figure 4.54: (80% 316L+20% VFA622), As-HIP (25X). 137
Figure 4.55: (80% 316L+20% VFA622), As-HIP (200X). 137
Figure 4.56: (80% 316L+20% VFA622), As-HIP (500X). 138
Figure 4.57: (80% 316L+20% VFA622), 1100°C (500X). 139
Figure 4.58: (80% 316L+20% VFA622), 1100°C (200X). 139
Figure 4.59: (50% Hastelloy C + 50% PremV), As-HIP (200X). 140
Figure 4.60: (50% Hastelloy C+50% Prem V), As-HIP (500X). 140
Figure 4.61: (50%Hastelloy C+50%PremV), As-HIP (500X). 141
Figure 4.62:(50% Hastelloy C + 50% Prem V), 1100°C (200X). 142
Figure 4.63: (50% Hastelloy C + 50% Prem V), 1100°C (500X). 143
Figure 4.64: (50% Hastelloy C+50% Prem V), 1100°C (500X). 143
Figure 4.65: Elemental scan of SP001008, As-HIP, (Across 123.3μm). 150
Figure 4.66: Elemental scan of VFA622+Fe, As-HIP, (Across 124.6μm). 151
Figure 4.67: Elemental scan of VFA622+Fe, As-HIP, (Across 504.3μm). 152
Figure 4.68: Elemental scan of VFA622+Fe, As-HIP, (Across 996.6μm). 153
Figure 4.69: Elemental scan of VFA622+Fe, heat treated, (Across 1011μm). 154
Figure 4.70 Elemental scan of 50% Hastelloy C + 50% Prem V (Across 1005μm) 155
Figure 4.71: Corrosion scan for Prem V, as-HIPped. 156
Figure 4.72: Corrosion scan for Prem V, heat treated. 156
Figure 4.73: Corrosion scan for VFA487, as-HIPped. 157
Figure 4.74: Corrosion scan for VFA487, heat treated. 157
Figure 4.75: Corrosion scan for VFA622, HIPped(2X). 158
Figure 4.76: Corrosion scan for VFA622, HIPped(2X) + heat treated. 158
Figure 4.77: Corrosion scan for SP001008, as-HIPped. 159

LIST OF FIGURES (continued)

Page

RESULTS (continued)

Figure 4.78: Corrosion scan for SP001008, heat treated. 159
Figure 4.79: Corrosion scan for VFA622 + Fe, as-HIPped. 160
Figure 4.80: Corrosion scan for VFA622 + Fe, heat treated. 161
Figure 4.81: Corrosion scan for 20% 316L+80%VFA622, heat treated 162
Figure 4.82: Corrosion scan for 50% 316L+ 50% VFA622, heat treated. 163
Figure 4.83: Corrosion scan for 80% 316L+20% VFA622, heat treated. 164
Figure 4.84: Corrosion scan for 50% Hast C + 50% PremV, heat treated. 165
Figure 4.85: Corrosion scan for PremV, heat treated. 166
Figure 4.86: Corrosion scan for VFA487, heat treated. 166
Figure 4.87: Corrosion scan for VFA622, HIPped twice. 167
Figure 4.88: Corrosion scan for VFA622, HIPped twice+ heat treated 167
Figure 4.89: Corrosion scan for VFA622+Fe (As-HIPped). 168
Figure 4.90: Corrosion scan for VFA622+Fe (Heat-treated). 169
Figure 4.91: Corrosion scan for 80% 316 + 20% VFA622, heat treated. 170
Figure 4.92: Corrosion scan for 50% PremV+50% Hast C heat treated. 171

DISCUSSION

Figure 5.1: Al-Fe phase diagram.[9] 180
Figure 5.2: Mill limit.[33] 182
Figure 5.3: Plastic deformation of spherical powder particles during HIPping.[34] 211
Figure 5.4: Diagram illustrating the effect of composition on the properties of the alloys, A - takes too long to convert to powder, B - Comes out of HIP as ferrite, C - comes out of HIP as sigma phase. 224
Figure 5.5: Parameters utilised in the examination of Arunsingh's and Heckel's homogenisation models. 226
Figure 5.6: Application of Larsson's model to the homogenisation of Fe-Cr and pure Fe particles. 229

LIST OF TABLES

Page

2. LITERATURE SURVEY

Table 2.1: Typical HIP parameters[34]. 31

3. EXPERIMENTAL PROCEDURE

Table 3.1: Composition of experimental melts(weight %). 78
Table 3.2: Thermomechanical processing prior to powder production. 83
Table 3.3: Size fractions used for HIPping. 84
Table 3.4: Composition of experimental melts VFA647 and VFA654 (wt %). 87
Table 3.5: Mill charge for mechanically mixed 4Mo-2Ni-2Al (SP001005) and Prem V with extra Fe (SP001008). 93
Table 3.6: Mix ratios for VFA543+Fe and VFA622+Fe. 94
Table 3.7: Summary of compositions. 95
Table 3.8: Composition of 316L atomised powder. 96
Table 3.9: Sieve analysis of as supplied powder. 96
Table 3.10: Composition of Hastelloy C (weight %). 96

4. RESULTS

Table 4.1: Chemical analysis of starting and milled powder (SP001008). 105
Table 4.2: Hardness vs time at 750°C for VFA647 and VFA654. 106
Table 4.3: EDS analysis of inclusion in Prem V. 118
Table 4.4: EDS analysis of SP001008. 129
Table 4.5: EDS analysis of precipitate in SP001008, HIP. 130
Table 4.6: EDS analysis of VFA622+Fe in Figure 4.47. 133
Table 4.7: EDS spot analysis of 50% 316L+50% VFA622. 136
Table 4.8: Microhardness results of 80% 316L+20% VFA622, as-HIP. 138
Table 4.9: EDS analysis of sigma phase at point B. 138
Table 4.10: Precipitate in Hastelloy C. 141
Table 4.11: EDS analysis of 50% Hast C + 50% PremV. 142
Table 4.12: Summary of EDS analyses. 144
Table 4.13: Summary of hardness results. 145
Table 4.14: Summary of microhardness results. 148
Table 4.15: Summary of corrosion data in 10 % H_2SO_4. 172
Table 4.16: Summary of corrosion data in 70% H_2SO_4 acid at 50°C. 173

5. DISCUSSION

Table 5.1: Nominal composition of grade 904L (wt %)[73]. 222
Table 5.2: Diffusion data and calculated diffusion coefficients at 1120°C (1393K).[97] 226

LIST OF EQUATIONS

		Page
1. $M \rightarrow M^{n+} + ne^-$	.....	38
2. $2H^+ + 2e^- \rightarrow H_2$	.....	38
3. $n = \pm B(\log \frac{i}{i_o})$	.....	39
4. $\frac{de}{dt_{applied}} = \frac{B_a.B_c}{2.3_1[B_a+B_c]}$	.....	48
5. $i = \frac{M.74}{slope}$	.....	48
6. $J = -D(\frac{\partial C}{\partial x})$	.....	61
7. $\frac{\partial C}{\partial t} = \frac{\partial}{\partial x}(D\frac{\partial C}{\partial x})$	.....	62
8. $D = D_o e^{-Q/RT}$	.....	62
9. $\overline{D} = D_1N_2 + D_2N_1$	.....	63
10. $C(x,t) = 0.5C_o[1 + erf(\frac{x}{2\sqrt{Dt}})]$	.....	64
11. $\frac{\partial C}{\partial t} = D(\frac{\partial^2 C}{\partial r^2} + \frac{2}{r}\frac{\partial C}{\partial r})$	.....	66
12. $\frac{\partial C}{\partial t} = D(\frac{\partial^2 U}{\partial r^2})$	.....	66
13. $C = -\frac{2aC_o}{\pi r}\sum_1^\infty \frac{(-1)^n}{n}\sin\frac{n\pi r}{a} e^{\frac{-n^2\pi^2 Dt}{a^2}}$	.....	66
14. $C = -\frac{2aC_o}{\pi r}\sin\frac{\pi r}{a} e^{\frac{-\pi^2 Dt}{a^2}}$	.....	67
15. $t = \frac{a^2}{D\pi^2}\log\frac{2C_o}{C}$	.....	67
16. $F = \frac{m_t}{m_\infty}$	.....	68
17. $\frac{\partial C}{\partial t} = D(\frac{\partial^2 C}{\partial r^2} + \frac{2}{r}\frac{\partial C}{\partial r})$	.....	68
18. $F = \frac{m_t}{m_\infty} = \int_0^{0.5l}(C_B - C(r)).4\pi r^2 / \int_0^{0.5l}(C_B - \overline{C}).4\pi r^2.dr$	.....	69
19. $F = 1.10 + 0.44\log_{10}[(\frac{Dt}{l^2})n^2Y]$	.....	70
20. $\frac{\partial C}{\partial t} = (\frac{\partial^2 C}{\partial X^2} + \frac{2}{X}\frac{\partial C}{\partial X})$	.....	73
21. $C_0^{j+1} = (1-6K)C_0^j + 6KC_1^j$	.....	74
22. $C_N^{j+1} = 2K\,C_{N-1}^j + (1-2K)C_N^j$	.....	74
23. $C_n^{j+1} = K(1-\frac{1}{n})\,C_{n-1}^j + (1-2K)C_n^j + K(1+\frac{1}{n})C_n^j$	.....	74
24. $\frac{Dt}{a^2} = 0.3$	.....	75
25. $0 = \frac{x}{2\sqrt{Dt}}$	.....	227
26. $\frac{X^2}{Dt} = k$	.....	231

INTRODUCTION

Stainless steel is a generic term for a range of alloys composed nominally of iron and chromium. These alloys are commonly used in numerous industrial and commercial applications due to their excellent corrosion resistance in numerous aggressive media and conditions. It has long been established[1] that the general corrosion resistance of the stainless steels typically increases with increasing chromium content. However, increasing the chromium content leads to the various problems of alloy embrittlement and difficulties in fabrication[2]. Commercially available alloys therefore only contain typically a maximum of thirty percent chromium. Steels which contain thirty to forty percent chromium have been termed ultra-ferritic alloys[3]. The work of European researchers in the 1970s and South African researchers in the 1980s and 1990s indicated that an ultra-ferritic stainless steel alloy containing forty percent chromium and minor ruthenium additions had many attractive properties which could render the alloy economically viable[4,5,6,7]. This research culminated in the commercial release of a new grade of cast steel under the tradename "Ruthalloy[TM]" in 1996[8].

In the course of fundamental research, a proprietary method of manufacturing an ultra-ferritic stainless steel powder was developed by Mintek. This was achieved by utilising the alloy's ease of embrittlement under the appropriate heat treatment conditions. Various applications for the powder were explored and it was felt that powder consolidation by Hot Isostatic Pressing (HIP) was the most suitable technology to fully exploit the commercial potential of the powder. This is because HIPping allows for the consolidation of materials which are usually difficult to manufacture by conventional means. The technique is also considered to be the state of the art in the production of many alloys, and is known to produce optimal material properties under the correct manufacturing conditions. An advantage of the technology is that it allows powders of vastly different composition to be diffusion bonded. These mixtures usually cannot be satisfactorily bonded by standard methods. Very little information is available in the literature relating the properties of this family of alloys when manufactured by powder metallurgical means. HIPping is primarily a method of solid-state consolidation by means of enhanced atomic diffusion. Whilst these diffusion mechanisms are not always of central importance in many conventional manufacturing processes such as casting, they are of primary importance in HIPping.

The primary aims of the project are thus to describe the unique peculiarities in alloy behaviour, microstructure and corrosion resistance which may be attributed to powder metallurgical manufacture, and to examine the underlying mechanisms which produce this behaviour. Possible commercial prospects for the material are also considered. The project has been separated into two sections: the HIPping of only the ultra-ferritic powder, and the consolidation of the ultra-ferritic powder when mixed with powders of different composition.

2. LITERATURE SURVEY

This literature survey outlines the general properties of ferritic stainless steels. Emphasis is placed on the research and development work which has been undertaken with regard to experimental ultra-ferritic steels with a nominal composition of forty percent chromium. The mechanical properties and corrosion behaviour of the alloy in the cast and wrought states are reviewed.

The densification of stainless steel powders by means of powder metallurgy methods is also mentioned, with particular reference to the specific consolidation technique known as Hot Isostatic Pressing (HIP). The methods by which metallic powders may be produced are reviewed. A specialised, proprietary powder manufacturing process, which was utilised in this project, is also discussed.

2.1 General stainless steel overview

Steels which contain over thirteen percent chromium are referred to as stainless steels. The addition of chromium provides good corrosion resistance through the formation of a protective passive layer in aggressive environments.

These steels are categorised as either ferritic, austenitic, martensitic, precipitation-hardening or duplex stainless steels according to the phases that are predominantly present. The austenitic types are the most widely used in industry due to their excellent resistance in oxidising, reducing and elevated temperature conditions. A review by Cortie[2] has shown that austenitic steels comprise approximately seventy percent of the total world stainless steel production, with the ferritic steels constituting about twenty five percent.

A drawback of the austenitic steels has been their susceptibility to stress corrosion cracking and pitting in chloride-containing environments. Also since austenitic steels contain significant additions of nickel, they are generally more costly than other types of stainless steel.

The ferritic stainless steels have often been considered as an alternative to the austenitic types. The ferritics are highly resistant to stress corrosion cracking and pitting attack in many environments which are unsuitable for austenitic stainless steels. When molybdenum is added, ferritic stainless steels exhibit corrosion resistance equivalent or superior to the austenitic grades.

Ferritic stainless steels also contain far smaller proportions of nickel and are generally less expensive than austenitic stainless steels. However, ferritic stainless steels have traditionally been susceptible to the problems of embrittlement, low toughness, as well as reduced formability and weldability, in comparison to the austenitic grades. This has hindered their use as a material of construction and fabrication.

A better understanding of the behaviour and characteristics of the ferritic stainless steels may be obtained by an examination of the Fe-Cr binary phase diagram (Figure 2.1). Commercial ferritic alloys contain between 12 and 30 percent chromium. The upper chromium limit is arbitrary and experimental alloys with up to forty percent chromium have been developed[2].

From the diagram it can be seen that alloys in the 12-40 percent chromium range do not have a FCC (face centred cubic) crystal structure at any temperatures up to their solidus. This is significant, since it indicates that ferritic steels do not exhibit the alpha to gamma phase transformation upon heating at high temperatures. These steels, therefore, cannot be hardened by the classic gamma to martensite mechanism. The gamma → alpha → gamma phase transformation is often employed as a technique of grain refinement. The absence of this transformation implies that the ferritic steels are vulnerable to grain growth at elevated temperatures. Large grains are generally undesirable in these alloys since room-temperature toughness and formability are impaired.

Another significant feature to be noted on the phase diagram occurs in the 20-70 percent chromium range between 820 and 600 degrees centigrade; sigma phase occurs in this region of the diagram. Sigma is a brittle intermetallic compound which is detrimental to the toughness and corrosion characteristics of the alloys in which it occurs.

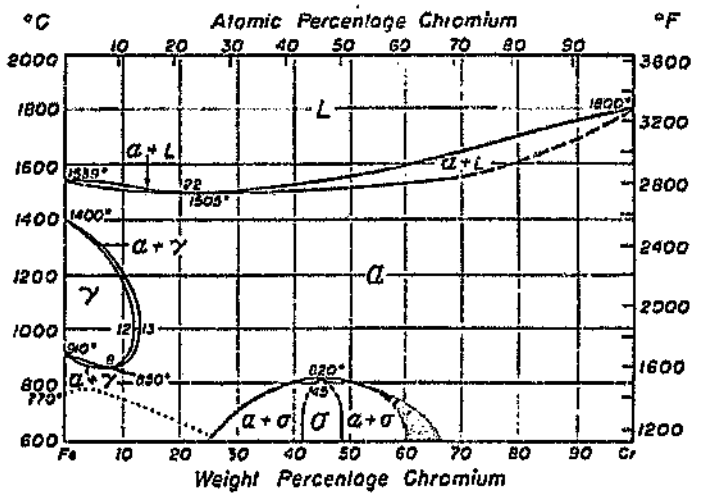

Figure 2.1: Cr-Fe phase diagram.[9]

2.2 The embrittlement of ferritic stainless steels

Due to the fact that ferritic steels exhibit a BCC (body centred cubic) structure they are subject to several embrittlement phenomena which are more pronounced than in alloys with an FCC structure. Amongst the more important of these phenomena is the exhibition of a ductile to brittle transition temperature which is close to room temperature. Although this characteristic may be modified by the addition of various alloying elements, the presence of such a high transition temperature has hindered the use of ferritic steels in many applications.

In plain chromium steels with high chromium contents, it was initially thought that embrittlement was actually due to the large amounts of chromium present. However, it was shown by Spendelow[10] in the 1950s that it was actually the presence of the interstitial elements, nitrogen and carbon, which were the cause of brittleness. Carbon and nitrogen are introduced during the steelmaking process and cannot be removed entirely.

The ferritic steels have a stable BCC crystal structure at temperatures up to their melting points. Since the BCC lattice does not have a high solubility for interstitial carbon and nitrogen, there is a tendency for the carbon and nitrogen to come out of solution in the form of brittle chromium-rich carbides and carbonitrides[3]. Consequently, the carbon and nitrogen levels have to be kept to a minimum, as low as 150ppm in some cases[4], in order to achieve acceptable toughness characteristics. These low levels have been made possible through the development of modern steelmaking technologies such as the Argon-Oxygen-Decarburisation (A.O.D.) and Vacuum Induction Melting (V.I.M.) processes. It has also been found[3] that the addition of certain "stabilising" elements such as Ti or Nb, lessens the effect of high interstitial element levels, by tying up carbon and nitrogen as Ti or Nb carbides and nitrides.

Modern ferritic alloys with above eighteen percent chromium and with low interstitial element contents are referred to as E.L.I. (Extra Low Interstitial) or superferritic stainless steels. However despite improvements in toughness, the superferritic grades are still only employed in sections of up to 12mm thickness[3]. This is due to embrittlement effects which would be apparent in thicker sections.

The three most common mechanisms of embrittlement are high temperature embrittlement, 475°C embrittlement and sigma phase embrittlement.

2.2.1 High temperature embrittlement

This form of embrittlement occurs when ferritic stainless steels are heated to above 1000°C and cooled. The precipitation of chromium-rich nitrides, carbides and carbonitrides during cooling results in decreased impact toughness and ductility. The exact mechanisms by which the precipitates form and affect the toughness of ferritic stainless steel are still the topic of much debate. It was suggested that embrittlement was due to the precipitation of carbides and nitrides at grain boundaries[5]. Alternately, Demo[11] considered that dislocation locking by intragranular precipitates was a possible explanation.

High temperature embrittlement is dependent on the carbon and nitrogen contents of the ferritic stainless steel. Since these interstitial elements have a relatively low solubility in ferrite, it can be seen that their amounts should be kept at a minimum. This becomes more critical as the amount of chromium is increased, since chromium decreases the solubility of carbon and nitrogen even further.

The addition of stabilising elements such as Ti and Nb has been used with some success[3] to tie up carbon and nitrogen as Ti or Nb compounds. This prevents the formation of detrimental Cr-rich nitrides and carbides and therefore results in increased toughness. However, it has been shown that the addition of excessive amounts of Ti and Nb produces a corresponding deterioration of properties.

2.2.2 475°C embrittlement

When ferritic stainless steels are heated in the 450-500°C temperature range, they become embrittled. This embrittlement results in decreased impact toughness, ductility and corrosion resistance[4]. Embrittlement effects become more severe with increasing chromium content[12]. Early studies observed that embrittlement occurred even in Fe-Cr alloys of high purity and low carbon and nitrogen contents. It was therefore deduced that embrittlement could therefore not be due to the formation of nitrides or carbides. Early investigators such as Heger[13] believed that 475°C embrittlement was caused by the formation of a transition lattice intermediate between the alpha and sigma phases, prior to the formation of the sigma phase at a higher temperature. However, the work of Houdremont[14] showed that this explanation was not feasible. Other studies[15] indicate that embrittlement eventually occurs due to the precipitation of a Cr-rich BCC phase, alpha prime, which forms due to the presence of a miscibility gap in the Fe-Cr phase diagram below 550°C. Two distinct ferrite phases, the Cr-rich alpha prime and the Fe-rich alpha, occur in alloys which are held at the appropriate temperature within the miscibility gap. The formation of these different enriched phases within a miscibility gap is known as spinodal decomposition. The products of the spinodal reaction differ in composition from each other and from the parent phase. However, the products share the same crystal structure as the parent phase. Spinodal decomposition has been reported in other alloy systems, most noticeably the Cu-Ni-Sn system, where it is utilised as a method of hardening the alloy[16]. The spinodal reaction differs from the classic mechanism of nucleation and growth in that discrete nuclei of the product phases do not form in the initial stages of decomposition from the parent phase. If the alloy is held at the necessary temperature, a gradual sinusoidal variation in composition with distance occurs instead. These variations in composition become more pronounced with time until the discrete product phases are eventually formed at the end of the reaction. Spinodal structures are typically extremely fine with distances between regions of identical composition being of the order of 50 to 1000 angstroms[16].

There is still some debate as to the exact mechanism of alpha prime formation and how it causes embrittlement. Grobner[15] proposed that alpha prime precipitation caused dislocation locking, whereas Jacobsen[17] suggested that subgrain strengthening due to alpha prime precipitation on subgrain boundaries was the cause of embrittlement. Interestingly, Cortie and others[18] have shown that the embrittlement caused by alpha prime precipitation is in any case preceded by embrittlement caused by the precipitation of minute CrN clusters which impede dislocation movement.

Alpha prime may be dissolved by sustained heating at above 550°C. However, the heating temperature should be below that which favours sigma phase precipitation.

2.3 Sigma phase embrittlement

The sigma phase is an equilibrium constituent of the binary Fe-Cr system and occurs in bulk form at 40-50 percent Cr content, after heating in the 500-900°C temperature range. Duplex structures, consisting of alpha and sigma have been reported in alloys containing between 20 and 70 percent Cr. The presence of sigma phase results in a decrease in room temperature toughness and ductility. The irregularly-shaped sigma particles may act as a stress raiser[19] or increase resistance to slip.

The sigma phase is a hard, brittle, non-magnetic, intermetallic compound and has the nominal composition FeCr. Sigma formation is favoured by increasing Cr content. In binary Fe-Cr alloys sigma phase takes a number of hours to form, even at favourable temperatures. The formation of sigma phase is affected by the presence of impurities, alloying elements, the degree of cold work present, and temperature. It appears that pressure may affect sigma formation. Otaguchi[20] found that a high Cr (45 atomic percent) steel, when subjected to a high hydrostatic pressure of 900MPa, formed sigma in half the time that it took to form at atmospheric pressure.

Premachandra[21] conducted an extensive examination into the mechanism and kinetics of sigma formation and determined the exact composition of various sigma phases. It must be mentioned that whilst it is mainly the ferritic stainless steels which are vulnerable to sigma phase formation, the phenomenon has also been observed in austenitic and duplex stainless steels.

2.4 Background to the 40 percent chromium alloys

It has been known since the 1970s, from the work of Tomashov and Chernova[32], that the optimum passivation properties of binary Fe-Cr alloys occurs at the 40 percent chromium level. It has also been shown that the passivating effects of platinum group metal (PGM) additions[33] are most effective at the 40 percent chromium level.

This Fe-40Cr alloy showed possible commercial potential as a highly corrosion-resistant steel in reducing and pitting environments. A significant amount of work was initiated by South African researchers in the 1980s and 1990s. The possibility of producing a cost-effective 40 percent chromium ferritic alloy which could compete with the more expensive austenitic or nickel-based grades was examined.

Early work by De Marsh[5] examined the effect of Ru, Ni, Ti, Nb and Al additions on impact toughness of the Fe-40Cr alloys. It was found that each of these elements, or combinations of these elements, reduced the ductile to brittle transition temperature of the alloy. Ni additions of two percent produced the greatest reduction in ductile-to-brittle transition temperature.

De Marsh[5] also investigated thermomechanical processing variables by rolling the Fe-40Cr alloy in the 650-950°C temperature range followed by high temperature annealing. The best toughness properties were obtained by an intermediate anneal at 800°C or 850°C , followed by a solution anneal at 1050°C for one hour. De Marsh attributed the differing ductile and brittle behaviour of the alloy to the presence of sigma phase. However, this postulation was contradicted by Van Zwieten[6], who considered the alternative possibility that brittle behaviour could instead be ascribed to the precipitation of Cr-rich carbides and nitrides.

Hermanus[4] concentrated on improving the toughness properties of the plain binary Fe-40Cr alloy. The effect of various melting, annealing and thermomechanical treatments on the toughness characteristics of the wrought plate material were examined. The role of C, N, Ru, Nb, Al , Ti and rare earth metal additions were also investigated. Hermanus concluded that tough Fe-40Cr alloys could be produced by rolling at temperatures between 1050 and 750 degrees centigrade, with a solution anneal at 950 degrees centigrade for one hour, followed by a water quench. Charpy impact values of 200J and a ductile-to-brittle transition temperature of -10 degrees centigrade were reported.

It was also found that toughness values decreased as the interstitial content of the alloy increased. It must be mentioned that the toughness values obtained by Hermanus were hampered by poor reproducibility within the investigation.

The embrittling effects of the interstitial elements C, N and O were studied by Van Zwieten[6]. He reported that even with as little as 130 ppm C+N and 260 ppm O, the plain Fe-40Cr alloy became severely embrittled. No intermediate annealing was utilised. Room temperature Charpy impact values of 15J/cm^2 and high ductile-to-brittle transition temperatures of 130°C were encountered. In this investigation, it was also shown that the dynamic fracture toughness test produced more reproducible results than the Charpy impact and slow bend tests used by Hermanus and De Marsh.

Wolff[7] examined plain Fe-40Cr alloys that had been annealed in the 750-850°C range. It was reported that mobile dislocations were formed in this temperature range, leading to improvements in toughness. The beneficial effects of Ni additions were also observed.

Tullmin[3] conducted a comprehensive investigation into the toughness, corrosion behaviour and weldability of same Fe-40Cr alloys. Significant information regarding the mechanisms by which the toughness and corrosion properties could be controlled were obtained in this study. Alloys were prepared by vacuum induction melting and hot rolling. Intermediate annealing treatments were undertaken at 850°C and followed by a solution anneal at 1050°C, culminating in a water quench. Elements such as Nb, Ru, Al, Nb, Mo, Ni and Ti were added to the melts.

With regard to toughness considerations, Tullmin[3] found that undesirable Cr-rich carbonitrides precipitated at grain boundaries despite using interstitial levels below 200 ppm and rapid quenching. It was found that the addition of a stabiliser element such as Nb, at concentrations of 14(C+N), could be used to prevent grain boundary precipitation.

An important finding of the study was that mobile dislocations were formed due to sigma phase dissolution during the 1050°C solution heat treatment. These mobile dislocations were considered essential in increasing the toughness of the alloy. Ni was also found to improve toughness by promoting deformation twinning. Deformation twinning favours plastic deformation during impact tests. Charpy impact values of up to 132J/cm^2 were reported in the Nb stabilised alloys. Fe-40Cr alloys with the correct alloying additions exhibited a gradual transition from ductile to brittle fracture over a large temperature range whereas alloys without the additions had a sharp DBTT.

Iorio, Witcomb and Cornish[24] performed a study with transmission electron microscopy on a Fe-40Cr alloy which exhibited a large variation in ductile behaviour. Variations in observed dislocation density, twinning and thus ductility were attributed to differences in the cooling rate after solution annealing, and the embrittling feature was deduced to be vacancy clusters.

Prior to Tullmin, very little work had been done describing the corrosion characteristics of the Fe-40Cr alloy. Work done by previous researchers[21] had concentrated chiefly on the cathodic modification of the alloy by addition of Ru and other platinum group metals.

Electrochemical corrosion testing was carried out by Tullmin[3]. It was found that additions of 2 percent Mo and 2 percent Ni were significantly beneficial in improving the passivation characteristics of the alloy under strongly reducing general corrosion conditions. The improvement in general corrosion resistance by the addition of 0.2 percent Ru was only considered to be moderate.

During pitting tests, pits were found to initiate at S- or Si- rich inclusions. Mo was found to greatly improve pit repassivation, whilst Ni and Ru additions produced no such improvement. Mo and Ni were also found to increase resistance to crevice corrosion, whilst Ru had minimal effect.

Tullmin[3] found that the Fe-40Cr alloys were vulnerable to sensitisation effects and thus intergranular corrosion, due to the precipitation of Cr-rich carbonitrides. He found that Nb stabilisation was beneficial in preventing sensitisation as well as in enhancing toughness properties. Unsensitised Fe-40Cr alloys were reported to exhibit significant resistance to pit initiation in corrosive environments.

Work was also initiated into the welding characteristics of the alloy[3]. This area of investigation had been ignored by previous researchers. It was found that good toughness and corrosion resistance could be obtained, in the as-welded condition, if laser or electron beam welding was employed. The presence of highly mobile dislocation densities and lack of harmful precipitates, due to low heat input during welding, was suggested as an explanation. TIG (Tungsten Inert Gas) welding was considered to be unsuitable due to the higher heat input which resulted in brittleness in the heat affected zone.

All the alloys used in the study were coarse grained. Grain refinement by means of cold working, followed by recrystallisation, was attempted. While the procedure was found to produce fine-grained microstructures, a number of these fine-grained Fe-40Cr alloys were found to be unacceptably brittle. It was surmised that recrystallisation effects had reduced the number of mobile dislocations, thereby resulting in embrittlement. After further experimentation Tullmin concluded that tough, fine-grained Fe-40Cr alloys could be produced by cold rolling, followed by recrystallisation at 800-1050°C, and a finishing cold rolling reduction of 2.5-5 percent. The effect of the final cold work, according to Wolff[7] was to generate additional mobile dislocations.

The effect of solution heat treating temperature (SHT) on the mechanical properties and grain growth of the high chromium steels had also been studied by Cortie et al[25]. The results of this work are shown in Figures 2.2-2.4. The Charpy impact values of a Fe-40Cr alloy were found to have a maximum at a SHT of approximately 1020°C. Solution heat treating temperatures which were either above or below this value produced a decrease in impact toughness (Figure 2.2). It was found that mechanical properties of the Fe-40Cr-2Ni-2Mo alloy deteriorated as the holding time at the SHT was increased (Figure 2.3). It was also found that grain growth increased and both ultimate tensile strength and percent elongation decreased as the SHT was increased from 1000°C to 1150°C (Figure 2.4).

Cortie et al[25] also conducted corrosion tests comparing the behaviour of the high chromium steels to several commercial alloys. The results are shown in Figures 2.5 and 2.6. The general corrosion resistance of Fe-40Cr-2Ni-2Mo and Fe-40Cr-0.2Ru in 10 percent sulphuric acid at 30°C was superior or comparable to superalloys such as Hastelloy C-276 and Al-6XN. The corrosion resistance was also found to be superior to a commercial super-ferritic alloy. The beneficial effects of cathodic modification by means of Ru additions to the basic Fe-40Cr alloy were also confirmed (Figures 2.5-2.7). The pitting resistance of Fe-40Cr-2Ni-2Mo in an aggressive chloride environment was found by Tullmin[1] to be comparable to Hastelloy-C276 and AL29-4C and superior to 904L and 316L.

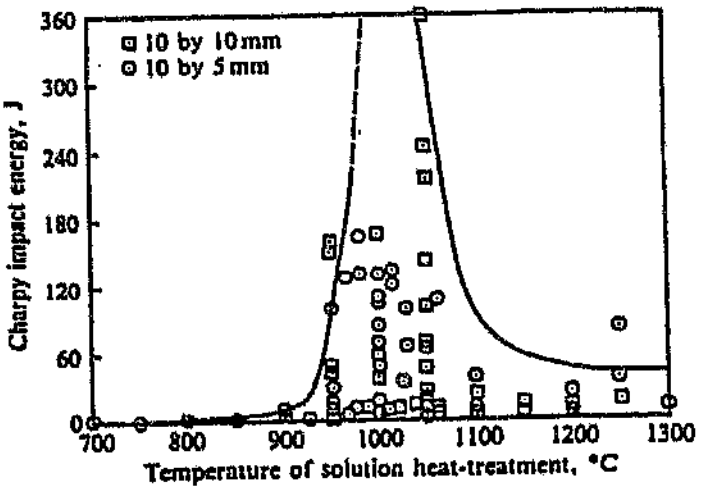

Figure 2.2: The effect of SHT (solution heat treatment) temperature on the room temperature Charpy toughness of Fe-40%Cr alloys.[25]

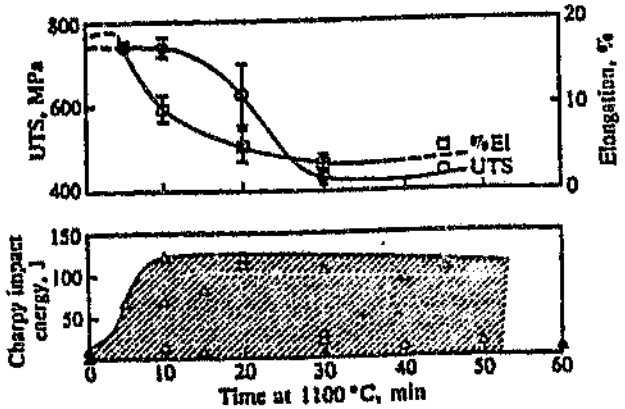

Figure 2.3: Mechanical properties of the warm-worked Fe-40Cr-2Ni-2Mo alloy as a function of SHT time at 1100°C.[25]

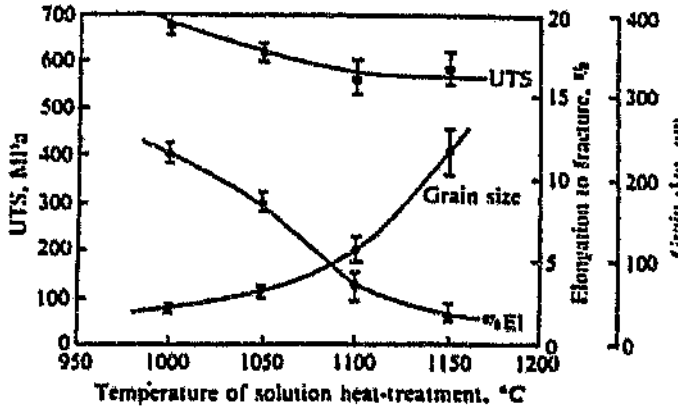

Figure 2.4: The effect of SHT temperature on the tensile properties of cold-worked Fe-40Cr-2Ni-2Mo. [25]

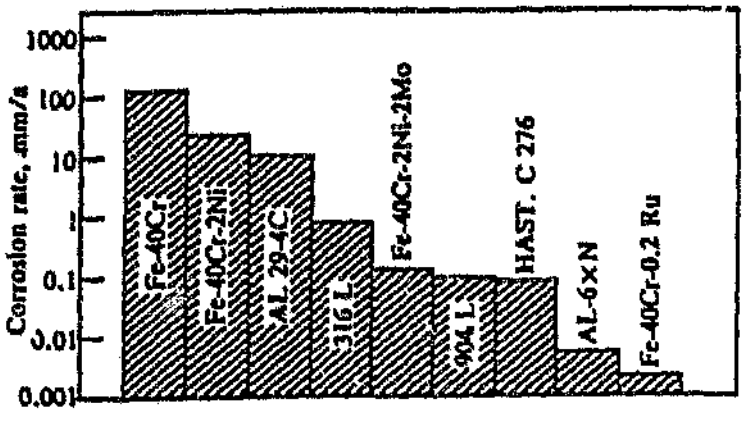

Figure 2.5: Corrosion rate (mm per annum) of several alloys in 10% H_2SO_4 at 30°C. [25]

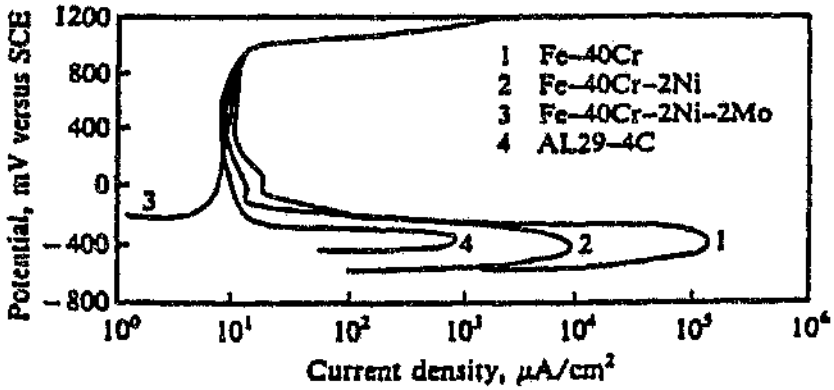

Figure 2.6: Potentiodynamic curves (against the standard calomel electrode) for the corrosion of four superferritic alloys in 10% H_2SO_4.[25]

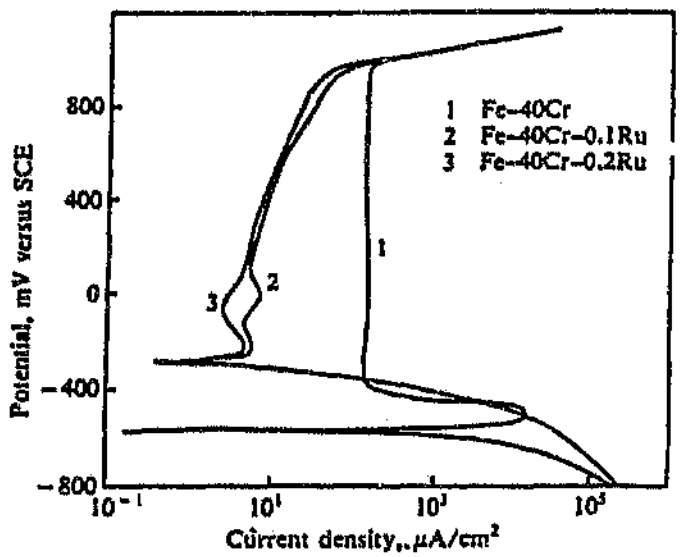

Figure 2.7: The effect of cathodic modification of Fe-40Cr with Ru in 0.5M H_2SO_4.[25]

2.5 The kinetics of sigma phase formation in Fe-40Cr alloys

The work of Tullmin[3] implied that the formation and dissolution of sigma phase was important in the establishment of mobile dislocations. The presence of these dislocations was considered essential if a tough Fe-40Cr alloy was to be produced. At the time of Tullmin's investigation, very little information was available regarding the kinetics of sigma phase formation in high chromium ferritic steels. It became apparent that establishing the kinetics of the reaction would be beneficial in terms of furthering the understanding of the Fe-40Cr alloy, as well as aiding in further development.

In 1993, Premachandra[21,26] conducted such a study and the kinetics and mechanisms of sigma phase precipitation in Fe-40Cr steels were determined for the first time. Time-temperature-transformation diagrams of sigma phase were established for the plain binary alloy, as well as for alloys with additions of Ni, Mo, Al, Ti, Zr and Nb (Figures 2.8-2.18)[21,26].

It was found that additions of Ni and Mo increased the kinetics of sigma phase formation in high-chromium ferritic steels. The addition of Nb as a stabiliser to the Fe-39Cr-2Mo-2Ni steels retarded sigma formation, whilst the addition of Ti and Zr increased the rate and temperature range at which formation occurred. A concentration of one percent Al was found to have a potent retarding effect on sigma growth. The greatest rate of sigma formation in the Fe-40Cr-2Ni-2Mo alloys was found to occur during isothermal heating at 750°C. Cold and hot working prior to isothermal heat treatment increased the rate of sigma formation (Figure 2.16)[21].

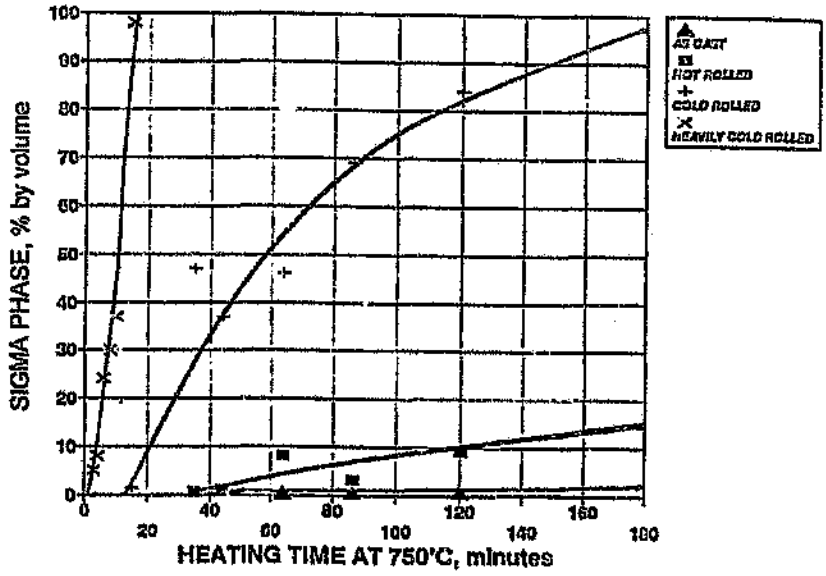

Figure 2.8: The effect of thermo-mechanical processing on sigma phase formation on alloy T15 at 750°C. [21]

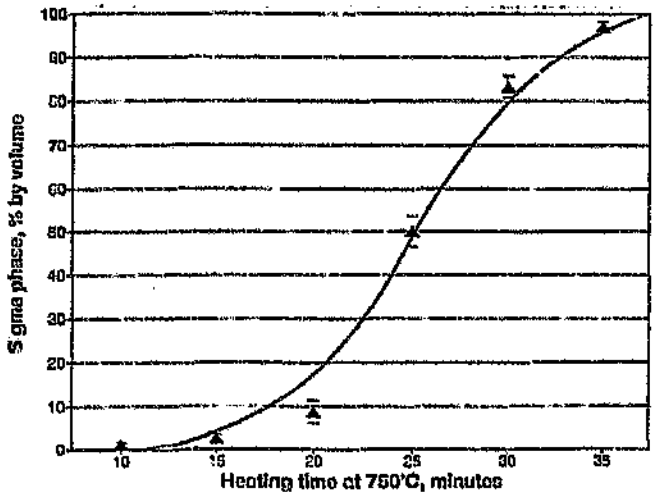

Figure 2.9: The rate of sigma phase formation in a 6Ni-40Cr-Fe as-cast alloy at 750°C. [21]

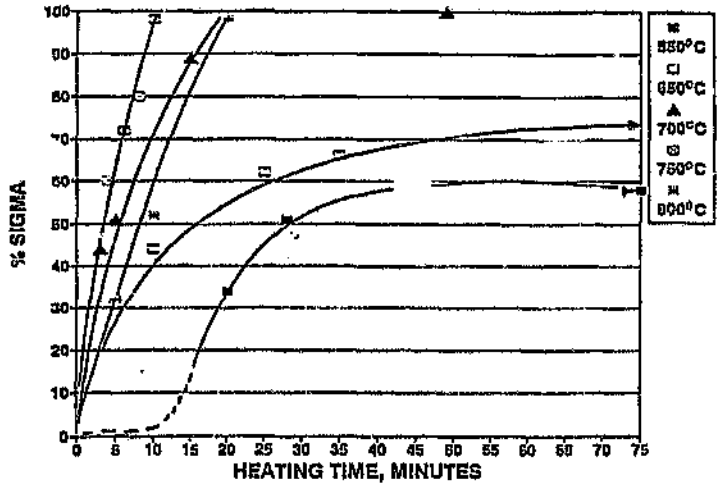

Figure 2.10: The rate of sigma phase formation in hot rolled 4Mo-39Cr-Fe at various temperatures.[21]

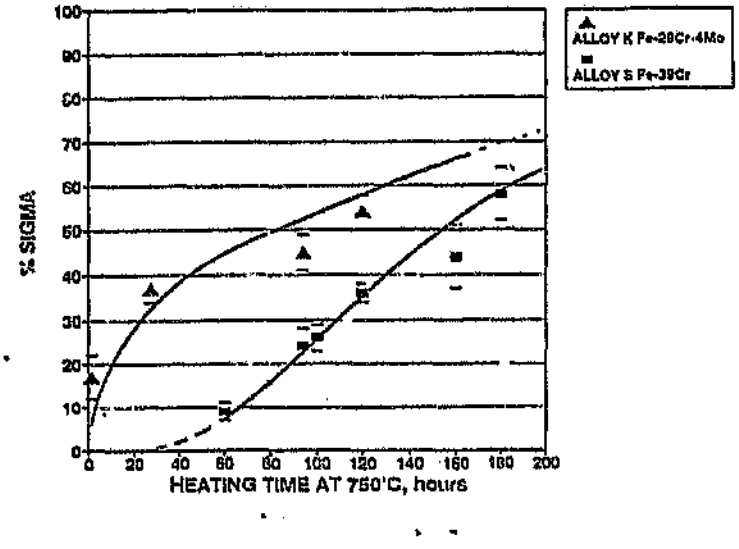

Figure 2.11: The rate of sigma formation in warm rolled (300°C) alloys K(4Mo-29Cr-Fe) and S(39Cr-Fe). [21]

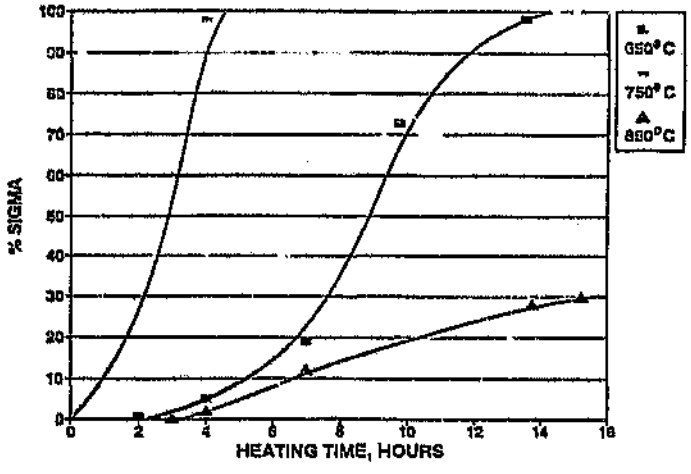

Figure 2.12: The rate of sigma phase formation in as-cast 2Ni-2Mo-39Cr-Fe at various temperatures.[21]

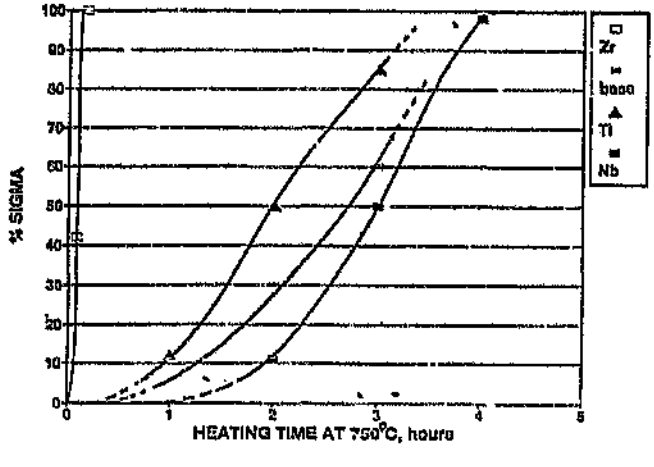

Figure 2.13 The rate of sigma formation at 750°C in the as-cast alloys containing 2%Mo and 2%Ni, with different stabilisers.[21]

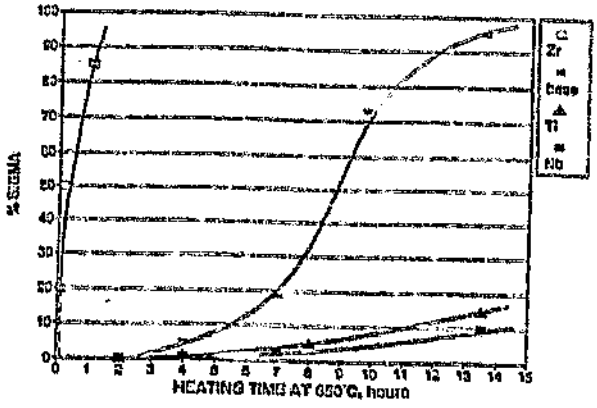

Figure 2.14 The rate of sigma phase formation at 650°C in the as-cast alloys containing 2%Mo and 2%Ni, with different stabilisers.[21]

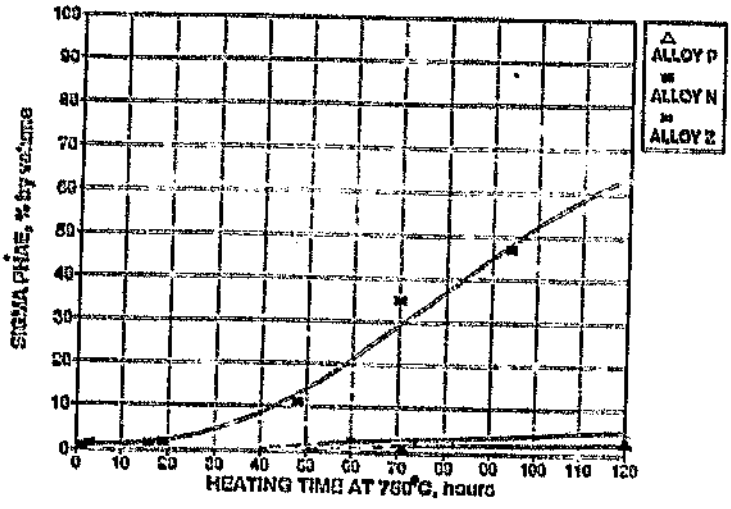

Figure 2.15 Formation of sigma phase in hot rolled alloys P (Al+Nb stabilised), N (Al+Zr stabilised) and Z (Al stabilised) at 750°C.[21]

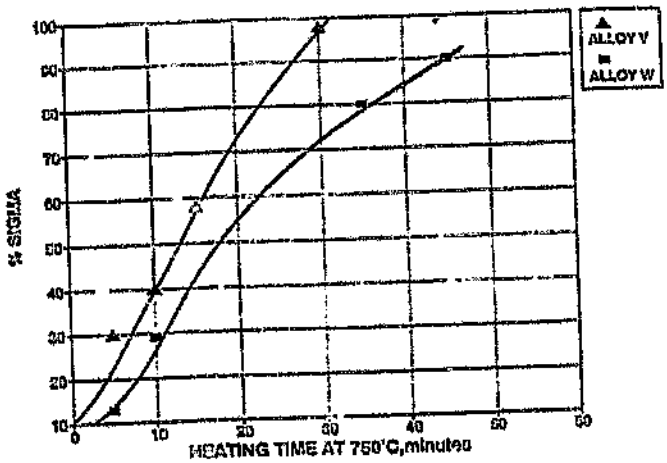

Figure 2.16 Formation of sigma phase in hot rolled 2%Mo and 2%Ni containing alloys V (unstabilised) and W (0.05% nitrogen) at 750 °C.[21]

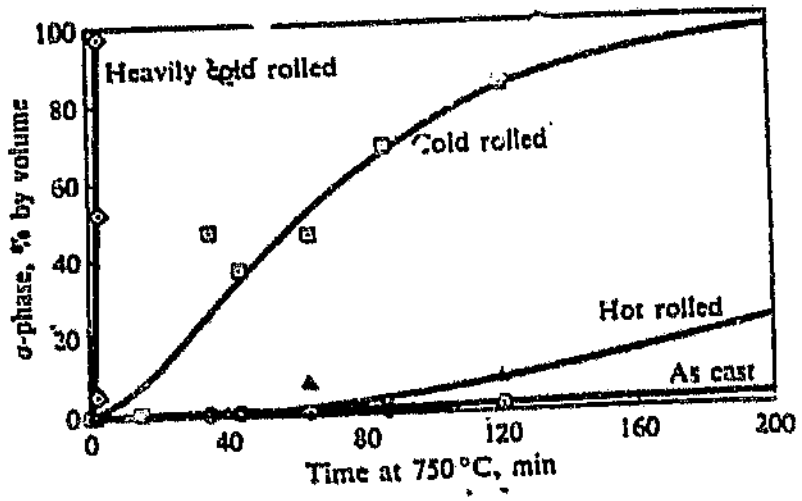

Figure 2.17 The effect of prior mechanical work on the formation of sigma phase in 2Ni-2Mo-40Cr-Fe.[28]

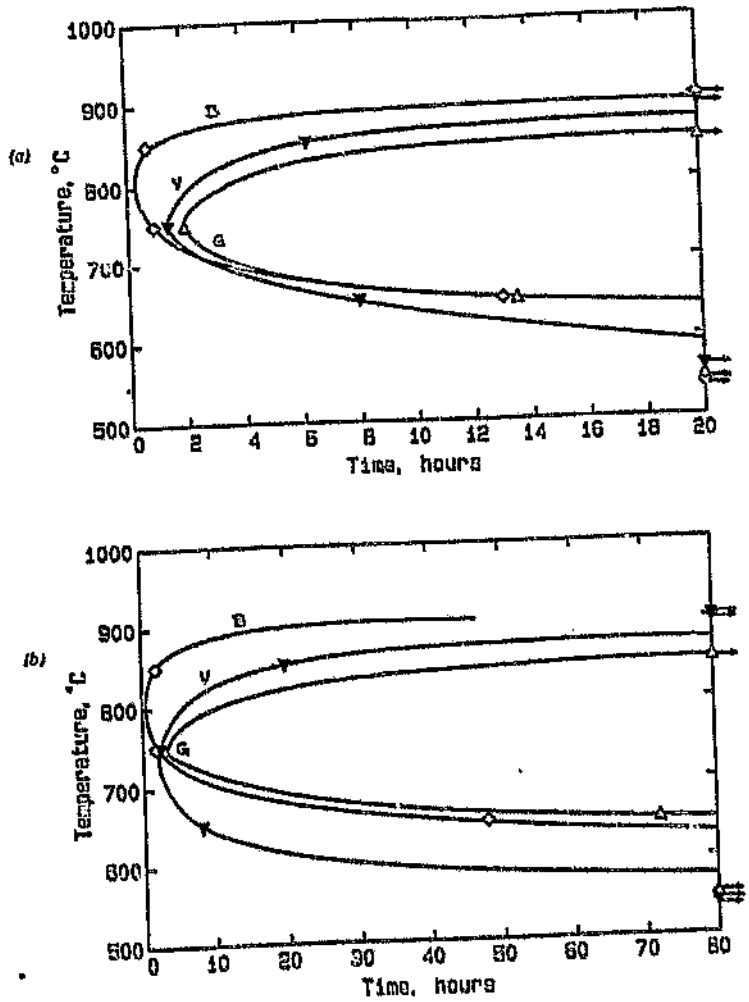

Figure 2.18. Time-temperature-transformation diagrams for the formation of sigma in as-cast unstabilised (V), Nb stabilised (G), Ti stabilised (B) alloys.[21]
(a) 10% sigma
(b) 50% sigma

2.6 The effect of alloying additions to Fe-40Cr

The addition of two percent Ni has been shown by previous workers[3] to improve toughness properties as well as corrosion resistance in reducing environments. However, higher levels are reported to promote stress corrosion cracking in ferritic stainless steels. Ni promotes the formation of sigma phase[21].

The presence of two percent Mo improves pitting resistance. Levels greater than two percent Mo are reported to result in loss of ductility in the presence of stabilising elements Ti and Nb[3]. Mo promotes the formation of sigma phase[21].

Both Nb and Ti are used as stabilisers and prevent sensitisation due to precipitation of Cr-rich carbides and nitrides. Nb narrows and retards the temperature range of sigma formation. Ti stabilisation is reported to result in decreased toughness[21]. Al may be used as a weld-ductilising element. The addition of one percent Al to Fe-40Cr is reported to have a potent retarding effect on sigma formation[26].

Additions of approximately 0.2 percent Ru improve the passivation characteristics of the alloy in reducing media[27]. Larger additions appear to produce no further beneficial effects on corrosion resistance. There is very little information regarding the influence of Ru on sigma phase. However, a recent (1998) publication by Wolff et al[28] indicates that Ru enhances the kinetics of sigma formation.

2.7 An economic assessment of the Fe-40Cr alloy

The Fe-40Cr alloy has certain economic and corrosion resistance advantages over many commercial Fe and Ni-based alloys. The results of a Mintek survey are shown in Figure 2.19. The material denoted "Mintek alloy" is a superferritic stainless steel containing 2%Ni and 0.2%Ru.

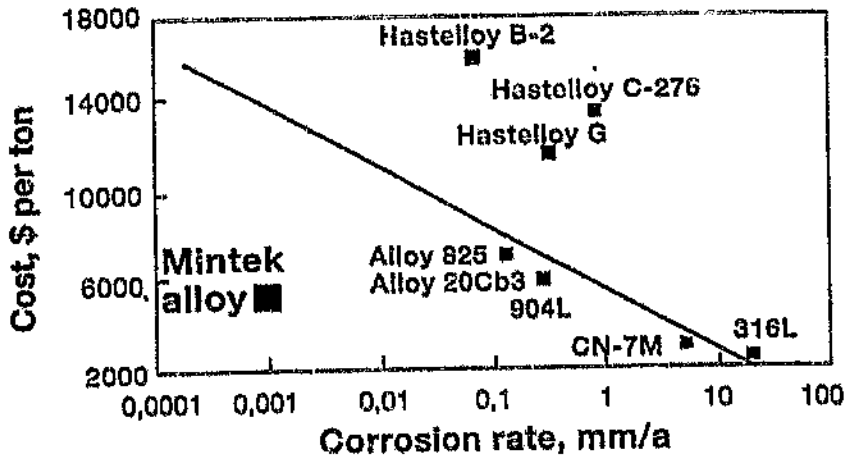

Figure 2.19: Cost-life comparisons in boiling 10% (by mass) sulphuric acid.[21]

2.8 Powder metallurgy

Powder metallurgy deals with the production of solid compacts from the consolidation of metallic powders. Metallic powders may be compacted to, or very close to, maximum theoretical density. Various techniques such as liquid phase sintering or hot isostatic pressing (HIP) are utilised in order to achieve consolidation. There are numerous advantages in utilising powder metallurgy processing. Powder metallurgy allows for the production of components from metals which are very difficult to produce by melting and casting, such as tungsten. Many composite materials, such as the cemented carbides, may only be manufactured by powder metallurgy. In addition, deliberately porous components, such as filters, are easily produced by this route. One of the major advantages of powder metallurgy processing is that it allows for the production of iron, nickel, aluminium and cobalt-based alloys which have superior microstructures and properties compared to the properties of the same alloy processed by casting and forging. Such powder metallurgy components or coatings typically exhibit greater wear resistance[30], enhanced mechanical properties and improved performance in service[31], compared to their conventionally-produced counterparts.

The advantages of powder metallurgy components are due to the characteristics of the starting powders. Depending on the manner of powder production, the powders generally have uniform, homogeneous, fine-grained microstructures with minimal segregation. Ideally, all powder particles could be considered "mini-ingots" with the nominal composition of the starting melt. Depending on the manner of powder manufacture and consolidation, material produced from these consolidated powders could therefore be expected to exhibit superior properties.

2.8.1 Production of stainless steel powders

There are numerous methods by which powders may be produced. These include communition of solid metal, precipitation from solution of a salt, thermal decomposition of a chemical compound, reduction of a compound, electrodeposition and the "atomisation" of molten metal. Only the methods relevant to the production of stainless steel powders will be reviewed here. Further information on the other processes is given in reference 33.

The majority of stainless steel powders are produced by water or gas atomisation of the melt. This method involves the disintegration and solidification of a thin stream of metal by the impingement of gas (usually inert) or water jets. Subsequently, each powder particle has the nominal composition of the parent melt. This process produces extremely fine, homogeneous microstructures with minimal segregation. However, the equipment required for powder atomisation is costly.

A novel method of producing powder from high-chromium ferritic steels has been developed and patented by Mintek[32]. The process appears to be specific to those alloy systems in which sigma phase is apparent. The technique involves embrittling the alloy by sustained heating in the temperature range of sigma formation. When sufficient sigma has formed, the material is subjected to mechanical communition in a ball mill. The powder which is produced by this method is reported to be free of surface oxide contamination, as well as having uniform composition. Numerous economic advantages have been claimed by this process. Standard milling and heat treating equipment, which are common in industry, may be employed in the powder production process. Minimal capital outlay (on new equipment or technology) is specified to be required in order to manufacture high-chromium ferritic stainless steel powder by this route. The costs of powder production by the process would therefore be expected to be far less than equivalent powder produced by atomisation.

2.9 Hot Isostatic Pressing

A number of methods may be used to consolidate a metal powder. Some of these methods are powder rolling, liquid phase sintering, the proprietary Ceracon[33] process and hot isostatic pressing (HIP).

Hot isostatic pressing (HIP) is a manufacturing technique which involves the simultaneous application of high gas pressures and an elevated temperature. The principle is straightforward. A component is placed within a specially designed pressure vessel. An inert gas, usually argon, is then pumped into the vessel. The temperature of the gas is raised, and this causes the gas pressure within the confines of the chamber to increase. Since a gas exerts uniform pressure in all directions, the nett result is the application of isostatic fluid pressure onto all surfaces of the component. Typical pressures would in the region of 1000bar (100MPa) at a temperature of 600-1300°C, depending on the composition of the alloy. The principle is illustrated in Figure 2.20.

The main effect of HIPping is the closure of internal pores within a metallic or metal enriched body e.g. cemented carbides. The upgrading of castings and sintered components is also a major industrial application of hot isostatic pressing. Some foundries and many cemented carbide manufactures specify the process as an essential stage in their manufacturing cycle. The detrimental stress-raising and weakening effects of internal porosity within a monolithic body are well documented and cannot be tolerated in many critical applications.

Another industrial application is the consolidation of metal powders to form fully dense components. The process involves placing the required metal powder into a mild steel canister of the desired shape. The canister is gas-tight and is evacuated, then sealed by welding, prior to HIPping. The high temperatures and pressures during HIPping results in yielding of the powder particles and enhanced atomic diffusion at their points of contact. The overall effect is to achieve complete metallurgical bonding of the powder particles which produces a fully-dense compact at the material's theoretical maximum density. A variety of materials such as stainless steels, tool steels and superalloys may be densified by this method. The major advantage of the technique is that all bonding occurs in the solid state. This avoids undesirable microstructural features such as the heterogeneous distribution of secondary phases and grain growth which are prevalent during solidification from the liquid phase. Since many metal powders (e.g. gas atomised powders) are typically manufactured with fine-grained, homogeneous microstructures these characteristics are preserved during HIPping.

The improvement in tensile, hardness and toughness properties in HIPped powder metallurgy alloys and HIPped castings is due to the removal of residual porosity and improved microstructure. Over the years, a number of workers have studied the differences between HIPped and unHIPped components. The findings indicate that hot isostatic pressing is a beneficial material enhancement technique for many alloy systems. Graphs which are illustrative of improvements in material properties in both powders consolidated by HIPping and castings which have undergone hot isostatic pressing are shown in Figures 2.21 and 2.22[34]. The temperatures used in HIPping are typically greater than $0.7T_m$(where T_m is the melting point). This ensures that sufficient atomic diffusion occurs to ensure complete particle bonding and pore closure within a reasonable time during commercial operation. Too low a temperature results in excessive cycle times, whilst too high a temperature introduces the risk of forming the liquid phase. The degree of pressure applied is usually derived from empirical data. Gas pressures between 80-100MPa have been found to be sufficient. A list of common temperatures for various materials is shown in Table 2.1.

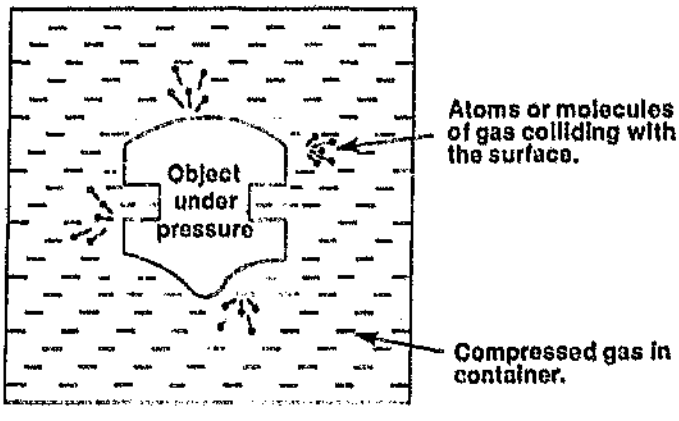

Figure 2.20: The principle of HIPping.[34]

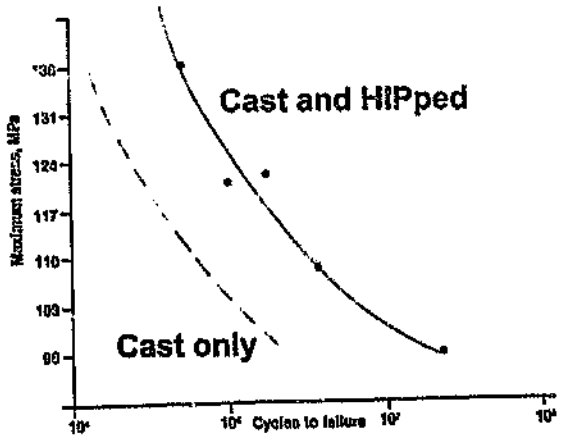

Figure 2.21: Comparison of material properties: as-cast and cast+HIPped. The material is Al-7 wt% Si alloy L99.[34]

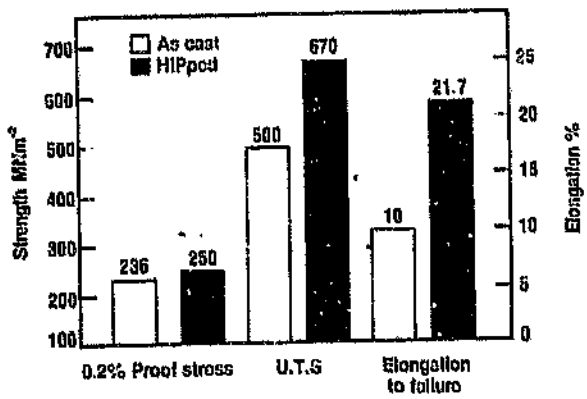

Figure 2.22: Illustrative comparison of material properties: as-cast and cast+HIPped.[34]

Table 2.1: Typical HIP parameters.[34]

Material	HIPping temperature (°C)	HIPping pressure (MPa)	Melting point (°C)
SiC	1850	200	2837
Al_2O_3	1500	100	2050
Al and Al alloys	500	100	660 (Al)
Nimonic and superalloys	1100-1280	100-140	1453 (Ni)
Steels	650-1160	100	1536 (Fe)
WC\Co	1350	100	2867 (WC)
Ti and Ti alloys	920	100	1670 (Ti)
Cu and Cu alloys	800-950	100	1083 (Cu)

From Table 2.1 it can be seen that HIPping is extremely versatile and can be applied to numerous materials. However, ceramics such as Al_2O_3 and carbides such as SiC, generally require extremely high temperatures. These temperatures can only be achieved with specialised HIP equipment and are usually not economically viable. Most commercial HIP facilities therefore only process materials which can be HIPped at 1400°C or below.

2.9.1 Diffusion bonding

HIPping may also be utilised to diffusion bond or join similar or dissimilar materials. The major advantage relative to traditional fusion welding is that no melting of the parent metals occurs. This minimises problems such as microstructural segregation and solidification cracking. Distortion is also decreased. Metallurgical bonds are produced in the process, and bond strengths are acceptable for commercial applications[35]. Diffusion bonding allows a far greater combination of alloys to be joined. Many of these combinations would be difficult or even impossible to produce in fusion welding processes. Some material combinations which are possible, typically for hardfacing or protective coating applications, are Stellite (cobalt-chrome) alloys/austenitic stainless steel, tool steel/stainless steel, nickel-based superalloys (e.g.Inconel)/Stellite, and Zircaloy/uranium oxide.

2.9.2 Industrial HIP

Whilst the earliest equipment for hot isostatic pressing was originally designed in the late 1950s by the Battelle Institute of America, the technique only became commercially successful in the 1970s. Only some companies in Europe and America generally offered the technology during this period. The world-wide value of finished HIP products in 1987 was estimated at over two billion pounds sterling[34]. In 1991 Ultra High Pressure Units made the process available to the South African industrial market for the first time.

2.9.3 The theoretical basis of powder consolidation during HIPping

Hot isostatic pressing relies on the simultaneous effects of applied temperature and pressure to achieve metallic diffusion bonding. There are a number of distinct stages. Initially, the elevated temperature reduces the yield strength of the powder particles such that the applied pressure results in compaction and plastic yielding of the powder particles. This causes the exposed surfaces of the particles to come in intimate contact with each other. The compact therefore consists of a network of powder particles with interconnected porosity. Further consolidation occurs by means of various creep mechanisms such as Nabarro-Herring and Coble creep which provide a means for matter transport. In the second stage, the bond interface consists primarily of bonded areas and residual voids. The driving for the removal of porosity is the overall reduction of the surface area of the compact. A reduction in surface area leads to a lowering in the overall energy of the system and is therefore thermodynamically favoured. Final bonding and pore removal occurs by means of atomic diffusion, as well as recrystallization and grain boundary migration[36].

The end result is complete bonding of all the powder particles in a compact which is at the theoretical density for that material. The various stages of HIP consolidation have been modelled mathematically by a number of workers[37]. These models are fairly involved, and are beyond the scope of this literature survey. A useful review and discussion of the various mathematical models may be found in the work of Eisen[38].

2.10 Milling

Milling involves the mechanical communition of a powder in order to reduce the size or alter shape of powder particles. It may also be used to coat the powder particles, or to mix or blend two or more materials.

There are a number of techniques in which milling is achieved. Different variations are vibratory, ball and attritor milling. Ball milling is one of the more commonly used methods. This involves placing a powder charge in a cylindrical tumbler which is filled with spherical milling media and a protective fluid (Figure 2.23). The milling media are usually produced from hard material such as cemented carbide or hardened steel. The protective fluid is usually a hydrocarbon such as acetone or hexane. In certain specialised cases, water may be used.

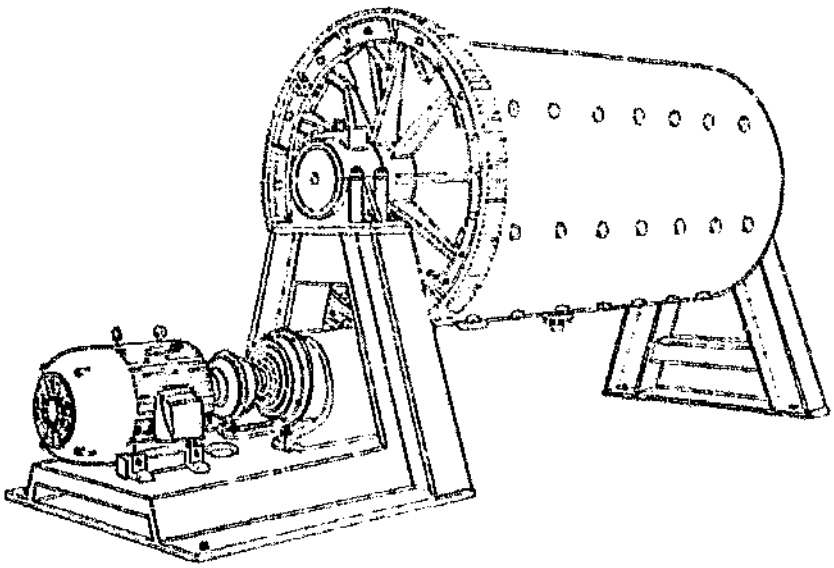

Figure 2.23: Tumbler used for milling metal powders.[34]

The principle of ball milling is straightforward. The tumbler is rotated at a certain angular velocity, causing relative motion between the milling media and the powder charge. This causes powder particles to become entrapped between the impacting milling media (Figure 2.24). A number of different responses to this impact are possible. Hard, brittle powder particles will tend to fracture with minimal deformation, whereas ductile materials will deform plastically and experience agglomeration and cold welding between particles.

There is a limit to the to the amount of particle size reduction which can be achieved by milling. Particles may agglomerate by means of cold welding or mechanical interlocking, and as the particles become finer, there is a tendency for the agglomeration forces to become stronger. Eventually, the agglomeration forces (cold welding) reach an equilibrium with the tendency for particle size reduction (fracture), and a minimum particle size is reached. A narrow particle size distribution is then obtained. Particles larger than average are reduced in size, whilst particles smaller than average are agglomerated (Figure 2.25). This means that excessive milling times are ineffective in achieving any further significant reduction in particle size.

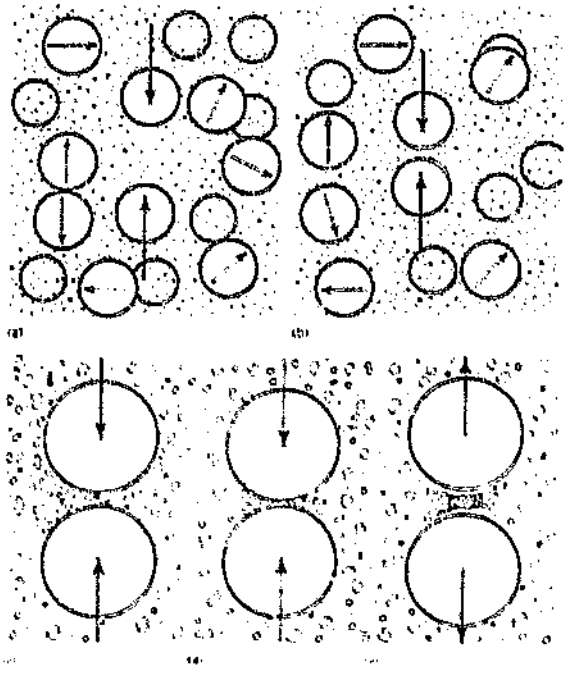

Figure 2.24: Representation of comminution by ball milling. The large circles represent the balls, whilst the particles around them represent the powder.[31]

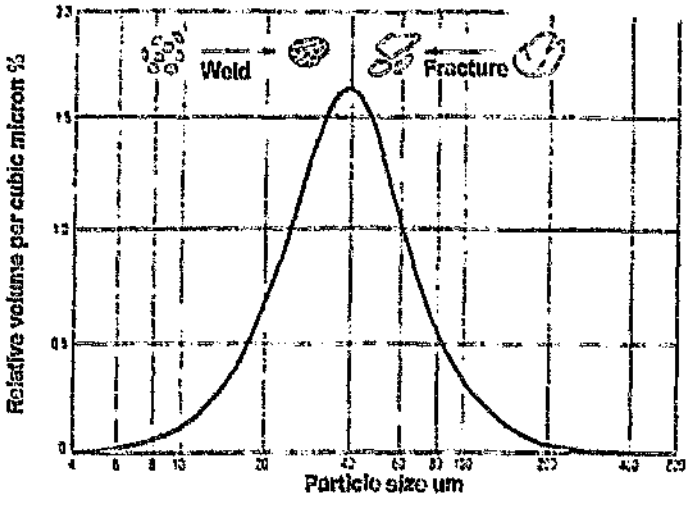

Figure 2.25: Narrow particle size distribution caused by tendency of small particles to weld and large particles to fracture.[32]

Milling is dependent on a number of factors such as angular velocity, media to powder ratio, type of protective liquid, milling time and the characteristics of the powder and mill media. As angular velocity increases, communition increases. However, once a critical velocity is exceeded, the balls will tend to be held against the walls of the mill chamber by centrifugal force, and minimal communition will occur. As the media to powder ratio is increased, the degree of communition and mixing increases, since there is a greater chance of a powder particle becoming entrapped between colliding balls.

The protective fluid interferes with cold welding, but absorbs the heat of communition and protects the reactive powder surfaces against oxidation from the atmosphere. The shape, size and material of the milling media affects the milling process. Brittle powders will tend to be communited more easily than ductile powders.

During ball milling, a great deal of cold welding occurs between the balls, powder particles and mill chamber. The continuous welding and fracturing (Figure 2.26) of individual particles results in homogenisation of the constituent powders. However, the homogenisation process is greatly enhanced and becomes truly effective only when the protective liquid environment is removed.

In this situation, the dry ball milling process is then referred to as mechanical alloying. Mechanical alloying may be treated as a separate branch of ball milling, and no further discussion on the topic is necessary at this time since the technique was not employed in this study. A more involved and mathematical analysis of the milling process is possible. These aspects will not be dealt with in this report, but can be found elsewhere[30].

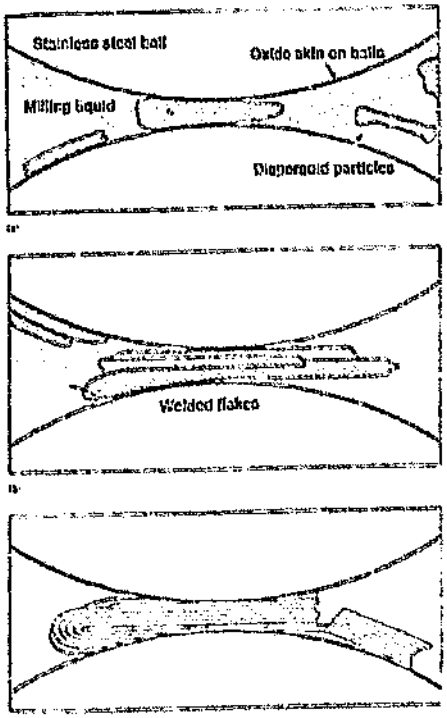

Figure 2.26: Cold welding of particles during ball milling.[31]

2.11 Duplex powders

The majority of work in the field of composite alloys and materials is concentrated on improving wear and strength characteristics of metallic alloys. The most common technique used is the mechanical alloying or mixing of metal powders with a fine dispersion of hard particles. These hard particles are typically carbides or oxides. Such materials are known as dispersion strengthened alloys or metal matrix composites and are said to produce desirable mechanical properties which are difficult to obtain by conventional means[40,41,42]. As an example, Velasco[42], found that the wear resistance of 316L stainless steel could be improved by 50 percent with the introduction of 4 weight percent yttria or alumina particles. The standard manufacturing route for metal matrix composites is mechanical milling/alloying of various powders followed by compaction and then conventional sintering techniques[33]. However, some workers such as Pierronnet and Raisson have utilised HIPping[43] in their study of the addition of various carbide particles to Ti and Ni alloys. These workers only used conventional mixing and blending techniques prior to hot isostatic pressing, and their chief finding was that HIP technology could be successfully used in the production of a metal-matrix composite.

No references could be found in the literature involving the simple mixing and HIP consolidation of different pre-alloyed metal powders. The only investigations in this area were examinations of the diffusion zone between bulk alloys which were bonded by HIPping. The work of Jarvenpaa[15], Zeedijk[44], and Raisson[45] provides a useful background to the field. Ashworth[46] conducted an interesting investigation into the strength of diffusion bonds, and found that high strength bonds could be produced between dissimilar materials, such as tool and stainless steels. However, none of these studies examined the reactions between powders of different composition which were mixed and HIPped together. The literature also indicates that almost no work has been done on producing a powder based composite alloy with the central aim of improving corrosion resistance.

2.12 Corrosion

Corrosion may be defined as the deterioration of a metal through mainly chemical interaction with its environment. Many metals in the pure state are not in their most thermodynamically stable forms. Corrosion is therefore the tendency of a metal to revert back to its most stable state. This state is typically some form of oxide. The electrochemical nature of this process may be demonstrated by considering a simplified corrosion reaction which may be represented by the following equations:

Oxidation (anodic reaction) $M \rightarrow M^{n+} + ne^-$ (1)
Reduction (cathodic reaction) $2H^+ + 2e^- \rightarrow H_2$ (2)

(Where M = metal).

During the oxidation process (reaction 1), the metal reverts from its metallic state to an ionised form. The electrons which are released are then taken up by a corresponding reductic process (reaction 2). A variety of reduction processes are possible and reaction (2) is only utilised as an example. The important feature to note is that an electrochemical cell is formed between the metal surface and a corrosive environment. Reactions (1) and (2) are therefore referred to as half-cell reactions. The reduction reaction occurs at the cathode, whilst oxidation occurs at the anode.

The electrochemical approach to the corrosion process allows for certain relationships between the cell potential and current to be defined. When an electrochemical cell is at equilibrium, there is no nett oxidation or reduction reaction i.e. the rate of reduction and oxidation is the same. There is no accumulation or deficiency of charge. At equilibrium a certain cell potential, n_e exists. These cell potentials are referenced with respect to the standard hydrogen electrode and are listed in the galvanic series. The rate of the reduction and oxidation reactions of the cell are expressed in terms of the exchange current density i_o (current per unit surface area). At equilibrium $i_{oxidation} = i_{reduction} = i_o$. The value of i_o is derived empirically and tables with the i_o measurements of various systems are available.

Metals which undergo corrosion form electrochemical cells which are not at equilibrium. Polarisation is then said to occur. This polarisation results in an overvoltage n, which represents a deviation from the equilibrium cell potential n_e.

Two types of polarisation, activation and concentration polarisation, can occur at an electrode. Activation polarisation is the electrochemical reaction which is controlled by the reaction kinetics at the metal-electrolyte interface. A reacting species must be adsorbed onto the metal surface before a reaction can occur. The rate of reaction at the interface is thus the rate-controlling step.

Concentration polarisation refers to electrochemical reactions which are controlled by the diffusion of reactant species through the electrolyte. In other words, the rate of reaction at the metal-electrolyte interface is far faster than the rate of diffusion towards the interface. The overall reaction rate is therefore governed by the diffusion of species through the bulk fluid, rather than the reaction at the interface.

Both activation and concentration polarisation can occur at an electrode. At high reaction rates, concentration polarisation is dominant, while low reaction rates activation polarisation is the dominant factor. Concentration polarisation is not usually a factor during corrosion.

The relationship between reaction rate and overvoltage is expressed by the following equation:

$$\mathbf{n = \pm B\ (\log \frac{i}{i_o})} \qquad \textbf{Activation polarisation} \quad \textbf{(3)}$$

n = overvoltage
B = the Tafel constant
i = rate of oxidation or reduction in terms of current density
i_o = rate of oxidation or reduction at equilibrium

In practice, B is typically assigned the value of 0.1 volt. If a plot of equation (3) is shown for a typical equilibrium reaction, the graph in Figure 2.27 is obtained. The graph is linear and the lines are the anodic and cathodic polarisation curves for the cell in question. It is apparent that small changes in overvoltage produce large changes in current density.

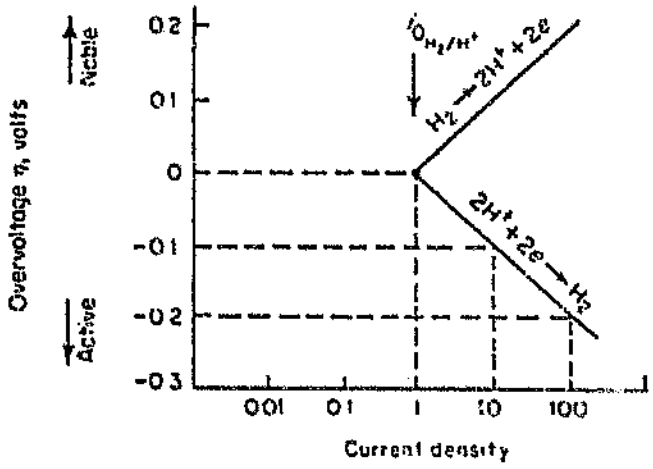

Figure 2.27: Overvoltage versus current density.[1]

2.12.1 Mixed potential theory

Mixed potential theory allows for the prediction of corrosion rates in systems in which more than one oxidation or reduction reaction takes place. The theory is based on two hypotheses:

1. Any electrochemical reaction can be simplified into two or more partial oxidation or reduction reactions.
2. There is no nett accumulation of charge during an electrochemical reaction, i.e. the rate of reduction must equal the rate of oxidation.

The case of zinc immersed in hydrochloric acid can be used as an illustrative example of the theory, as shown in Figure 2.28.

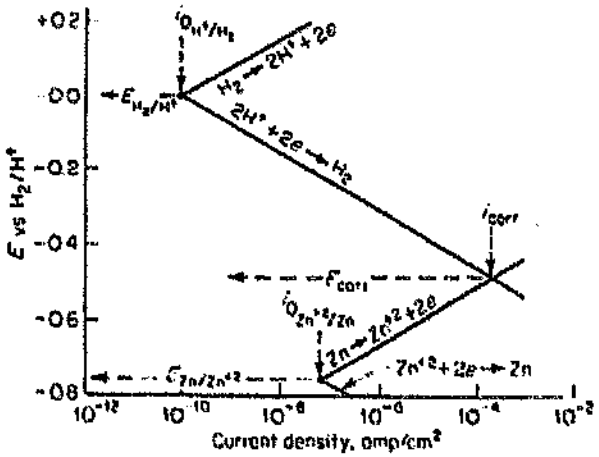

Figure 2.28: Electrode kinetic behaviour of Zn in acid solution.[1]

From the graph it can be seen that the zinc and hydrogen reaction cannot lie at their equilibrium potential values since charge must be conserved. Therefore the only point at which equivalent reaction rates can occur will be at the intersection points of the hydrogen reduction and zinc oxidation lines. The current density at this point of intersection is referred to as i_{corr}, the critical current density, and the corresponding overvoltage value as E_{corr}. The value of i_{corr} can then be utilised to determine the corrosion rate of the system.

In complex systems with more than two oxidation and reduction reactions, the overall reduction and oxidation rate has to be determined. Fontana[1] provides a more detailed explanation of the principles and procedures involved.

2.12.2 Passivity

Passivity is the loss of reactivity of a metal in certain environments. The phenomenon is due to the formation of a relatively inert film on the metal surface. The film or passive layer is extremely thin and is estimated to be of the order of 30 angstroms in thickness[1]. Its composition is thought to be oxides and water of hydration. The behaviour of a metal which does not exhibit passivity under increasing oxidising conditions is shown in Figure 2.29.

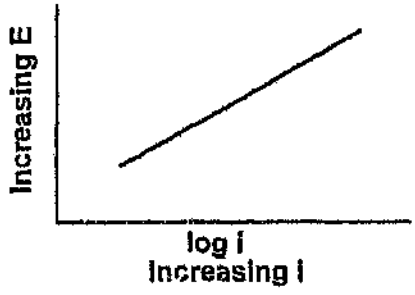

Figure 2.29: Behaviour of non-passive metal.

Metals such as chromium, titanium, nickel and their alloys have the ability to passivate. The typical behaviour of these metals is illustrated in Figure 2.30.

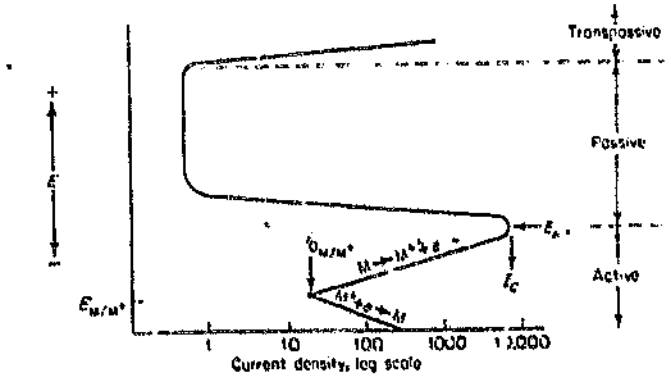

Figure 2.30: Typical anodic dissolution behaviour of an active-passive metal.[1]

From the Figure 2.30 it can be seen that as the overvoltage is increased above the equilibrium potential, then the current density (corrosion rate) increases as well. The metal is termed to be in its active state. At the primary passivation potential E_{pp}, the anodic current density achieves its maximum value I_c , the critical anodic current density.

At overvoltages greater than E_{pp} the current density decreases drastically until it remains at a fairly constant value. In this potential range the oxide layer is stable and corrosion occurs at a very low rate. The metal is then said to be in its passive state. As the overvoltage is increased, the passive layer is eventually broken down at E_p and the current density increases accordingly. This is the transpassive region.

The effect of increasing temperature and acid concentration on passivation behaviour is shown in Figure 2.31.

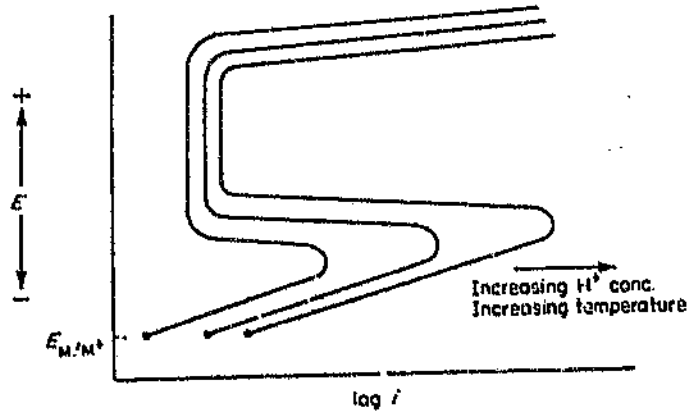

Figure 2.31: The effect of temperature and acid concentration on passivation.[1]

Increasing acid concentration and temperatures produces a higher I_c. However, I_{pass} and E_{pp} are relatively unchanged. The passive film is stable over a smaller potential range with increasing temperature and acid concentration. It is therefore apparent that metals or alloys which have a low anodic current density and an active primary passivation potential will be more easily passivated.

2.12.3 Galvanic coupling

A galvanic couple is formed when two dissimilar metals are joined . The more noble metal exhibits decreased corrosive attack, whilst the less noble metal experiences an increase in corrosion rate. The mixed potential theory provides an explanation for this phenomenon. Figure 2.32 indicates the behaviour of corroding metals M and N before and after galvanic coupling.

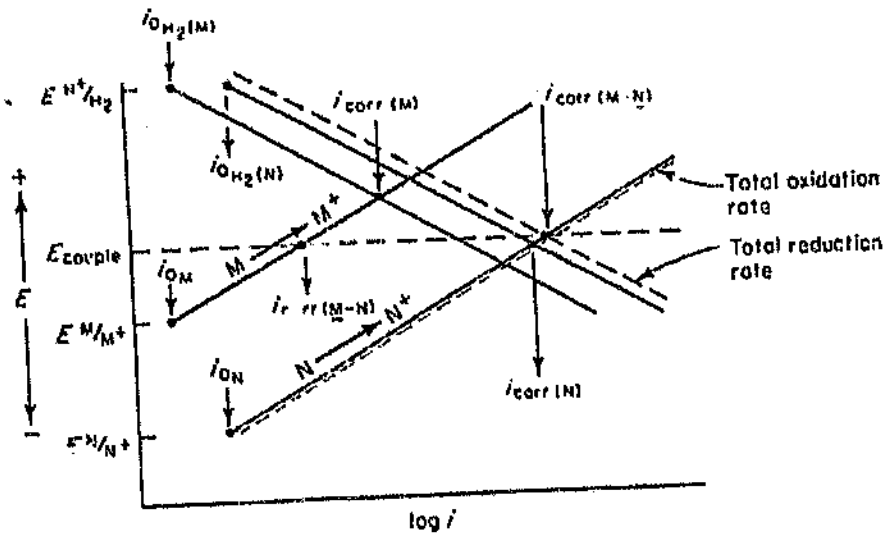

Figure 2.32: Galvanic couple between two corroding metals.[1]

Metal M is more noble than N and has a lower corrosion rate. When the M and N are joined, the entire redox system changes. The corrosion potential occurs at E_{couple} and the overall behaviour of the system is defined by considering the total oxidation and reduction rates which occur. E_{couple} occurs where the lines representing the total oxidation and reduction rates intersect. The corrosion rate of metal M decreases to i_{corr}(M-N), whilst the corrosion rate on metal N increases to i_{corr}(M-N).

The mixed potential theory can also be used to describe the alloy engineering technique known as noble metal alloying or cathodic modification. The technique extends the range of environments, concentrations and temperatures over which an alloy exhibits passivity. A review of the field has been performed by Higginson[27] and further details may be found in the references.

It has been observed[27] that chromium and titanium passivate spontaneously when galvanically coupled or alloyed to the platinum group metals (PGM). This is due to the fact that the platinum group metals are extremely noble and raise the voltage of the Cr/Ti-PGM galvanic couple into the potential region in which Cr or Ti passive layer is stable. As a consequence of the change in overpotential after alloying, the rate of the cathodic (hydrogen evolution) reaction is increased, hence the term cathodic modification. It has been established[27] that in order for cathodic modification to be successful certain criteria have to be satisfied. The first criterion is that the reversible cathodic (hydrogen evolution) potential must be greater than the primary passivation potential. The second criterion is that the cathodic (hydrogen evolution) process must supply a current density which is greater than the critical current density required for passivation.

Three cases with different cathodic (hydrogen evolution) conditions are illustrated in Figure 2.33.

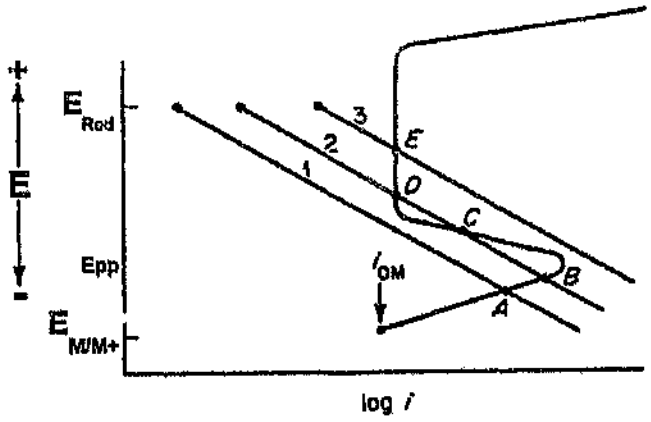

Figure 2.33: Requirements for cathodic modification [1]

In case one, intersection of the anodic and cathodic reactions can only occur at point A. Point A is at a potential below E_{pp}. The alloy will therefore corrode actively. In case two, three intersection points are possible. Only B and D are stable, so the metal can exist in both the passive or the active state under identical environmental conditions. This situation is not desirable since the metal will not exhibit consistent corrosion behaviour. The third case is one which satisfies all the requirements for successful cathodic modification. Passivation will occur spontaneously and the addition of a PGM will be successful. In other words, the addition of a PGM will modify the electrochemical behaviour of the alloy such that overall electrochemical system follows the behaviour of case three. The requirements for cathodic modification are only satisfied by the chromium and titanium alloy systems with PGM additions.

2.12.4 Corrosion tests

Mixed potential theory is a valuable tool in corrosion studies. Graphs of overvoltage versus the logarithm of current density provide useful information with regard to the behaviour of a metal. Values of I_{pass}, I_C,E_{pp} , E_P and the range over which the passive film is stable, allow the corrosion characteristics of a metal to be determined. In addition, these graphs allow the corrosion rate of a metal to be measured by means of Tafel and linear polarisation.

2.12.4.1 The linear polarisation method

The linear polarisation method is a common technique for determining corrosion rates from anodic and cathodic polarisation curves. The principle is based on the observation of a region of apparent linearity near the origin of a polarisation curve. The slope of this linear region is inversely proportional to the corrosion rate. The linear region typically occurs over a restricted range, as shown in Figure 2.34.

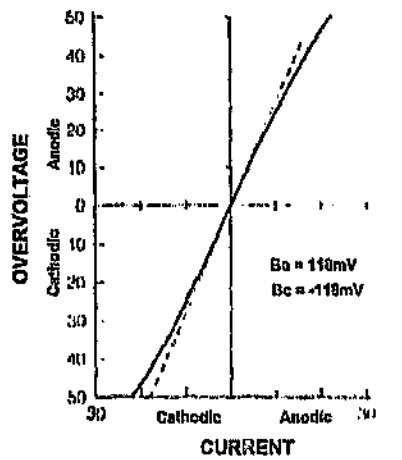

Figure 2.34: Linear region in cathodic and anodic polarisation curves.[47]

It can be shown[47] that the following relationship exists between the slope of the linear region and the corrosion current density:

$$Slope = \frac{de}{di(applied)} = \frac{B_a.B_c}{2.3i[B_a+B_c]} \qquad (4)$$

Where:

de = potential change from the steady state corrosion potential E_{corr} (mV)

di(applied) = applied polarisation current density (uA/cm^{-2})

B_a = anodic Tafel constant (mV)

B_c = cathodic Tafel constant (mV)

i = corrosion current density (μA/cm^{-2})

It has been shown[47] that the Tafel constants may be approximated by $B_a = B_c =$ 100mV to achieve good correlation with experimental results. The use of such an approximation has been shown to produce a maximum error in calculated corrosion rate of a factor of two, and is within the experimental scatter of plant corrosion data. In addition, relative corrosion rates rather than absolute values are generally of more importance in laboratory studies. Equation (4) may therefore be simplified to the following form:

$$Slope = \frac{de}{di(applied)} = \frac{21.74}{i}$$

Rearranging for i yields

$$i = \frac{21.74}{slope} \qquad (5)$$

A further calculation is required to convert i to a corrosion rate. For stainless steels, a current density of 1μA.cm^{-2} corresponds to a corrosion rate of approximately 0.011mm per year.

2.12.4.2. Tafel extrapolation

Tafel extrapolation is another method which may be used to determine corrosion rates from electrochemical potentiodynamic corrosion tests. During potentiodynamic tests it is found that in the absence of an applied current, the measured potential corresponds to the corrosion potential of the test specimen in the test media with respect to the reference electrode. If a current is applied then the graph of potential versus the log of the current appears as shown in Figure 2.35. The curve of applied current is non-linear at low currents but becomes linear as the current is increased. The linear region is referred to as the Tafel region. Extrapolation of the Tafel region to the corrosion potential E_{corr} provides a value for i_{corr} at the point of intersection. The main restriction of this method is that the Tafel region must extend over at least one order of magnitude to achieve reliable results for i_{corr}. Additionally, the method can only be applied to systems in which one reduction process occurs. If more than one reduction process is present, then the Tafel region becomes distorted. The advantages of Tafel extrapolation are that it allows for the measurement of extremely low corrosion rates and provides good accuracy[1].

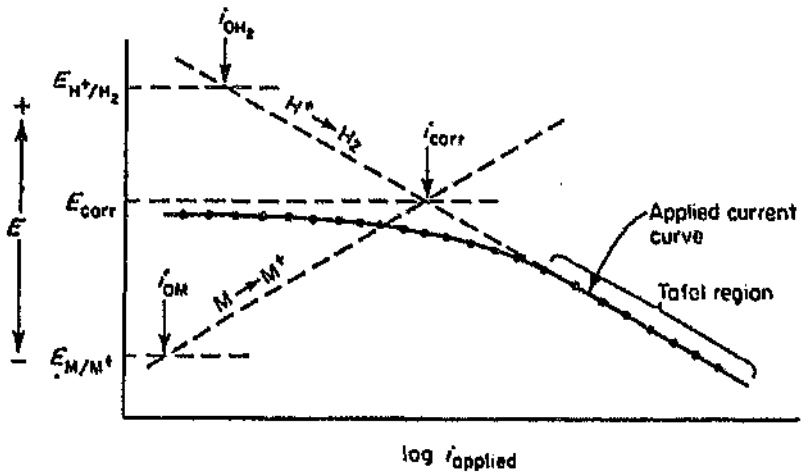

Figure 2.35: Applied current cathodic polarisation curve of a corroding metal showing Tafel extrapolation.[1]

2.12.5 Corrosion of the Fe-40Cr alloys

Interest in the Fe-40Cr alloys can be generally attributed to the work of Tomashov and Chernova[48] who studied the passivation behaviour of Fe-Cr-Pd alloys with varying amounts of chromium. Tomashov determined that the optimal effect of a 0.2%Pd addition occurred at a chromium content of 40 percent (Fe-40Cr-0.2Pd). These results prompted further research in the field, and Higginson[27] and Streicher[49] found that the substitution of Ru instead of Pd yielded similar results in sulphuric acid solutions. The lower cost of Ru relative to Pd was a motivating factor.

Initial corrosion tests were on the binary Fe-40Cr or Fe-40Cr-0.2Ru alloys and were conducted in H_2SO_4 and HCl environments[27]. These tests concentrated on general corrosion, and no localised corrosion tests were performed. The work of Higginson[27] provides some information on the behaviour of the Fe-40Cr-Ru alloys with varying Ru content. It was found that Fe-40Cr-0.1Ru and Fe-40Cr-0.2Ru alloys underwent spontaneous passivation in 0.5M HCl and 0.5M H_2SO_4 at 25°C. The addition of 0.2%Ru was found to be more beneficial than 0.1%Ru, and the potential-time curves are shown in Figure 2.36.

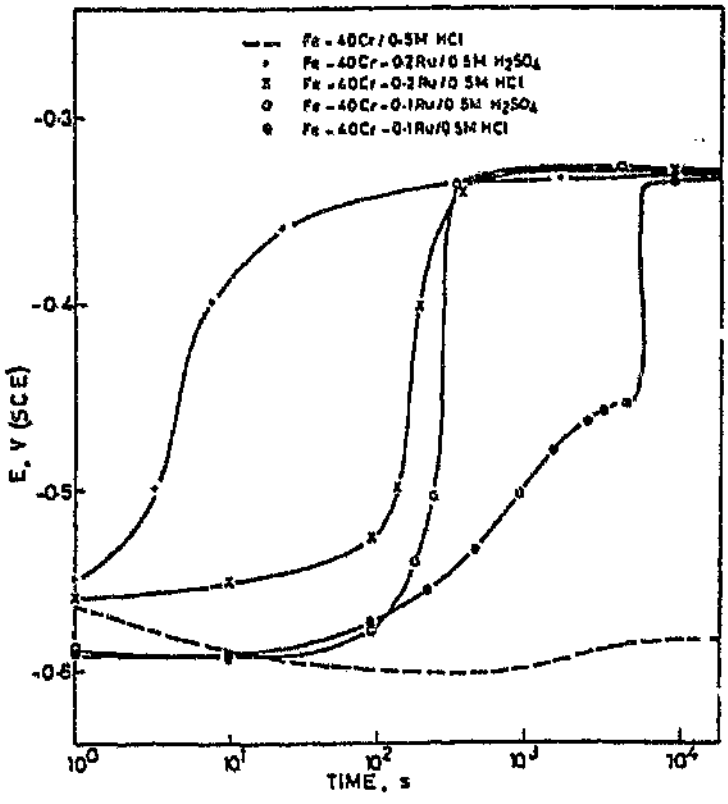

Figure 2.36: Potential-time curves for Fe-40Cr-Ru alloys displaying spontaneous passivation in 0.5M acids at 25°C.[27]

Higginson, Newman and Procter[50] studied the passive films on the Fe-40Cr-Ru alloys by Auger spectroscopy. They were found to be similar to those formed in conventional stainless steel, and were not enriched in Ru. Only in conditions of borderline passivity (in which the passive layer is only metastable) did Ru become the major alloying constituent of the film.

Tullmin[3] conducted a fairly comprehensive study on the general and localised corrosion characteristics of Fe-40Cr alloys, with and without Ni, Mo, Cu, Nb Ti, V and Ru additions. Comparisons were also made with alloys available on a commercial basis: 904L, Hastelloy C276, 316L, AL29-4C and AL-6XN. The test solutions used were 10 volume percent de-aerated H_2SO_4 at 30°C and 20 volume percent de-aerated H_2SO_4 at 40°C (with 100ppm KSCN).

The latter solution was utilised in order to obtain satisfactory active to passive polarisation behaviour in the alloys which contained Mo. For accelerated electrochemical pitting tests, Tullmin utilised 3 percent NaCl at 60°C and industrial effluent at 50°C. Crevice corrosion tests were conducted in de-aerated 3.5 percent NaCl at 30°C. In the study, the compositions of the passive layers were examined by means of XPS surface analysis. The results of the study indicated that simultaneous additions of two percent Ni and two percent Mo were essential in producing general corrosion resistance which was comparable to the commercial alloys. Binary Fe-40Cr or Fe-40Cr-Ni alloys were found to have lower corrosion resistance than 316L in the test environments. The addition of 0.2% Ru alone was find to only have a limited beneficial effect i.e. 2%Mo and 2%Ni alone were as good as 0.2%Ru alone in certain environments. Some of the results of the study are shown in Figures 2.37 and 2.38.

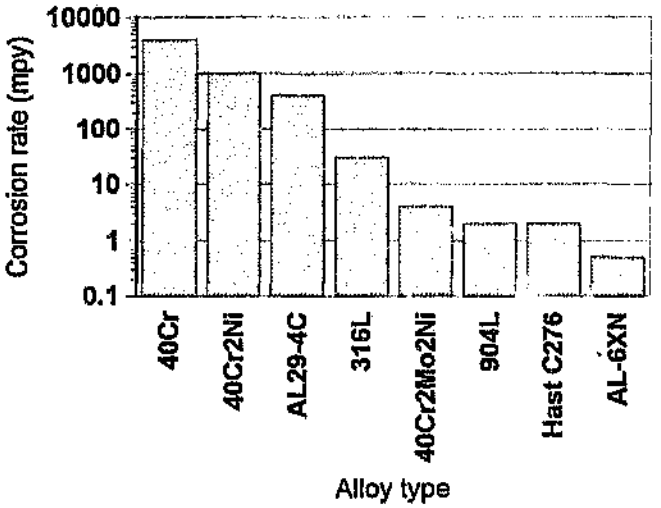

Figure 2.37: General corrosion rates of Fe-40Cr alloys and commercial stainless steels in 10% H_2SO_4 at 30°C.[3]

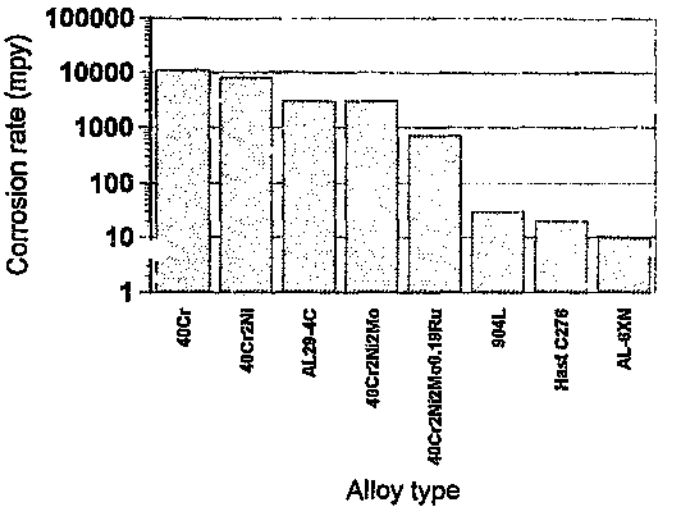

Figure 2.38: General corrosion rates of Fe- 40Cr alloys and commercial stainless steels in 10% H_2SO_4 +100ppm KSCN at 40°C.[3]

The pitting and crevice corrosion tests in the study[3] indicated that Fe-40Cr alloys without Mo additions had poor resistance to pitting and crevice corrosion. The presence of Ru was found to have only a minimal beneficial effect on pitting resistance in the test environment. Some results are shown in Figure 2.39.

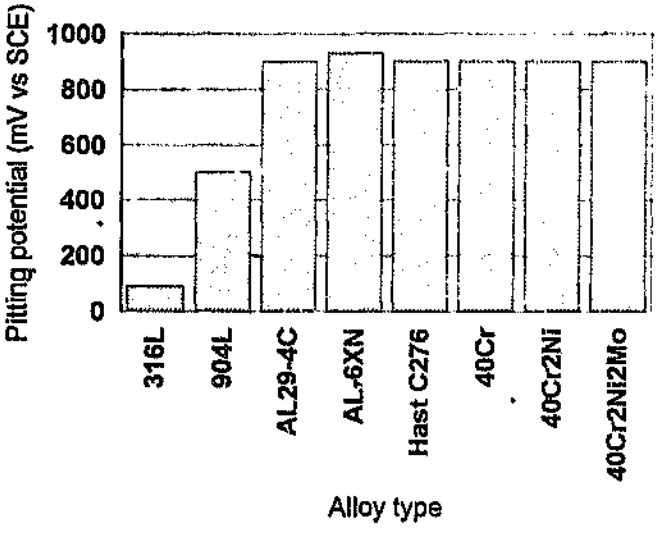

Figure 2.39: Pitting potentials of 40Cr-Fe alloys and commercial stainless steels in 3%NaCl at 60°C.[3]

Tullmin[3] found evidence from XPS (X-ray photo-spectrometry) analysis that CrO(OH) and water of hydration were the main constituents in the passive layers of the Fe-40Cr alloys. No Ni, Mo or Cu enrichment was observed in the layer. Mo enrichment was only found on the surfaces during active dissolution. This enrichment was thought to be responsible for pitting resistance.

The standard addition of 0.2% Ru to the Fe-40Cr alloys[3] was a direct substitution of the 0.2% Pd utilised by Tomashov[48]. Since the platinum group metals could exhibit differences in behaviour, Potgieter and Van Bennekom[51] conducted an investigation as to whether this amount of Ru was the optimal value for maximum corrosion resistance. Tests were conducted in de-aerated ten mass percent H_2SO_4. The Ru content was varied between 0 and 0.2 percent for both Fe-40Cr and Fe-30Cr alloys. The findings of the study are shown in Figures 2.40-2.43.

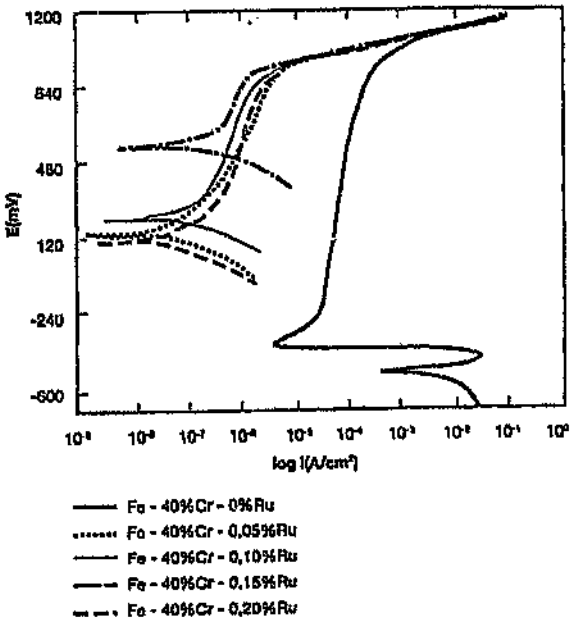

Figure 2.40: Potentiodynamic responses of Fe-40%Cr-Ru alloys in 10% H_2SO_4 at 25°C. [51]

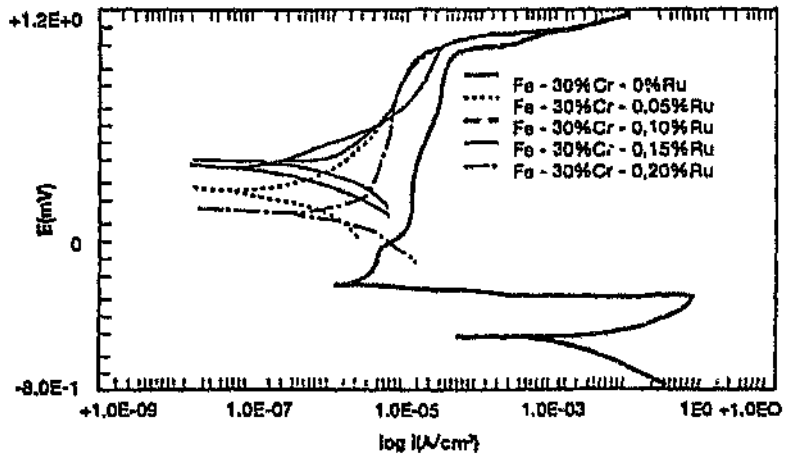

Figure 2.41: Potentiodynamic responses of Fe-30%Cr-Ru alloys in 10% H_2SO_4 at 25°C.[51]

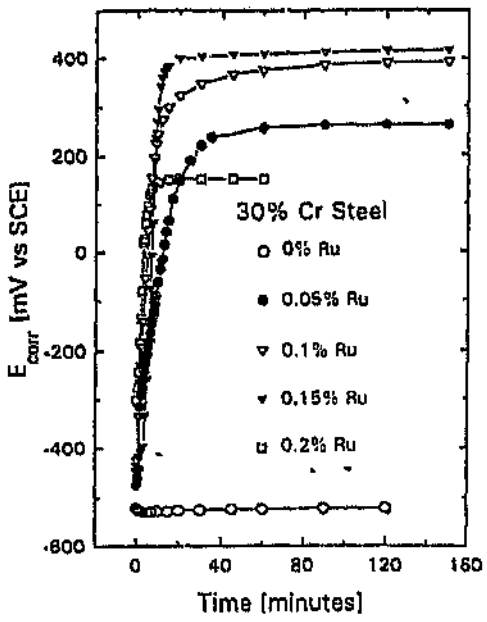

Figure 2.42: Open circuit corrosion potential variations with time of Fe-30%Cr-Ru alloys in 10% H_2SO_4 at 25°C.[51]

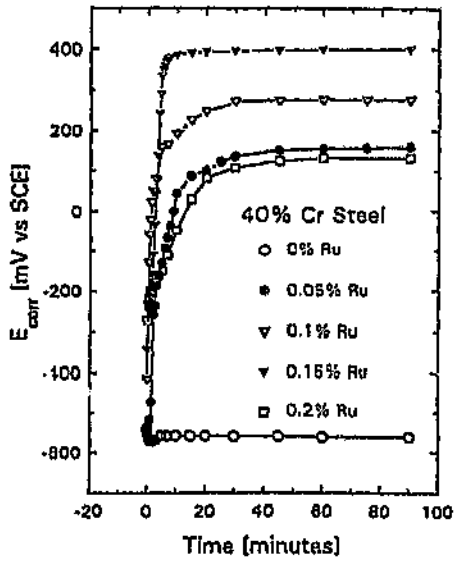

Figure 2.43: Open circuit corrosion potential variations with time of Fe-40%Cr-Ru alloys in 10% H_2SO4 at 25°C.[51]

Compared to the base alloy, additions as low as 0.06% Ru were found to induce spontaneous passivation in the test solution[51]. A Ru content of 0.15 percent was found to produce the most noble open-circuit corrosion potential value as well as the best overall corrosion resistance. This behaviour was observed in both the Fe-40Cr and Fe-30Cr materials. The Fe-40Cr and Fe-30Cr alloys exhibited similar characteristics in the test solution. The investigators felt the cathodic modification of the Fe-30Cr alloy would be more appropriate due to the fact that the technology already exists to produce the Fe-30Cr alloys on a commercial basis and only a minimal improvement is gained by increasing the chromium content.

At the time of this study it appears that no research is available comparing the corrosion characteristics of HIPped or powder metallurgical steel and conventional Fe-40Cr alloys.

2.12.6 Sigma phase and corrosion resistance

Although it is generally accepted that the presence of sigma phase is deleterious to corrosion resistance, minimal information is available on the effect of the phase in the corrosion of Fe-40Cr alloys. However, some workers have examined the effect of sigma phase in duplex stainless steels.

Wilms et al[52] investigated sigma precipitation in a Fe-25Cr-7Ni-4Mo-0.3N alloy. The investigation was mainly concerned with the crevice and pitting corrosion of the alloy in artificial and natural sea water. In addition, the effect of the sigma phase on impact toughness was also examined. In their work, Wilms et al described a technique for artificially induced crevice corrosion. The results of the polarisation scans are shown in Figures 2.44-2.45.

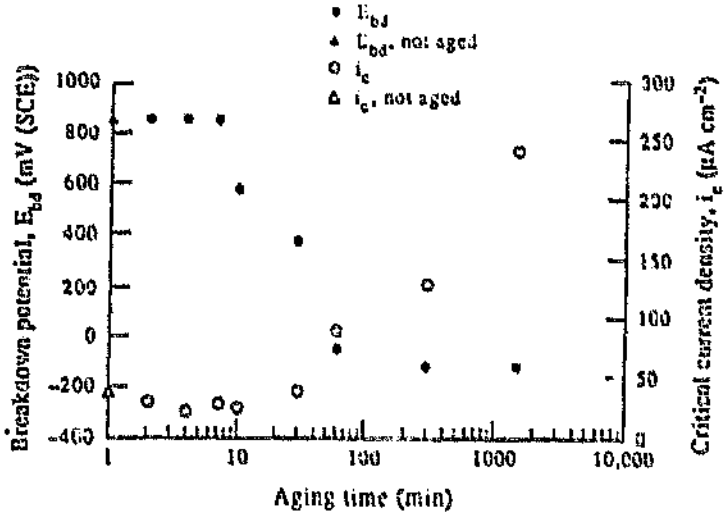

Figure 2.44: Breakdown potential (E_{bd}) and critical current density (i_c) as a function of ageing time (i.e increasing sigma content).[52]

E_{bd} is the potential value at which a current density of 10μA.cm^{-2} is reached. I_c is the largest anodic current density measured while increasing potential, before passive behaviour is attained.

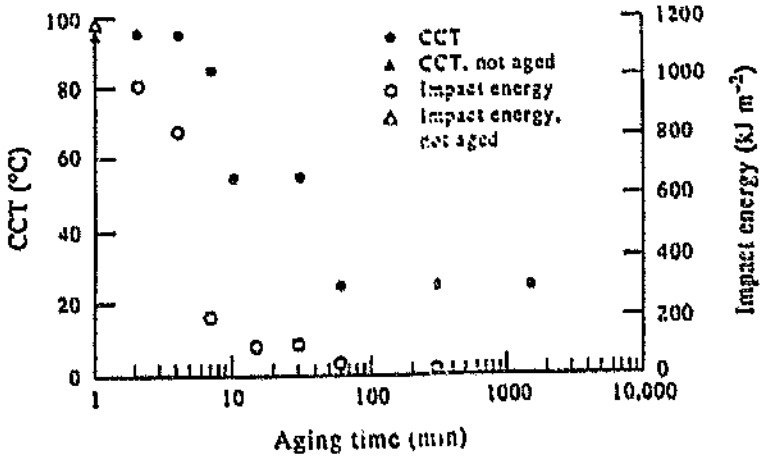

Figure 2.45: Critical crevice corrosion temperature (CCT) and impact value as a function of ageing time (i.e. increasing sigma content).[52]

Critical crevice corrosion temperature (CCT) is defined as the highest temperature at which a material remains free from crevice corrosion. The significant decrease in impact toughness with increasing sigma content is also apparent in this graph.

This work[52] indicated that as the amount of sigma phase increases, the resistance to localised corrosion decreases. This was shown in the continual drop of the CCT with sigma content. Local corrosion was found to originate at regions adjacent to the sigma phase and was postulated to be due to Cr and Mo depletion of these zones. An important point raised was that sigma phase tends to have a far more dramatic effect on the impact resistance of the steel than on the corrosion resistance. In other words, a steel with sigma phase would be rejected on the grounds of poor mechanical characteristics long before the deterioration of corrosion properties became a factor.

Potgieter[53] investigated the influence of sigma phase on the general and localised corrosion resistance of 2205 duplex stainless steel. The test solutions were ten mass percent H_2SO_4 at 25°C and 3.5% NaCl. The effects on general corrosion are shown in Figure 2.46.

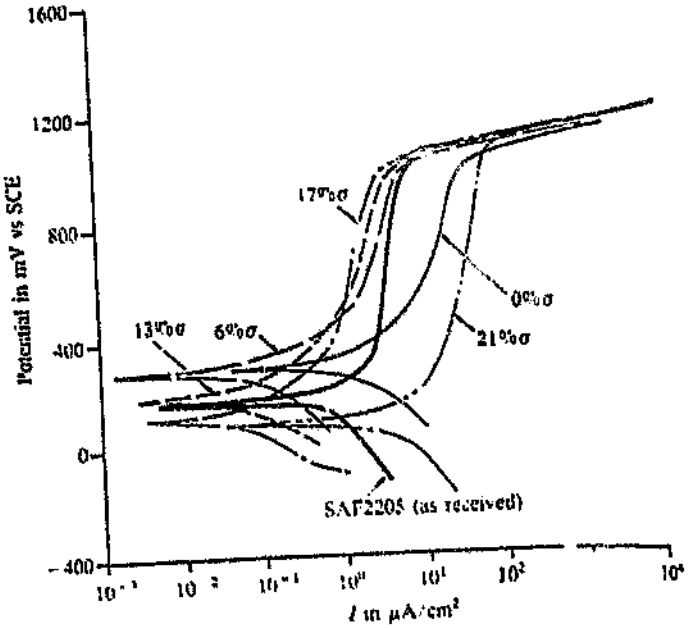

Figure 2.46: Potentiodynamic responses for SAF2205 duplex stainless steel with various sigma phase contents at 10% H_2SO_4 at 25°C.[53]

It was shown that even at a sigma content of 21 percent, the alloy did not undergo active dissolution, and E_{corr} remained positive in all cases. No active peak formation was observed. The corrosion rates for all alloys were very low and Potgieter deduced that even a sigma content of as high as 21 percent did not significantly affect the corrosion resistance of the steel in the test environment. No explanation was offered as to why the steels with 6-17% sigma had a lower corrosion rate than the sigma-free alloy.

The results of localised corrosion tests in NaCl showed a significant difference, as shown in Figure 2.47.

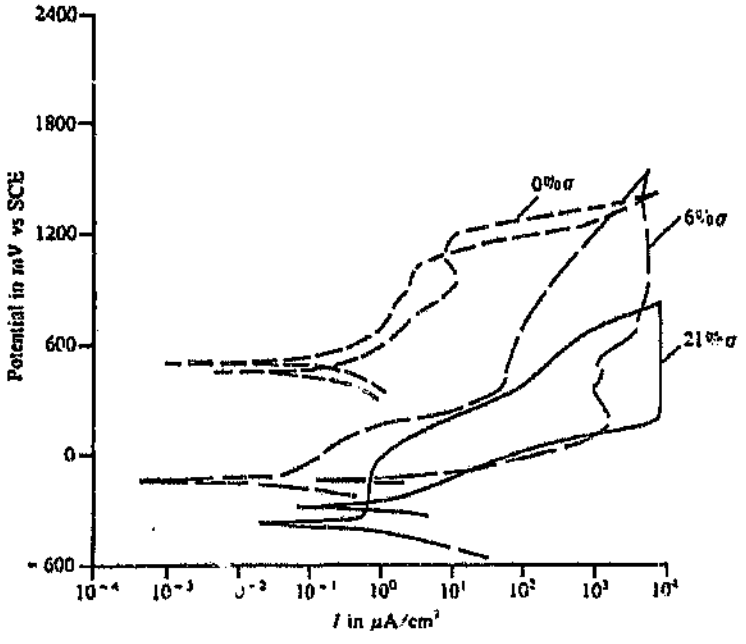

Figure 2.47: Anodic pitting polarisation curves of duplex alloy SAF2205 with various sigma phase contents exposed to 3.5% NaCl solution at 25°C.[53]

E_{cor} occurred at lower potentials and the pit initiation potential was lowered dramatically. Considerable impairment of localised corrosion resistance in 3.5% NaCl was therefore found in alloys with the sigma phase. It was concluded that sigma precipitation was far more deleterious on localised than general corrosion resistance. Potgieter observed that pitting occurred in both the ferrite and austenite phases, and not in the ferrite only. This is in agreement with Wallis[53] who found evidence that pit nucleation was due to an impairment of the passive layer at the intermetallic phase boundary. This was attributed to lattice irregularities and mismatch, and not to the depletion of certain elements in the matrix, as is commonly held[53].

2.13. The mathematics of diffusion

The behaviour of many solid state processes such as phase change and homogenisation is governed by the rate of mass transfer or diffusion within that state. Diffusion usually occurs down a concentration gradient and always down a potential gradient, in order to reduce the free energy of the system. An example is shown in Figure 2.48 which shows a metal slab with the ends A and B held at different concentrations C_0 and C_1, where $C_0 > C_1$. Matter will therefore flow from region A to region B down the concentration gradient. The problem of mathematically describing the diffusion process was first attempted by Fick in 1855.

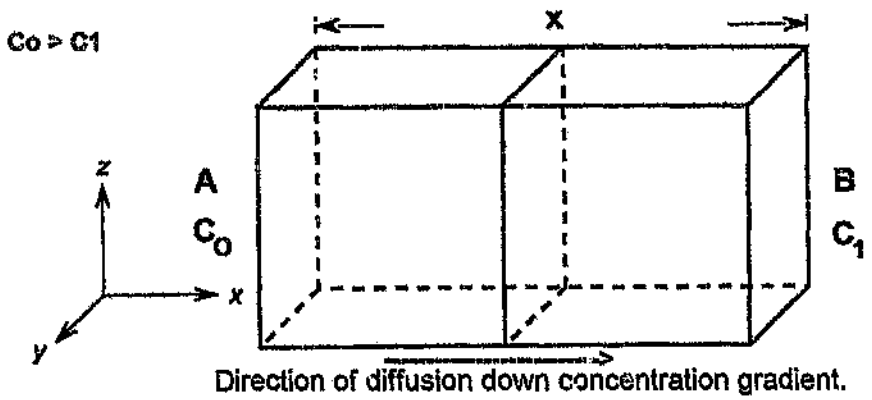

Figure 2.48: Basis for derivation of Fick's first law.[53]

Fick's first law is defined as:

$$J = -D\left(\frac{\partial C}{\partial x}\right) \qquad (6)$$

Where:
J is the flux of material parallel to the concentration gradient ($kg.m^{-2}.s^{-1}$).
D is the mathematical constant referred to as the diffusion coefficient ($m^{-2}.s^{-1}$).
C is the concentration along the x axis ($kg.m^{-3}$).
x is the position along the x axis (m).

Equation 6 therefore states that the flux across a given plane is proportional to the concentration gradient across that plane.

Fick also proposed his second law which provided a mathematical relationship between concentration, position and time.

Fick's second law is defined as:

$$\frac{\partial C}{\partial t} = \frac{\partial}{\partial x}(D\frac{\partial C}{\partial x}) \qquad (7)$$

Where:
t is time (s).
D is the proportionality constant referred to as the diffusion coefficient ($m^2.s^{-1}$).
C is the concentration along the x axis ($kg.m^{-3}$).
x is the position along the x axis (m).

The negative symbol in equation 6 indicates that diffusion occurs in the direction opposite to the concentration gradient. The mathematical reasoning and derivation of equations 6 and 7 is given in reference 56

It can therefore be seen that the description of many situations involving diffusion involves obtaining and solving the appropriate differential equations. The solutions to Fick's first and second laws are highly dependent on the selection of the initial mathematical boundary conditions. In many cases the solutions are not trivial, and require an in-depth knowledge of advanced calculus and algebraic techniques. The work of Crank[56] provides an excellent insight into the mathematics involved. Additionally, an analytical solution is not always possible and numerical methods often have to be employed. Certain illustrative applications of Fick's laws will be discussed.

A knowledge of the diffusion coefficient D is necessary to calculate the parameters of many diffusion systems. The value of D has to be determined empirically for each particular diffusion system. Fortunately fairly comprehensive tables for D are available in the literature[57]. The value of D is highly temperature dependent and the variation with temperature may be calculated according to Equation 8.

$$D = D_o e^{-Q/RT} \qquad (8)$$

Where:
D is the coefficient at temperature T ($m^2.s^{-1}$).
D_o is the frequency factor ($m^2.s^{-1}$).
e is the base of the natural logarithm.
Q is the activation energy for the diffusion process ($kJ.mole^{-1}$)
R is the universal gas constant ($8.314\ JK^{-1}.mole^{-1}$).
T is the temperature (K).

2.13.1. The Kirkendall Effect

It is known that metals of a uniform composition experience random self-diffusion[58] which is best measured by the tracer self diffusion coefficient D*. However, when a binary alloy is joined in a couple with a pure metal the diffusion coefficients in the alloy are not the same in each component of the couple. This effect was first observed by Kirkendall in 1947[58]. In Kirkendall's experiment a rectangular bar of brass(70% Cu - 30% Zn) was wound with molybdenum wire, to mark the original boundaries of the brass, and then plated with pure Cu. A diagram of the couple is shown in Figure 2.49.

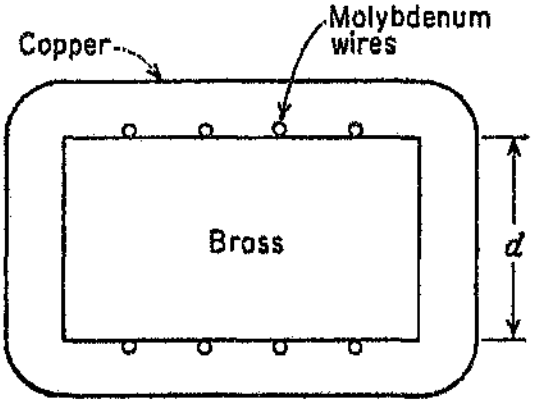

Figure 2.49: Diffusion couple used by Kirkendall.[58]

After successive anneals the distance d, defining the width of the brass, was measured. It was found that d decreased monotonically with time. The shift could only be explained if the flux of Zn atoms outward past the markers was greater than the inward flux of Cu atoms I.e. $D_{Zn} > D_{Cu}$. It therefore follows that for a diffusion couple involving metals of different composition a more general, overall value of D is required. It can be shown[30] that chemical diffusion coefficient $\overline{D}$ may be defined as follows:

$$\overline{D} = D_1N_2 + D_2N_1 \quad (9)$$

Where:

$\overline{D}$ is the chemical diffusion coefficient ($m^2.s^{-1}$).

D_1 and D_2 are the diffusion coefficients of metals 1 and 2 ($m^2.s^{-1}$).

N_1 and N_2 are the mass fractions of metals 1 and 2 in a binary alloy.

$\overline{D}$ provides an overall diffusion coefficient value for a particular diffusion couple. Equation 9 is often referred to as Darken's equation and is only valid for isothermal diffusion in an infinite couple or in dilute solutions.

2.13.2. The infinite diffusion couple

The infinite diffusion couple is one of the simplest applications of Fick's second law. An example of an infinite diffusion couple is shown in Figure 2.50, where the boundary between the bars is at $x=0$. The couple is infinite in that the bars are considered to be of infinite length and their ends do not change composition with time. The concentration profile may be calculated by solving:

$$\frac{\partial C}{\partial t} = \frac{\partial}{\partial x}(D\frac{\partial C}{\partial x})$$

for the following boundary conditions:

$C = 0$ at $x<0$ and $t=0$

$C=C_0$ at $x>0$ and $t=0$

It can be shown[55] that the solution is:

$$C(x,t) = 0.5C_0[1 + \text{erf}(\frac{x}{2\sqrt{Dt}})] \qquad (10)$$

Where:
erf is the error function.

Equation 10 is only valid for infinite systems and short diffusion times, but may be used as a first order approximation for certain diffusion systems which satisfy the boundary conditions. Equation 10 is shown graphically in Figure 2.50 which indicates the concentration profile across the couple.

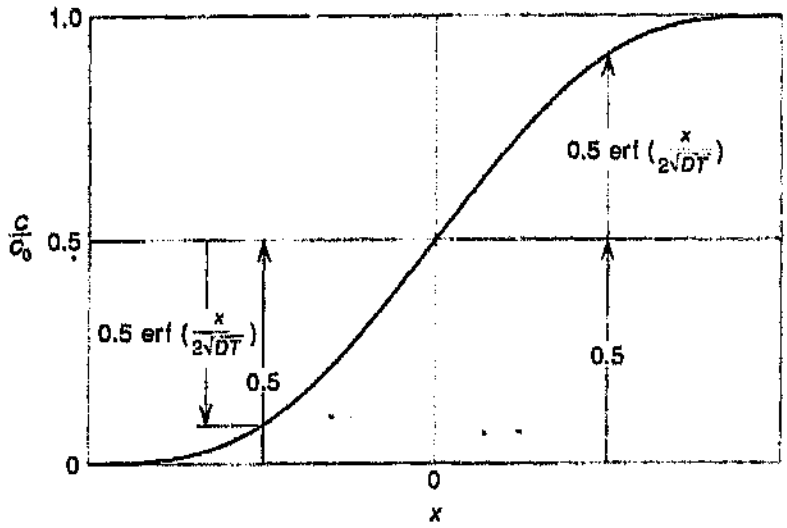

Figure 2.50: Normalised concentration profile produced by diffusion in an infinite diffusion couple.[55]

2.13.3. The mathematics of homogenisation

Although the process of homogenisation is extremely important in metallurgical systems there are few references to mathematical models in the literature. Rhines and Colton[59] performed some of the earliest work in the field in 1942. However, other workers such as Karlsson[60], Aaron[61] , Arunsingh[62], Purdy[63] and Heckel[64] have provided some results and approaches to the mathematical solution of the homogenisation problem A number of these approaches have involved the kinetics of secondary phase dissolution in bulk alloys[61,63,65]. Arunsingh[62], Heckel[64] and Larsson[66] have suggested models which may be utilised in powder metallurgy systems. The three powder metallurgy models are relevant to this study and will be described in further detail.

Certain assumptions are common to all three models. All diffusion is assumed to occur in a single phase i.e. no phase changes occur during homogenisation and a spherical powder particle model is assumed. The spherical model is employed since Fisher and Rudman[67] found that such an assumption provided a valid approximation to the behaviour of many real systems. Additionally, the spherical geometry allows for certain simplifications in the solution of Fick's second law equation. It must be mentioned that models also exist for cylindrical and planar particle shapes[64], although these models are not as commonly utilised.

2.13.4. Arunsingh's homogenisation model

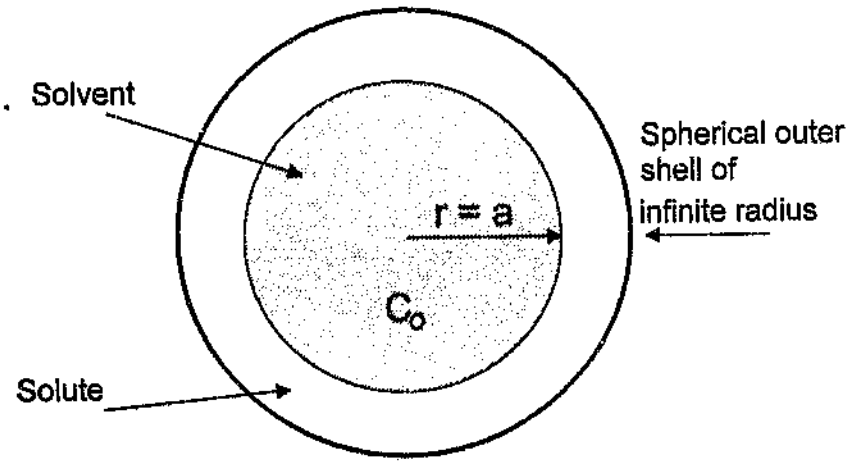

Figure 2.51: Arunsingh's model[62].
C_o = concentration (%) of A atoms within radius *a*. C_o= 100 % before interdiffusion begins.

Arunsingh's model[62] assumes solvent atoms of type A within a sphere of radius *a*. The solute atoms of phase B lie on the shell outside (Figure 2.51). D is assumed independent of composition. If the origin is taken as the centre of the solvent matrix and spherical coordinates are used, Fick's second law equation becomes:

$$\frac{\partial C}{\partial t}=D\left(\frac{\partial^2 C}{\partial r^2}+\frac{2}{r}\frac{\partial C}{\partial r}\right) \qquad (11)$$

putting U=Cr reduces the equation to:

$$\frac{\partial C}{\partial t}=D\left(\frac{\partial^2 U}{\partial r^2}\right) \qquad (12)$$

For the following boundary conditions:

U=0 at r = 0 for all t
U=0 at r = ∞ for all t (since C=0 at r=*a*)
U=C_or at t=0 for 0<r<*a*

the solution can be shown to be:

$$C=-\frac{2aC_o}{\pi r}\sum_1^{\infty}\frac{(-1)^n}{n}\sin\frac{n\pi r}{a}e^{\frac{-n^2\pi^2 Dt}{a^2}} \qquad (13)$$

where n is a natural number.

Since subsequent terms in this infinite series decrease rapidly, only the first term in the series need be retained. Therefore for large t, the solution becomes

$$C = -\frac{2aC_o}{\pi r}\sin\frac{\pi r}{a}e^{\frac{-\pi^2 Dt}{a^2}} \qquad (14)$$

which (for $r \rightarrow 0$) finally reduces to:

$$t = \frac{a^2}{D\pi^2}\log\frac{2C_o}{C} \qquad (15)$$

Where:
D is the diffusion coefficient of metal B in metal A.
C is the concentration of metal A at the centre of the sphere at homogenisation.

Equation (15) provides an expression for the time at which the centre of the spherical particle achieves homogeneity.

Arunsingh evaluated the model by comparing its results with those obtained by experiment. In a trial involving the homogenisation of compacts composed of 56 atomic percent Cu and 44 atomic percent Ni, the model predicted a homogenisation time of 5.3×10^5 seconds. This was less than the reported experimental time of 2×10^6 seconds. The agreement was considered to be acceptable in light of uncertainties in the actual particle size and solute distribution[62].

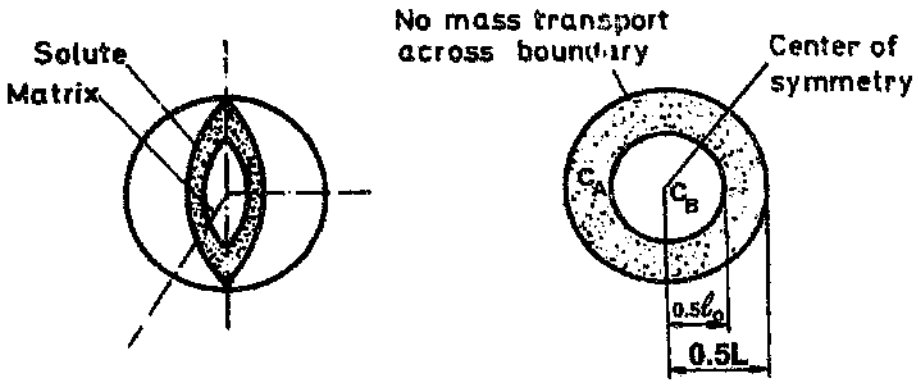

gure 2.52: Heckel's model.[64]

As shown in Figure 2.52 Heckel's model[64] assumes a sphere of concentration C_B and radius $0.5l_o$ surrounded by a shell of radius 0.5L and concentration C_A. Th model assumes $C_A=0$ and $C_B=1.0$, i.e. strictly speaking the model should only be applied to mixtures of elemental powders. However, it can be shown that the model may be utilised for mixtures where $0 < C_A < C_B < 1.0$. Heckel took a different approach to solving the homogenisation problem by defining the "degree of interdiffusion" parameter F. The parameter is the ratio of mass transferred across a spherical surface at radius $0.5l_o$, after a diffusior time t, to the mass transferred at $t = \infty$.

$$F=\frac{m_t}{m_\infty} \qquad (16)$$

In the case of complete homogenisation F=1.

Now, from first principles:

$$\frac{\partial C}{\partial t}=D\left(\frac{\partial^2 C}{\partial r^2}+\frac{2}{r}\frac{\partial C}{\partial r}\right) \qquad (17)$$

with the following boundary conditions:

$C = C_B$ for $0 \leq r \leq 0.5l$

$C = C_A$ for $0.5l \leq r \leq 0.5L$

$\frac{\partial C}{\partial r} = 0$ at r=0 and r=0.5L

$$F = \frac{m_t}{m_\infty} = \int_0^{0.5l} (C_B - C(r)).4\pi r^2 \Big/ \int_0^{0.5l} (C_B - \overline{C}).4\pi r^2.dr \qquad (18)$$

$\overline{C}$ = the mean composition of the compact = $(\frac{l}{L})^3$. The $\overline{C}$ expression is valid for C_A=0 and C_B=1.

C_{max} occurs at r=0 and C_{min} occurs at r=0.5L.

Using similar reasoning, Heckel obtained expressions for cylindrical and planar geometries. The expressions are shown graphically in Figure 2.53.

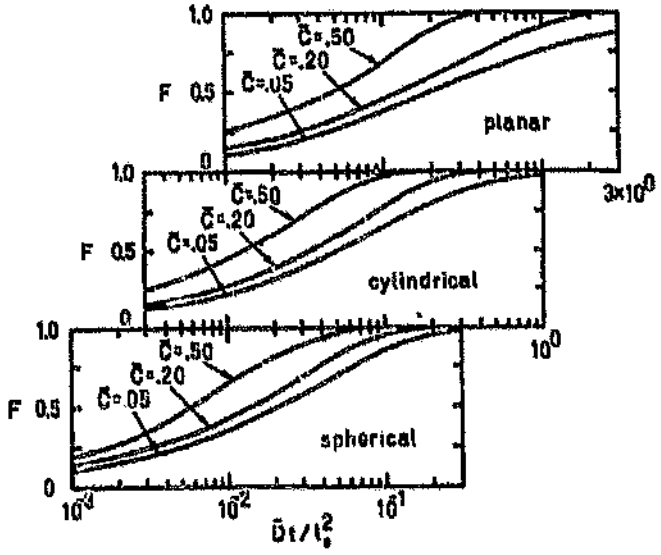

Figure 2.53: Homogenisation behaviour of planar, cylindrical and spherical models in terms of the degree of interdiffusion F, as a function of normalised homogenisation time, for various mean compositions $\overline{C}$ [64]

Due to the similarity of the curves, Heckel derived a general expression which approximated the behaviour of the spherical, cylindrical and planar geometries. This general expression was :

$$F = 1.10 + 0.44\log_{10}[(\frac{l_0}{l_c})n^2Y] \qquad (19)$$

where:
n is the geometry factor, n=1,2,3 for planar, cylindrical and spherical geometries respectively.
Y is a function of $\overline{C}$ as shown in Figure 2.54.

Equation 19 (plotted in Figure 2.54) provides a general description of the homogenisation problem and includes most of the significant variables involved.

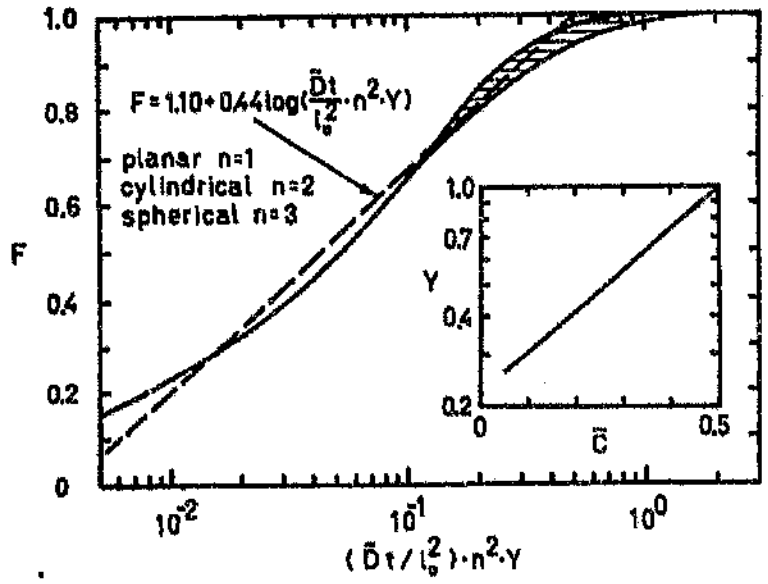

Figure 2.54: Normalised degree of interdiffusion F as a function of D, t, l_o, n and Y.[64]

Comparisons of the model with numerous experimental data were performed. The comparisons are shown in Figures 2.55-2.56.

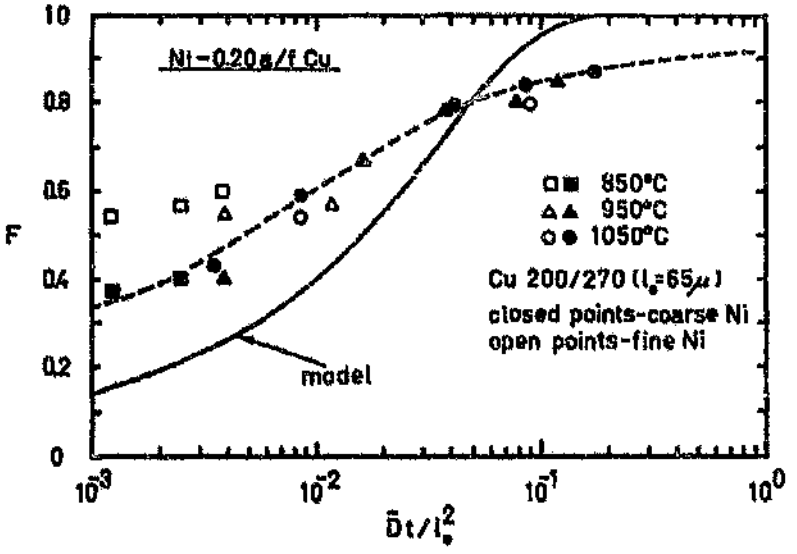

Figure 2.55: Comparison of experimental F data on Ni-0.20Cu compacts with model predictions.[64]

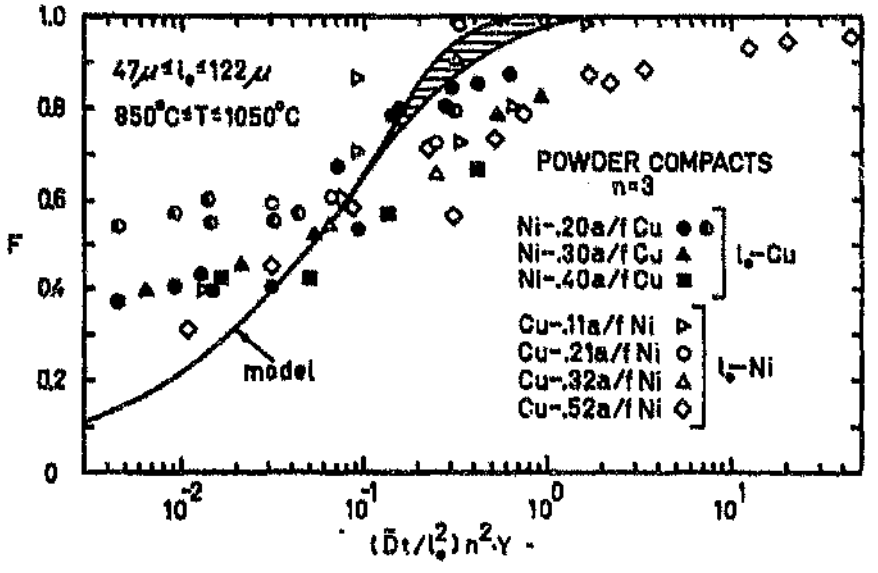

Figure 2.56: Comparison of data from two alloy systems (Ni-Cu) and (Cu-Ni) with model predictions.[64]

The comparisons of the concentric sphere models were found to be useful in the prediction of the relative effects of the major process variables. Absolute predictions of the degree of homogeneity were found to be too low when the degree of homogeneity was low and too high when the degree of homogeneity was high. These deviations were attributed to the fact that the model assumes that the minor elements are surrounded by a continuous matrix of major elements. In practice, non-ideal mixing and the presence of localised groupings of contiguous particles are unavoidable.

2.13.6. Larsson's homogenisation model

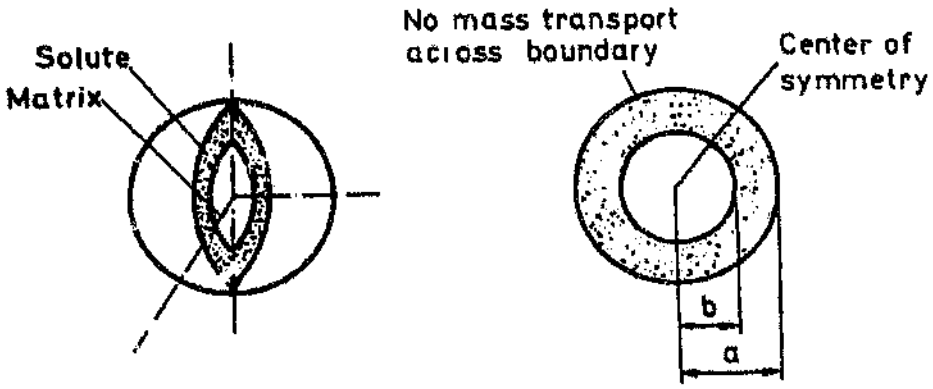

Figure 2.57: Larsson's model of homogenisation.[66]

In Larsson's model[66] of a sphere of radius b enclosed by a shell of radius a (Figure 2.57), the following definitions are required:

c is the concentration at any time t at any position x (arbitrary units).
C_s is the concentration of solute in the shell.
$\overline{C}$ is the average final concentration in the alloy (arbitrary units).

$C = \frac{c}{\overline{c}}$; $X = \frac{x}{a}$; $T = \frac{Dt}{a^2}$ (T is normalised time).

Fick's second law transforms to:

$$\frac{\partial C}{\partial T} = \left(\frac{\partial^2 C}{\partial X^2} + \frac{2}{X}\frac{\partial C}{\partial X}\right) \qquad (20)$$

The following boundary conditions were assumed:

$$\text{At } X=0 \text{ and } X=1, \ \frac{\partial C}{\partial X} = 0, \text{ for } T \geq 0.$$

With the following starting conditions:

$$\text{For } X \leq \frac{h}{a}: \ C=0 \text{ at } T=0;$$
$$\text{For } \frac{h}{a} < X \leq 1, \ C=C_s \text{ at } T=0.$$

Larsson employed a finite difference approximation to equation 20 and arrived at the following solutions for homogenisation at the centre and boundary of the sphere:

Centre: $$C_0^{j+1} = (1-6K)C_0^j + 6KC_1^j \quad j=0,1,2... \qquad (21)$$

Boundary: $$C_N^{j+1} = 2K\,C_{N-1}^j + (1-2K)C_N^j \quad j=0,1,2... \qquad (22)$$

General: $$C_n^{j+1} = K(1-\tfrac{1}{n})\,C_{n-1}^j + (1-2K)C_n^j + K(1+\tfrac{1}{n})C_n^j \qquad (23)$$
$$K=N^2\Delta T$$

where:
n=1,2...N-1 (index for space)
j=0,1,2,... (index for time)
N is the number of nodes or discrete subdivisions used to approximate the solution to the differential equation.
$\Delta T=0.25(\frac{1}{N^2})$ (time step)
Homogenisation was considered complete when $C_{centre}=0.99C_{boundary}$. Plots of equations 21 and 22 for various starting surface concentrations are shown in Figure 2.58.

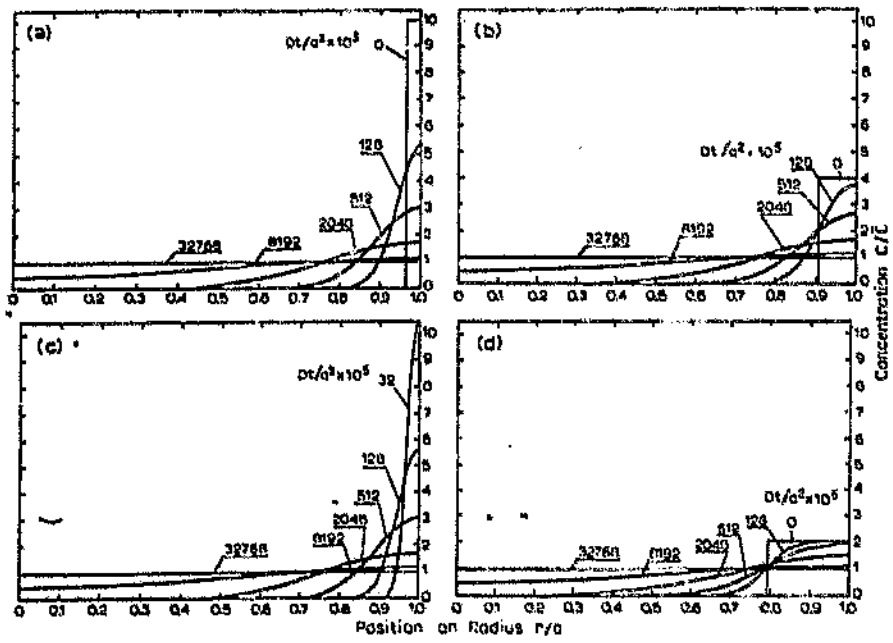

Figure 2.58: Concentration profiles along radius of sphere after various homogenisation times. Relative starting surface concentrations were: (a)10, (b)4, (c)∞, (d)2.[16]

From Figure 2.58 it can be seen that for various surface concentrations complete homogenisation is predicted to occur at:

$$\frac{Dt}{a^2} = 0.3. \qquad (24)$$

The model therefore implies that the same time is required to remove a "large" inhomogeneity as a "small" one. Larsson did not compare the model's predictions with any experimental data, but did provide a comparison with the planar homogenisation model proposed by Lavender and Jones[68] (Figure 2.59). Large deviations in predicted behaviour of the two models were observed. The deviations were attributed to the choice of different geometries.

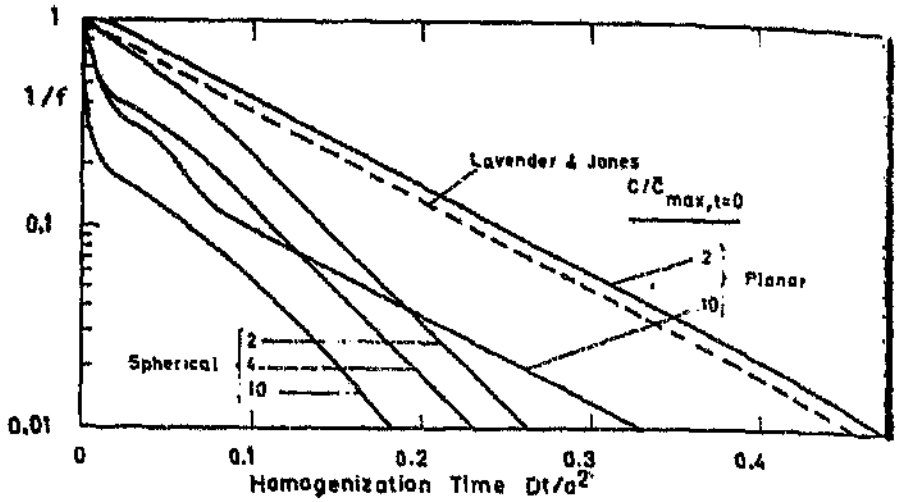

Figure 2.59: Comparison between predicted homogenisation behaviour based on the equation of Lavender and Jones and Larsson's study. Numbers on the curves show surface concentrations at $\frac{Dt}{a^2} = 0.$[66]

Larsson also extended the model to include surface concentration, which varied as a function of time. However, this aspect is beyond the scope of the current investigation, since it is primarily applicable to liquid-solid alloying.

2.14. Summary

The Fe-40Cr alloys possess a number of desirable properties which render them economically attractive. These alloys, with the correct additions, are highly resistant to corrosion and pitting in reducing environments. The alloys therefore have potential as cost-effective competitors to traditional nickel and cobalt-based superalloys in corrosion applications.

Suitable heat treatments and nominal compositions for a tough, corrosion resistant alloy have already been established for the cast alloy. The effect of various processing parameters on the mechanical properties and formation of secondary phases has also been studied in the cast form.

The literature survey has indicated that the production of an Fe-40Cr alloy by means of powder metallurgy processing and hot isostatic pressing appears feasible. The composition of the alloy may have to be modified by the addition of sigma stabilisers or retardants. This would be required in order to facilitate powder production as well as to minimise post-HIP heat treatments. However, the effect of these additions on corrosion resistance and mechanical properties would have to be assessed.

The effect of subjecting the alloy to extended periods at elevated temperatures would also have to be examined closely. This extended exposure would be an unavoidable aspect of the HIP process.

Certain mathematical models exist which attempt to describe the homogenisation process in metallic powders. The applicability of these models may be evaluated by comparing their predicted results with experimental data.

3. EXPERIMENTAL PROCEDURE

This dissertation is divided into two areas of investigation: the Fe-40Cr alloys produced from a single composition of powder and alloys manufactured from mixtures of powders of differing compositions.

3.1 Alloys produced from a single powder: Introduction

This section examines various Ni, Mo and Ru additions to a base 40Cr-Fe alloy. The effect on powder production, rate of sigma phase formation, response to HIPping, heat treatment and corrosion resistance is evaluated. The role of starting particle size, contamination during processing and the effects of HIPping on the as-cast material are discussed.

Alloys of the following compositions were prepared at Mintek. All melts were vacuum melted, with the exception of DS-1 and DS-C, which were air melted. Samples of approximately 5kg mass were produced. The compositions are shown in Table 3.1

Table 3.1: Composition of experimental melts (weight percent).

Element	Melt ID: VFA 390	391	392	393	395
C	0	0.01	0.01	0	0
Si	0.04	0.05	0.05	0.05	0.06
Mn	0.05	0.05	0.05	0.05	0.05
P	0	0.01	0.01	0.01	0.01
S	0	0	0	0.01	0.01
Cr	37.9	38	38.2	38.2	37.6
Ni	2.3	0.6	0.99	1.67	0.02
Mo	0.06	0.45	0.95	1.34	1.81
Cu	<0.005	<0.005	<0.005	<0.005	<0.005
Al	0.02	0.01	0.01	0.01	0.01
V	<0.005	<0.005	0.01	0.01	0.01
Ti	0.01	0.01	0.01	0.01	0.01
Nb	<0.005	<0.005	<0.005	<0.005	<0.005
Fe	58.9	60.2	59.1	58.1	60.2

Element	Melt ID: VFA 417	419	420	422	423	487	552 / Prem V
C	0	0.01	0.01	0.01	0.01	0.01	0.02
O	0.05	0.05	0.02	0.05	0.04	-	0
N	0	0	0	0	0	-	0.09
Cr	37	37.1	37.1	37	37.1	36.4	38.8
Ni	2.36	2.4	2.38	3.38	2.36	2.32	2.2
Mo	4.15	4.32	4.35	4.29	4.35	2.03	2.04
Al	0.21	0.21	0.35	0.34	0.22	0.01	<0.02
Si	0.58	0.58	0.6	0.55	0.6	0.09	0.09
Ru	0	0.2	0.1	0	0	0	0
Ir	0	0	0.1	0.1	0.21	0	0
Fe	bal	bal	bal	bal	bal	bal	bal

Table 3.1: Composition of experimental melts (continued).

Element	Melt ID: VFA				
	543	553	622	DS-C	DS-1
C	0.015	-	-	-	0.07
O	-	-	-	-	-
N	0.004	-	-	-	-
Cr	39.7	39	40	36	35.7
Ni	2.40	2.4	2	2	2.56
Mo	3.80	2.1	2	4	4.35
Al	0.010	3.2	-	0	0
Nb	0.4	0.4	0.4	-	-
Si	0.10	0.1	-	-	0.6
Ru	0.21	-	0.15	0.25	0
Fe	balance	balance	balance	balance	balance

3.2 Alloy description.

Prem V was an Fe-39Cr-2Ni-2Mo alloy derived from the work of Premachandra[21,26]. This composition was used as a basic starting point from which other alloys could be developed.

VFA 390-395 were Fe-38Cr alloys with variations in Ni and Mo content. The amounts of Ni and Mo were varied between 0.02 and 2.3 percent. No additions of stabilising elements or platinum group metals were made. These alloys were used to ascertain the minimum Ni and Mo levels which would be required in order to produce a readily sigmatised material suitable for powder production.

VFA 417, 419, 420, 423 were Fe-37Cr-2.4Ni-4.3Mo alloys with additions of Ru and Ir. These alloys were produced to examine the effect of different combinations of Ir and Ru on corrosion resistance. The Mo content was increased in order to improve pitting corrosion resistance, as well as promote the formation of sigma phase. Greater amounts of Al and Si were added than in the VFA 300 series. No stabilising elements were added.

VFA 422 was an Fe-37Cr-3Ni-4Mo alloy with 0.1% Ru, and was used to ascertain the effect of increasing both the Ni and Mo content simultaneously.

VFA 487 was an Fe-36Cr-2.3Ni-2Mo alloy and was used to establish whether a decrease in Cr content would lead to a significant reduction in sigma phase after HIPping.

VFA 543 had the nominal composition Fe-40Cr-2Ni-4Mo with an addition of 0.4 percent Nb.

VFA 553 had the nominal composition Fe-40Cr-2Ni-4Mo with an addition of 3.2 percent Al. The Al (which inhibits sigma formation) was utilised to determine if an inhibitor could be introduced as part of the alloy composition, whilst still allowing for powder manufacture.

DS-1 and DS-C were air melted Fe-36Cr-2Ni-4Mo alloys. DS-1 and DS C were produced in order to determine if air melting techniques could be used as a satisfactory alternative to vacuum melting. DS-C contained an addition of 0.2 percent Ru.

VFA622 was a 2Ni-2Mo-0.4Nb-0.2Ru-40Cr alloy. It was decided that increasing the Cr content to 40Cr would improve corrosion resistance without significantly increasing sigma phase formation. An addition of 0.4%Nb was included in order to improve intergranular corrosion resistance. It was assumed that the Nb would tie up interstitial C and N in the form of Nb carbides and nitrides and therefore prevent the formation of deleterious Cr carbides and nitrides.

3.3 Powder production

All samples were heated in air to 750°C or 850°C and held at this temperature. This was done in order to induce sigma phase embrittlement. The work of Premachandra[21,26] had shown that sigma phase formation was most favourable at 750°C. Consequently, this temperature was used as the basis of most of the heat treatments.

After heat treatment, all samples were impacted with a hammer. Samples which were not embrittled were then subjected to hot forging which is known to promote sigma formation and given further heat treatments at either 750°C or 850°C.

Samples which were clearly embrittled were then subjected to further comminution. Each slab was subjected to an initial comminution stage by manual crushing with a pestle and mortar. The broken-down material was exposed to further comminution in a jaw crusher. The powder was then milled for a period of thirty seconds in a vibratory Seib mill and sieved on an automated screening unit. All crushing equipment was visually inspected and dusted and cleaned before use. The vibratory mill was cleaned by crushing silica sand in the mill and removing the silica debris by means of a compressed air stream.

A chemical analysis of the alloy VFA622, before and after Seib milling, was made. These analyses were undertaken at Mintek and at the Ultra High analytical laboratory. Carbon contents were determined by wet chemical analysis.

No further heat treating or comminution was attempted on alloys which were still ductile after 121 hours of heat treatment since it was obvious that these alloys could not be viably produced by this route.

The thermomechanical processing of each alloy is summarised in Table 3.2.

Table 3.2: Thermomechanical processing prior to powder production

Melt	Processing procedure
Prem V / VFA 552	Held isothermally at 850°C for 14 hours. Heated to 1150°C and hot worked (50% reduction) at that temperature. Slow cooled to 850°C and held isothermally for 24 hours.
VFA 390-395	Held isothermally at 750°C for 196 hours. Heated to 1100°C for 3 hours and then hot worked (50% reduction). Slow cooled to 758°C and held isothermally for a further 96 hours.
VFA 417, 419, 420, 423, 487	Heated to 1100°C for 3 hours and then hot worked (50% reduction). Slow cooled to 758°C and held isothermally for a further 96 hours.
VFA 422	Held isothermally at 850°C for 14 hours. Heated to 1150°C and hot worked (50% reduction) at that temperature. Slow cooled to 850°C and held isothermally for 24 hours.
VFA 563	Held isothermally for 121 hours at 750°C
DS-1 , DS-C	Hot worked at 1150°C and held at 850°C for 21 hours Slow cooled to room temperature
VFA 543, VFA 622	Heated up to 1050°C and hot worked to a 50% reduction in thickness. Held isothermally at 750°C for 4.5 hours

3.4 Hot Isostatic Pressing

The powders were packed into mild steel canisters, evacuated, sealed and HIPped at 1120°C for a period of four hours. The canisters were cylinders, 20mm in diameter and 50mm in length. After the four hour dwell period, the specimens were slow cooled in the HIP unit. The HIP unit cooled from 900 to 600°C in approximately 80 minutes. The particle size fractions used to produce the HIPped test pieces are shown in Table 3.3 and Figure 3.1.

Table 3.3: Size fractions used for HIPping

Alloy	Size fraction (f) (microns)
Prem V	150>f>75
DS-1	<106
DS-C	<45
VFA543	Unsized (See Malvern analysis)
VFA 417	106>f>75
VFA 419	106>f>75
VFA 420	106>f>75
VFA 423	106>f>75
VFA 487	212>f>106
VFA622	150>f>106

Size µms.	% under	Size µms.	% under	Size µms.	% under	Size µms.	% under
0.50	0.0	2.20	0.4	9.66	6.5	42.4	34.4
0.55	0.0	2.41	0.5	10.6	7.6	46.5	37.7
0.60	0.0	2.64	0.6	11.6	8.3	51.1	41.3
0.66	0.0	2.90	0.8	12.7	9.3	56.0	45.1
0.72	0.0	3.18	0.9	14.0	10.5	61.4	49.0
0.79	0.0	3.49	1.1	15.3	11.8	67.4	53.1
0.87	0.0	3.83	1.4	16.8	13.1	73.9	57.4
0.95	0.0	4.20	1.6	18.5	14.6	81.1	61.9
1.05	0.0	4.61	1.9	20.3	16.1	89.0	66.4
1.15	0.1	5.06	2.3	22.3	17.8	97.6	70.8
1.26	0.1	5.55	2.7	24.4	19.6	107	75.2
1.38	0.1	6.08	3.2	26.7	21.5	117	79.2
1.52	0.1	6.67	3.8	29.4	23.6	129	84.3
1.66	0.2	7.32	4.4	32.2	25.8	141	88.6
1.83	0.3	8.02	5.0	35.4	28.3	155	92.9
2.00	0.3	8.80	5.7	38.7	31.4	170	100

Result source=Sample
Record No. = 0
Focal length = 100 mm.
Presentation =1407
Volume distribution
Beam length = 2.2 mm.
Obscuration =0.2068
Volume Conc. = 0.0960 %
Residual = 3.205%
Model indp

D(v,0.5) = 62.86 µm
D(v,0.9) = 145.60 µm
D(v,0.1) = 13.40 µm
D(4,3) = 70.63 µm
D(3,2) = 35.29 µm
Span = 2.1
Spec. surf. area
0.2068 sq.m./cc.

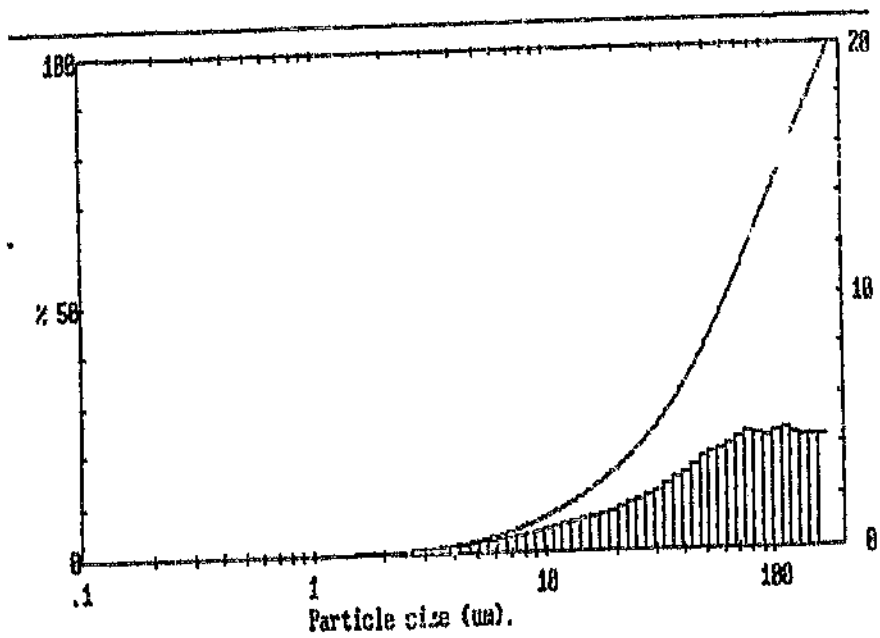

Figure 3.1: Particle size distribution of VFA543 (as received)
The upper curved line is the cumulative distribution of the particle sizes.

3.5 Heat treatment and metallographic examination

After HIPping, all specimens were subjected to a solution anneal at 1100°C for a period of two hours. The specimens were then quenched in water at room temperature.

Specimens were mounted, polished and examined metallographically both after HIPping and after solution annealing. Three different etchants were used during microstructural examination: Murakami's reagent (for carbides) and potentiostatic etching (8V) in 5 weight percent KOH and an $FeCl_3$+HCl mix for the general microstructure. Ferrite is revealed as dark brown areas by the $FeCl_3$+HCl etchant, whilst sigma phase is not attacked. The composition of the $FeCl_3$+HCl mix was: 5g $FeCl_3.6H_2O$ + 50ml HCl(55%) + 100ml H_2O.

3.6 Heat treatment comparison between cast and HIPped VFA622

A trial was undertaken to determine if there was any difference between the cast and HIPped materials when subjected to the same heat treatment. A small 15x10x2mm specimen of the cast VFA622 material was solution annealed, then HIPped, to determine the effect of the HIP thermal cycle on a sample which was initially free of sigma. To determine the effect of repeated exposures to the HIP thermal cycle, a fully-dense specimen of HIPped VFA622 was deliberately HIPped for a second time. The microstructures and hardness values of the cast and HIPped materials were analysed by optical microscopy and a Vickers hardness tester.

3.7.Examination of hardness versus time at 750°C

For the majority of the trials in this study the embrittlement of the high chromium alloys during heat treatment was characterised on a qualitative basis. Test slabs were hot rolled at 1050°C to a 50 percent reduction in thickness. These slabs were then held isothermally at 750°C . At various time intervals the slabs were removed from the furnace and struck with a mallet. If the slab fractured easily, the material was deemed sufficiently brittle to allow powder production by vibratory milling.

In order to provide more quantitative data on the degree of embrittlement with respect to time at 750°C, two melts were made up with compositions shown in Table 3.4.

Table 3.4: Composition of experimental melts VFA647 and VFA654 (wt%).

	VFA647	VFA654
C	0.012	0.010
Si	0.07	0.09
Mn	0.05	0.05
P	0.007	0.010
S	0.003	0.003
Cr	36.0	36.6
Ni	2.45	2.19
Mo	1.86	1.86
Cu	0.002	0.005
Al	0.022	0.016
V	0.01	0.013
Ti	0.005	0.006
Nb	<0.005	0.34
Fe	60.4	58.2
N	0.002	0.003

Both alloys were nominally 36Cr-2Ni-2Mo-Fe alloys, and were produced in order to examine the effect of lowered chromium content on the rate of embrittlement.

The use of hardness values is considered an appropriate technique to estimate the degree of embrittlement of these high Cr alloys. As the percentage of brittle sigma phase within the microstructure increases, the hardness increases.

A small test piece approximately 1x1x2cm in size was cut from each hot rolled parent slab. These test pieces were then held isothermally at 750°C. At various intervals each specimen was removed from the furnace and quenched in water. The Rockwell C (HRc) hardness of the material was measured and then the specimen was then returned to the furnace for further heat treatment. VFA647 was heat treated for 89 hours, whilst VFA 654 was heat treated for 12 hours.

3.8 Extra communition of VFA543(24h)-(SP001012)

The effect of starting particle size was examined by subjecting the VFA543 powder to communition in a ball mill. The mill charge was 200g VFA543, 1800g steel milling media and 500ml acetone. The mill period was 24 hours. The cylindrical mill body has an outer diameter of 165mm and a length of 145mm. The speed of rotation was 45 r.p.m. The mill body is fabricated from a steel of unknown composition. The milling media were steel balls with a diameter of 11mm. The spherical milling media were analysed chemically and metallographically to ascertain a possible influence on the composition of the powder during the milling process. Drying was performed in air, for a period of 15 hours. No screening of the powder was carried out.

Samples were HIPped, solution annealed at 1100°C for 2 hours and quenched in water held at room temperature. The specimens were subjected to metallographic analysis.

3.9 Experimental procedure for potentiodynamic corrosion tests

Tests were conducted at the Mintek corrosion laboratory (Physical Metallurgy division) on an AutoTafel potentiostat. Scans were performed on small disks approximately 15mm in diameter and 3mm thick. All surfaces were polished to a 1200 grit finish, and were cleaned with acetone prior to testing. Two test environments were selected: 10 weight percent sulphuric acid solution at room temperature and 70 weight percent sulphuric acid at 50°C. Distilled water was used to make up the solutions. The solutions were not de-aerated and were exposed to the atmosphere. When placed in the test medium the mounted specimens were allowed to stabilise to the equilibrium corrosion potential E_{corr}. Scans were conducted from 100mV below E_{corr} to 700mV above E_{corr} at a scan rate of 12mV per minute. A fresh solution was supplied for each test. All results are referenced with respect to the standard calomel electrode.

Some investigators prefer the use of de-aerated sulphuric solutions. However, this is very much an artificial condition. De-aerated solutions are not commonly encountered in many industrial environments. These trials are aimed at determining relative corrosion behaviour between different alloys, and the determination of absolute corrosion rates is not critical at this stage. Hence the use of the sulphuric acid solution exposed to air and conducted at various temperatures is felt to be sufficient for this purpose.

3.10 Experimental procedure for field trials

Laboratory tests provide valuable information on the corrosion characteristics of an alloy. However, the best indicator of the behaviour of a particular alloy under service conditions is to run an actual field trial. Field trials expose the material to environments which cannot be simulated in the laboratory. It was suggested that a test component should be manufactured out of a Fe-40Cr alloy and subjected to field trials.

A suitable application was found in an industrial leaching process. Components known as "spring locks" were manufactured. Each spring lock is approximately 20mm in diameter and 20mm in length as shown in Figure 3.2. Although exact details regarding the leaching process are not available, due to the proprietary information involved, some factors can be mentioned. It is known that the spring lock is subjected to alternating streams of concentrated nitric and sulphuric acid at boiling point. These streams move at a high velocity relative to the surface of the springlock and are further agitated through the addition of air bubbled through the solution. This environment is very aggressive and 904L superaustenitic stainless steel is the material currently utilised for these components.

Two test springlocks were manufactured out of alloy VFA622 (HIPped twice) and solution annealed at 1100°C. Machining was performed at Ultra High Pressure Units Engineering. No problems were reported during the machining process. One spring lock was immersed directly into the corrosive solution whilst the other was placed in close proximity to the solution where it was exposed to only the corrosive fumes. Reference springlocks of the same dimensions and geometry were manufactured from 904L stainless steel and were placed alongside the experimental springlocks. This ensures exposure to identical environmental conditions. Periodic mass loss measurements and visual inspections were conducted on the different materials.



Figure 3.2: Experimental springlock used in industrial field trial.

3.11. Duplex powders

This section examines the effects of mixing highly alloyed Cr-Fe powders with powders of dissimilar composition e.g. pure iron, 316L and Hastelloy C powder. These duplex powders mixtures were HIPped and the degree of the interaction between the different powder particles was observed. The influence of the various powders on sigma formation, microstructure and corrosion resistance was evaluated. Different methods of mixing the powders were utilised, and SEM analysis of the diffusion zone between dissimilar particles was performed.

There are two distinct goals in experimentation with duplex powders. Firstly, the possibility of inhibiting sigma phase formation with the addition of retarding agents such as Al and Fe. The second goal is to manufacture a synthetic duplex stainless steel alloy by mixing the austenitic and ferritic phases together. This should combine the advantages of the separate ferritic and austenitic starting materials and allow the various phases to be present in pre-defined proportions. Some advantages associated with duplex stainless steels are excellent resistance to stress corrosion cracking, resistance to localised corrosion and pitting, good mechanical properties and a lower nickel content than the austenitic stainless steels.

3.12. Inhibition of sigma phase formation by mechanical mixing

3.12.1 Mechanical mixing with 2%Al (SP001005)

A 200 gram batch of Fe-4Mo-2Ni-2Al (SP001005) alloyed powder was mechanically mixed in a ball mill at Ultra High Pressure Units. Mill dimensions have already been described in Section 3.8. The mill body and mill media were cleaned in acetone, prior to use. The Prem V alloy with extra Fe additions (SP001008) was milled with the same parameters. A Malvern particle size analysis of the milled and starting Fe powder used in SP001008 was performed. The mill charge make-up for SP001005 and SP001008 is shown in Table 3.5.

Table 3.5: Mill charge for mechanically mixed 4Mo-2Ni-2Al (SP001005) and Prem V with extra Fe (SP001008).

SP001005 Constituent	Mass(g)
VFA543	245
Al	5
Steel milling media	1800

	Cr	Ni	Mo	Al	Nb	Fe	Ru
SP001005 desired final composition (weight %)	39	1.96	3.92	2	0.39	52.5	0

SP001008 Constituent	Mass(g)
Prem V	150
Fe	50
Steel milling media	1800

	Cr	Ni	Mo	Al	Nb	Fe	Ru
SP001008 desired final composition (weight %)	30	1.5	3	0	0.3	65.05	0.15

Mill period = 24 hours
Acetone added = 500ml

The powder was dried for 16 hours in air and packed in a sealed plastic container. No screening of the powder was carried out.

The powder was encapsulated in a 20mm diameter mild steel tube and HIPped. A circular cross-sectional sample, approximately 3mm thick, was cut from the HIPped tube. The sample was solution annealed at 1100°C, in air, for a period of two hours at Mintek. This was followed by quenching in water (room temperature).

Microstructural examination and potentiodynamic corrosion testing (in 10 and 70 volume percent sulphuric acid) of both the as-HIPped and solution annealed material was performed.

The HCl etchant was used during metallographic examination.

3.13. The addition of extra Fe to VFA543 and VFA622 by hand mixing

Additions of Fe powder were made to VFA543 and VFA622 powder. The mix ratios are shown in Tables 3.6-3.7. No communition or milling took place. The powders were mixed by shaking and stirring by hand for a period of 4 minutes. The mixed powders were then HIPped and solution annealed (1100°C, 2 hours, water quench-room temperature). Microstructures and the hardnesses of the alloys were evaluated.

Table 3.6: Mix ratios for VFA543+Fe and VFA622+Fe

Constituent of VFA543 + extra Fe	Mass(g)								
VFA543 (unscreened)	150			Ni	Mo	Cr	Nb	Ru	Fe
Fe	50		Desired final composition of VFA543 + extra Fe (weight %)	1.5	3	30	0.3	0.15	65
Constituent	Mass(g)								
VFA622 (106< f< 150μm)	150			Ni	Mo	Cr	Nb	Ru	Fe
Fe	50		Desired final composition of VFA543 + extra Fe (weight %)	1.5	1.5	30	0.3	0.11	66.6

Table 3.7: Summary of compositions

	Alloy identification				
	SP001005 *	SP001008 *	SP001012 *	VFA543+ Fe **	VFA622 + Fe **
Element					
C	-	0.18	>0.015	-	-
O	-	0.281	-	-	-
Cr	39	30	39.7	30	30
Ni	1.96	1.5	2.40	1.5	1.5
Mo	3.92	3	3.80	3	1.5
Al	2	-	0.01	-	-
Ru	-	0.15	0.21	0.15	0.11
Nb	0.39	0.3	0.4	0.3	0.3
Fe	balance	balance	balance	balance	balance

* = Ball milled
**=hand mixed

3.14 The manufacture of a synthetic duplex alloy

3.14.1 Experimental procedure - duplex powders

Small (100g) batches of duplex powders consisting of VFA622, 316L , Prem V and Hastelloy C were produced by hand mixing. This trial was performed to determine the suitability of the Fe-40Cr alloys as a possible combination material with the Hastelloy powders. The combination with the 316L material was used to examine if 316L could be used with the Fe-40Cr alloy to produce a synthetic duplex stainless steel with predetermined proportions of the austenite and ferrite phases. Required quantities of the powders were placed into a small cylindrical container (OD=40mm, length=58mm) and agitated by hand for approximately 120 seconds. This was followed by encapsulation and HIPping under standard conditions. Short cylindrical test pieces, approximately 15mm in diameter and 3mm thick were parted from the HIPped compact. These pieces were subjected to solution annealing at 1100°C for 2 hours, followed by a room temperature water quench. Microstructural examinations were carried out in the as-HIPped and solution annealed state. Corrosion tests in 10 weight percent sulphuric acid at room temperature were performed on the heat treated specimens.

Data on the 316L and Hastelloy C powder are shown in Tables 3.8-3.10.

Table 3.8: Composition of 316L atomised powder (as-supplied).
Values are weight percentages

C	Si	Mn	P	S	Cr	Ni	Mo	Fe	Particle size
0.028	0.59	1.44	0.019	0.004	17.2	12.2	2.72	Balance	<500μm

Table 3.9. Sieve analysis of as supplied powder.

	500μm	250μm	125μm	100μm	63μm	45μm	Tap density (g.cm^{-3})
%<	96.6	81.1	48.1	39.3	20.9	11.8	5.21

Table 3.10:Composition of Hastelloy C (weight %) (as-supplied).
Particle size < 53μm

Cr	Mo	W	Fe	Si	Mn	C	Co	Ni
15.55	17.30	3.90	5.12	0.07	0.24	0.01	0.04	Bal

The following duplex alloys were manufactured: (Values are in weight percent) 20% VFA622 + 80% 316L ; 50% VFA622 + 50% 316L; 80% VFA622 + 20% 316L; 50% Prem V + 50% Hastelloy C.

3.15. Hardness and micro-hardness tests

Vickers hardness tests were carried out on all specimens, using Ultra High Pressure Units' equipment. The average of three readings was taken. All specimens were in the final polished condition. A load of 30kg was used. Micro-hardness tests were performed on DS-1, DS-C, VFA543 and 80% 316 + 20% VFA622. A dwell time of 10 seconds was used. The results are an average of three measurements. The smaller 25 grams force load was utilised on alloys DS-1 and DS-C in order to produce an indentation which was of a similar size to the sigma phase precipitates. The micro-hardness tests were conducted at the University of the Witwatersrand on a LECO M-400A micro-hardness tester.

3.16. Experimental procedure: SEM examination

3.16.1. Elemental scans

SEM elemental scans are an extremely useful analytical technique. The electron beam is automatically guided across a pre-determined linear path on the specimen. As the beam traces the path, the intensities of the X-rays originating from the various elements are recorded. Relative troughs and peaks in surface topography are also simultaneously measured. The presence of certain elements at specific points along the path can therefore be determined. However, the technique has limitations. The scan does not produce absolute values regarding the elemental content at each point in the scan. Instead, the content of each specific element relative to the content of that same element at other points of the scan is recorded. Multiple scans on the same path are performed. The greater the number of scans, the greater the accuracy. The method is most useful when typical minimum and maximum values are already known. This allows for an approximate scale to be introduced to the resulting graphs and a rough upper and lower limit can be established.

Surface topography is largely dependent on surface preparation prior to analysis. A finely polished specimen would have a more uniform topography compared to one which is only roughly ground. Identification of hard phases and precipitates, which typically would project above a softer matrix, can really only be performed in this method when analysis of surface topography is coupled with visual examination of the region being scanned. This prevents precipitates from being confused with other raised regions on the surface.

Polished and etched specimens of 50% Hastelloy C + 50% Prem V, 80% 316L + 20% VFA622, 20% 316L + 80% VFA622, SP001008, and VFA622 + Fe were analysed on the SEM (model JEOL JSM-840). Energy dispersive spectroscopy (EDS) spot analyses were conducted on the diffusion zone of 50% Hastelloy C + 50% Prem V with a LINK AN10000 system. Unfortunately elements below Be, such as O and C, could not be detected. Similar analyses were also performed on the phases in 50% 316L+50% VFA622. The local Fe, Cr, Mo and Ni content of each material was analysed over lengths of 125-1000 microns. An analysis of surface roughness or topography was also undertaken. Since the average particle sizes are all less than 1000 microns and in most cases less than 125 microns, an elemental gradient analysis which is representative of the bulk material should be obtained. The electron beam has a penetration depth of approximately 1 micron.

3.17. Experimental procedure for potentiodynamic corrosion tests on duplex materials

Corrosion tests on the alloys formed from duplex powders wer conducted using the same conditions as described in section 3.9. All results are measured with respect to the standard calomel electrode. Different specimens of the 80% 316L + 20% VFA622 alloy were used in the 10% and 70% s ' ic acid solutions.

4. RESULTS

4.1 Powder manufacture:

4.1.1. Single powders

Alloys VFA 390-395 and VFA553 failed to embrittle sufficiently after over 100 hours of heat treatment. No powder was made from these alloys. VFA 422 did not embrittle after 24 hours of heat treatment. No powder was produced. All the other alloys were sufficiently embrittled to form powder. A micrograph of FeCr powder after Seib milling is shown in Figure 4.1.



Figure 4.1:Micrograph of FeCr powder particles.
FeCr powders after Seib milling.

4.1.2. Carbon and oxygen analysis of VFA622 (Fe-40Cr-2Ni-2Mo-0.4Nb)

The carbon content of the as-cast VFA622 material was analysed at Mintek and found to be 0.015 weight percent C. After Seib milling the values were 0.024 weight percent C and 0.090 weight percent O_2. The analysis after Seib milling was conducted at Ultra High Pressure Units.

4.1.3 Duplex powders

4.1.3.1 Mechanical mixing with Al (SP001005)

The unscreened VFA543 starting powder has an uneven particle size distribution. The powder is fairly coarse, with a large proportion of particles over one hundred microns in size. Only a small percentage is under fifty microns. Micrographs of the ball milled powder are shown in Figures 4.4-4.5.

Ball milling produced a normal particle size distribution (Figure 4.3), with an average particle size of four microns. Ninety percent of the powder is below eight microns, whilst ten percent is below two microns. This powder could not be HIPped since it combusted energetically during the welding stage of the encapsulation process.

Size µm.	% under	Size µm.	% under	Size µm.	% under	Size µm.	% under
0.50	0.0	2.80	0.4	9.66	6.5	42.4	34.4
0.55	0.0	3.08	0.5	10.6	7.3	46.5	37.7
0.60	0.0	3.39	0.6	11.6	8.3	51.1	41.3
0.66	0.0	3.73	0.8	12.8	9.4	56.0	45.1
0.72	0.0	4.10	0.9	14.0	10.5	61.4	49.0
0.79	0.0	4.51	1.1	15.4	11.8	67.4	53.1
0.87	0.0	4.96	1.3	16.9	13.1	73.9	57.4
0.96	0.0	5.46	1.5	18.6	14.6	81.1	61.9
1.05	0.0	6.00	1.8	20.4	16.1	89.0	66.4
1.16	0.0	6.60	2.1	22.4	17.8	97.6	70.9
1.27	0.0	7.26	2.4	24.7	19.6	107	75.5
1.39	0.0	7.98	2.8	27.1	21.6	117	79.9
1.53	0.0	8.78	3.2	29.8	23.7	129	84.3
1.68	0.0	9.65	3.7	32.7	26.0	141	88.6
1.85	0.0	10.6	4.2	35.9	28.5	155	92.9
2.03	0.3	11.7	4.8	39.5	31.4	170	100
2.00	0.3	0.80	5.7	30.7	31.4		

Result source=Sample
Record No. = 0
Focal length = 100 mm.
Presentation =1HRI
Volume distribution
Beam length = 2.4 mm.
Obscuration =0.2068
Volume Conc. = 0.0960 %
Residual = 3.205%
Model indp

Div(0.1) = 69.46 µm
Div(0.5) = 145.60 µm
Div(0.9) = 13.40 µm
D(4,3) = 70.63 µm
D(3,2) = 35.29 µm
Span = 2.1
Spec. surf. area
0.2068 sq. m./cc.

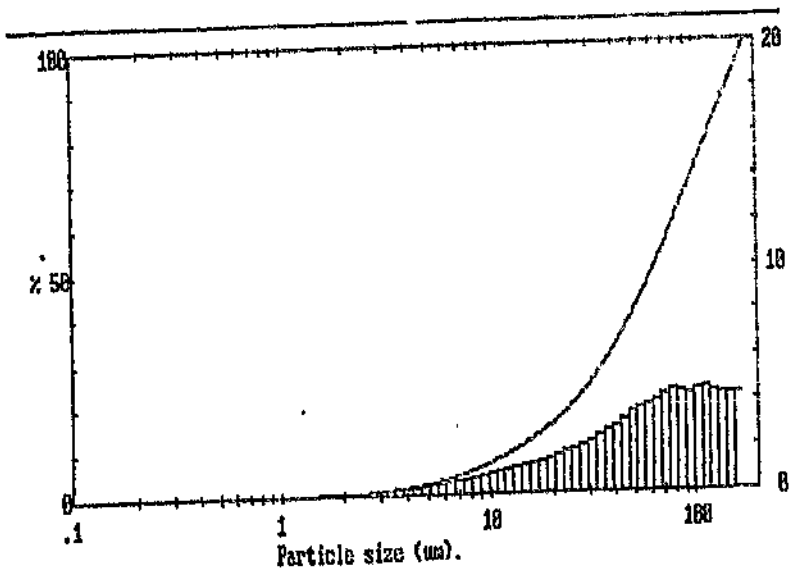

Figure 4.2: Malvern analysis of VFA543.

Size µms.	% under	Size µms.	% under	Size µms.	% under	Size µms.	% under
0.50	0.0	2.20	14.7	9.66	93.9	42.4	100
0.55	0.0	2.41	19.2	10.6	95.5	46.5	100
0.60	0.0	2.64	24.3	11.6	96.8	51.1	100
0.66	0.0	2.90	29.8	12.7	97.7	56.0	100
0.72	0.0	3.18	35.7	14.0	98.4	61.4	100
0.79	0.1	3.49	41.9	15.3	98.9	67.4	100
0.87	0.2	3.83	48.3	16.8	99.2	73.9	100
0.96	0.4	4.20	54.8	18.5	99.5	81.1	100
1.05	0.7	4.61	61.2	20.2	99.7	89.0	100
1.15	1.1	5.05	67.3	22.2	99.8	97.6	100
1.26	1.7	5.54	72.9	24.4	99.9	107	100
1.38	2.6	6.08	77.9	26.7	99.9	117	100
1.52	3.9	6.67	82.4	29.3	99.9	129	100
1.66	5.6	7.32	86.1	32.1	100	141	100
1.83	8.0	8.02	89.3	35.3	100	155	100
2.00	11.0	8.80	91.9	38.7	100	170	100

Result source=Sample
Record No. = 6
Focal length = 100 mm.
Presentation =1407
Volume distribution
Beam length = 2.2 mm.
Obscuration =0.2248
Volume Conc. = 0.0115 %
Residual = 1.227%
Model indp

D(v,0.5) = 3.92 µm
D(v,0.9) = 8.22 µm
D(v,0.1) = 1.95 µm
D(4,3) = 4.49 µm
D(3,2) = 3.50 µm
Span = 1.6
Spec. surf. area
1.7592 sq.m./cc.

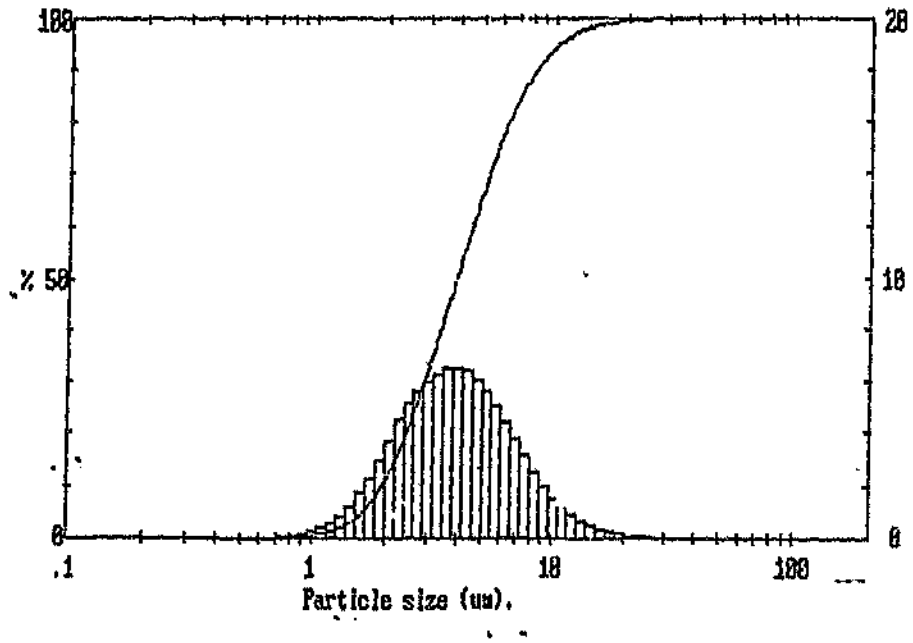

Figure 4.3: Malvern analysis of SP001005.

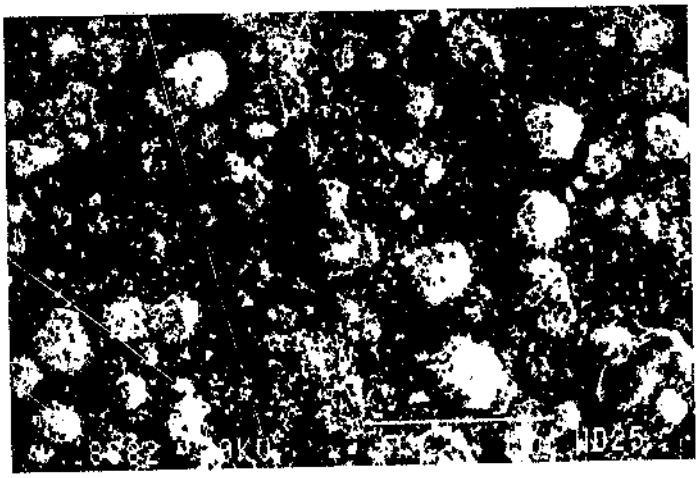

Figure 4.4: FeCr-Al agglomerates after ball milling (SEM image in secondary electron mode).

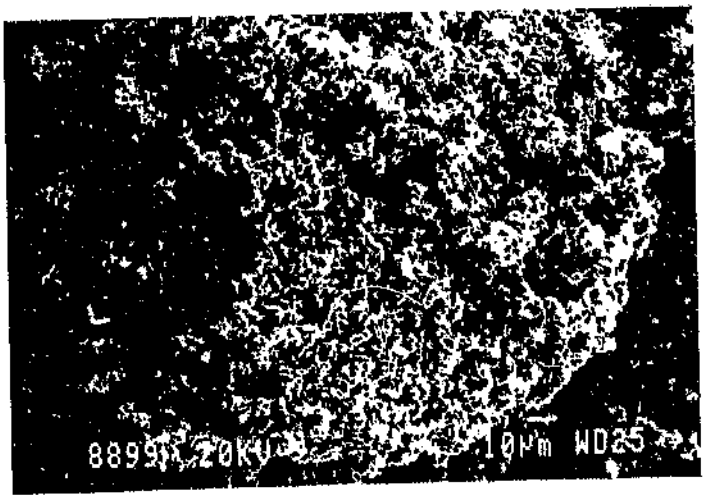

Figure 4.5: Detail of FeCr-Al agglomerate (SEM image in secondary electron mode).

4.1.3.2 Mechanical blending with added Fe (SP001008)

The Fe powder has a broad range of particle sizes, with an average size of approximately 11 microns (Figure 4.6). The Malvern particle size distribution of SP001008 is shown in Figure 4.7. A normal distribution is evident, with a slight peak in the 1 to 3 micron size segment. The average particle size is approximately 6 microns with 90 percent of the material below approximately 14 microns, and 10 percent below three microns.

Size pas.	% under	Size pas.	% under	Size pas.	% under	Size pas.	% under
0.50	0.0	2.20	2.7	9.65	46.4	42.4	87.9
0.55	0.0	2.41	4.0	10.6	48.7	46.5	90.1
0.60	0.0	2.64	5.6	11.6	52.8	51.1	92.0
0.66	0.0	2.90	7.3	12.7	55.9	56.0	93.8
0.72	0.0	3.16	9.0	14.0	58.8	61.4	95.3
0.79	0.0	3.49	11.0	15.3	61.6	67.4	96.5
0.87	0.0	3.83	13.3	16.8	64.2	73.9	97.4
0.95	0.0	4.20	15.9	18.5	66.8	81.1	98.2
1.05	0.1	4.62	18.3	20.3	69.3	89.0	98.9
1.15	0.1	5.08	20.3	22.3	71.7	97.6	99.1
1.26	0.1	5.58	22.6	24.4	74.0	107	99.4
1.38	0.2	6.08	24.1	26.7	76.4	117	99.6
1.52	0.3	6.67	25.6	29.3	78.7	129	99.7
1.66	0.5	7.30	26.1	32.1	81.0	141	99.8
1.83	1.0	8.02	29.6	35.2	83.4	155	99.9
2.00	1.7	8.80	43.0	38.7	85.7	170	100

Result source=Sample
Record No. = 0
Focal length = 100 mm.
Presentation =2207
Volume distribution
Beam length = 2.2 mm.
Obscuration =0.2275
Volume Conc. = 0.0272 %
Residual = 0.315%
Model indp

D(v,0.5) = 10.70 µm
D(v,0.9) = 46.40 µm
D(v,0.1) = 3.33 µm
D(4,3) = 17.54 µm
D(3,2) = 7.98 µm
Span = 4.0
Spec. surf. area
0.7857 sq.m./cc.

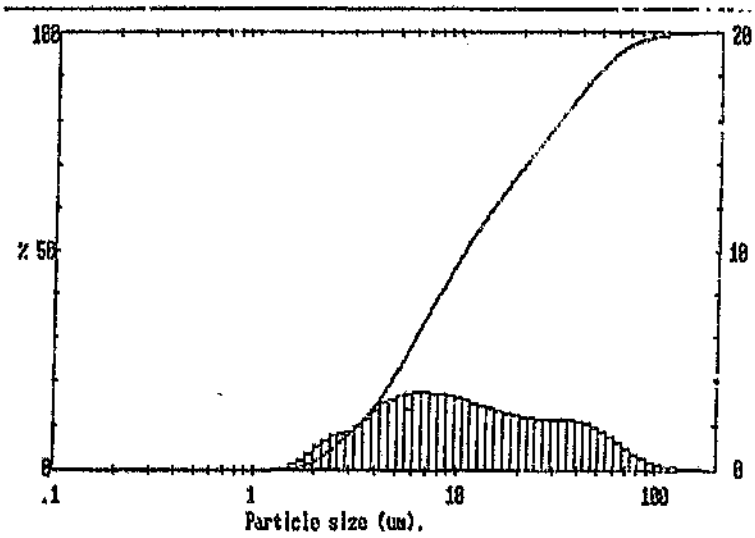

Figure 4.6: Particle size distribution of Fe powder.

Size µm.	% under	Size µm.	% under	Size µm.	% under	Size µm.	% under
0.50	0.0	2.20	5.1	9.66	76.0	42.4	99.9
0.55	0.0	2.41	7.4	10.6	80.5	46.5	100
0.60	0.0	2.64	9.8	11.6	84.6	51.1	100
0.66	0.0	2.90	12.4	12.7	88.0	56.0	100
0.72	0.0	3.18	14.8	14.0	90.8	61.4	100
0.79	0.0	3.48	17.6	15.3	93.1	67.4	100
0.87	0.0	3.83	21.1	16.8	94.9	73.9	100
0.95	0.1	4.20	25.8	18.5	96.3	81.1	100
1.05	0.1	4.61	32.2	20.3	97.4	89.0	100
1.15	0.2	5.05	41.2	22.2	98.2	97.6	100
1.26	0.3	5.54	52.4	24.4	98.8	107	100
1.38	0.5	6.08	62.6	26.7	99.2	117	100
1.52	0.7	6.67	69.4	29.3	99.4	129	100
1.66	1.0	7.32	73.5	32.1	99.6	141	100
1.83	2.0	8.03	75.3	35.2	99.8	155	100
2.00	3.3	8.80	76.0	38.7	99.9	170	100

Result source=Sample
Record No. = 6
Focal length = 100 mm.
Presentation =3207
Volume distribution
Beam length = 8.0 mm.
Obscuration =0.0021
Volume Conc. = 0.0161 %
Residual = 0.426%
Model indp

Div,0.5) = 6.34 µm
Div,0.9) = 13.59 µm
Div,0.1) = 2.66 µm
D[4,3] = 7.24 µm
D[3,2] = 5.35 µm
Span = 1.7
Spec. surf. area
1.1071 sq.m./cc.

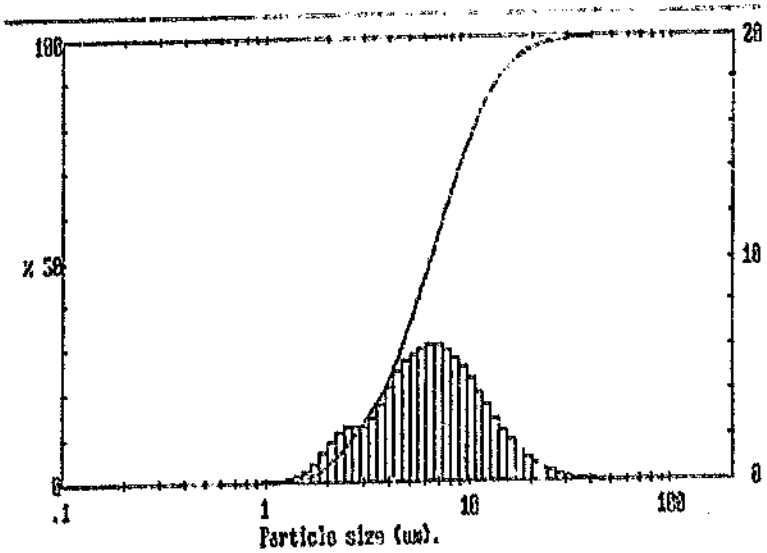

Figure 4.7: Particle size distribution of SP001008 (Extra Fe).

Table 4.1: Chemical analysis of starting and milled powder (SP001008). Analysed at Ultra High Pressure Units.

	weight % carbon	weight % oxygen
UHPU Fe (starting powder)	0.050	0.078
VFA843 (starting powder)	0.025	0.141
SP001008 (milled powder)	0.176	0.281

4.2 Hardness vs time at 750°C for VFA647 and VFA654

The results of the heat treatment comparison of VFA647 and VFA654 are shown in Table 4.2

Table 4.2: Hardness vs time at 750°C for VFA647 and VFA654.

Time at 750°C (hours)	Hardness of VFA647 (Rockwell C)	Hardness of VFA654 (Rockwell C)
0	16	13
2	11	-
4	13	49 (Cracks appear in material)
8	11	58
12	11	59
16	16	-
24	22	-
44.75	34	-
48	42	-
80	54	-

- indicates that no readings were taken

The results are shown graphically in Figure 4.8.

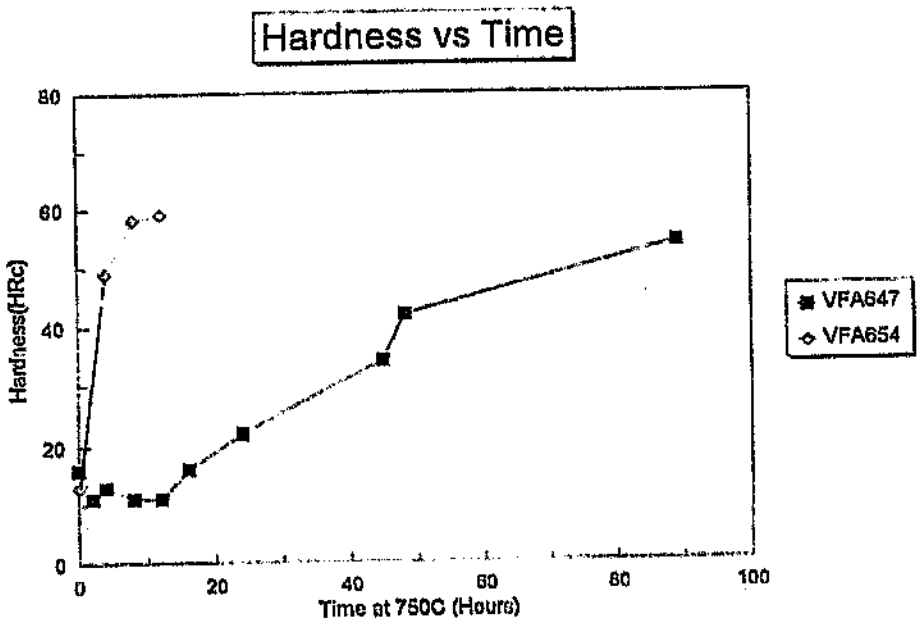

Figure 4.8: Hardness vs time at 750°C.

Alloy VFA654 embrittles readily within twelve hours. On the other hand, VFA647 was not sufficiently brittle for powder manufacture, even after 89 hours isothermal annealing at 750°C.

4.3 Metallography results

Metallographic examination of all as-HIPped specimens, in which the canister stayed intact, revealed complete bonding. Certain features were common to all specimens and these included the phenomena described below.
Entrapped contaminant inclusions were apparent at all particle boundaries. Various inter-particular inclusions were also observed. Alloys DS-1 and DS-C (both air melted) had a far higher proportion of contaminating inclusions than the vacuum melted alloys.

Widespread sigma phase precipitation was observed in all alloys. The amount of sigma present varied from between 20 and 70 percent. In alloys with greater than 20 percent sigma, extensive macro-cracking was apparent after polishing. Alloy V exhibited the least amount of sigma (20 percent) after HIPping.

Examination of the samples after solution annealing and quenching revealed that sigma was removed from most of the alloys. However, sigma phase was still apparent in DS-C, DS-1 and VFA 423 alloys. The sigma appeared to have formed preferentially on particle boundaries. Inter- and intragranular precipitates were also observed

Sigma phase is revealed by the HCl and electrolytic etchants as a light phase, whilst the ferrite is darker etching.

The micrographs are presented as Figures 4.9-4.64 and have accompanying notes with them. All micrographs were taken by optical techniques.

4.3.1 Microstructures of the Fe-38Cr-4Mo-2Ni alloys (As-HIPped)

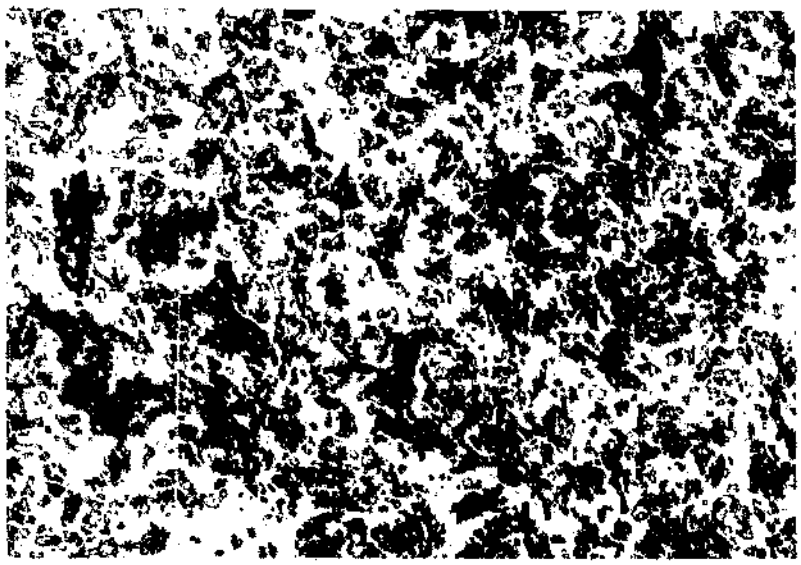

Figure 4.9: VFA543, as-HIPped, unetched (100X), optical image.

The microstructure exhibited severe cracking after HIPping and casual handling, as shown in Figure 4.9.

4.3.2 Microstructures of the 2Ni-4Mo-38Cr-Fe alloys (Solution annealed)

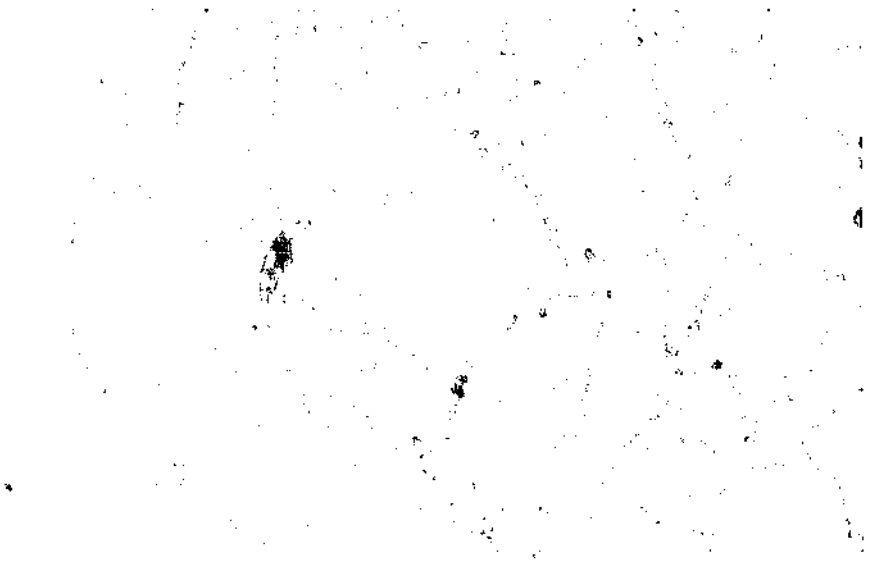

Figure 4.10: DS-1, (1100°C), KOH electrolytic etch, (200X), optical image. Ferrite with residual sigma phase, as shown in Figure 4.10.



Figure 4.11: DS-1, (1100°C), KOH electrolytic etch, (500X), optical image. Detail of residual sigma phase.



Figure 4.12: DS-C, (annealed 1100°C), KOH electrolytic etch, (200X), optical image.
Ferrite with secondary phase precipitation.



Figure 4.13: DS-C, (annealed 1100°C), KOH electrolytic etch, (500X), optical image.
Detail of precipitates.

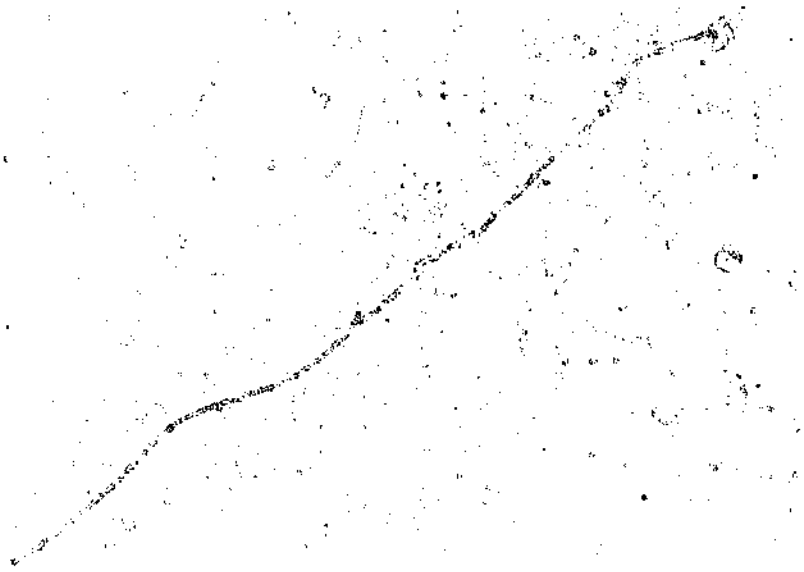

Figure 4.14: VFA417, (annealed 1100°, HCl etch, (200X), optical image.
Large crack running through sigma-ferrite microstructure, with a higher number of particles near the crack.

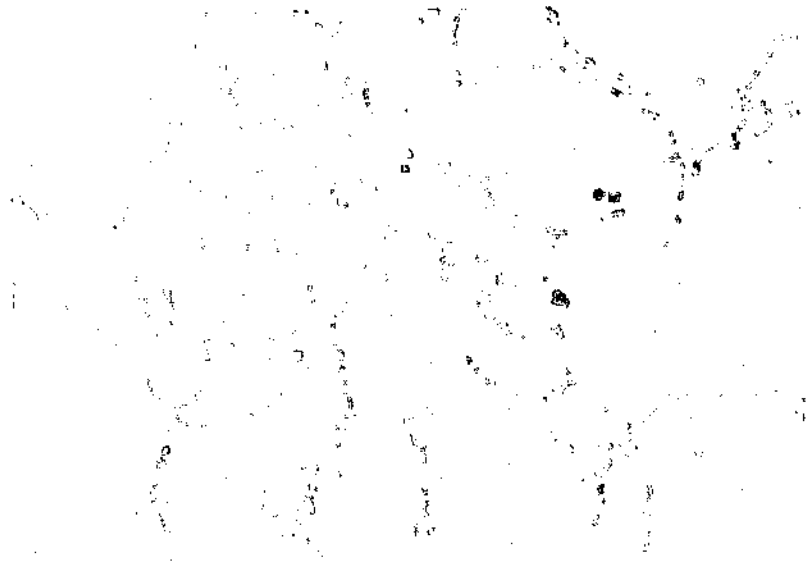

Figure 4.15: VFA417, (annealed 1100°, HCl etch,) (500X), optical image.
Duplex sigma (lighter etching) - ferrite (darker etching) microstructure.

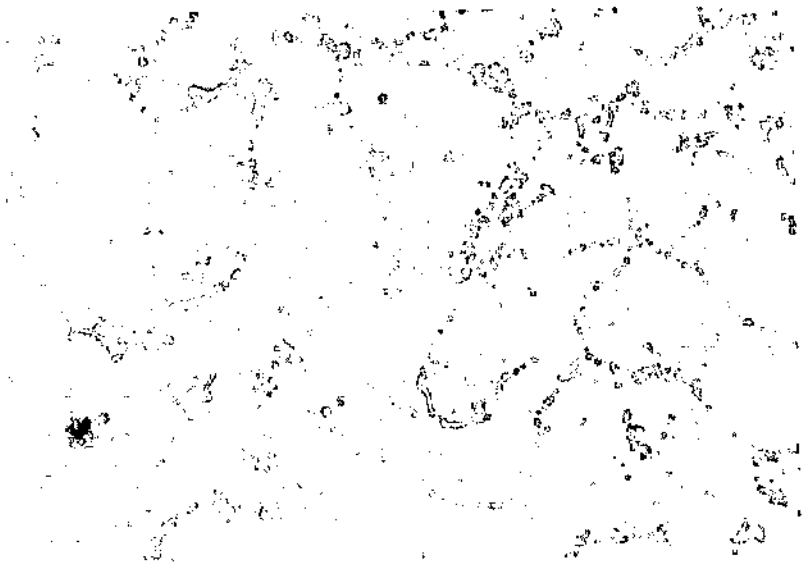

Figure 4.16: VFA419, (annealed 1100°C), HCl etch, (200X), optical image.
Duplex ferrite (darker etching) - sigma (lighter etching) microstructure.

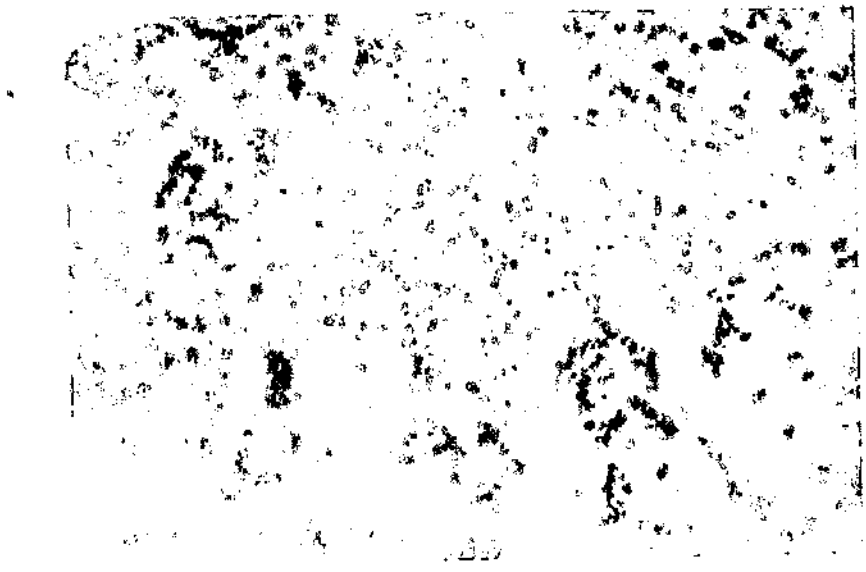

Figure 4.17: VFA419, (annealed 1100°C), HCl etch, (500X), optical image.
Detail of precipitates.

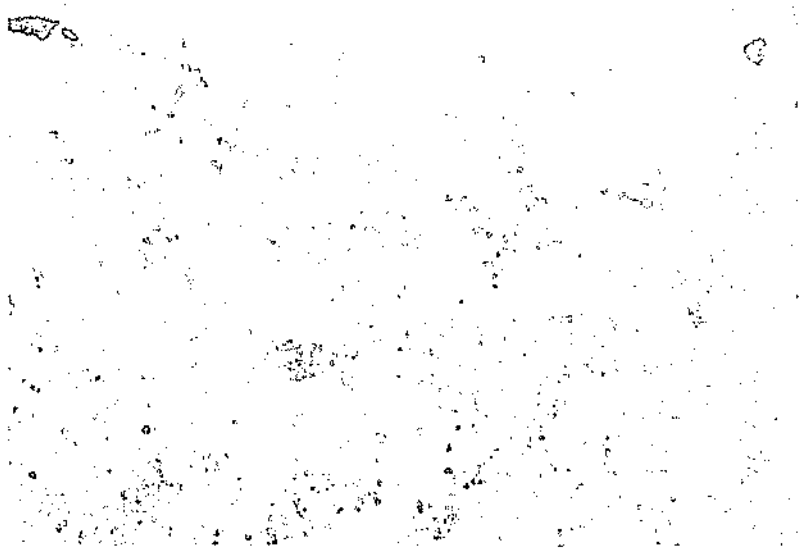

Figure 4.18: VFA420, (annealed 1100°C), HCl etch, (200X), optical image.
Ferrite (darker etching) - sigma (lighter etching) microstructure.

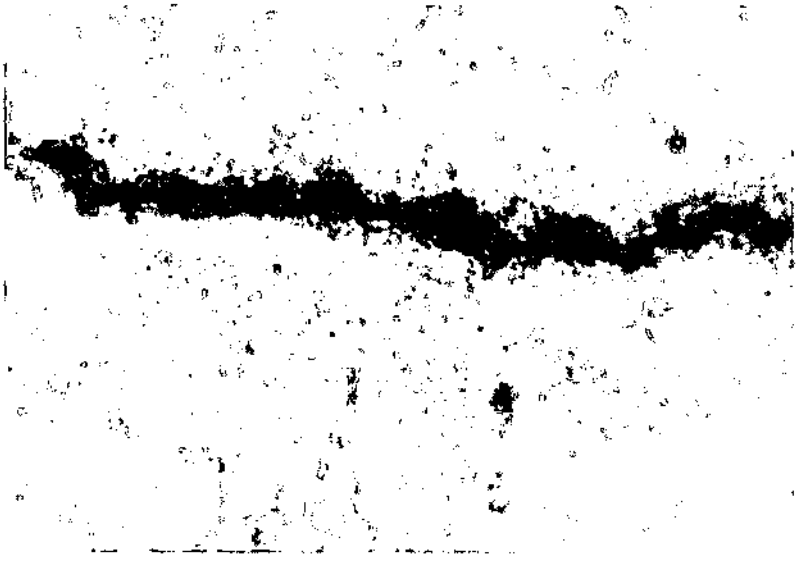

Figure 4.19: VFA420, (annealed 1100°C), HCl etch, (500X), optical image.
Large crack passing through sigma and ferrite phases.

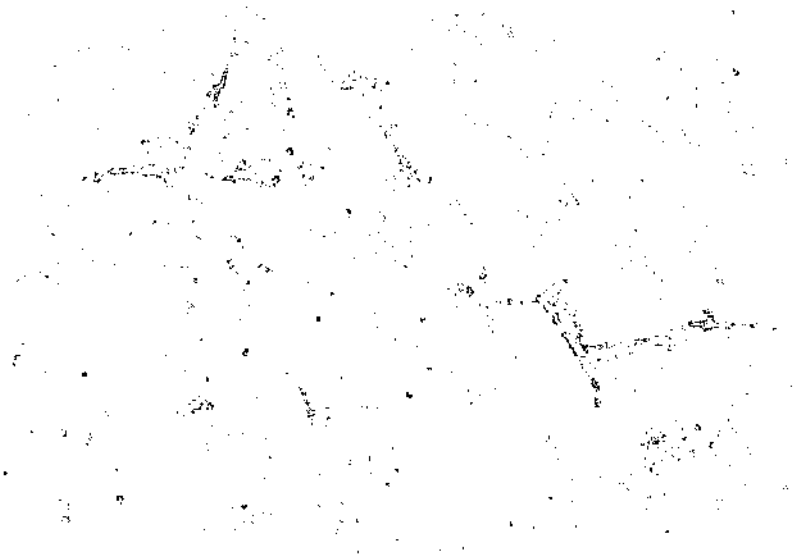

Figure 4.20: VFA423, (annealed 1100°C), HCl etch, (200X), optical image. Residual sigma in ferrite matrix.

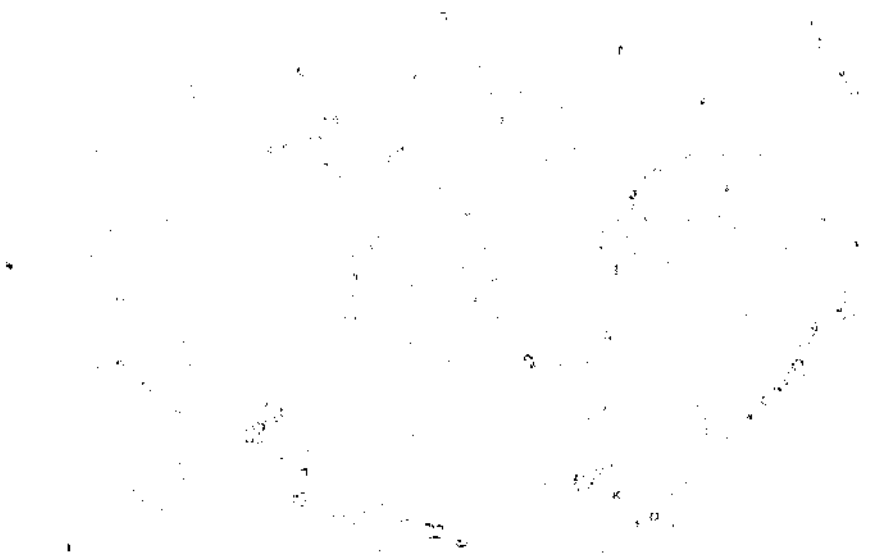

Figure 4.21: VFA423, (annealed 1100°C), HCl etch, (500X), optical image. Ferrite grains with inclusions at particle boundaries.

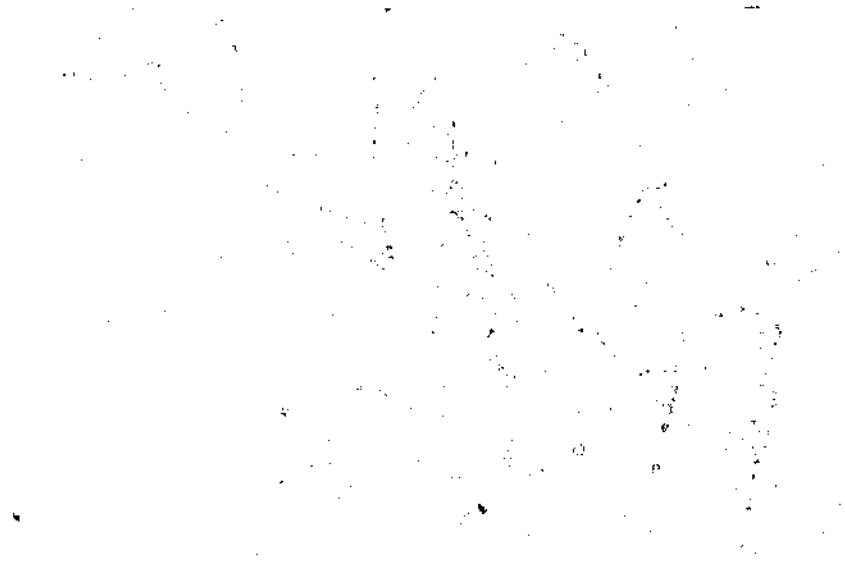

Figure 4.22: VFA543, (annealed 1100°C), HCl etch, (500X), optical image.

4.3.3 The 2Ni-2Mo alloys

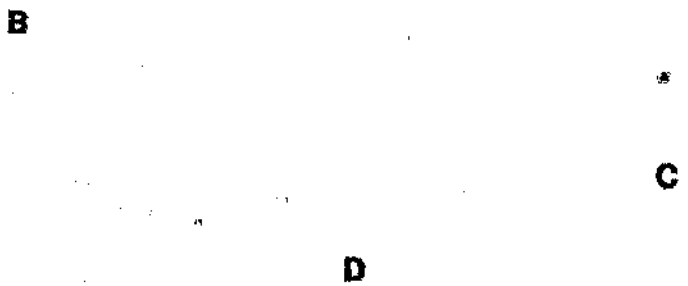

Figure 4.23: PremAlloy V, (as-HIPped), HCl etch, (100X), optical image. Secondary phases in Diffusion zone. C is the mild steel canister; D is the diffusion zone; B is the Prem V compact.

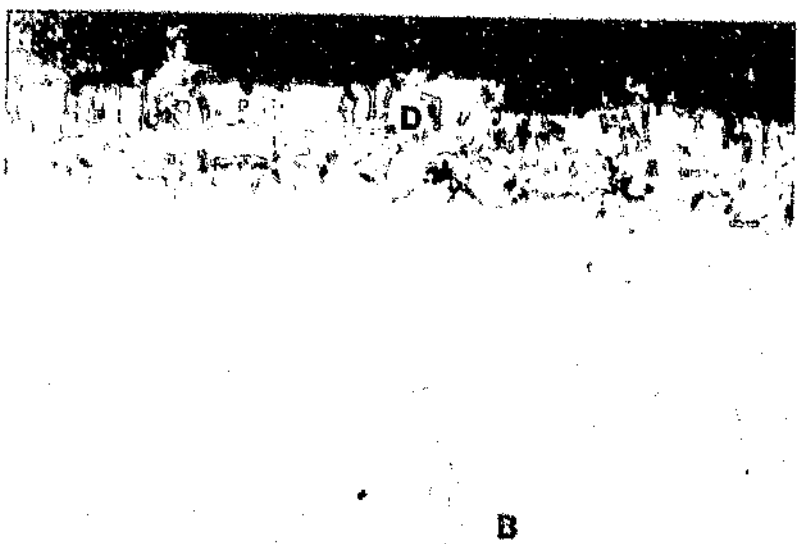

Figure 4.24: PremAlloy V, (annealed 1160°C), HCl etch, (100X), optical image. Secondary phases in diffusion zone after solution annealing. D is the diffusion zone; B is the Prem V compact.

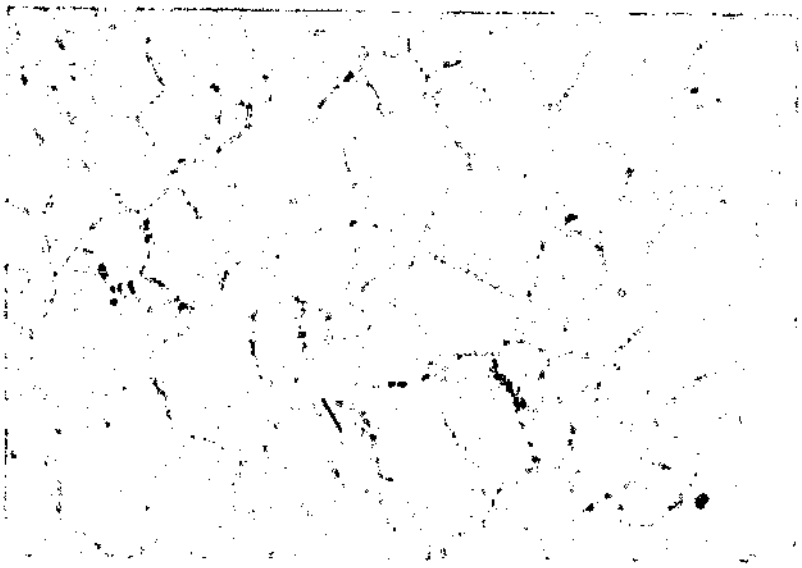

Figure 4.25 PremAlloy V, (annealed 1100°C), HCl etch, (200X), optical image. General ferritic microstructure with a number of dark grey inclusions. The inclusions were analysed with EDS techniques.

Table 4.3: EDS analysis of inclusion in Prem V.

		Spot analysis (weight percent)							
Alloy	Micrograph	Mo	Cr	Fe	Ni	W	Ti	Al	Other
Prem V	Inclusion in Figure 4.25	-	47.6	1.3	-	-	23.3	1.7	0.8% Nb Balance could be C or O

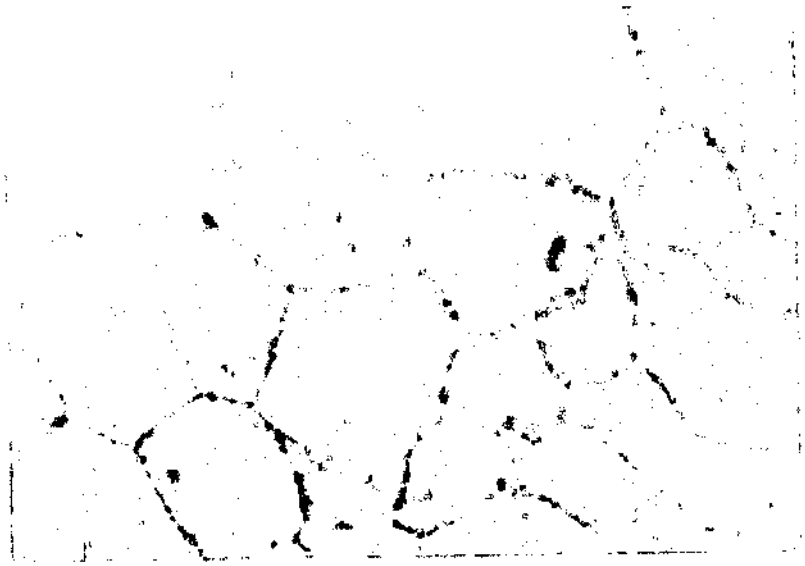

Figure 4.26: PremAlloy V, (annealed 1100°C), HCl etch, (500X), optical image. Ferritic microstructure with a combination of large and fine precipitates.



Figure 4.27: VFA487, (as-HIPped), HCl etch, (100X), optical image.
Plastic deformation around indentation.

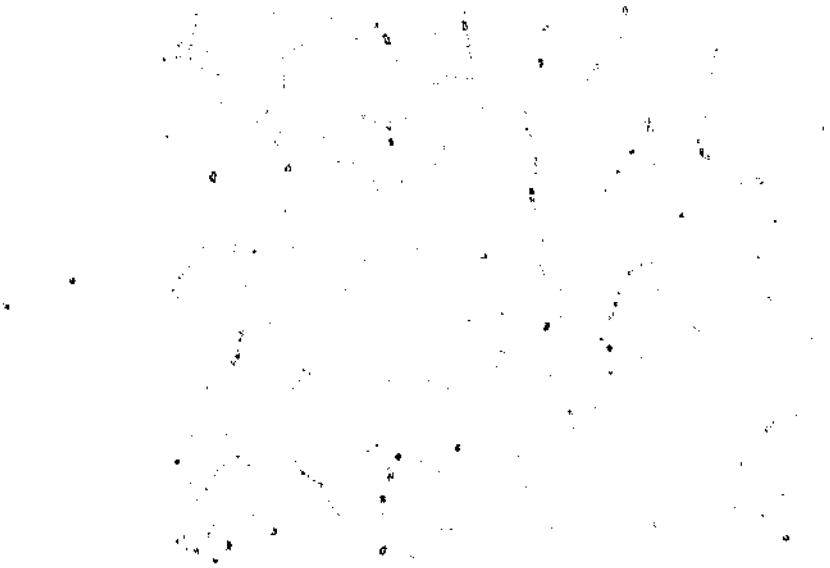

Figure 4.28: VFA 487, (annealed 1100°C), HCl etch, (200X), optical image.
Ferritic microstructure with traces of sigma.

..3.4 Metallographic results of VFA622

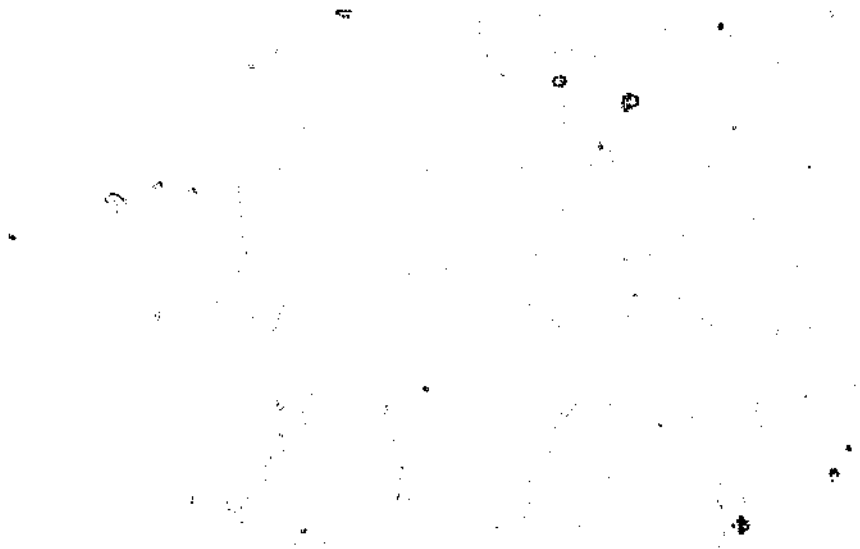

Figure 4.29: VFA622, (HIPped + annealed 1100°C), HCl etch, (200X), optical image.
Ferrite grains free of sigma phase.

Figure 4.30: VFA622, (HIPped + annealed 1100°C), HCl etch, (500X), optical image.
Ferrite grains without residual sigma.

4.3.5. Comparison of HIPped and cast material VFA622.

Figure 4.31: VFA622 , (Cast and HIPped), HCl etch, (200X), optical image.
Widespread intragranular precipitation of spherical carbides and nitrides.

Figure 4.32: VFA622 , (Cast and HIPped), HCl etch, (500X), optical image.
Detail of precipitates.



Figure 4.33: VFA622 , (HIPped+solution annealed), HCl etch, (500X), optical image.
Ferrite grain with prominent precipitates, especially on prior grain boundaries.

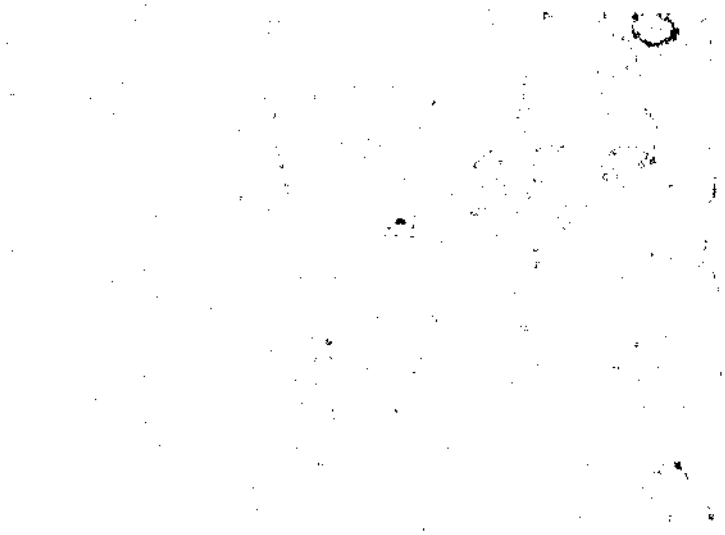

Figure 4.34: VFA622 , (HIPped twice only), HCl etch, (200X), optical image.
Preferential sigma phase formation at particle boundaries.

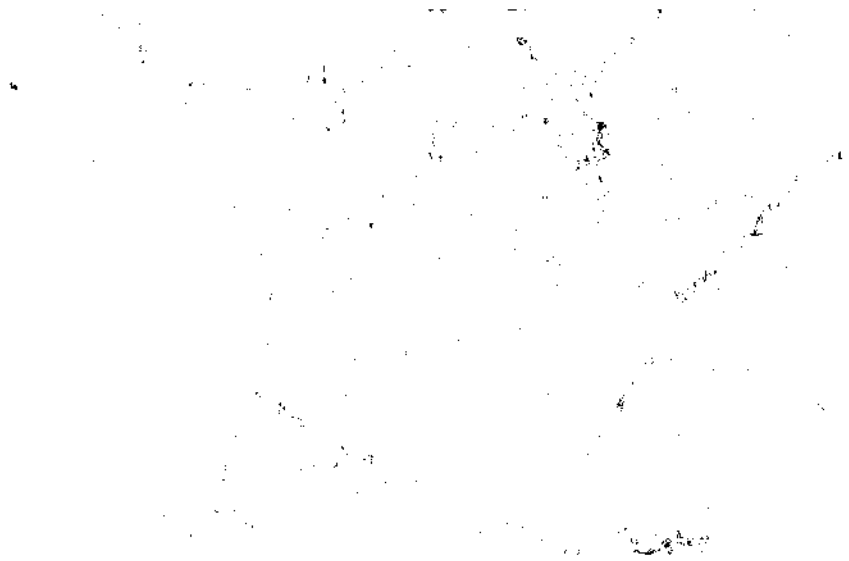

Figure 4.35: VFA622 , (HIPped twice only), HCl etch, (500X), optical image. Preferential sigma phase growth at particle boundaries.

4.3.6. Extra milled VFA543(SP001012)

4.3.7. Analysis of milling media

The milling media was found to contain 0.275 percent C and 90 percent Fe by mass. Analysis was performed at Ultra High Pressure Units using wet analytical techniques.

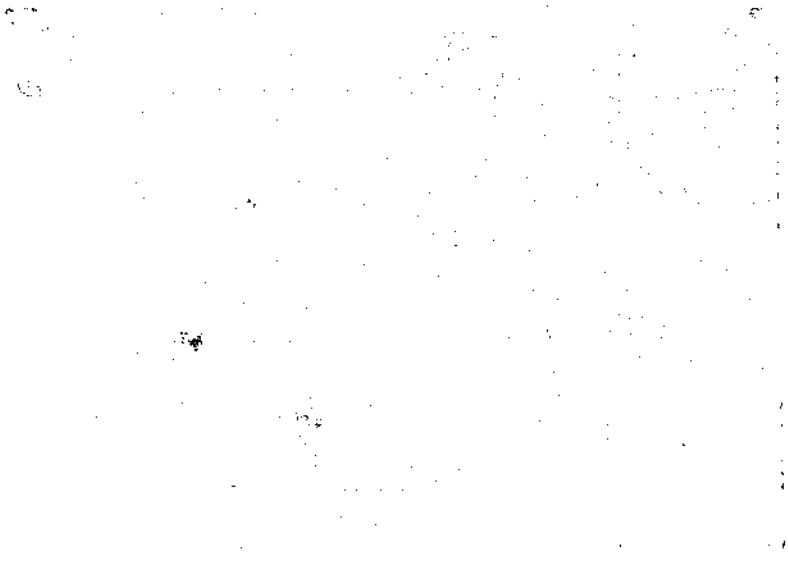

Figure 4.36: Microstructure of steel milling media, (500X), optical image. A martensitic microstructure is present.

Size µm.	% under	Size µm.	% under	Size µm.	% under	Size µm.	% under
0.50	0.0	2.20	5.1	9.66	76.0	42.4	99.9
0.55	0.0	2.41	7.3	10.6	80.5	46.5	100
0.60	0.0	2.64	9.8	11.6	84.6	51.1	100
0.66	0.0	2.90	12.3	12.7	88.0	56.0	100
0.72	0.0	3.18	14.8	14.0	90.8	61.4	100
0.79	0.0	3.49	17.6	15.3	93.1	67.4	100
0.87	0.0	3.83	21.1	16.8	94.9	73.9	100
0.96	0.1	4.20	25.3	18.5	96.3	81.1	100
1.05	0.1	4.61	30.3	20.2	97.4	89.0	100
1.15	0.2	5.05	35.7	22.2	98.2	97.6	100
1.26	0.3	5.54	41.3	24.4	98.8	107	100
1.38	0.4	6.08	47.2	26.7	99.2	117	100
1.52	0.7	6.67	53.4	29.3	99.4	129	100
1.66	1.2	7.32	59.5	32.1	99.6	141	100
1.83	2.0	8.02	65.3	35.3	99.8	155	100
2.00	3.3	8.80	70.8	38.7	99.9	170	100

Result source=Sample
Record No. = 0
Focal length = 100 mm.
Presentation =2207
Volume distribution
Beam length = 2.2 mm.
Obscuration =0.202%
Volume Conc. = 0.0151 %
Residual = 0.426%
Model indp

D(v,0.5) = 6.34 µm
D(v,0.9) = 13.58 µm
D(v,0.1) = 2.66 µm
D(4,3) = 7.24 µm
D(3,2) = 5.55 µm
Span = 1.7
Spec. surf. area
1.1571 sq.m./cc.

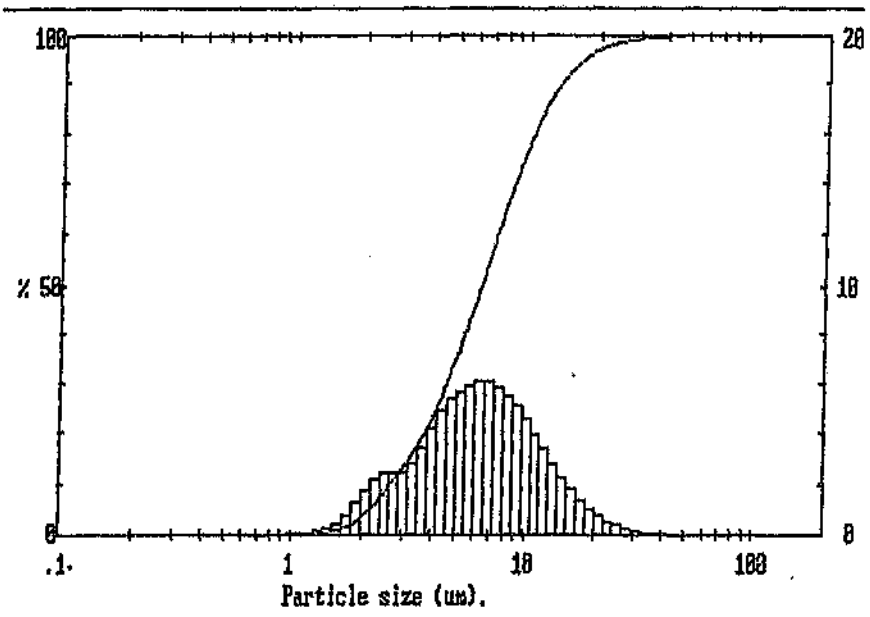

Figure 37: Frequency and cumulative particle size distribution of extra milled VFA543 (SP001012)

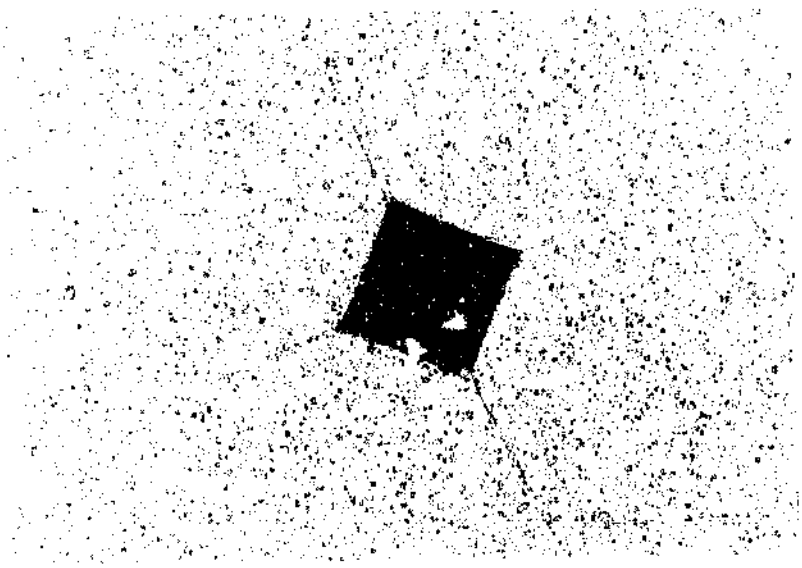

Figure 4.38: Extra-milled VFA543 (SP001012), (As-HIPped), HCl etch, (100X), optical image.
Palmqvist cracks are present at the corners of the hardness indentation.

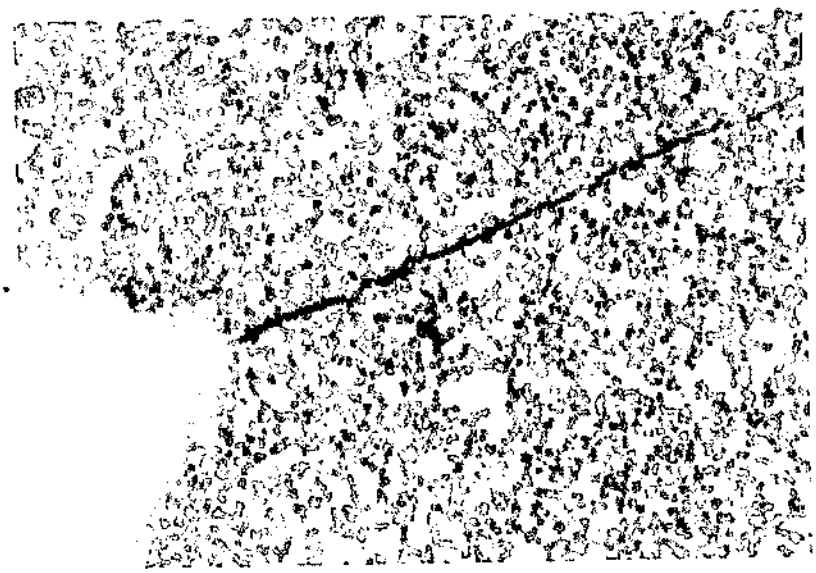

Figure 4.39: Extra milled VFA543 (SP001012), (As-HIPped), HCl etch, (500X), optical image.
Detail of corner of indentation.

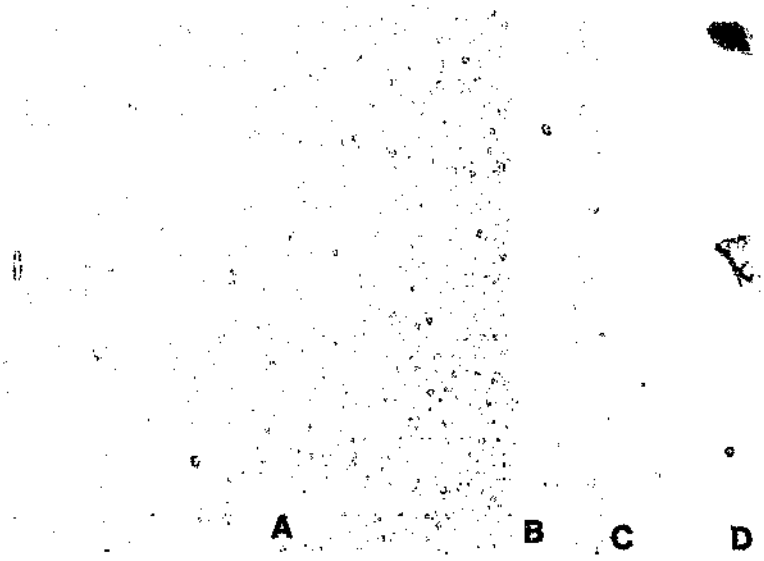

Figure 4.40: Extra-milled VFA543 (SP001012), (As-HIPped), Murakami etch, (200X), optical image.
Diffusion zone of powder in contact with the mild steel canister. A is the core of the compact; B and C are the diffusion zone; D is the mild steel canister.

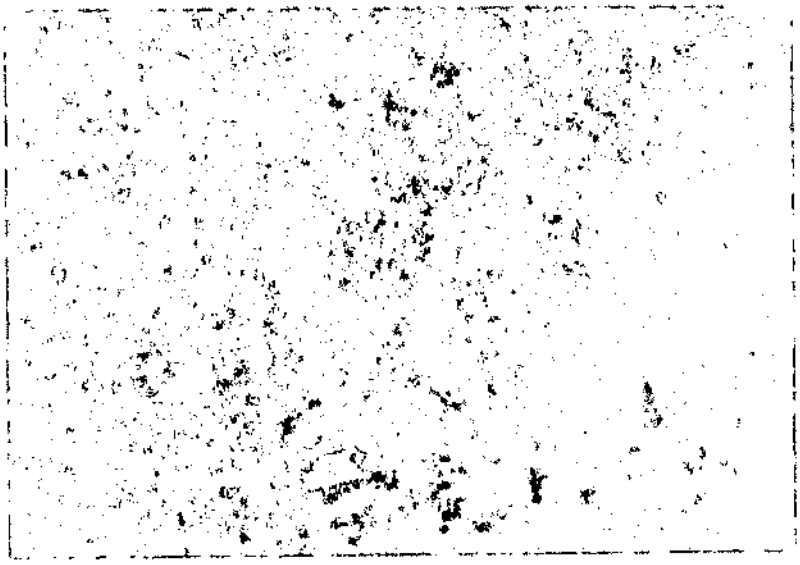

Figure 4.41: SP001012, (annealed 1100°C), HCl etch, (500X), optical image.
Fine duplex ferrite-sigma microstructure. The sigma is the lighter etched phase.

4.3.8. Microstructures of alloys made from duplex powders.

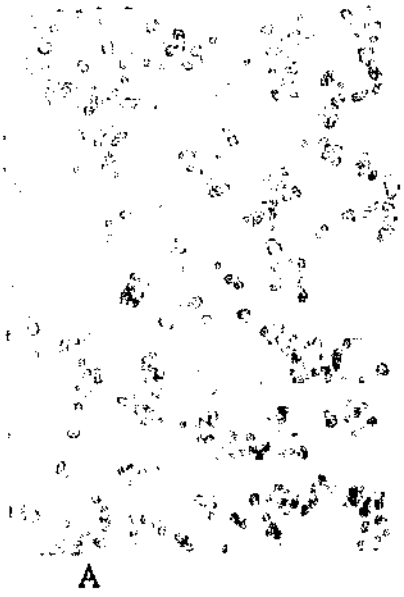

Figure 4.42: Microstructure SP001008, (As-HIPped), 200X
A cross-section of the diffusion zone between the mild steel canister (D) and the powder particles (A, B, C). EDS analyses were performed in regions A and B.

Table 4.4: EDS analysis of SP001008.

		Spot analysis (weight percent)				
Alloy	Micrograph	Mo	Cr	Fe	Ni	Other
SP001008	Diffusion zone B in Figure 4.42	1.8	22.7	74.1	0.9	0.3% Si
SP001008	Core region A in Figure 4.42	1.8	28.3	68.2	1.1	0.5% Si

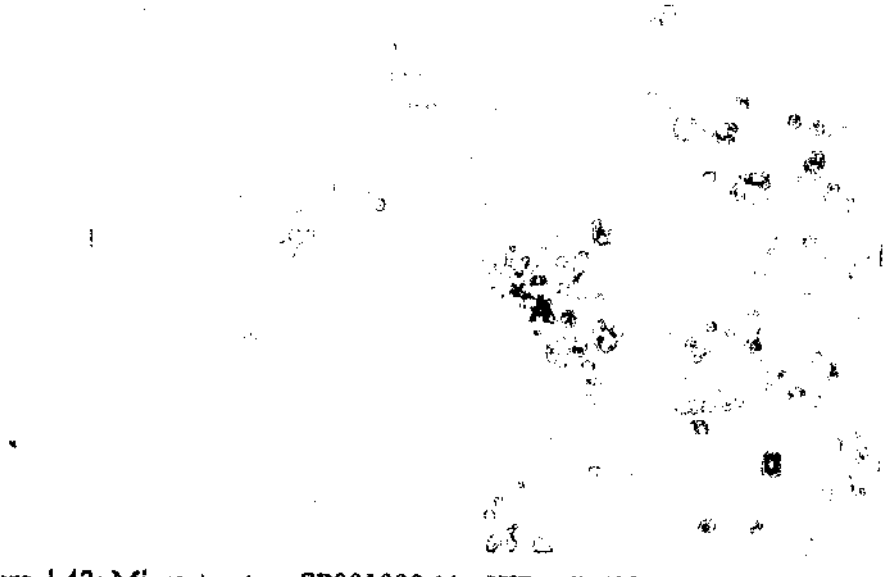

Figure 4.43: Microstructure SP001008 (As-HIPped) 500X, optical image. Ferrite matrix . This core region contains coarse complex Cr-Fe-Mo carbides. The precipitate at point A was analysed by EDS analysis.

Table 4.5: EDS analysis of precipitate in SP001008, as-HIPped.

		Spot analysis (weight percent)				
Alloy	Micrograph	Mo	Cr	Fe	Ni	Other
SP001008	Precipitate A in Figure 4.43	4.8	57.1	24.3	0.7	0.6%Si Balance should be C

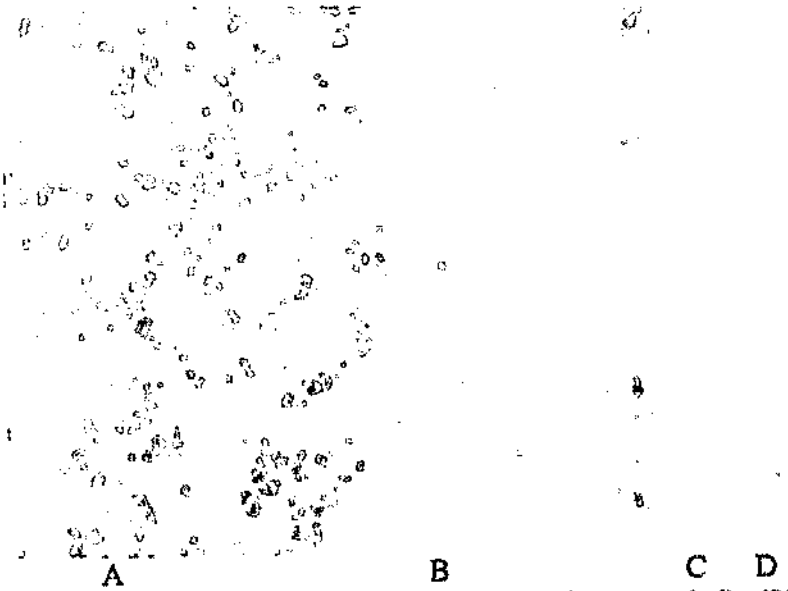

Figure 4.44: Microstructure SP001008 (HIPped + solution annealed), (200X), optical image.

The diffusion zone appears unchanged after annealing. The precipitates in section C have gone into solution. A is the core of the compact; B and C are the diffusion zone; D is the mild steel canister.

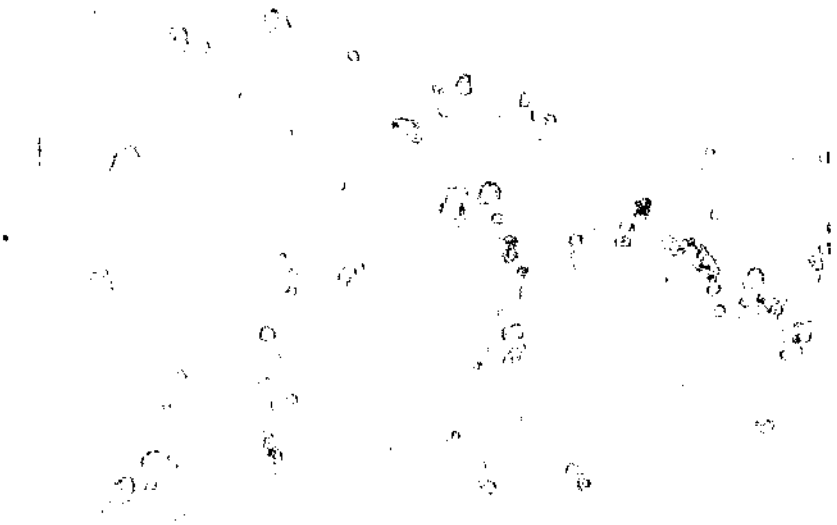

Figure 4.45: Microstructure SP001008 (solution annealed 1100°C) 500X, optical image.

Core region with coarse Cr-Fe-Mo carbides.

4.3.9. The addition of extra Fe to VFA543 and VFA622 by hand mixing

Figure 4.46: VFA622+Fe (as-HIPped), HCl etchant, (200X), optical image.
Detail of area near Vickers indentation showing strain lines within a ferritic microstructure. There is a combination of large and fine particle sizes as indicated by the darker precipitates on the particle boundaries.

Figure 4.47: VFA622+Fe (1100°C anneal), HCl etchant, (200X), optical image. Ferritic microstructure without areas of preferential attack by etchant. Points A1, A2 and A3 were subjected to EDS analysis.

Table 4.6: EDS analysis of VFA622+Fe in Figure 4.47.

		Spot analysis (weight percent)							
Alloy	**Micrograph**	**Mo**	**Cr**	**Fe**	**Ni**	**W**	**Ti**	**Al**	**Other**
VFA622+Fe (As-HIPped)	Average of three spot analyses in Figure 4.47	1.35	34.2 Max:35 Min:32	62.3	1.4	-	-	-	0.2%Si 0.1%Nb

Figure 4.48: VFA622+Fe (1100°C anneal), HCl etchant, (500X), optical image. Detail of ferrite grain.

4.3.10. Microstructures of duplex powders.



Figure 4.49: (20% 316L+80% VFA622), As-HIP (200X), HCl etch , optical image.
Large non-metallic inclusion in alloy.



Figure 4.50: (20% 316L+80% VFA622), As-HIP (500X), HCl etch , optical image.
Morphology of sigma phase in the duplex alloy.

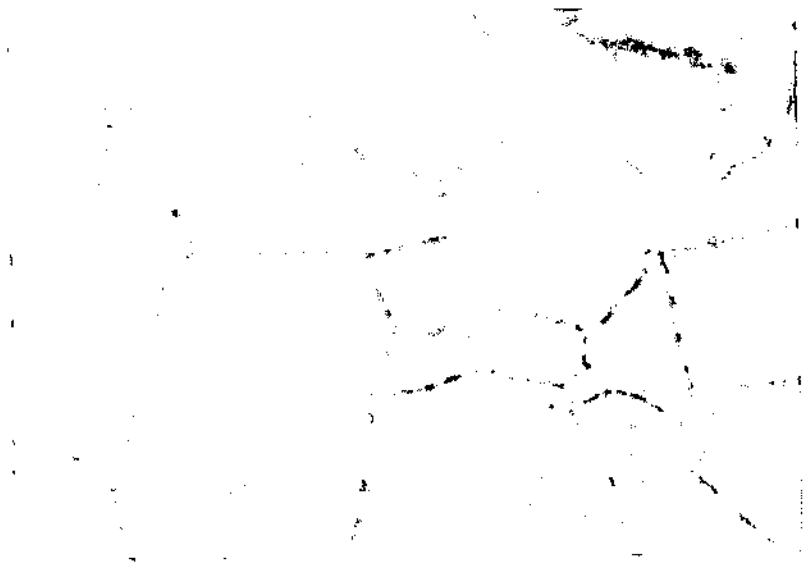

Figure 4.51: (20% 316L+80% VFA622), 1100°C,(500X), HCl etch , optical image.
Predominantly ferritic microstructure.

Figure 4.52: (50% 316L+50% VFA622), As-HIP,(200X), HCl etch , optical image.
Duplex ferritic (etched dark) - austenitic (etched light) microstructure.

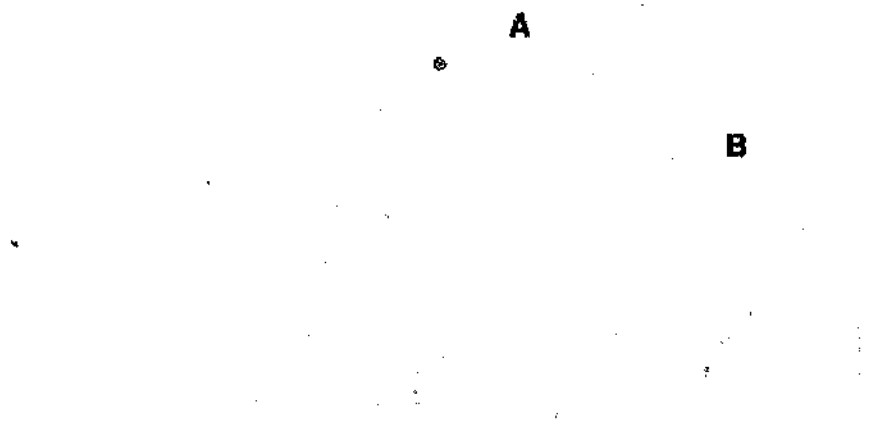

Figure 4.53: (50% 316L+50% VFA622), 1100°C(200X), HCl etch , optical image.
Decrease in proportion of etched light (austenitic) phase after annealing. Points A and B were examined by SEM spot analysis.

Table 4.7: EDS spot analysis of 50% 316L + 50% VFA622.

		Spot analysis (weight percent)			
Alloy	Micrograph	Mo	Cr	Fe	Ni
50% 316L + 50% VFA622	Figure 4.53 Etched dark area B.	1.2	38.7	56.3	3.8
50% 316L + 50% VFA622	Figure 4.53 Etched light area A.	1.4	28.2	63.6	6.8

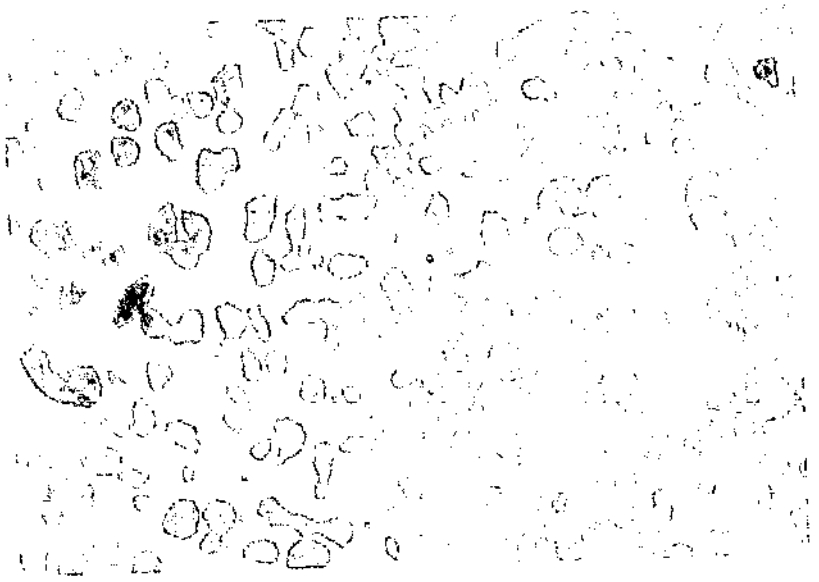

Figure 4.54: (80% 316L+20% VFA622), As-HIP (25X), HCl etch , optical image.
Well distributed ferrite (dark) particles within an austenite (316L) matrix.



Figure 4.55: (80% 316L+20% VFA622), As-HIP(200X), HCl etch , optical image.
Sigma in bulk and lamellae morphology.



Figure 4.56: (80% 316L+20% VFA622), As-HIP (500X), HCl etch , optical image.

Comparison between different sigma phase morphologies. Micro-hardness tests were taken at points A and B. The composition of the sigma phase at point B was analysed and is shown in Tables 4.8-4.9.

Table 4.8: Microhardness results of 80% 316L+20% VFA622, as-HIP.

Alloy	Micrograph	Microhardness value with 50 grams-force load.
80%316 + 20%VFA622 (Solution annealed) , ferrite phase	Point A in Figure 4.56	339
80%316 + 20%VFA622, (Solution annealed) , sigma phase	Point B in Figure 4.56	529
VFA543, as-HIP, Reference alloy consisting of near 100% sigma phase	Figure 4.9	1555

Table 4.9: EDS analysis of sigma phase at point B and C.

		Spot analysis (weight percent)			
Alloy	Micrograph	Mo	Cr	Fe	Ni
80% 316+ 20% VFA622 (As-HIPped)	Sigma phase at point B in Figure 4.56	6.4	53	37.4	2.2
80% 316+ 20% VFA622 (As-HIPped)	Sigma phase at point C in Figure 4.56	3.5	39.6	51.8	4.2
Overall composition of VFA622 base alloy		2	40	55	2

Figure 4.57: (80% 316L+20% VFA622), 1100°C (500X), HCl etch , optical image.
VFA622 particle in 316L matrix, with higher precipitate concentration at grain boundaries.

A

Figure 4.58: (80% 316L 20% VFA622), 1100°C (200X), HCl etch , optical image.
Three phase microstructure consisting of austenite, ferrite and sigma phase. The diffusion zone between a VFA622 particle and the surrounding 316L is indicated at region A.

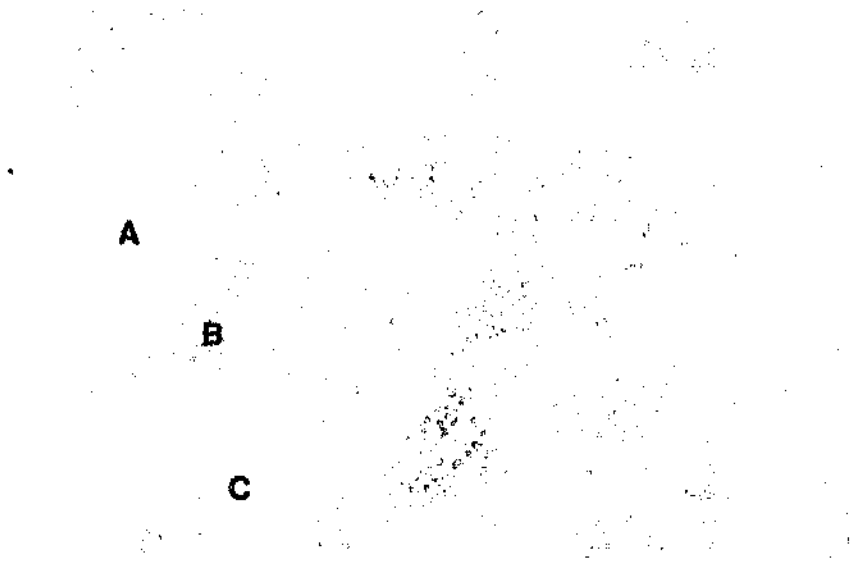

Figure 4.59: (50% Hastelloy C + 50% PremV), As-HIP (200X), HCl + Murakami's etch, optical image.
Region showing diffusion zone (C) between Prem V (A) and Hastelloy particles (B).



Figure 4.60: (50% Hastelloy C+50% Prem V), As-HIP (500X), HCl + Murakami's etch , optical image.
Prem V particle exhibiting a high proportion of sigma (light) phase. An inclusion is indicated at point A.

A

Figure 4.61: (50%Hastelloy C + 50%PremV), As-HIP (500X), HCl +Murakami's etch, optical image.
A carbide-rich Hastelloy region. The carbide at point A was subjected to EDS analysis (Table 4.10).

Table 4.10: Precipitate in Hastelloy C.

		Spot analysis (weight percent)					
Alloy	Micrograph	Mo	Cr	Fe	Ni	W	Other
50% Hastelloy C + 50% Prem V	Precipitate A in Figure 4.61	25.2	26.6	15.6	23.2	8.0	Balance should be C

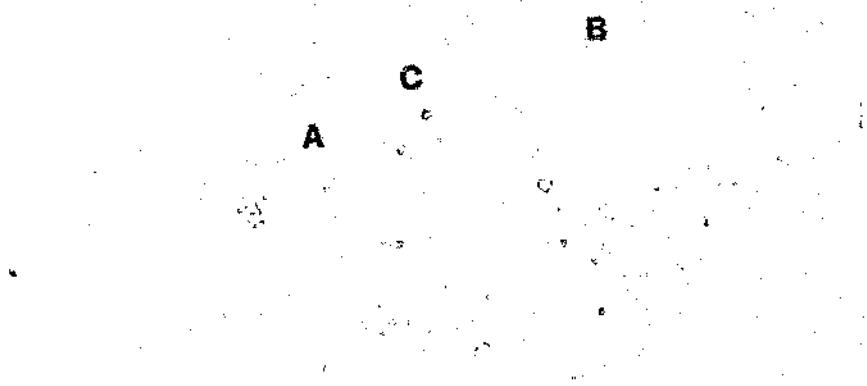

Figure 4.62:(50% Hastelloy C + 50% Prem V), 1100°C (200X), HCl +Murakami's etch, optical image.

Overall microstructure after heat treatment. The centre of a Prem V particle (A) and centre of a Hastelloy C particle (B) were subjected to EDS analysis (Table 4.11).

Table 4.11: EDS analysis of 50° Hastelloy C+ 50% Prem V.

		Spot analysis (weight percent)				
Alloy	Micrograph	Mo	Cr	Fe	Ni	W
50% Hastelloy C + 50% Prem V	Centre of Prem V particle in Figure 4.62.	7.0	38.0	36.7	17	1.3
50% Hastelloy C + 50% Prem V	Centre of Hastelloy C particle in Figure 4.62.	7.9	26.2	23.6	39.1	3.1
50% Hastelloy C + 50%Prem V	Figure 4.62 Diffusion zone	4.2	36.1	35.5	24.2	Not analysed

Hastelloy C typically contains 4 percent W. This element was not included in the analysis of the diffusion zone and could therefore cause minor deviations in the results.

Figure 4.63: (50% Hastelloy C + 50% Prem V), 1100°C (500X), HCl +Murakami's etch, optical image.
Detail of Prem V particle. EDS spot analysis was performed on the diffusion zone at point A.

Figure 4.64: (50% Hastelloy C+50% Prem V), 1100°C (500X), HCl +Murakami's etch , optical image.
Hastelloy-rich region with complex M_6C carbides in a Ni-Cr-Mo matrix.

Table 4.12: Summary of EDS analyses.

		Spot analysis (weight percent)							
Alloy	Micrograph	Mo	Cr	Fe	Ni	W	Ti	Al	Other
Prem V	Inclusion in Figure 4.25	-	47.6	1.3	-	-	23.3	1.7	0.8% Nb Balance could be C or O
SP001005 powder	Particle surface as shown in Figure 4.5	3.1	44.1	48.8	1.9	-	-	1.5	0.6% Si
SP001008	Diffusion zone in Figure 4.42	1.8	22.7	74.1	0.9	-	-	-	0.3%Si
SP001008	Core region in Figure 4.42	1.8	28.3	68.2	1.1	-	-	-	0.5%Si
SP001008	Precipitate A in Figure 4.43	4.8	57.1	24.3	0.7	-	-	-	0.6%Si Balance should be C
VFA622+Fe (As-HIPped)	Average of three spot analyses in Figure 4.47	1.35	34.2 Max:35 Min:32	62.3	1.4	-	-	-	0.2%Si 0.1%Nb
80% 316+ 20% VFA622 (As-HIPped)	Sigma phase at point B in Figure 4.56	0.4	53	37.4	2.2	-	-	-	1.2%Si
80% 316+ 20% VFA622 (As-HIPped)	Sigma phase at point C in Figure 4.56	3.5	39.6	51.8	4.2	-	-	-	1.1%Si
50% 316L + 50% VFA622	Figure 4.53 Etched dark area B.	1.2	38.7	56.3	3.8	-	-	-	-
50% 316L + 50% VFA622	Figure 4.53 Etched light area A.	1.4	28.2	63.6	6.8	-	-	-	-
50% Hastelloy C + 50% Prem V	Precipitate A in Figure 4.61	25.2	26.6	15.6	23.2	8	-	-	Balance should be C
50% Hastelloy C + 50% Prem V	Centre of Prem V particle in Figure 4.62	7	38	36.7	17	1.3	-	-	-
50% Hastelloy C + 50% Prem V	Centre of Hastelloy C particle in Figure 4.62	7.9	26.2	23.6	39.1	3.1	-	-	-
50% Hastelloy C + 50% Prem V	Diffusion zone in Figure 4.62	4.2	36.1	35.5	24.2	Not analysed	-	-	-
		Mo	Cr	Fe	Ni	W	Ti	Al	

The EDS spot analysis examines a roughly drop shaped region on the specimen surface encompassing a volume of approximately $1\mu m^3$. The actual shape is dependent on the atomic number.

4.4. Summary of hardness results.

All solution annealing carried out at 1100°C for a period of two hours. Quenching was done in water at room temperature. A typical example of plastic deformation around an indentation is shown in Figure 4.27.

Table 4.13: Summary of hardness results.

Alloy	Condition	Vickers hardness (Hv30)	Comments
DS-1	As-HIPped	836	Massive cracking in material
DS-1	Solution annealed	276	
DS-C	As-HIPped	775	Massive cracking in material
DS-C	Solution annealed	269	Plastic deformation around indentation
Prem V	As-HIPped	289	Plastic deformation around indentation
Prem V	Solution annealed	252	Plastic deformation around indentation
SP001012 (VFA543 milled for 24h)	As-HIPped	876	Well defined indentation. Palmqvist cracks at indentation corners
SP001012 (VFA543 milled for 24h)	Solution annealed	318	Well defined indentation
VFA417	As-HIPped	876	Massive cracking in material
VFA417	Solution annealed	263	
VFA419	As-HIPped	890	Massive cracking in material
VFA419	Solution annealed	277	Plastic deformation around indentation
VFA420	As-HIPped	817	Massive cracking in material
VFA420	Solution annealed	736	Duplex microstructure
VFA423	As-HIPped	>800Hv	Unmeasurable indentation. Massive cracks in material.

Table 4.13 (continued) Alloy	Condition	Vickers hardness (Hv30)	Comments
VFA423	Solution annealed	277	Plastic deformation around indentation
VFA487	As-HIPped	274	Plastic deformation around indentation
VFA487	Solution annealed	321	Plastic deformation around indentation
VFA543	Solution annealed	275	
SP001012 (VFA543 milled for 24h)	As-HIPped	876	Well defined indentation. Palmqvist cracks at indentation corners
SP001012 (VFA543 milled for 24h)	Solution annealed	318	Well defined indentation
VFA622	As-HIPped (once)	>800Hv	Unmeasurable indentation. Massive cracks in material.
VFA622	Solution annealed	253	Plastic deformation around indentation
VFA622 (Test piece)	HIPped (twice)	282	Plastic deformation around indentation
VFA622 (Spring lock)	HIPped (twice)	257	Plastic deformation around indentation
VFA622	Cast, sigmatised and solution annealed	238	Plastic deformation around indentation
VFA622	Cast and HIPped	276	Plastic deformation around indentation
Steel mill media	As-received	715	Martensitic microstructure
SP001008 (VFA543+extra Fe)	As-HIPped	262	Well defined indentation
SP001008 (VFA543+extra Fe)	Solution annealed	281	Well defined indentation
VFA543+extra Fe (hand mix)	As-HIPped	238	Plastic deformation around indentation

Alloy	Condition	Vickers hardness (Hv30)	Comments
VFA543+extra Fe(hand mix)	Solution annealed	242	Plastic deformation around indentation
VFA622+extra Fe(hand mix)	As-HIPped	224	Plastic deformation around indentation
VFA622+extra Fe(hand mix)	Solution annealed	212	Plastic deformation around indentation
20% 316L + 80% VFA622	As-HIP	286	
20% 316L + 80% VFA622	Solution annealed	219	
80% 316L + 20% VFA622	As-HIP	194	
80% 316L + 20% VFA622	Solution annealed	Off-scale <185Hv	
50% 316L + 50% VFA622	As-HIP	272	
50% 316L + 50% VFA622	Solution annealed	248	
50% Hastelloy C + 50% Prem V	As-HIP	401	
50% Hastelloy C + 50% Prem V	Solution annealed	357	

Table 4.13 Summary of hardness values(continued).

Table 4.14: Summary of microhardness results.

Alloy	Micrograph	Microhardness value with 25 grams-force load.	Microhardness value with 50 grams-force load.
DS-1, DS-C (Solution annealed) (Ferrite phase)	Figure 4.10 Figure 4.12	357	-
DS-1, DS-C (Solution annealed) (Sigma phase)	Figure 4.10 Figure 4.12	507	-
VFA543, as-HIP, (Reference alloy consisting of 100% sigma phase)	Figure 4.9	1750	-
80%316+VFA622 (Solution annealed) (Ferrite phase)	Point A in Figure 4.56	-	339
80%316+VFA622, (Solution annealed) (Sigma phase)	Point B in Figure 4.56	-	529
VFA543, as-HIP, (Reference alloy consisting of 100% sigma phase)	Figure 4.9	-	1555

4.5. Elemental scans

The elemental scans (Figures 4.65-4.70) provide data on the surface topography and distribution of elements over a pre-defined area. The first scan, designated SE, indicates the roughness of the area i.e. areas which are raised or lowered relative to surrounding areas. Analyses for Mo, Cr, Fe and Ni are also shown. The surface topography is highly dependent on the degree of polishing and surface preparation of the specimen.

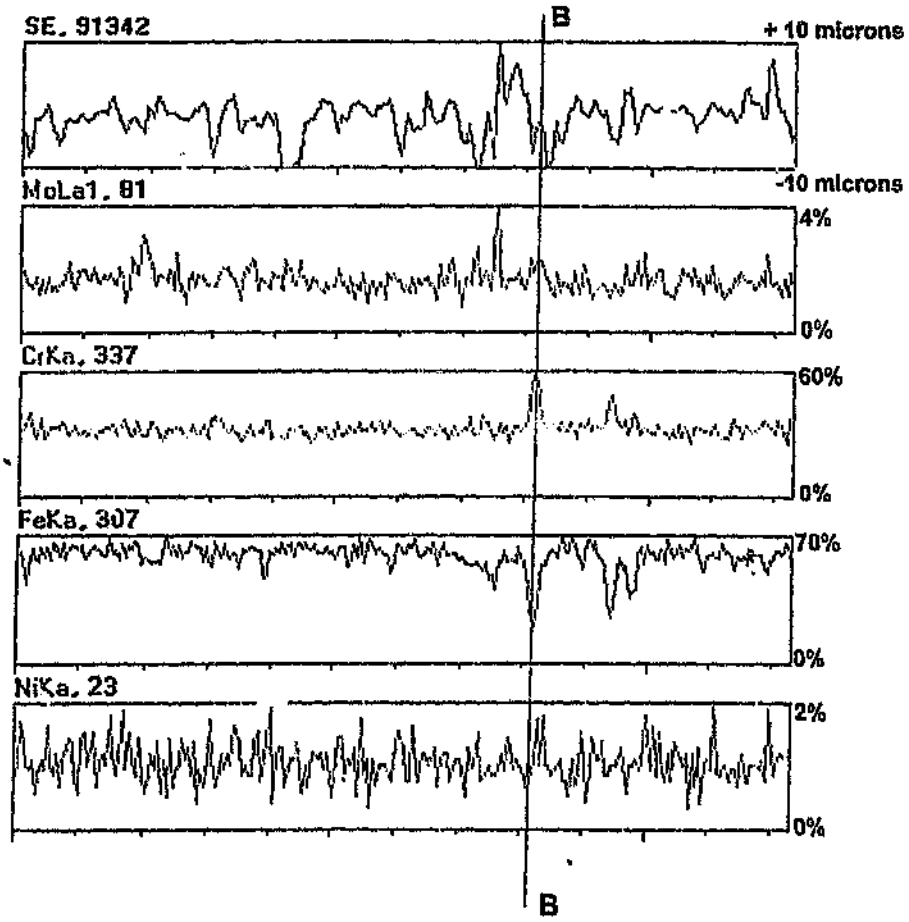

Figure 4.65: Elemental scan of SP001008, As-HIP, (Across 123.3μm).
A Cr-enriched precipitate is shown at B.

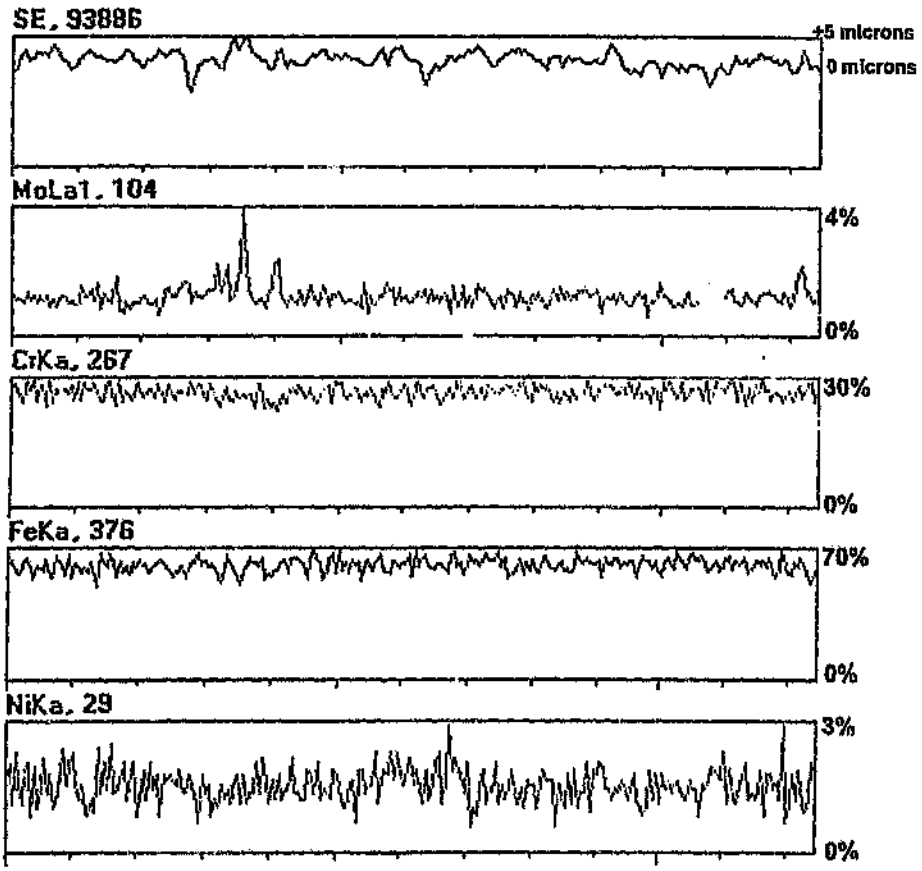

Figure 4.66: Elemental scan of VFA622 + Fe, As-HIP, (Across 124.6μm). Uniform Fe and Cr distribution.

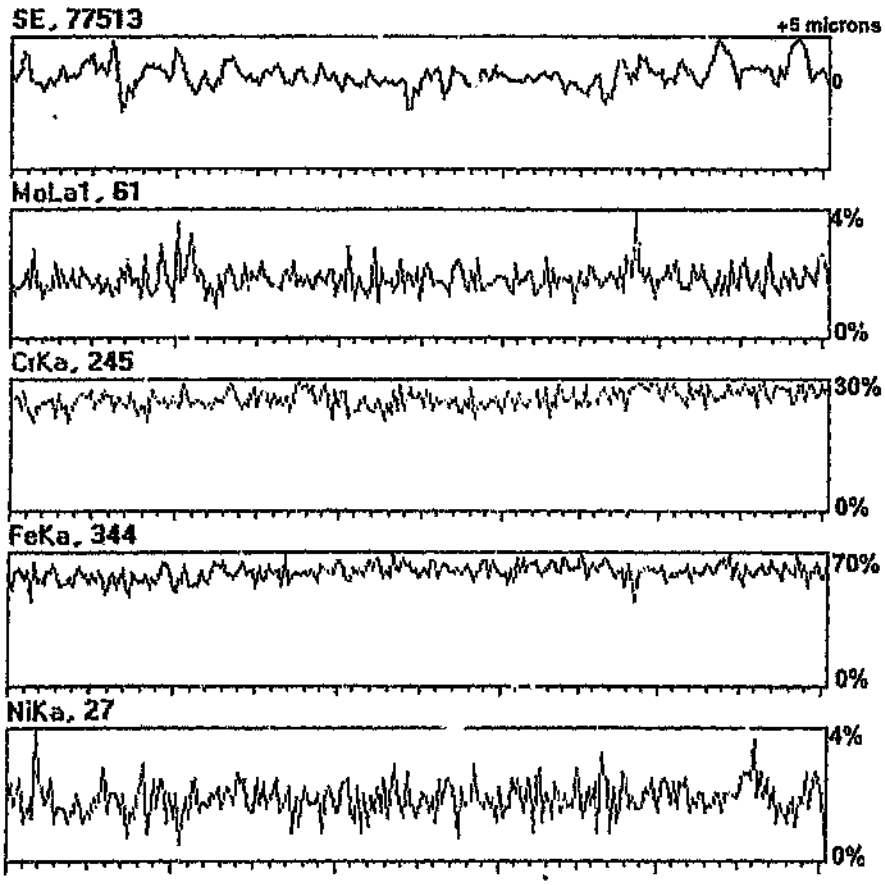

Figure 4.67: Elemental scan of VFA622 + Fe, As-HIP, (Across 504.3μm). Uniform Fe and Cr distribution.

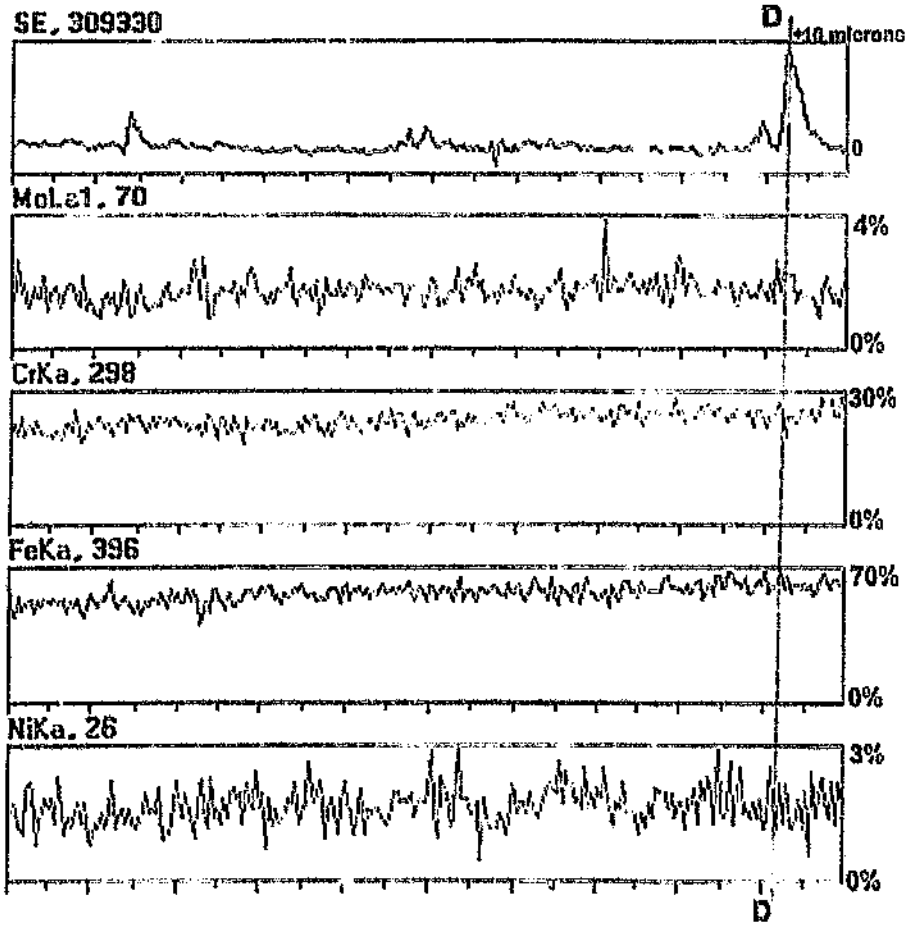

Figure 4.68: Elemental scan of VFA622 + Fe, As-Hill (across 996.6μm). Uniform Cr and Fe distribution.

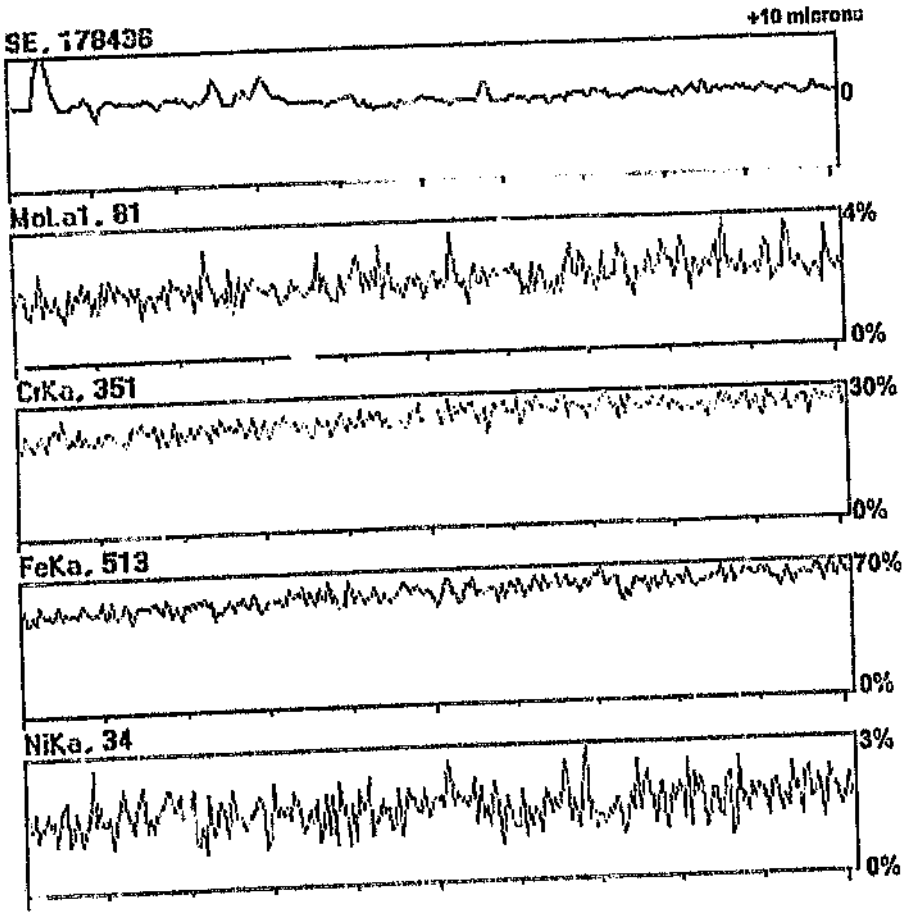

Figure 4.69: Elemental scan of VFA622 + Fe, heat treated, (Across 1011μm). Uniform Cr and Fe distribution after heat treatment.

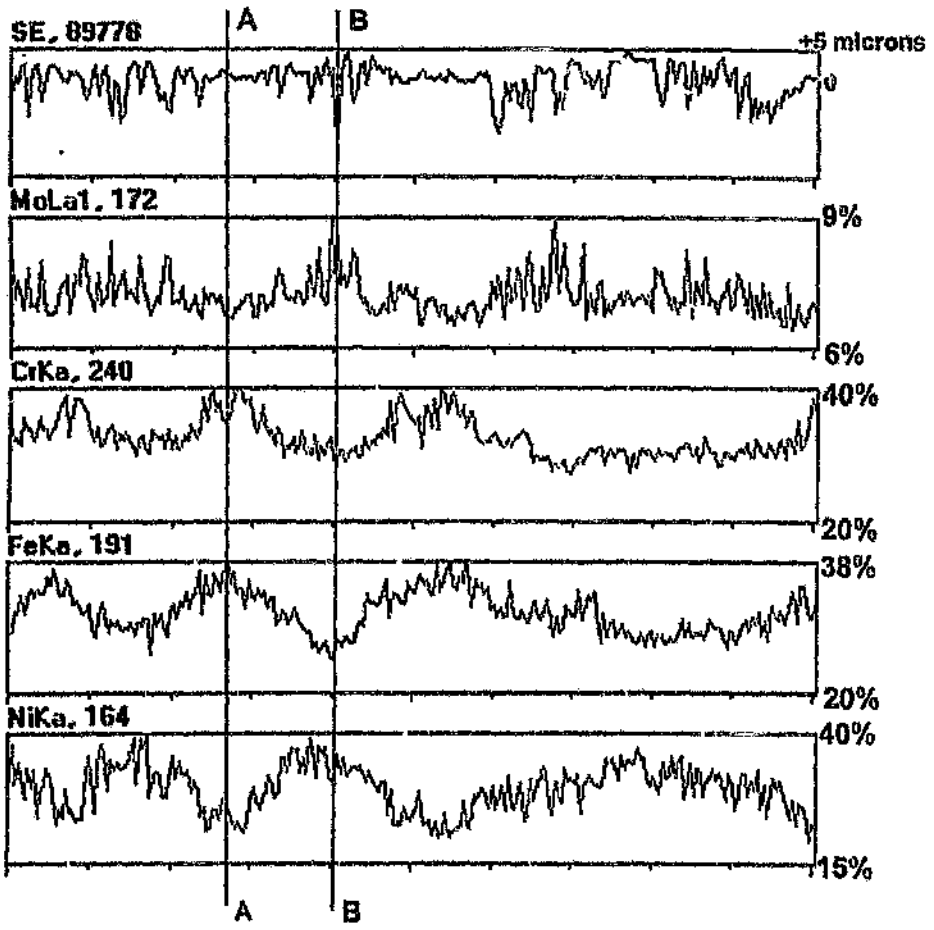

Figure 4.70 Elemental scan of 50% Hastelloy C + 50% Prem V (Across 1605μm).

Large variation in composition as different particles are crossed. The Ni-enriched regions (B) are Hastelloy particles, whilst the Fe-enriched areas are Prem V particles (A).

4.6. Corrosion results in 10% sulphuric acid.

The corrosion results for the alloys tested in 10% sulphuric acid, at room temperature, are presented in Figures 4.71-4.84. The graphs are accompanied by notes.

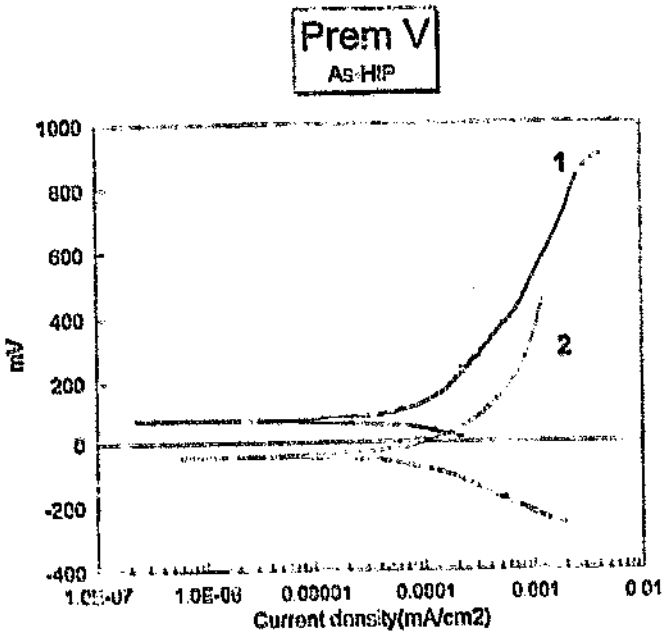

Figure 4.71: Corrosion scan for Prem V, as-HIPped.

Spontaneous passivation in Figures 4.71-4.72.

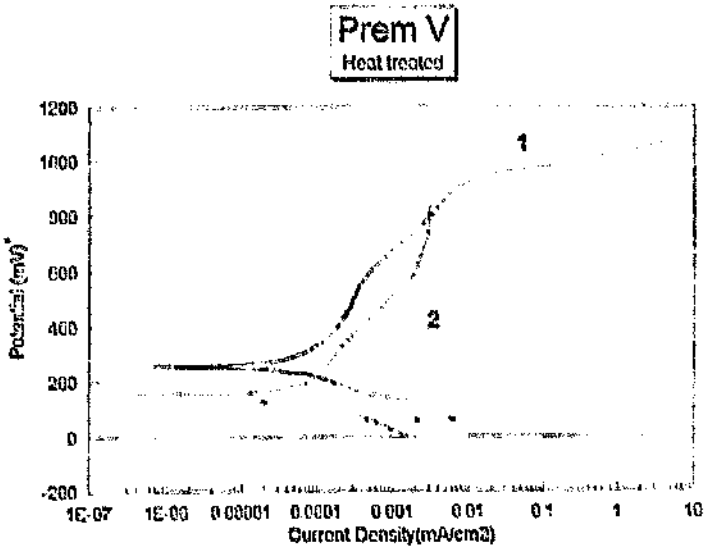

Figure 4.72: Corrosion scan for Prem V, heat treated.

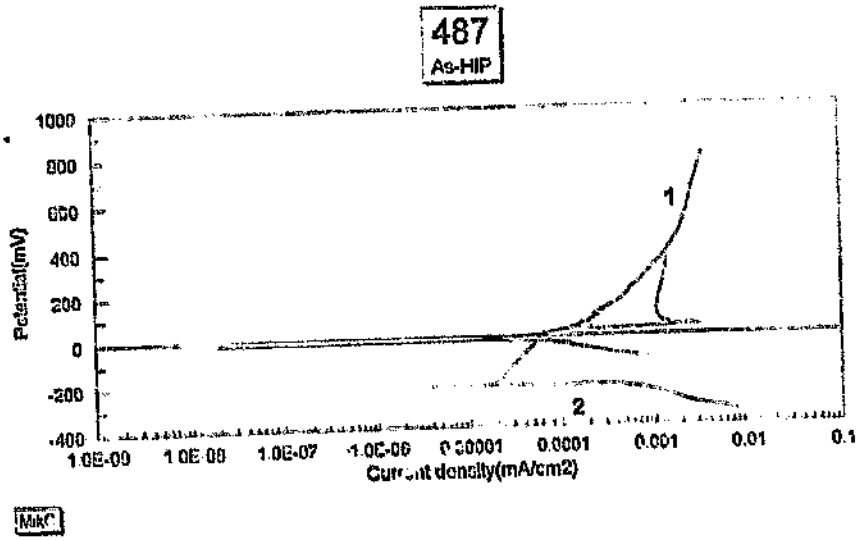

Figure 4.73: Corrosion scan for VFA487, as-HIPped.
Spontaneous passivation. The second scan is non-representative due to poor electrical connection.

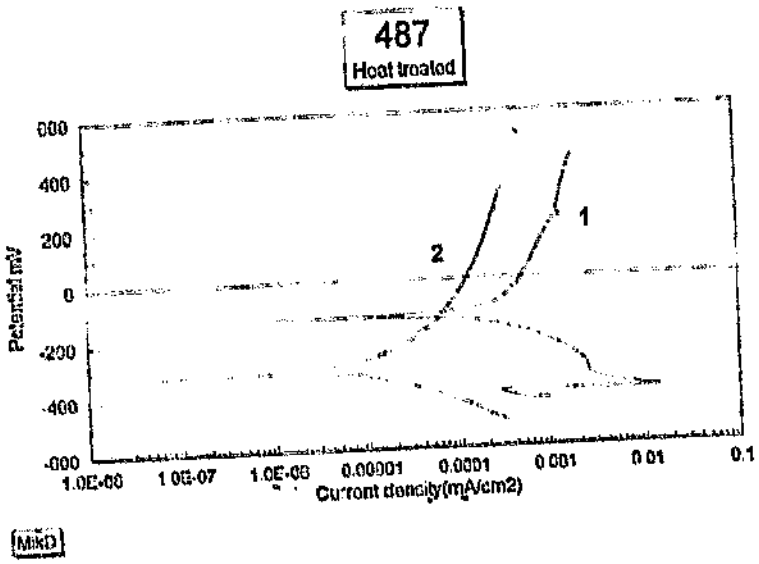

Figure 4.74: Corrosion scan for VFA487, heat treated.
Spontaneous passivation in both scans.

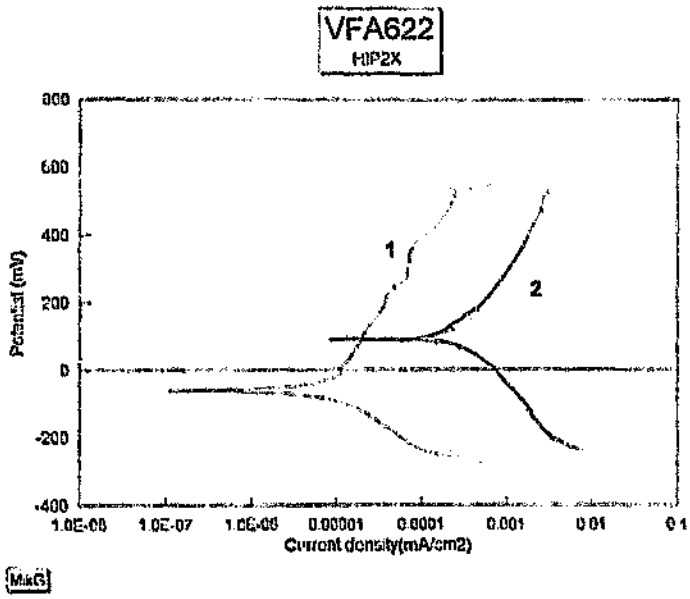

Figure 15: Corrosion scan for VFA622, HIPped(2X).
Spontaneous passivation occurred in both scans.

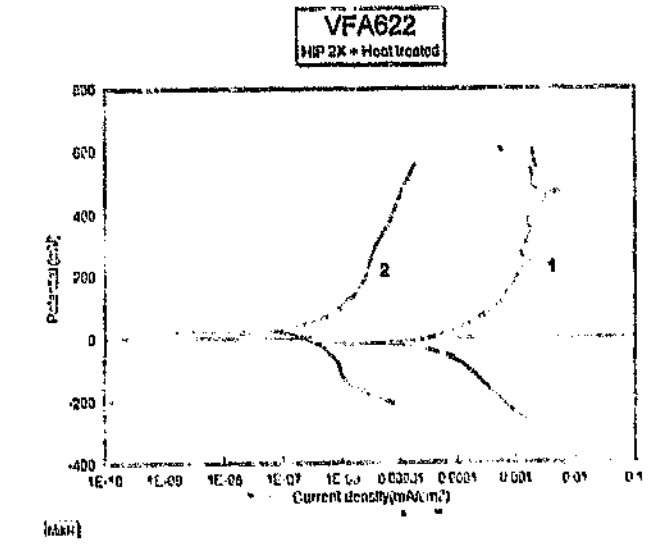

Figure 4.76: Corrosion scan for VFA622, HIPped(twice)+ heat treated.
Spontaneous passivation in the test media.

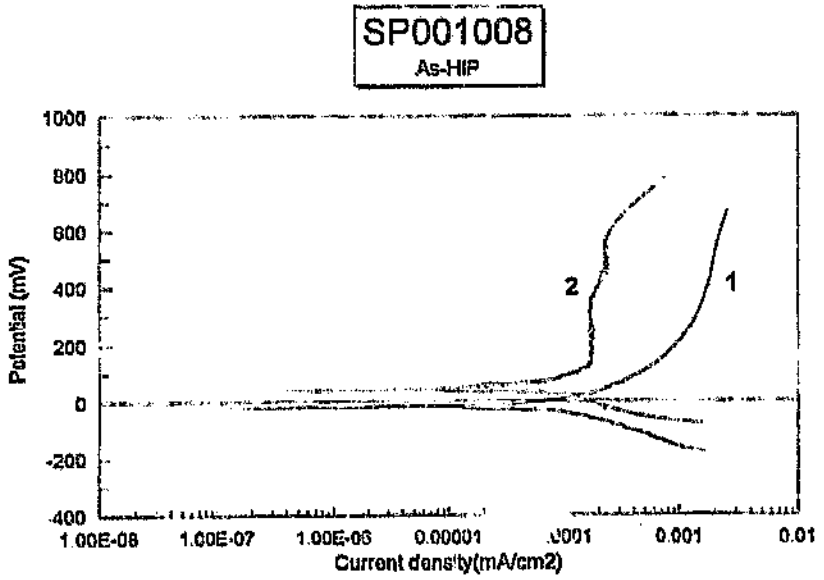

Figure 4.77: Corrosion scan for SP001008, as-HIPped.
Spontaneous passivation in the test medium. The first scan in Figure 4.78 is inconsistent, and should be ignored.

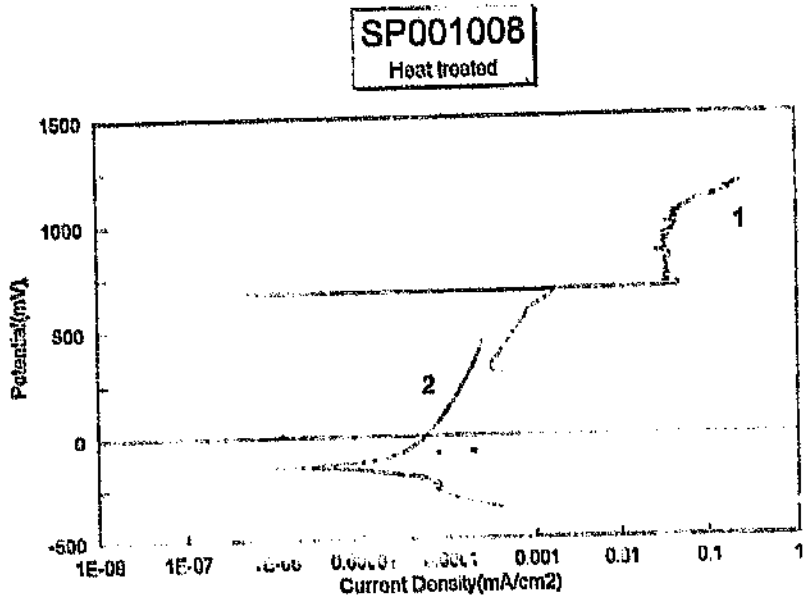

Figure 4.78: Corrosion scan for SP001008, heat treated

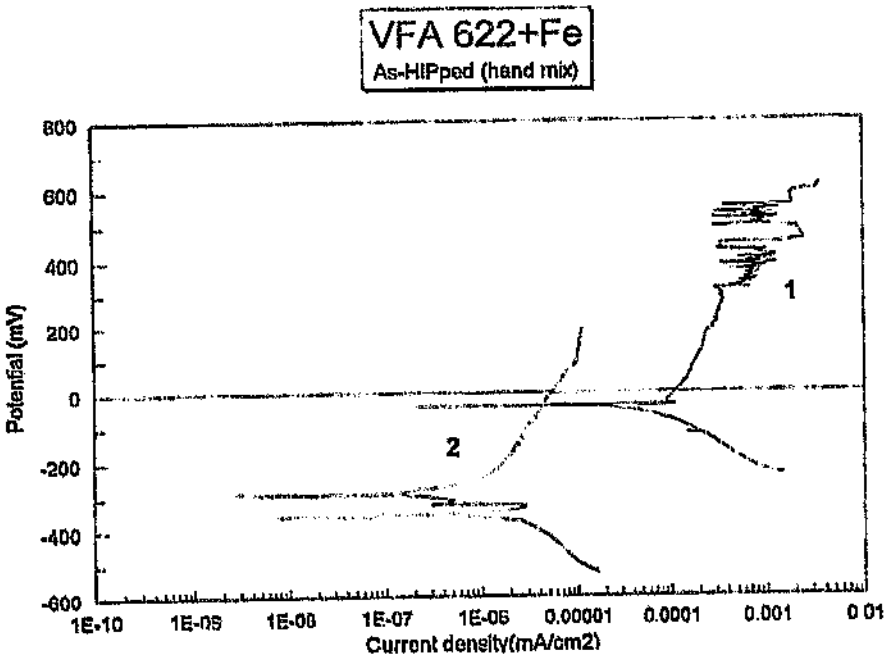

Figure 4.79: Corrosion scan for VFA622 + Fe, as-HIPped.
Spontaneous passivation with unusual behaviour in the first scan of Figure 4.79.

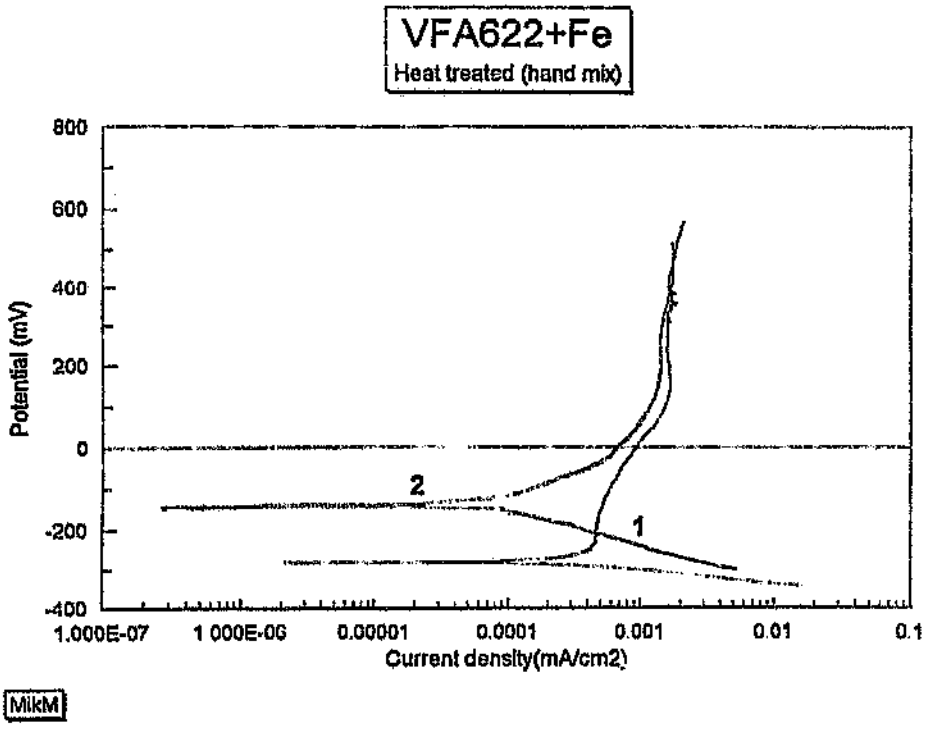

Figure 4.80: Corrosion scan for VFA622 + Fe, heat treated.
Spontaneous passivation in the test medium.

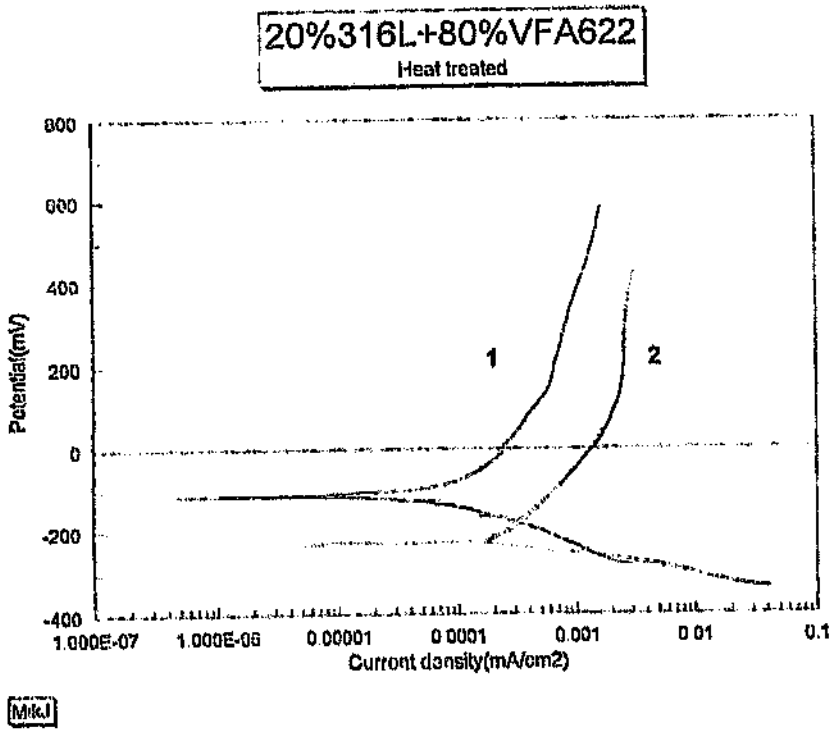

Figure 4.81: Corrosion scan for 20% 316L+80% VFA622, heat treated. Spontaneous passivation with a large variation in E_{corr}.

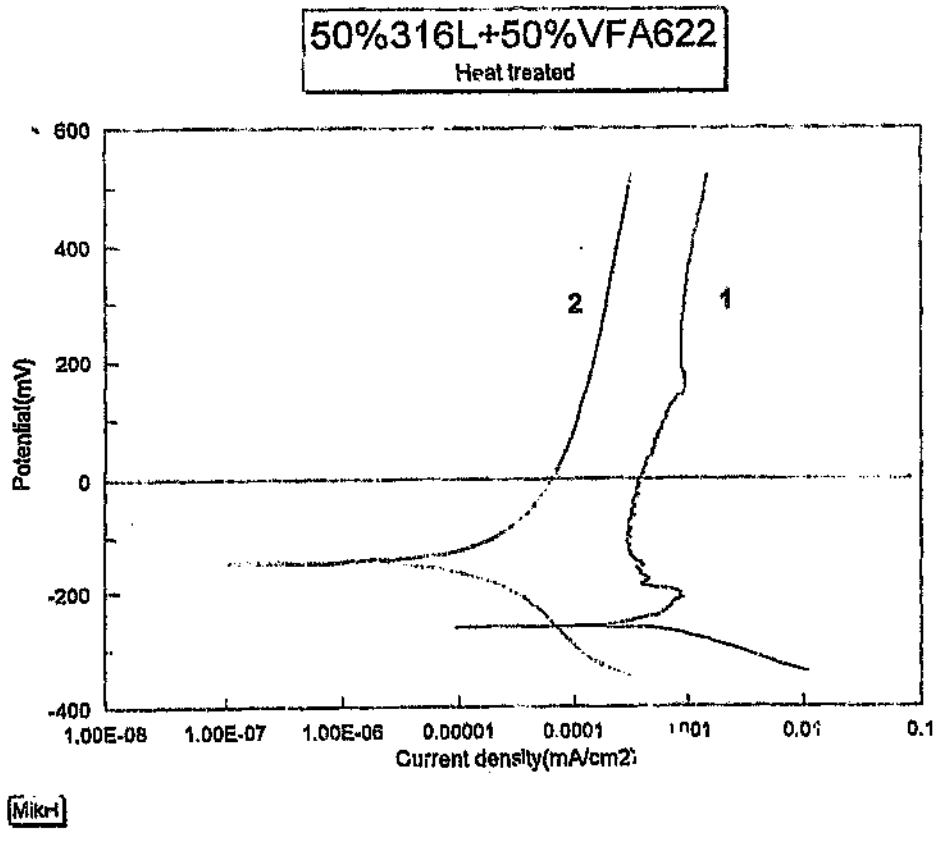

Figure 4.82: Corrosion scan for 50% 316L + 50% VFA622, heat treated.
A small active loop followed by passivation at increasing potential was observed in the first scan. In the second scan, the material passivated spontaneously. A large difference in the E_{corr} values of the two scans was observed.

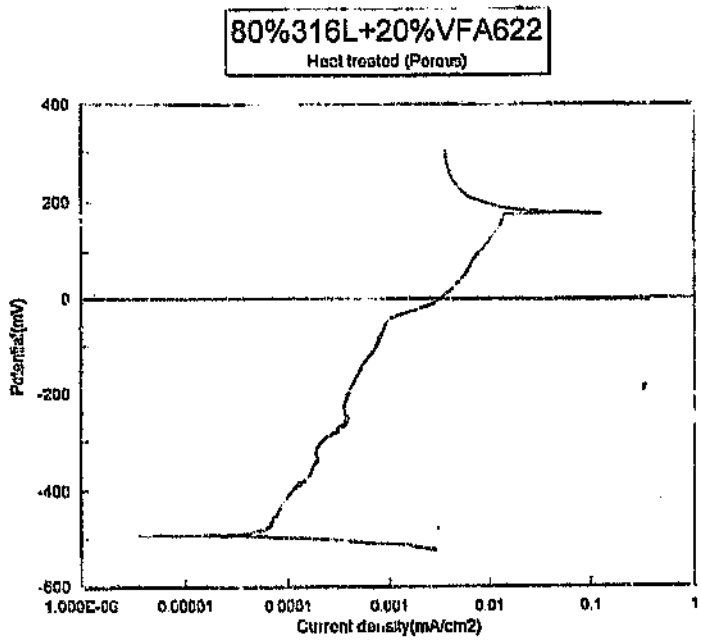

Figure 4.83: Corrosion scan for 80% 316L+20% VFA622, heat treated.
Inconsistent corrosion behaviour arising due to widespread porosity in the HIPped compact. The 80% 316L + 20% VFA 622 specimen contained significant porosity which can produce unpredictable results during potentiodynamic scanning. The scan therefore could not be utilised to characterise the corrosion behaviour of the material.

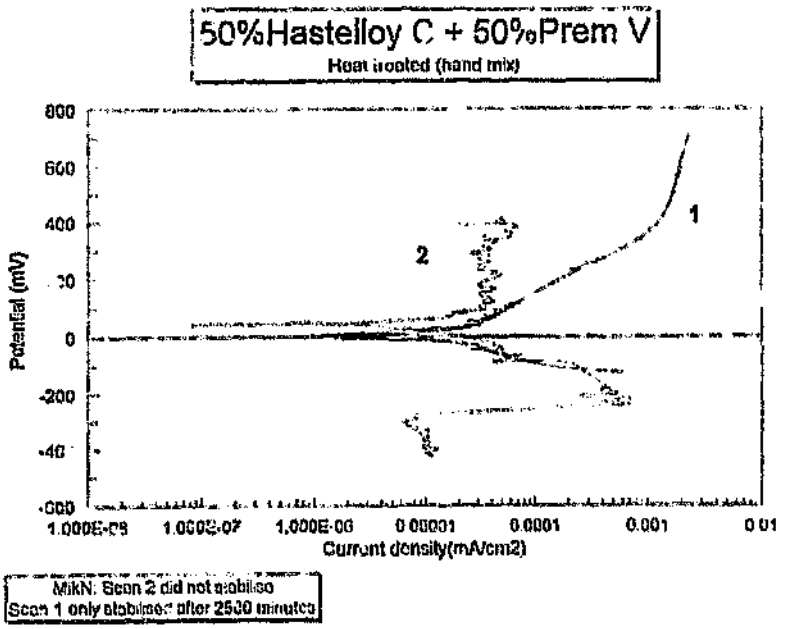

Figure 4.84: Corrosion scan for 50% Hastelloy C + 50% Prem V, heat treated.

This composite alloy required long periods of over 2500 minutes to stabilise in the 10 percent sulphuric acid solution. The potentiodynamic scan is shown in Figure 4.84 (Scan 1). In the first scan, the composite passivated spontaneously with a fairly uniform potentiodynamic curve. In the second scan, the alloy was not allowed to stabilise. This scan exhibited distinct anodic and cathodic curves. However, large degrees of fluctuation were present in both the anodic and cathodic regions of the graph.

4.7. Corrosion results in 70% sulphuric acid at 50°C.

The corrosion results for the alloys tested in 70% sulphuric acid, at 50°C, are presented in Figures 4.85-4.92. The graphs are accompanied by notes.

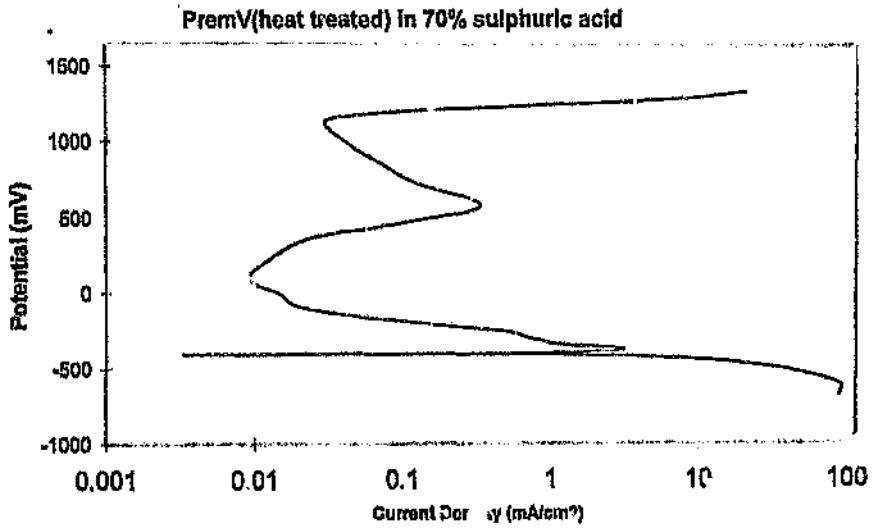

Figure 4.85: Corrosion scan for PremV, heat treated.
Two minima are present in the passive region.

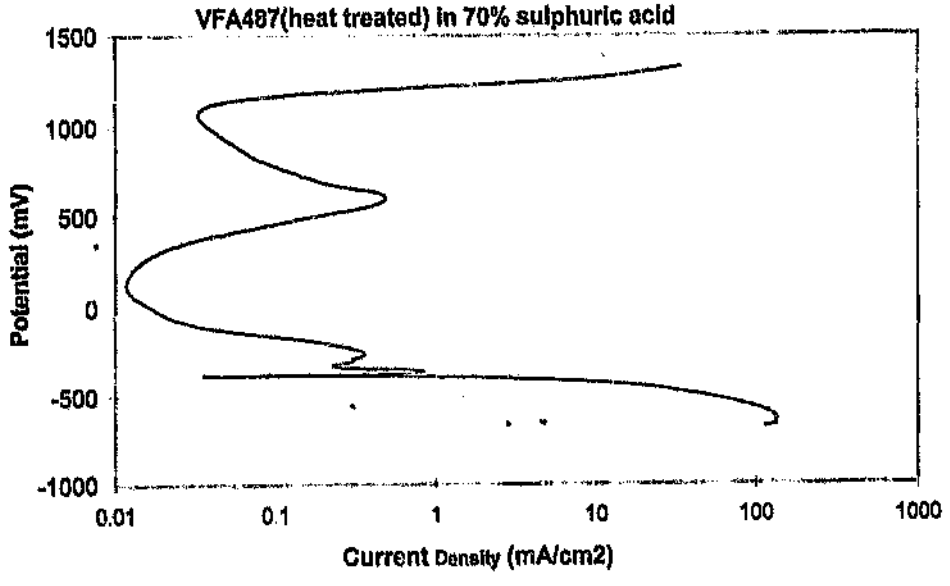

Figure 4.86: Corrosion scan for VFA487, heat treated.
Two minima are present in the passive region.

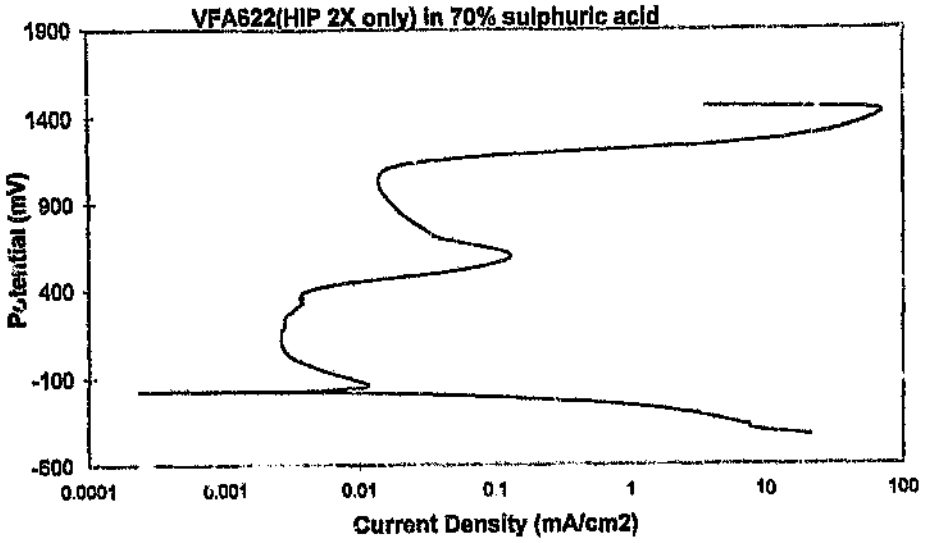

Figure 4.87: Corrosion scan for VFA622, HIPped twice.
A distinct anodic loop is present with two minima in the passive region.

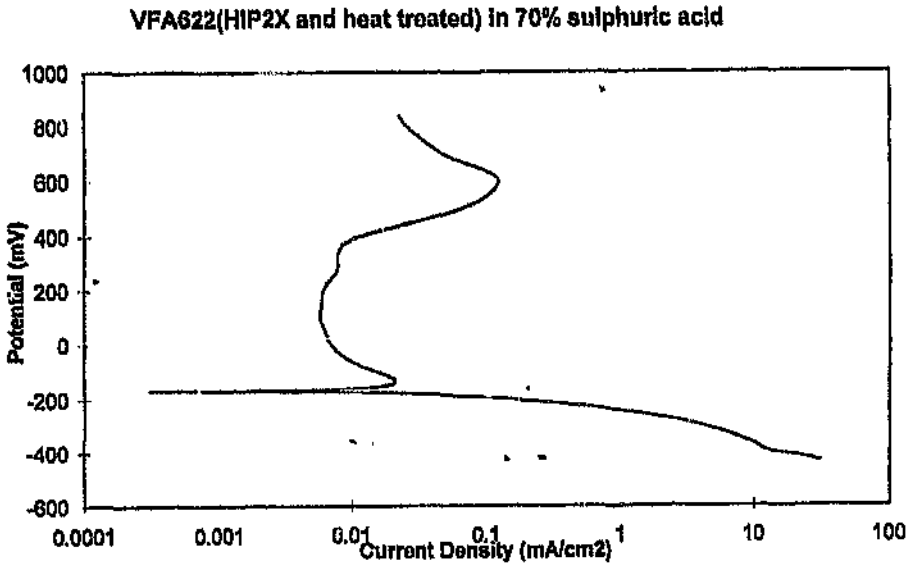

Figure 4.88: Corrosion scan for VFA622, HIPped twice - heat treated.
A distinct anodic loop is present with two minima in the passive region.

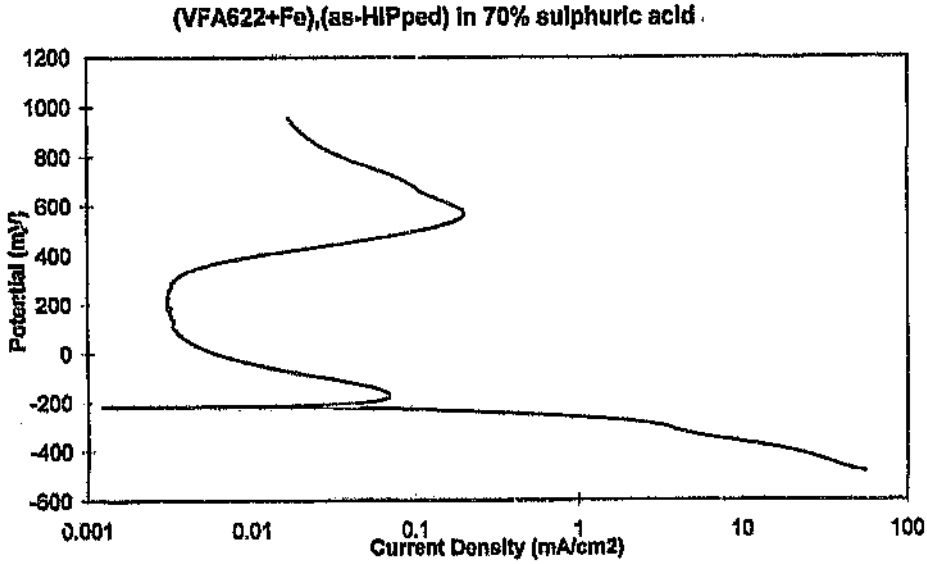

Figure 4.89: Corrosion scan for VFA622+Fe (As-HIPped).
The duplex alloy passivated according to classical behaviour, but exhibited a second minimum in current density in the transpassive region. Solution annealing did not appear to result in significant difference in corrosion behaviour.

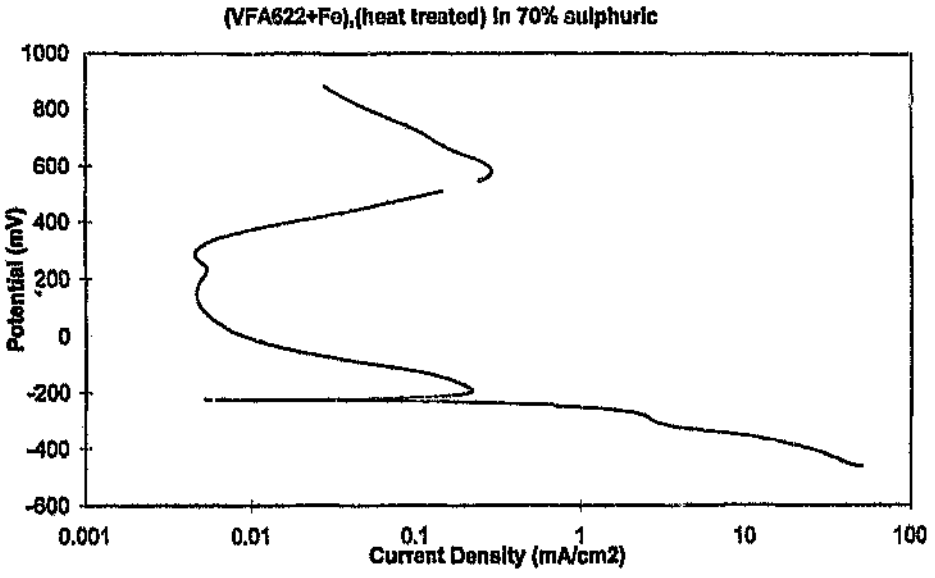

Figure 4.90: Corrosion scan for VFA622+Fe (Heat-treated).

The alloy passivated, but exhibited a fairly high critical current density of 0.6 mA/cm^2.

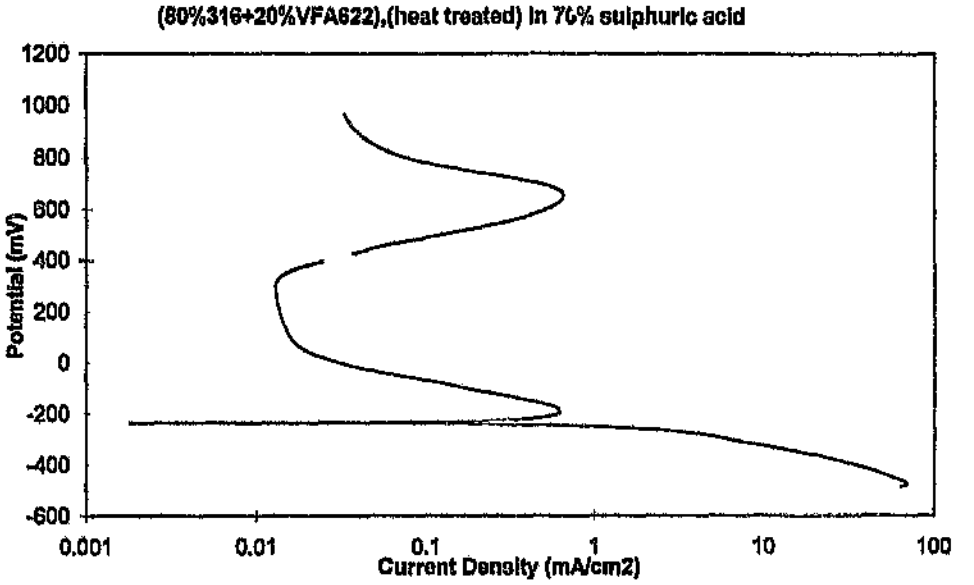

Figure 4.91: Corrosion scan for 80% 316 + 20% VFA622 (Heat-treated).
The alloy had a stable passive region and the transpassive region was not reached, even at an overpotential of 1000mV.

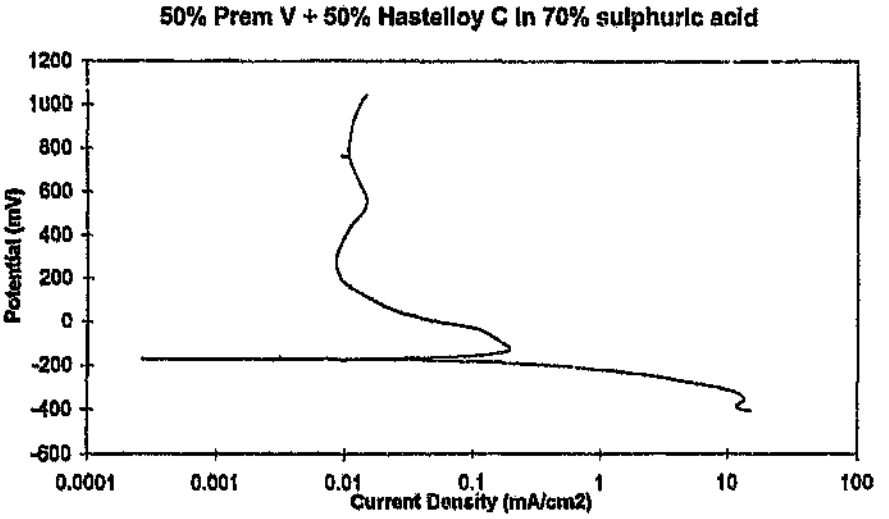

Figure 4.92: Corrosion scan for 50% Prem V + 50% Hastelloy C (Heat-treated). A distinct anodic loop is observed. The alloy remained passive up to an overpotential of 1000mv.

The corrosion results in 10 weight percent sulphuric acid (room temperature) and 70 weight percent sulphuric acid (50°C) are given in Tables 4.15-4.16.

Table 4.15: Summary of corrosion data in 10 % H_2SO_4.

Alloy	Average E_{corr} Relative to SCE (mV)	Anodic intercept (i_{corr}) (mA/cm^2)	Corrosion rate in 10 weight% H_2SO_4 (mm/year)
Prem V As-HIPped	15.56	Average $7x10^{-5}$	0.0008
Prem V Heat treated	209.02	Average $5.34x10^{-5}$	0.0006
VFA487 As-HIPped	-13.82	Scan 1 $10.1x10^{-5}$	0.011
VFA487 Heat treated	-223.38	Scan 2 $2.91x10^{-5}$	0.0003
VFA622 HIPped twice	14.36	Scan 1 $6.97x10^{-5}$	0.0008
VFA622 HIPped twice + heat treated	0.37	Scan 1 $20.8x10^{-5}$	0.0023
SP001008 Heat treated	-146.27	Scan 2 $3.9x10^{-4}$	0.0004
VFA622+Fe (Hand mix,As-HIP)	310.96	Scan 2 $1.03x10^{-5}$	0.0001
VFA622+Fe (Hand mix, heat treated)	-166 41	Scan 2 $68x10^{-5}$	0.0075
80%316L+ 20%VFA622 Heat treated	Porous	Porous	Porous
50%316L+ 50%VFA622 Heat treated	-201.43	Scan 2 $4.18x10^{-5}$	0.0005
20%316L+ 80%VFA622 Heat treated	-172.7	Scan 2 $21.8x10^{-5}$	0.0024
50%Hastelloy C +50% Prem V (Hand mix, heat treated)	22.19	Scan 1 $1.58x10^{-5}$	0.0002

Table 4.16: Summary of corrosion data in 70% H_2SO_4 acid at 50°C.

Alloy	E_{corr} (mV)	i_{crit} (mA/cm²)	Corrosion rate at i_{crit} (mm/year)	i_{pass} (mA/cm²)	Corrosion rate at i_{pass} (mm/year)
VFA552 / Prem V Heat treated	-402.9	3.1	31	$9.3x10^{-3}$	0.093
VFA487 Heat treated	-378.4	0.8	8	$1.1x10^{-2}$	0.11
VFA622 HIPped twice only	-173.5	$1.1x10^{-2}$	0.11	$2.6x10^{-3}$	0.026
VFA622 HIPped twice + heat treated	-168.3	$2x10^{-2}$	0.2	$5.8x10^{-3}$	0.058
SP001008 Heat treated	-96.6	$1.2x10^{-2}$	0.12	$4.4x10^{-3}$	0.044
VFA622+Fe HIP only	-216	$6.9x10^{-2}$	0.69	$3.2x10^{-3}$	0.032
VFA622+Fe Heat treated	-255.4	0.2	2	$4.5x10^{-3}$	0.05
80%316L+20 %VFA622 Heat treated	-235.5	0.6	6	$1.6x10^{-2}$	0.16
50%Hastelloy C + 50% Prem V Heat treated	-173	0.19	1.9	$8.6x10^{-3}$	0.086

4.8. Field trials

At the start of the field trial the two springlocks had masses of 25.309g and 25.228g. After over 5 months exposure in the field trial, no visible corrosive attack was apparent and no mass losses were reported. The sensitivity of the scale used in the trial was 0.2g. No detectable mass losses were reported for the reference 904L springlocks.

5. DISCUSSION

5.1 Powder production

It was noted from the thermomechanical processing procedures that mechanical working of all the experimental alloys was required in order to produce sufficient sigma in a reasonable time. This was in agreement with the results of Cortie et al[25], which indicated that prior working promoted sigma formation. The thermomechanical procedures are summarised in Table 3.2.

The fact that Prem V sigmatised sufficiently after only 24 hours exposure at 850°C indicated that the choice of Fe-39Cr-2Ni-2Mo as a base material was reasonable. The effect of variations in Mo and Ni (sigma stabilisers) content on the ease of powder production could therefore be gauged with regard to this reference alloy.

Important results were obtained from the VFA 390-395 series. These alloys had a combined Ni+Mo (sigma stabiliser) content of less than 3 percent. These materials did not embrittle sufficiently to produce powder, despite prior hot working and over 96 hours heat treatment at 758°C. When these results were compared to those obtained for Premalloy V, it was apparent that minimum levels of approximately 4 percent Ni+Mo were required in order to produce an alloy suitable for powder production.

Alloys VFA 417, 419, 420, 423 (Fe-37Cr-2Ni-4Mo) contained a greater proportion of sigma stabilisers than Premalloy V. However, these alloys required over 96 hours of heat treatment at 758°C in order to embrittle them. This is in direct contrast to the results obtained by Premachandra[21] (Figure 2.10) for an Fe-38Cr-4Mo alloy, in which 90 percent sigma formed after only 15 minutes exposure at 750°C. A possible explanation for this inconsistency may be due to the relatively high Al contents of the VFA alloys. These Al contents ranged from 0.2 to 0.35 percent. It was established by Premachandra[21] that the addition of one percent Al to the Fe-40Cr alloys has a potent retarding effect on sigma formation. Examination of the behaviour of Premalloy V reinforces this possibility. Prem V contained less than 0.02 percent Al and was sufficiently embrittled after 24 hours heat treatment. This compares favourably with previous results obtained for this alloy (Figure 2.16). From Figure 2.12 it can be seen that a temperature of 750°C should be more conducive to powder production.

The air melted alloys DS-1 and DS-C (Fe-36Cr-2Ni-4Mo) embrittled in 21 hours at 850°C, after hot working at 1150°C. DS-1 and DS-C were essentially air-melted equivalents of VFA 417 and VFA 419. Subsequent SEM analysis of DS-1 and DS-C indicated that these alloys did not contain any Al. The longer time required for embrittlement of VFA 417 and 419 may therefore be attributed to their Al content.

The hot working of the Fe-40Cr-2Ni-2Mo-0.4Nb (VFA622) alloy, followed by isothermal annealing at 750°C for four and a half hours produced a structure of virtually 100 percent sigma. This is in line with the results obtained by Premachandra[21] and represents a significant decrease in the time required to embrittle the alloy. Heat treatments over periods of 100 hours, utilised in earlier trials, are thus excessive and unnecessary. This result has important ramifications for the commercial aspects of the alloy. A 2Ni-2Mo alloy may now be embrittled in a substantially shorter time, and thus at a correspondingly lower cost. The most effective procedure for powder production therefore appears to be the combination of hot working an alloy to a 50% reduction in thickness followed by annealing at 750°C.

Crushing and vibratory (Seib) milling of the VFA622 powder proceeded easily. A thin, green layer is present on the surface of the alloy after hot working and heat treatment. This is an oxide scale produced by exposure to air at elevated temperatures. The scale was not removed and was milled into the powder This is undesirable since the scale particles would behave as inclusions in the material. It is recommended that the alloy should be protected by an anti-scaling additive, prior to exposure at elevated temperatures. Alternatively, the alloy could be descaled by the addition of a pickling stage prior to powder manufacture.

An examination, by wet chemical analysis, of the carbon content of VFA622 after vibratory milling (0.024%C) compared to the carbon content of the starting material (0.015%C) indicates that minimal carbon pick-up took place. This is due to the short milling period utilised, as well as the fact that the powder temperature did not rise above ambient. Carbon pick-up would be expected due to interaction with the milling media. The carbon levels in both analyses are at the level recommended for this type of alloy.

5.2 Powder particles

The sharp angular features of the powder particles, in Figure 4.1, are due to the brittle nature of sigma phase. High intensity milling during powder manufacture shatters the sigma thereby producing the characteristic appearance of the particles. Spherical, atomised powders are usually preferred for HIP applications, due to their higher flowability and consequently more even packing densities. However, these trials have shown that the conchoidally fractured powders are also acceptable. The larger powder size distributions, typically less than 500 microns, are the more easily packed. Smaller size fractions of under 45 microns are less useful since there is a tendency to form agglomerates. The agglomerates result in less efficient packing of the powder and consequently uneven shrinkage during consolidation.

5.3. The effect of time at 750°C on hardness

VFA654 exhibits a dramatic increase in hardness from 13 to 49HRc after only 4 hours heat treatment, as shown in Table 4.2 and Figure 4 8. The appearance of macroscopic cracks in the region of the hardness indentation are indicative of material embrittlement. Additional isothermal treatment for a further 4 hours resulted in a hardness of 58HRc. Another 4 hours of exposure produced an increase of only one hardness point to 59HRc. This indicates that a hardness plateau is reached (Figure 4.8) and that further heat treatment is unlikely to produce significant increases in hardness.

Alloy VFA647 (Figure 4.8) exhibited different behaviour. The alloy softened from 16HRc to 11HRc after two hours at 750°C. After 8 hours heat treatment, the material remained at this hardness value This data indicated that no sigma phase formed during this period. The decrease in hardness from 16HRc to 11HRc is most likely due to stress-relief brought about by the isothermal annealing. After rolling, the plastically deformed material retained residual stresses, which tend to increase the hardness. Heat treatment removes these stresses, hence the lowered Rockwell C values.

Appreciable hardening of VFA647 only began after 16 hours of heat treatment. The trend was very gradual and after approximately 45 hours the hardness was only 34 HRc. Finally, after 89 hours, a maximum of 54HRc was obtained. At this value the material was not sufficiently brittle for powder production. It can therefore be seen that the kinetics of sigma phase formation in VFA647 are far slower than in VFA654. The important result from this trial is that that alloy VFA654 embrittled sufficiently after twelve hours heat treatment, and that a hardness of 59HRc has to be achieved before the alloy is ready for powder production.

The vastly differing behaviour between VFA647 and VFA654 is considered unusual, since both alloys are very similar in composition. VFA654 contains 0.6 percent more Cr than VFA647, but has 0.26 percent less Ni. Both elements promote sigma formation. However, VFA654 also has 0.34 percent Nb, allegedly a sigma retardant. Therefore, from a purely compositional basis, it would be expected that VFA647 would have the greater tendency to be embrittled.

A possible explanation could be that the 36Cr-2Ni-2Mo-Fe alloy is at the lower limit of the composition range for "quick" sigma formation. Another possibility is that slight differences in the working of the material lead to large differences in the rate at which sigma is formed.

The results of these trials indicate that 36Cr-2Ni-2Mo-Fe is the minimum alloy composition which should be considered when manufacturing powder to be used in hot isostatic pressing. In addition, powder can be manufactured when the steel reaches a hardness of 59 HRc or greater. Hardness values can thus be utilised as an easily-monitored indicator during any future powder manufacturing processes.

5.4 Mechanical mixing of Al (SP001005)

As can be seen from Figures 4.2-4.3, ball milling is successful in greatly reducing the particle size of the alloy. A reduction in average particle size from 63 microns to 4 microns took place. This implies that the sigmatised material can be successfully communited by ball milling if such a requirement should ever arise.

The combustion of the powder during welding is unexpected. An examination of the literature provides possible explanations[33]. It is well known that the reactivity of a metal powder increases as the particle size decreases. This is due to the fact that a greater free surface area is exposed. When this free surface area is exposed to the appropriate atmosphere and the necessary temperatures, there exists the high probability that a chemical reaction between the metal and atmosphere will occur, at an accelerated rate. In the case of aluminium a typical reaction in air would be :

$$2Al(solid) + 1.5\ O_2(gas) \rightarrow Al_2O_3\ (solid)$$

Heat of formation = -1692 kJ/mole

This reaction is highly exothermic and it is for this reason that powdered Al is often used in high energy rocket propellants and explosives. In fact, Al is often the primary ingredient in many explosive applications.

It is considered probable that this reaction is the cause of the flames observed during encapsulation. The necessary activation energy would be supplied by heat from the weld arc, with localised temperatures reaching over 1000°C, whilst oxygen would be derived from the atmosphere.

Other deductions may be made from this trial. A successfully mechanically alloyed material should contain powder particles with a uniform and desired composition throughout each powder particle. It is considered unlikely that a homogeneous 2Ni-3Mo-2Al-40Cr-Fe alloy would be easily combustible since the Al atoms would be a minor alloying constituent, held in solid solution. Incomplete alloying would result in an Al layer enclosing each 40Cr-Fe particle. It is this Al layer which would combust during welding. This is highly probable when it is considered that an acetone lubricant was used during milling. The acetone effective acts as a barrier between the milled particles and hinders diffusion of Al into the Fe-Cr particles. The results of SEM and EDS examination of the mechanically mixed powder are shown in Figures 4.4-4.5 and Table 4.12. The micrograph (Figures 4.4) indicated the powder particles had formed into ovoidal agglomerates during milling.

A detailed examination in Figure 4.5 revealed the agglomerates to consist of a porous network of mechanically bonded Fe-Cr particles. No distinct Al particles were observed or detected by EDS analysis. The analysis of individual powder particles (Table 4.12) confirmed the presence of Al on surface of the Fe-Cr particles.

Free aluminium would also pose a number of problems during the actual HIP stage itself. From the Al-Fe phase diagram (Figure 5.1), it can be seen that Al-Fe alloys containing 85 percent Al or greater have a liquidus temperature of under 1000°C. Since HIPping occurs at 1120°C it can be seen that a liquid phase would be present. In addition, the L + θ region has as its lower limit the 655°C [L $\rightarrow \theta$+(Al)] eutectic temperature. Thus any temperature in excess of this for alloys of more than approximately 62% Al will have some liquid phase, and higher temperatures will mean a higher proportion of the liquid phase. This is highly undesirable because a liquid phase would be deleterious to the microstructure of a powder, since it could induce hot cracking at grain boundaries. In addition, the molten metal attacks the mild steel canister and results in canister leakage and destruction.

In view of the potential dangers involved it is recommended that further work on the mechanical mixing of Al-40Cr-Fe powders should be discontinued.

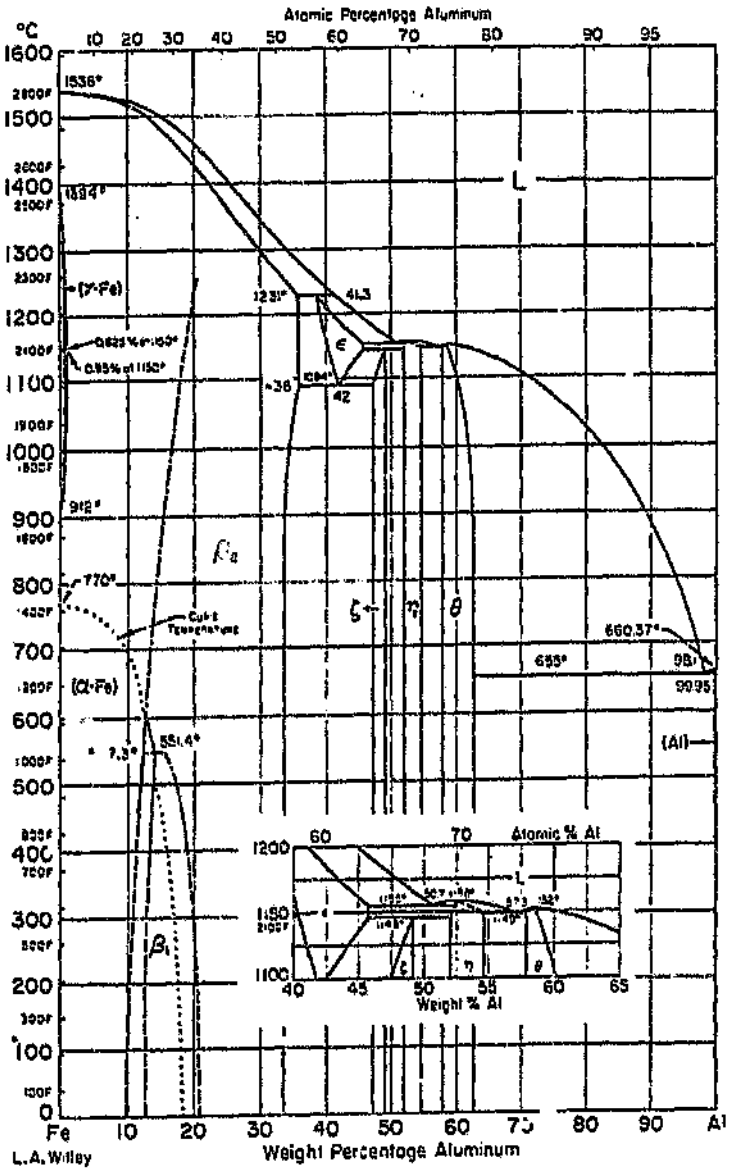

Figure 5.1: Al-Fe phase diagram.[9]

5.5. Mechanical mixing with extra Fe (SP001008)

Alloy SP001008 had an average particle size of 4 microns after 72 hours milling (Figure 4.3). After only 24 hours milling the average particle size of SP001008 was reduced from 63 microns to 6 microns (Figure 4.7). This particle size is close to that of SP001012 and indicates that a milled particle size limit exists. It therefore appears that milling for periods beyond 24 hours are ineffective in achieving any further significant particle size reduction. This is important if material communition is the central aim in the use of ball milling, since it shows that more and more energy input is required, with diminishing returns. The concept of a mill limit is shown in Figure 5.2. The effect of the Fe alloying addition on particle size is considered minimal, since Fe is relatively soft compared to the sigmatised 40Cr powder and is already fine.

Since both this alloy and SP001005 have a normal size distribution, it may be taken that this is the response of the 40Cr-Fe material to the mill parameters used. It must be mentioned, that any modification of the mill parameters will generally produce a different result in the distribution of the final particle size fractions.

The chemical analyses of the starting and final powders (Table 4.1) are particularly interesting. The starting materials have a carbon content between 0.025 and 0.056 percent and an oxygen content between 0.078 and 0.141 percent. The milled product contains 0.176 percent carbon and 0.281 percent oxygen. The increase in carbon and oxygen content therefore cannot be due to the existing levels in the starting material. In all likelihood, the carbon pick-up occurred by interaction of the mill media and powder. Considering the very nature of high energy mechanical mixing, in which cold welding is promoted, it is considered likely that carbon from the milling media and mill body contaminated the powder. Oxygen pick-up could be also be due to interaction with milling media. However, another possibility exists in that oxidation of the reactive, milled powder surfaces could have occurred during the drying (acetone removal) stage. During this sixteen hour period, the powder was completely exposed to the atmosphere.

These results are important since they indicate certain pitfalls inherent in the mechanical mixing technique. The 40Cr-Fe alloys require extremely low carbon and nitrogen contents, usually each of the order of 0.02 percent and less. Extreme care is taken in the preparation of these alloys, e.g. in the use of vacuum melting, to ensure low interstitial levels. It is therefore apparent that the raised carbon and oxygen levels brought about during milling are undesired. Ball milling, and mechanical mixing as such, should not be completely excluded from future work, since certain rectifications are possible. Milling media with a low carbon content could be used. Acetone removal can also be achieved in the presence of a vacuum.

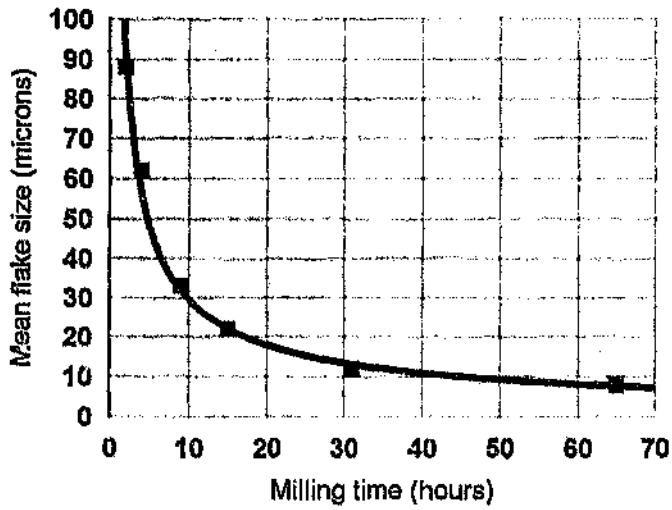

Figure 5.2: Mill limit.[33]

5.6 Metallographic examination of alloys from single powders

A summary of the compositions of alloys manufactured from a single powder is given in Table 3.1, whilst the hardness values are summarised in Table 4.13. The observation of inclusions at particle boundaries is a common feature of HIPped powders and was not unexpected. Powders have a high surface area, and are vulnerable to surface oxidation. In addition, contamination of powders during milling often occurs. Even gas atomised powders exhibit a certain amount of interparticular inclusions. However, the powders produced by the Mintek process have a far higher degree of these inclusions than observed in gas atomised powders. These inclusions are detrimental since they interfere with the diffusion bonding process. However, their effect on the properties of the current alloys has yet to be evaluated. It is significant to note, however, that the inclusions are not continuous at the particle boundaries. A continuous contaminant film would be highly deleterious, and it is known[34] that mechanical properties are greatly affected if such a film is present

The air-melted alloys, DS-1 and DS-C exhibited a far greater amount of inter- and intraparticular inclusions than the vacuum-melted alloys. This was a direct result of the air melting process, since the melt would have had a far greater chance of reacting with the atmosphere or other agents. The detrimental nature of inclusions has already been mentioned. The degree of contamination within these alloys would be sufficient for rejection of the powder, if the acceptance standards for gas atomised powders were applied.

The quality of any powder is dependent on the quality of the initial melt. A clean, contaminant-free powder is always desirable. Therefore, whilst producing alloys by air-melting may offer certain initial economic advantages, it appears that improved final results would be obtained by using vacuum melting instead. Cleaner powders result in a improved final properties. This is important since the HIP process does not remove any impurities which are already present within a powder.

After HIPping, all the Fe-38Cr-4Mo-2Ni alloys contained interconnected networks of sigma occupying between 70 and 100 percent of the microstructure. Severe macroscopic cracking occurred in all specimens during sample cutting and preparation. Since the cracking occurred to a similar extent in all the alloys the microstructure of VFA543 is shown in Figure 4.9 as a representation of these alloys. Many of the alloys did not respond well to solution annealing. Sigma contents of between 90 and 30 percent were still present in some of the alloys (VFA 417,VFA 419). These are shown in Figures 4.9-4.22.

The microstructure of DS-1 after solution annealing is shown in Figures 4.10-4.11, and appears ferritic with some sigma phase at the particle boundaries. The annealed microstructure of DS-C, in Figures 4.12-4.13 is ferritic, with heavy sigma phase precipitation at some particle boundaries. A ferrite and sigma duplex microstructure was observed in VFA417 (Figures 4.14-4.15). The large crack running through the material, shown in Figure 4.14 was present in the as-HIPped state and could not be removed by heat treatment. A higher concentration of fine precipitates near the crack is noticeable. Figure 4.16 shows a high concentration of precipitates was present at the particle boundaries of VFA419. The precipitates also occurred within individual sigma and ferrite regions, in Figure 4.17, and generally appeared finer in the sigma phase. The overall microstructure of VFA 419 consisted of ferrite and sigma phase. The microstructure of VFA420, in Figure 4.18, indicated only partial transformation from sigma to ferrite after solution annealing. A large number of precipitates were present in both phases. A large crack passing through both ferrite and sigma may be seen in Figure 4.19, confirming that heat treatment alone does not provide a driving force for crack closure. VFA423 with residual sigma in a ferrite matrix is shown in Figures 4.20-4.21. Inclusions at the particle boundaries are apparent in Figure 4.20. VFA543 (solution annealed) in Figure 4.22 was mainly ferritic with localised bodies of sigma phase.

The Fe-40Cr-2Ni-2Mo alloys were less likely to form high proportions of sigma phase. Prem V and VFA487 (Figures 4.23-4.28) exhibited approximately 20 percent sigma after HIPping and had hardnesses of 289Hv and 274Hv respectively. The sigma phase occurred in large, isolated and sometimes transparticular bodies in Prem V, whilst in VFA 487, it occurred preferentially at particle boundaries.

After solution annealing, both alloys only exhibited traces of sigma. Secondary phases which were found only in the diffusion zone were apparent in Prem V. These phases were definitely harder than the ferrite phase since they did not exhibit the same degree of polishing scratches as the matrix (Figure 4.23). These phases were possibly a form of sigma phase. Their occurrence in the diffusion zone would imply that they would have a slightly different composition to the sigma found in the core of the compact. This could allow them to be more resistant to solution annealing and could explain their presence after heat treatment. Their morphology and scratch resistance are consistent with the properties of sigma phase. The difference in appearance of the boundary zone relative to the bulk of the compact is due to the diffusion between the mild steel and the Fe-40Cr alloy. VFA 487, in Figure 4.27, provided an example of plastic deformation around a Vickers hardness indentation.

Slip lines were clearly seen in the immediate vicinity of the indentation. The plastic deformation produced the uneven edges of the indentation.

Solution annealing removed most of the bulk sigma in Prem V and VFA487, as can been seen in Figures 4.24-4.28. Some secondary phases in the diffusion zone of Prem V (Figure 4.24) were not removed. The extensive white region at the top of the micrograph is the area which was in intimate contact with the mild steel canister, and therefore has a decreased corrosion resistance. The region is thus more readily attacked by the HCl etchant. Figure 4.25 shows the general ferritic microstructure of Prem V. Inclusions (dark grey) , heavily enriched in Cr and Ti, whilst being deficient in Fe, were observed both within the particles and at the particle boundaries. The composition of these inclusions is given in Table 4.3. The high Ti (23%) content of the inclusions implied that they were definitely not a precipitate or phase inherent to the Fe-40Cr-2Ni-2Mo alloy. The presence of the inclusions within the actual particle body, and not at the particle boundary, indicates that the inclusions were most likely introduced during the casting process and were not due to contamination during powder manufacture.

VFA622 was severely cracked after HIPping and had transformed to virtually one hundred percent sigma phase. No hardness measurements could be taken, since massive cracking obscured the Vickers indentation. However, a value in excess of 800Hv would be expected. The as-HIPped microstructure is not shown, since it is similar to Figure 4.9. Solution annealing was successful and all visible signs of the sigma were removed. The hardness was measured at 253Hv. Figures 4.29-4.30 show ferrite grains rich in intergranular/interparticular precipitates without any traces of residual sigma. The precipitates were extremely fine and barely resolvable at 1000X magnification.

The comparative microstructures of VFA622 in the HIPped and solution annealed state, cast and HIPped state and HIPped twice state are shown in Figures 4.29-4.35. The cast material, initially fully sigmatised, had a fully ferritic microstructure after solution annealing. The annealed hardness value was 238Hv. The HIPped, annealed material still exhibited traces of sigma, and had a hardness of 253Hv. The cast, solution annealed alloy increased in hardness from 238Hv to 276Hv after HIPping. The ferritic microstructure and large grain size of VFA622 (cast and HIPped) is shown in Figure 4.31. Widespread intragranular precipitation of fine spherical carbides and nitrides can be observed. Figure 4.32 shows a detailed view of precipitates within a ferrite grain of VFA622 (cast and HIPped). The prior grain boundaries can clearly be seen.

The HIPped and solution annealed microstructure of VFA622, in Figure 4.33, appeared similar to the cast material in that the matrix consisted of ferrite grains with fine but prominent precipitates. However, the particle/grain size of the HIPped steel was finer. This was due to the smaller particle size of the starting powder. Prior particle boundaries are also apparent in Figure 4.33. A ferrite matrix with sigma forming preferentially at the particle boundaries of VFA622 (HIPped twice) may be seen in Figure 4.34. There was a low concentration of the sigma ase compared to the sample which was only HIPped once (Figure 4.9). Figure 4.35 shows preferential sigma growth at particle boundaries, with some nucleation within the ferrite particles.

One aim of this investigation was the development of an alloy which could be easily converted to powder, and yet still remain free of sigma phase after passing through the slow HIP cooling cycle. The fact that all specimens exhibited sigma phase after HIPping indicated that a suitable composition had not yet been established. The proportion of sigma in the specimens, after HIPping, varied between 20 and 70 percent. These results were unexpected. Over 96 hours of sustained heating was required to form sufficient sigma in order to produce powder, and yet 70 percent sigma was formed in certain alloys after passing through a single HIP cooling cycle. This may be due to certain forging effects exerted on the powder particles during the HIP process. The applied pressure would increase the tendency for the formation of lattice defects whilst the application of heat would tend to anneal the defects. The differences in the rate of sigma formation may also be due to the use of continuous cooling as opposed to isothermal conditions.

Premalloy V (Fe-39Cr-2Ni-2Mo) exhibited the least sigma (20 percent) after HIPping. Attempts to decrease the Ni and Mo content by small amounts were unsuccessful since the resulting alloys did not embrittle sufficiently to form powder. A 2 percent increase in the Mo content (VFA 417) resulted in a substantial increase in percentage sigma. Decreasing the Cr content (VFA487) had no discernable effect. These results highlight the sensitivity of the Fe-37Cr alloy to slight variations in the amount of sigma stabilisers added, i.e. small variations in Mo content have a greater effect on sigma formation than equivalent variations in Cr content.

The fact that most of the alloys were free of sigma after solution annealing and quenching indicated that the procedure could be used successfully to remove the phase after HIPping.

However, VFA 423 (Fe-37Cr-2Ni-4Mo-0.2Ir), DS-1 (Fe-36Cr-2.6Ni-4Mo) and DS-C (Fe-36Cr-2Ni-4Mo-0.3Ru) still retained residual sigma. The behaviour of VFA423 and DS-C could be due to the possibility that the platinum group metals act as sigma stabilisers. However, at present there is no direct evidence to support this suggestion. The behaviour of DS-1 (cast in air) was initially considered unusual since an equivalent alloy of similar composition, VFA 417 (cast in vacuum), responded favourably to solution annealing. However, VFA417 did contain 0.21 percent Al which would inhibit sigma formation.

The presence of sigma after HIPping may not be entirely detrimental. There is evidence[3] that the dissolution of sigma phase, in the appropriate morphology, may improve toughness by inducing mobile dislocations after solution annealing. This aspect should be kept in mind in future work.

5.7. Fe-40Cr-4Mo-2Ni alloys

Alloys such as Prem V and VFA 487 have a nominal composition of 2Ni-2Mo-38Cr. It was felt that the corrosion resistance of these alloys could be increased with the further additions of 2 percent molybdenum. Furthermore, additions of ruthenium and iridium, singly and together, were also made. The aim of the trial was therefore, in terms of chemical composition, to produce a highly alloyed 38Cr steel with the maximum corrosion resistance.

All of the 2Ni-4Mo alloys exhibited severe cracking after HIPping. This effect was not as easily observed in earlier trials since specimens with a smaller circular cross section were used. On larger test pieces, the cracks were more readily apparent and are due to the formation of bulk sigma throughout the microstructure. Since Mo is known to be a potent sigma former, it is apparent that the extra Mo additions promoted the bulk sigma formation. The cracking is sufficient to render useless any component produced from these alloys. Therefore, whilst from a corrosion standpoint a four percent Mo addition would appear theoretically justified, the resulting HIP alloys are far too brittle to withstand the rigours of cutting and machining. In fact, the alloys may have even cracked during casual handling. The use of powder metallurgical versions of these alloys in any commercial application is therefore not recommended.

The hardness values of the HIPped alloys, summarised in Table 4.13, provide an indication of the amount of sigma present in the microstructure. A fully sigmatised microstructure has a hardness of approximately >890Hv. A solution-annealed material consisting exclusively of ferrite has a hardness of about 240Hv. Microstructural examination, coupled with hardness values, indicates that a hardness in excess of 250Hv should be indicative of the presence of some sigma in the microstructure.

All of the as-HIPped 2Ni-4Mo alloys have hardness values between 710Hv and 890Hv, showing that large amounts of bulk sigma phase are present. This explains the widespread cracking and brittleness of the alloys. It is interesting to observe the cracks extending from the corners of the hardness indentation. These cracks are referred to as Palmqvist cracks and are often utilised in the hardmetals industry to provide approximate values of the toughness of cemented carbides. However, the principle is extended to other brittle materials as well, such as the sigma phase. A shorter crack length is thus indicative of greater toughness within a brittle material.

Heat treating does not result in crack closure. However, in terms of characterising the further behaviour of the Fe-40Cr-4Mo-2Ni alloys, heat treatments are informative. Initial trials with these alloys involved solution annealing at 1200°C for 2 hours, followed by an iced brine quench. It was felt that these parameters, while generally effective, were too severe and could lead to component distortion. In addition, many commercial furnaces have an operating limit of 1200°C.

It was therefore decided to pursue a less extreme annealing treatment at 1100°C for two hours followed by quenching in water held at room temperature. The new solution annealing conditions provided mixed results. Alloys such as DS-1, DS-C, VFA 417, VFA419, VFA423, and VFA543 softened appreciably to values of 274-277Hv. The similar hardness values, after solution annealing, are indicative of the similar compositions of these alloys, and indicate a consistent response to solution annealing. VFA 420 exhibited very little sigma phase dissolution, with an annealed hardness value of 736Hv. Thus this trial indicated that the solution annealing treatment can be used effectively on most of these alloys.

5.7.1 Microstructure of VFA543 (2Ni-4Mo-0.4Nb-40Cr)-As-HIPped

This composition was devised in order to test the effectiveness of niobium additions. It was felt that a 40Cr-Fe alloy with a 4 percent molybdenum and 0.4 percent niobium content should offer excellent pitting and intergranular corrosion resistance.

After HIPping, the alloy consisted of approximately 90 percent sigma. The microstructure is shown in Figure 4.9. The brittle nature of the sigma phase is highlighted by the fact that widespread macroscopic cracking across the entire cross section of the specimen occurred. These cracks were clearly visible on the fresh, newly cut surface, and were obviously not brought about by grinding or polishing, but were rather due to casual handling after HIPping. The addition of 4 percent molybdenum, whilst enhancing corrosion resistance, enhances the formation of sigma phase to an excessive degree. This as-HIPped alloy is unusable and would break apart during any machining operation.

The inclusion content was fairly high, and certain measures would have to be undertaken to improve the cleanliness of the powder production process.

A large number of inter- and intraparticular precipitates are present in the microstructure. The interparticular precipitates have different sizes and morphologies compared to those which occurred within the particles. The latter within the particles are widespread and homogeneously distributed, and have a rounded, spherical morphology and correspond to the usual morphology of niobium carbides. Conversely, the precipitates on the particle boundaries are larger and appear ovular, rather than spherical in shape. The composition of these precipitates is probably also linked to the niobium additions.

5.7.2 Microstructure of VFA543 (2Ni-4Mo-0.4Nb-40Cr)-heat treated

A microstructure consisting of ferrite (Figure 4.22) and approximately 5 percent sigma is apparent after heat treatment. Some of the sigma is localised and appears to follow the path of the pre-existing cracks. This might be due to some type of strain effect associated with the material surrounding the crack, which enhances the stability of the sigma, such that the phase can resist solution annealing or reform quickly during the quenching stage.

The cracks which were present after HIPping are still visible after heat treatment. This is expected since there is no driving force for crack closure during heat treatment under atmospheric pressure. The appearance of the inter- and intra particular precipitates was unchanged. This is an indication of the stability of the precipitates.

5.8. 38 or 40Cr alloys with 2Mo-2Ni

In these trials, alloys with 38Cr-2Ni-2Mo (Prem V, VFA 487) exhibited the best overall characteristics. They embrittled easily to facilitate powder manufacture whilst still forming the lowest amount of sigma (20 percent) after HIPping.

It was felt that corrosion resistance could be improved by increasing the alloying additions. Trials with the 4Mo-2Ni compositions indicated that further Mo additions were deleterious. It was decided that the chromium level could be increased to forty percent Cr without excessive embrittlement. An addition of 0.4% Nb was considered to be beneficial in terms of promoting resistance to intergranular corrosion, as well as inhibiting the sigma phase. Ru (0.15%) was added to enhance cathodic modification.

VFA622 (40Cr-2Mo-2Ni-0.4Nb) underwent massive cracking after HIPping, with virtually 100 percent sigma formation and a Vickers hardness in excess of 800Hv. This result is unexpected, since the increase in Cr and Nb was considered minor. This indicates that, when alloyed with Ni and Mo, the high Cr alloys are most likely extremely sensitive to Cr content. Therefore, the small increase in Cr, from 38 to 40 percent, could have increased the rate of sigma phase formation dramatically. Another possibility is that the Nb additions promote the sigma phase. However, work by Premanchandra[21] indicated that this should be unlikely. It is plausible that the 0.15 percent Ru played a role, considering the work of Wolff et al[28].

The response of VFA622 to solution annealing is satisfactory, with a solution annealed hardness of 253Hv. However, the cracks occurring after HIPping were not closed. This composition therefore cannot be used in commercial applications when manufactured by this specific route.

5.9. The extra-communited powder VFA543 (SP001012)

The microstructure of the milling media was martensitic and is shown in Figure 4.36. The chemical analysis is shown in section 4.5.1. The hardness of the steel media was 715Hv. A normal size distribution, in Figure 4.37, was apparent after the extra milling of VFA543. The average particle size was 6 microns. There was a mild peak in the number of particles occurring in the three to one micron size range.

SP001012, in Figure 4.38, consisted totally of sigma phase after HIPping. Palmqvist cracks were present at the indentation corners, indicating the brittleness of the phase. A detail of the indentation corner may be seen in Figure 4.39. The Palmqvist cracks passed directly through the individual sigma particles and did not travel preferentially around the particle boundaries. The particle/grain size was extremely fine. Figure 4.40 shows the diffusion zone, which was similar in appearance to the zones in alloy SP001008. However, SP001012 had a far finer dispersion of precipitates. The duplex microstructure of ferrite (dark areas) and sigma (light areas), after solution annealing, may be seen in Figure 4.41. The grain size was very fine and individual grains were not readily discernable. The sigma dispersion was homogeneous throughout the material.

The shape of the size distribution curve of the powder produced by ball milling is similar to those observed in previous trials, and the average particle size is similar to SP001008. Therefore, it appears that when similar milling parameters are utilised, there is a fair amount of reproducibility in the ball milling process.

The aim of milling the 2Ni-4Mo-0.4Nb-40Cr alloy to below six microns in size was to determine the effect of reduction in starting particle size would have on sigma formation and on the toughness of the material. The same milling equipment and similar milling and powder charge parameters, as described for batch SP001008, were utilised. Although no carbon content analysis was made on this heavily milled material, it is expected that similar levels of carbon contamination (in the range of 0.2%C) would have occurred.

5.9.1 Microstructure of extra-communited VFA543 (SP001012)-As-HIPped

The HCl etched surface has few discerning features, apart from entrapped bodies outlining individual particle boundaries (Figures 4.38-4.39).

When etched with Murakami's reagent (Figure 4.40), the as-HIPped material exhibited the typical three zone diffusion layer. The core is rich in carbides, which is expected, due to the high level of carbon contamination occurring during milling.

The HCl etchant revealed a microstructure consisting of over 95 percent sigma. This was confirmed by the Vickers hardness value of 876Hv and the distinct Palmqvist cracks at the corners of the indentation. These cracks run directly through the particles of the hard phase, and do not follow the particle boundaries.

It is clearly evident that the starting particle size influences the microstructure. Precipitates and sigma phase grain size are finer and more homogeneously distributed throughout the microstructure.

The only possible benefit of having a very fine particle size appears to be a slight improvement in the grinding and polishing characteristics of the material. This could be due to the small particle size having a certain, limited effect in retarding crack growth during grinding.

The reduction in particle size produced a marginal improvement in the toughness of the alloy. The homogeneous dispersion of fine isolated sigma particles instead of a single large sigma body occupying the same volume is attributable to the milling process. For example, during sample cutting, preparation and polishing, there was a somewhat diminished susceptibility to cracking. This is most likely due to the fine particle size. Cracks would have to propagate through individual sigma particles instead of large bulk bodies of sigma. Crack propagation occurs more easily through large brittle bodies than through smaller brittle bodies.

However, the fact that some specimens still cracked during sample preparation highlights the minimal improvement to be gained from this microstructural modification.

5.9.2 Microstructure of extra-communited VFA543 (SP001012)-heat treated.

The microstructure (Figure 4.41) consisted of an extremely fine ferrite matrix with a widespread, homogeneous dispersion of sigma phase particles. A fine, even dispersion of precipitates was also present. The particle boundaries of the individual grains are not clearly defined and are difficult to discern, even at a magnification of 1000X.

The presence of the sigma particles after solution annealing indicates that not all of the sigma was taken into solution during the 2 hours at 1100°C, or that the cooling rate during quenching was too slow to prevent sigma formation. This alloy has a hardness of 318Hv, which is consistent with the presence of some sigma.

The presence of sigma after solution annealing is unusual since the same alloy, with a larger average particle size, responds successfully to the same heat treatment. This implies that the degree of sigma formation is correlated to the size of the starting powder particles. A smaller particle size provides a greater boundary area on which sigma can nucleate.

In terms of commercial application, this composition is still too brittle for use. The slight improvement in toughness gained by particle size reduction and homogenisation is insufficient to justify any further development work on this particular alloy.

5.10.1. Microstructure of Fe (SP001008). - As-HIPped

Figure 4.42 shows a cross section of the region in which the powder was in contact with the canister. Four distinct zones are present: the mild steel cylinder (D), a region of particle or powder grain growth (C), a zone which is free of large precipitates (B) and a zone which is rich in large precipitates (A). There are also fine precipitates at individual particle boundaries. No sigma phase was observed. A detailed view of the core section (A) with precipitates in a ferrite matrix is shown in Figure 4.43. The microstructure after solution annealing (Figure 4.44) appeared very similar to the as-HIPped material, except that the precipitates, at the boundaries of the enlarged particles (C), went into solution. Figure 4.45 shows that the core microstructure (A) appeared unchanged after solution annealing. In Figure 4.45, no obvious distinction was apparent between the starting pure Fe and the 40Cr-Fe particles. The ferrite microstructure did not show any areas of preferential attack, which would be indicative of a Cr deficient region. This was confirmed by the elemental scans (Figure 4.65) and EDS spot analysis (Table 4.4) which indicated that there were no large scale Cr deficient regions or variations in Cr content. The higher magnification examination in Figure 4.43 reveals that the greyish precipitates, which were readily apparent in the VFA622 alloy (Figure 4.32), were not visible in the VFA622+Fe microstructure. The precipitates in the core section (A) were identified as carbides by virtue of their etching characteristics in Murakami's reagent. EDS analysis, shown in Table 4.5, indicated that the precipitates were enriched primarily in Cr, Fe, and Mo. The areas surrounding the precipitates thus would be expected to be more vulnerable to corrosion due to depletion of Cr and Mo from the matrix.

The fine bodies surrounding each powder particle are probably contaminants or surface oxides trapped on the particle surfaces. The presence of these bodies is unavoidable, although their number could be minimised. The inclusions arise due to exposure to the atmosphere or pickup during the powder manufacturing process. Even high purity gas atomised powders exhibit these inclusions. Work at Ultra High Pressure Units has shown that certain concentrations of these inclusions are not necessarily harmful to the properties of the material.

The three distinct regions in the as HIPped material are essentially brought about by diffusion processes. The left-most region of the microstructure (A-Figure 4.43) is rich in carbide or carbo-nitride precipitates, since they were preferentially etched by Murakami's reagent. The precipitates are not evenly dispersed throughout the core of the microstructure and regions which are distinctly free of precipitates are evident.

This may be due to incomplete mechanical mixing as well as insufficient diffusion, homogenisation during the HIPping process. The following mechanism is proposed to explain the variation in microstructure. If it is assumed that the carbon gained during milling is evenly distributed throughout the individual Fe as well as the 40Cr-Fe particles, it can be seen that there is a greater tendency to form precipitates in the regions with 40Cr-Fe. This is because the solubility of carbon and nitrogen, in Cr-Fe alloys, decreases as the proportion of Cr increases. Carbon and nitrogen precipitate as carbides and nitrides when their solubility limit in the ferrite phase is exceeded. The excess carbon would thus tend to enhance precipitate formation in 40Cr-Fe particles. On the other hand, the iron rich regions (particles) would tend to retain the interstitial elements in solution, and no precipitates would form. This is because they have a low chromium content, and therefore a far higher solubility for interstitial elements than the surrounding alloyed powder particles. Thus, there would be iron-rich regions of the microstructure with an absence of large precipitates.

A precipitate free zone (B) occurs throughout the circular cross-section, at a uniform distance from the mild steel canister. It is considered unlikely that a lower level of carbon should be present in this zone relative to the core. The 40Cr-Fe alloy, in contact with the mild steel canister, should actually act as a carbon sink. The low carbon content of the alloy, lower than the levels present in industrial grade mild steel, would cause a concentration gradient between the alloy and the mild steel. Carbon would therefore have a tendency to diffuse from the mild steel into the alloy. Therefore, a higher concentration of precipitates should actually be observed adjacent to the canister. This apparent contradiction between observation and theory can explained by considering another possibility. The mild steel contains no chromium, whilst the powder alloy is chromium rich. It is probable that chromium diffused from the powder alloy and into the mild steel. This would result in a lowering of the chromium content of the affected particles. A lowered chromium content would increase the interstitial element solubility of the alloy. This would mean that there would be a reduced tendency for precipitation. The tiny, 50 micron thickness of the precipitate-free zone, would be due to the relatively poor mobility of the chromium atoms, during diffusion. At a diffusion distance of greater than 50 micron from the canister, insufficient chromium loss would have occurred in order to affect interstitial element solubility to any great extent. Hence, precipitate formation occurs in the core only. This theory was verified by SEM spot analysis (Table 4.4) of the precipitate-free regions. The core region was found to contain 28.3 percent Cr whereas the precipitate-free diffusion zone (B) contained only 22.7 percent Cr. Since the solubility of carbon increases with decreasing Cr content in high Cr-Fe alloys it can seen that the assumption regarding the preferential precipitation of carbides in specific regions of the HIPped compact was justified.

The third zone, zone C, consists of a region of enlarged particles adjacent to the mild steel canister. This zone is extremely thin, of the order of 10 microns. These particles are free of large precipitates internally, although other fine, well defined precipitates occur at the particle boundaries. It is felt that these regions could not be mistaken as being grains of the mild steel canister. This is verified by examination of the mild steel grains, in which it can be seen that the grains are many orders of magnitude larger than the particles in zone C. In addition, the enlarged particles are still present in the microstructure, even after the mild steel has been removed by nitric acid. The reason for the lack of internal precipitates is as mentioned previously. At present, no explanation can be offered as to the reason for this preferential particle growth. Such phenomena has not been encountered in work involving other alloy powders.

The entire object of mechanical mixing is the retardation of sigma phase. In this respect the trial is successful. No sigma phase is apparent in the microstructure. Sufficient diffusion occurred such that the overall Fe level was increased, and therefore the formation of sigma was inhibited. However, as mentioned previously, there is reason to suspect that the alloy is not entirely homogeneous. This would affect the mechanical and corrosion properties of the alloy. Corrosion and mechanical testing is required. This would be informative, since SP001008 is nominally similar in composition to AL-29-4-2, a well known, commercial superferritic alloy. Appropriate comparisons could therefore be made.

5.10.2 Microstructure of Fe (SP001008), - heat treated

The microstructure of the solution annealed alloy appeared very similar to the as-HIPped material (Figures 4.44-4.45). The three distinct zones were still present. The core was still rich in precipitates. The only apparent difference is in the zone with enlarged particles. The precipitates at these grain boundaries are absent since they have gone into solution. This strengthens the theory that they are indeed precipitates and not some form of entrapped inclusion. Solution annealing did not affect the bodies surrounding the powder particles at the core of the specimen. Another aspect which this trial revealed is the stability of the Cr-Fe-Mo carbides. The EDS analysis of the carbides is shown in Table 4.5. These did not go into solution, and have a similar size and morphology as in the as-HIPped material. From a purely microstructural viewpoint, this indicates that this particular alloy does not respond well to the current heat treatment.

It must be mentioned that during the majority of applications, the diffusion zone will most likely be removed during initial machining. The diffusion zone will therefore not play a role in commercial applications of the alloy.

5.11. Extra Fe alloys (hand mixed)

The microstructures of hand-mixed VFA543 and VFA622 with Fe additions are shown in Figures 4.46-4.48. No immediately obvious sigma phase or large carbide bodies were apparent after HIPping. The as-HIPped hardness values of VFA543+Fe and VFA622+Fe were 238Hv and 224Hv respectively. The microstructures of VFA543+Fe and VFA622+Fe are similar, therefore only the microstructure of VFA622+Fe is shown. The hardness values are 242Hv (VFA543+Fe) and 212Hv (VFA622+Fe). The micrograph of VFA622+Fe in Figure 4.46 was taken near the edge of a Vickers indentation around which plastic deformation was apparent. Strain or slip lines caused by the indentation are apparent in one of the particles. A number of relatively coarse inclusions were present within the particle. The microstructure after solution annealing of is shown in Figures 4.47 and 4.48.

The addition of extra Fe to VFA543 and VFA622, by hand mixing, provided information on whether the process can be used as an alternative manufacture route for powders. The aim of adding the extra Fe is to produce an alloy which is free of sigma phase after HIPping. This would work by effectively lowering the overall Cr content of the alloy, thereby inhibiting the tendency for sigma formation. The trial also provided information on the degree of homogeneity brought about by diffusion processes during HIPping.

The results of EDS spot analysis and elemental scans are given in Table 4.6 and Figures 4.66-4.69 respectively. These indicated that reasonable homogeneity in composition was achieved and that no pure Fe particles remained after HIPping.

Comparisons can also be made on the effectiveness of simple hand mixing versus ball milling in providing a homogeneous, HIPped structure.
After HIPping, both of the hand-mixed alloys appear to be free of any obvious sigma phase (Figures 4.46-4.48). This is reflected in the low hardness values of 238Hv (VFA543+Fe) and 224Hv (VFA622+Fe). The hardness tests were taken at variety of positions within the cross section of the test piece and were found to be reproducible. No "hard" or "soft" spots were found. The unalloyed powders have as-HIPped values in excess of 800Hv.

The results indicate that it is likely that sufficient diffusion between the alloy and Fe particles did occur such that the sigma phase was inhibited. This was confirmed by the EDS spot analysis of 34.2%Cr (Table 4.6) and the elemental scan in Figure 4.69. Perhaps a more important result derived from the EDS analysis was that the combined Mo and Ni content was less than four percent. Earlier trials with alloys VFA390-395 showed that a combined minimum content of at least four percent was required for bulk sigma formation Fe-40Cr-Ni-Mo alloys.

The lack of large carbides in the mixed powders is an advantage over ball milled material. The existing ball milling process introduces undesirable levels of carbon into the powder. The hand mixed alloys exhibit very little change in microstructure after solution annealing. VFA543+Fe remained virtually unchanged at 242Hv, whilst VFA622+Fe softened slightly to 212Hv. This indicates that there could have been small traces of sigma which were removed, or perhaps some of the carbide precipitates had gone into solution. The small changes in hardness indicate that these reactions should only have occurred to a limited extent.

The main advantage of using hand mixing is that it is a quick and inexpensive means of adding controlled amounts of an alloying element to a powder. Hand mixing allows for very low levels of contamination and requires minimal energy input.

The disadvantage is that hand mixing cannot achieve the same degree of powder homogeneity as high energy ball milling, but instead has to rely on diffusion processes during HIPping to achieve compositional uniformity. In terms of corrosion resistance, inhomogeneous areas in the cross-section which have low Cr contents would tend to be attacked preferentially in aggressive environments.

In addition, both hand mixing and ball milling require Fe powder of high purity to be obtained. This contributes to increasing the overall cost of the final alloy. Also, the addition of the actual mixing stage adds another step to the powder production process and renders it more complex. Another disadvantage is that only relatively small volumes of powder can be manufactured. Any future use of hand mixing will depend on the homogeneity of an alloy after HIPping as well as the added costs required.

5.12. Microstructure of duplex alloys

Microstructures of the synthetic duplex alloy manufactured from various proportions of 316L and VFA622 powder are shown in Figures 4.49-4.58.

5.12.1. 20% 316L+80% VFA622

In Figure 4.49 (20% 316L + 80% VFA622) prior particle boundaries are evident. The smaller, rounded particles are 316L material, whilst the larger, irregularly shaped regions are VFA622. The dark region in the centre of the micrograph is a non-metallic inclusion. Figure 4.50 shows sigma phase in the microstructure in the duplex alloy. The sigma phase is evenly dispersed and does not occur in large contiguous bodies. The sigma morphology differs from that found in HIPped VFA622 in having a lamellar appearance and is far finer in appearance compared to the standard VFA622 material in which bulk sigma was formed. The sigma bodies occupy approximately 10 percent of the microstructure. Figure 4.51 showed that after solution annealing, the microstructure appeared predominantly ferritic. This indicated that heat treatment was successful in removing the sigma phase.

The as-HIPped alloy exhibits only small amounts of sigma phase, as can be seen by the fairly low hardness value of 286 Hv. The addition of the 316L material seems to have a retarding effect on sigma formation. The retarding effect of the 316L material is possibly due to the diffusion of chromium from the VFA622 regions to the 316L regions and the diffusion of iron in the reverse direction. The overall effect would be a lowering of the chromium content of the VFA622 particles. The lowering of the chromium content would therefore inhibit sigma formation. The Mo contents of 316L and VFA622 are similar and there would be little tendency for Mo diffusion. Ni diffusion could also occur, but due to the smaller difference in content the diffusion gradient would not be as large as for chromium or iron. Heat treatment successfully removes all the residual sigma and this is apparent in the lowered hardness value of 219Hv. There does not appear to be a readily observable diffusion zone in the regions in where the two materials are in contact. The appearance of large non-metallic inclusions (Figure 4.49) may be traced back to impurities which were introduced in the VFA622 powder manufacturing process. It was difficult to avoid the additions of some inclusions during the casting process. In addition, the equipment used to mill the VFA622 powder had traces of silica which were impossible to remove completely prior to milling. In commercial applications the cleanliness of the powder would have to be improved to above the current level.

5.12.2. 50% 316L+50% VFA622

The 50%316L+50%VFA622 material is shown in Figures 4.52-4.53. No prior particle boundaries were observed in the as-HIPped 50% 316L + 50% VFA622 material (Figure 4.52). There appeared to be roughly equivalent areas of etched light (austenitic-316L) and dark (ferritic-VFA622). The light etched regions occurred as both large and smaller isolated bodies. After solution annealing, the average size of the light etched (possibly austenitic) regions had decreased (Figure 4.53). There was also a smaller number of the light etching isolated bodies compared to the as-HIPped state. Points (A and B) were analysed by SEM spot analysis.

This composite alloy exhibits the most interesting response to HIPping. A classical duplex ferrite-austenite microstructure is observed without any prior particle boundaries. The distribution of the ferrite amongst the austenite is not particularly homogeneous and large bodies of ferrite are found in close proximity to smaller isolated ferrite regions (Figure 4.52). The decrease in hardness from 272Hv (as-HIPped) to 248Hv (after solution annealing) indicates that some sigma phase may have been taken into solution. The decrease of 24 hardness points is not particularly large, and since any sigma phase material only comprises a proportion of the VFA622 particles it would therefore tend to have a smaller influence on properties.

5.12.3. 80% 316L + 20% VFA622

Figure 4.54 shows the 80% 316 L+ 20% VFA622 alloy in the as-HIPped state. The microstructure consists of well distributed ferrite (dark) particles within an austenite (316L) matrix. The micrograph of the as-HIPped alloy in Figure 4.55 indicated the presence of sigma-phase (etched light) within a particular ferrite particle. The sigma appears to have formed in two distinct morphologies: bodies of bulk sigma and fine lamellae. Figure 4.56 highlights the comparison between the different sigma phase morphologies. The lamellae are fairly fine and individual branches were barely resolvable at 500X magnification. Certain areas with lamellae appeared to run directly into bodies of bulk sigma. The results of microhardness and EDS analysis of the lamellar sigma phase are given in Tables 4.8-4.9 and show that the sigma lamellae are harder than the ferrite matrix. The sigma phase was enriched in Mo and Cr and had a composition which differs from the bulk VFA622 alloy. The effect of solution annealing may be seen in Figure 4.57, which shows a VFA622 particle in 316L matrix. Ferrite grains were readily apparent within the particle. Small sigma phase regions were present at the grain boundaries, as well as at intergranular positions within the ferrite. A three phase microstructure consisting of austenite, ferrite and sigma phase may be seen in Figure 4.58. The austenitic 316L phase and sigma phase were untouched by the etchant.

The VFA622 particles were clearly distinguishable by their jagged, irregular appearance. Darker etched ferrite regions were easily noticeable as was the appearance of sigma phase within the ferrite. Some of the VFA622 particles exhibited a clear diffusion zone with the surrounding 316L particles (marked as point A).

The fairly uniform distribution of VFA622 particles in this alloy indicates that relatively simple mixing techniques are effective in producing a satisfactory particle dispersion (Figure 4.54). The 316L appears to have some effect on the VFA622 microstructure since the sigma phase shows a greater tendency to occur as lamellae. The diffusion zone in the as-HIPped steel is apparent, and can be seen by the tendency of the ferrite particles to respond less readily to etching in certain regions (Figure 4.58).

The solution annealing treatment is able to remove most of the sigma, as can be seen in Figure 4.57. It must be mentioned that the hardness values obtained from this alloy are misleading. Canister leakage occurred during the HIP process. Argon gas was trapped in the pores and full densification was not achieved. The pores are not easily seen on the etched surface, but are readily apparent in the unetched state. The effects of porosity in a steel are well documented. Increasing porosity leads to a decrease in corrosion resistance, tensile strength, impact toughness and hardness. This can be seen from the low hardness of the as-HIPped steel at 194Hv and the decrease after heat treatment to below the limits of the Hv30 scale. However, valid microstructural characteristics may still be obtained from this alloy. The dark etched regions occupied approximately 40 percent of the microstructure, whereas they should only occupy twenty percent of the visible areas since only 20% VFA622 was added. This could be due to inefficient mixing, resulting in segregation of the VFA622 particles. Certain areas of the compact could have a greater number of VFA622 particles than other regions. Alternately, ferrite stabilisation of the areas surrounding each VFA622 particle could have taken place, thereby producing a greater percentage of dark etched areas.

The results of micro-hardness tests are informative. A distinct difference in the hardness of the ferrite ($339H_{micro}$) and sigma lamellae ($529H_{micro}$) was observed. This confirmed that the lamellae were composed of a harder phase. However, a reference hardness test performed on an alloy containing near 100 percent sigma phase (VFA543) produced a value of $1555H_{micro}$. The lower hardness value of the sigma lamellae relative to the reference alloy can be attributed to the far softer ferrite phase which formed between the sigma lamellae. The micro-hardness result was therefore an overall value obtained over a region containing both sigma phase and ferrite.

The presence of fine porosity in the compact is not considered to affect the micro-hardness results since the porosity could only occur at the interfaces between individual powder particles and all micro-hardness results were taken at intraparticular regions. The appearance of sigma lamellae is not restricted solely to the ultra-ferritic alloys and similar morphologies have been reported by Jackson[60] in duplex stainless steels.

An interesting result is obtained upon examination of the chemical composition of individual sigma lamellae (Table 4.9). The sigma is significantly enriched in both chromium and Mo relative to the bulk alloy. An important finding by Premachandra[21] was that the sigma phase was formed by two different mechanisms which influenced the composition of the phase. In the first mechanism the conversion from ferrite to sigma would occur without any major partitioning of the elements to either ferrite or sigma. Short range diffusion across an incoherent reaction interface would occur and the Fe and Cr atoms in the ferrite would simply re-arrange into the sigma structure. There would therefore be minimal compositional difference between the sigma phase and the bulk alloy. It was found that the bulk alloy composition had to lie within the sigma phase field of the phase diagram for this first mechanism to be dominant. The second mechanism was more involved and occurred when the composition of the bulk alloy lay within the duplex sigma plus ferrite region of the complex phase diagram. In this situation the composition of the sigma phase would differ from that of the bulk alloy and be determined by the appropriate tie lines on the phase diagram. Certain elements would thus partition preferentially to either the ferrite or sigma phase. In effect, the following eutectoid reaction would occur:

$$\alpha(\text{metastable}) \rightarrow \alpha\ (\text{stable}) + \sigma$$

The presence of lamellae and the composition of the sigma phase may therefore be explained by the occurrence of the second sigma formation mechanism. However, this implies that the regions which exhibited the sigma lamellae have local compositions which lie in the duplex sigma plus ferrite region of the phase diagram. Since the lamellae morphology was not observed in the plain VFA622 alloy it may be deduced that the bulk composition of the alloy most likely lies within the sigma only phase region. Therefore the second mechanism would only occur if there was some diffusion between the VFA622 and 316L material. This could then shift the composition of localised regions of the VFA622 particles into the sigma plus ferrite region such that the eutectoid mechanism of sigma formation would be dominant.

5.12.4. 50% Hastelloy C + 50% Prem V

Figure 4.59 shows a microstructure consisting of Prem V particles surrounded by equal proportions of Hastelloy C particles. The ferrite grains (A) were etched dark, whilst the sigma phase within the Prem V particles was etched light. The adjacent Hastelloy regions (B) consisted of numerous carbides embedded in a Ni-Cr-Mo matrix. A distinct diffusion zone (C) was apparent between the Fe-Cr and Hastelloy regions. A Prem V particle exhibiting a high proportion of sigma phase in the ferrite matrix is shown in Figure 4.60. Very fine precipitates were also barely resolvable at the 500X magnification. The percentage of sigma was expected from the behaviour of the Prem V alloy. The diffusion zone was generally free of sigma phase, carbides or any other precipitates. The well-defined, spherical particles (point A in Figure 4.60) were inclusions which were introduced during the melting and powder manufacturing process. A Hastelloy region which was rich in carbides may be seen in Figure 4.61. These carbides were irregular in shape, and were not all evenly dispersed. There was a tendency for the carbides to segregate in groups. However, this segregation was not severe and the carbides occurred throughout the matrix. The Ni-Cr-Mo matrix was not attacked by the HCl or Murakami's etchant and no grain or prior particle boundaries were observed.

Figure 4.62 shows the overall microstructure and the effect of heat treatment. The diffusion zone between the two materials is more defined. A carbide phase is present at the boundaries of the stainless steel particles. This carbide phase has a "stained" appearance. A detailed view of a Prem V particle is given in Figure 4.63. The material responded successfully to heat treatment and no sigma phase was immediately apparent. The diffusion zone around the particle appeared smaller than in the as-HIPped specimen. SEM spot analysis was performed on point A. The Hastelloy-rich regions in Figure 4.64 were essentially unchanged in appearance after solution annealing and consisted of complex carbides in a Ni-Cr-Mo matrix. The main effect of the heat treatment was an increase in the average size of the carbide precipitates.

The diffusion zone between the different particles (Figure 4.62) is expected since Hastelloy C and Prem V have greatly differing compositions. The zone is characterised by a region which is generally free of carbides and other precipitates. The Hastelloy C regions consist of a Ni-Cr-Fe matrix which is rich in complex carbides. The EDS analysis of these precipitates its given in Table 4.10. The compounds were found to be enriched in Mo, Cr, W, and Fe. These carbides have been verified in the literature as being of the M_6C type[70,71]. A detailed description of the crystal structures and lattice parameters of the various precipitates which can appear in Hastelloy C is available in reference 70.

The sigma forming tendency of Prem V appears to be unaffected by diffusion from the surrounding Hastelloy. This could be due to the high Ni and Mo content of Hastelloy.

In fact, it is surprising that sigma growth is not even promoted to a greater extent. Solution annealing at 1100°C removes sigma from the Prem V particles. However, no precipitates in the Hastelloy were taken into solution. Some carbide growth due to the heat treatment was observed in the Hastelloy. This may be explained by considering the fact that Hastelloy is designed for high temperature applications (in the region of 1200°C). The recommended solution annealing temperature for the alloy is 1220°C[70]. The current heat treatment is thus below the minimum temperature required and this produces coarsening of the carbides.

This duplex alloy has a fairly high hardness value (401Hv) after HIPping. The hardness decreases to 357Hv (a relatively high value) after solution annealing. It can thus be deduced that it is the precipitates in the Hastelloy matrix, and not the sigma phase in Prem V, which have the dominant influence on hardness.

The "stained" appearance of the diffusion zone in the heat treated alloy could be due to the movement of carbon into the zone, with the corresponding formation of carbides. It is unusual that the Hastelloy should be so rich in the carbide phases, since its starting carbon content of 0.01%C is very low. It may be possible that some carbon contamination could have entered the powder during mixing with the Prem V powder, although this is considered unlikely.

5.13. Elemental scans

5.13.1. Alloys with pure Fe additions: SP001008 (as-HIP) and VFA622+Fe

Figure 4.65 shows the elemental scan for SP001008, as-HIPped, over a length of 123 microns. The region analysed contained lowered and raised regions, one of which was a precipitate (B). The Cr and Fe contents were fairly uniform. This implied that the Cr and Fe had diffused nearly completely. However, there was a sharp dip in the Fe content accompanied by a simultaneous rise in the Cr content at the precipitate B. The Ni and Mo contents were relatively uniform throughout the analysis.

SP001008 was manufactured by ball milling pure Fe powder with 40Cr-Fe material. Since SP001008 has a relatively fine particle size (11μm) a small scan length (123.3μm) is used. This provides more detail on a localised area. The Cr and Fe contents were generally uniform throughout the scan. This is an important result: it indicates that sufficient diffusion occurred during HIPping to provide a certain degree of chemical homogeneity. If some homogenisation had not taken place, then distinct Fe rich regions with minimal Cr contents would be observed in the scan.

Some Cr enriched, Fe deficient areas were detected in SP001008 (B-Figure 4.65). Visual identification of the etched surface revealed these to be precipitates. The precipitates were not prominent on the topography scan since the surface is relatively uneven. These Cr-enriched precipitates could possibly be Cr carbides due to their etching characteristics in Murakami's reagent (Figure 4.60). This would be consistent with the high levels of carbon (0.176%C) which were detected in this material and the low solubility of carbon in ferrite. Chromium carbides are generally undesirable in stainless steels since they deplete the surrounding matrix of Cr, thereby decreasing the corrosion resistance in that localised region. A Cr deficient region, would therefore be expected adjacent to the precipitate. This is not observed and it could be possible that during HIPping Cr from the surrounding Cr-enriched areas might have diffused into the Cr deficient zone, thereby returning the Cr content in that region to its original level. This is plausible if it is considered that the overall Cr content is high (30%) and that none of the original pure Fe additions are detected.

The multiple fluctuations in the Mo and Ni readings are not considered significant. This is because the upper and lower limits would typically be between two and zero percent. The fluctuations are therefore in the region of fractions of a percent and should not denote any major changes in composition. The Cr and Fe values are an order of magnitude larger and any fluctuations in these elements are more dominant.

The VFA622+Fe (as-HIP) specimen (Figure 4.66) had a very smooth, uniform surface topography without any large peaks or troughs across a length of 125 microns. The Fe and Cr contents were uniform and tended to remain at the upper limit of the measurement scale. There was a small, localised Mo peak in the first quarter of the scan whilst the Ni had minor fluctuations. As the length of the scanned area was increased to 504 microns (Figure 4.67) few distinguishing features with regard to surface roughness were observed. Cr and Fe remained at fairly even levels and only minor variations are apparent in Ni and Mo content. When the scanned length was increased to 997 microns (Figure 4.68) , the surface finish on the specimen was fairly smooth with only a raised region at the tail end of the scan. The elemental compositions were still relatively uniform throughout. There was no elemental depletion or enrichment at the raised point D, indicating that the raised area was due to surface preparation and not due to the presence of a wear-resistant precipitate. After solution annealing, in Figure 4.69, Fe, Cr, Mo and Ni do not display any major deviations across the scan. Only minor peaks were apparent in the topography.

Scans of VFA622+Fe (as-HIPped) were conducted over lengths of 124.6μm, 504.3μm and 996.6μm. This provides more data on micro-segregation. The curves on all three graphs are very similar with very little variation in Cr and Fe, even on the higher resolution 124.6μm scale. This is important , since it provides some evidence to indicate that HIPping results in a degree of homogenisation of the blended ferritic powders. This is particularly interesting since the starting powders particle sizes are significantly coarser (160<particle size<150μm: VFA622 and 11μm:Fe) than for SP001008. The coarser particle sizes result in a decreased surface area along which atomic diffusion can take place. However, despite the larger particle size, the alloy appears to have a uniform distribution of elements. No immediately obvious changes in composition are noticed in the heat treated specimen (Figure 4.69) although some further diffusion would be expected due to the kinetic energy supplied during solution annealing. These results are important since they imply that additions of pure Fe particles by simple mixing could possibly be a viable method of producing a homogeneous high chromium alloy which does not easily form sigma phase after HIPping. This would remove the necessity for ball milling and minimise carbon contamination of the duplex powder. The important factor is the distribution of chromium. Chromium, above a minimum level of approximately 12 percent, is the chief element responsible for corrosion resistance in stainless steels. The major test of homogeneity will therefore occur during corrosion tests. In an aggressive environment, any localised region which is deficient in chromium should corrode more readily than surrounding chromium-rich areas.

It must be mentioned that the homogenising effects of hot isostatic pressing have been reported by other workers[34] in castings and welds which have been HIPped[72].

5.14. Duplex powders with 316L additions

Whilst the diffusion behaviour of VFA622 with pure Fe additions is relatively straightforward, the diffusion reactions between VFA622 and 316L are more complex. This is because the 316L used in this study is alloyed with approximately 17%Cr, 12%Ni and 3%Mo. There should therefore be a general tendency for Cr to diffuse into the 316L particles, whilst Ni should diffuse out into the 40Cr-Fe regions. Fe and Mo diffusion should also occur. However, the ratios of Fe and Mo are comparatively similar in both materials and therefore a reduced driving force for diffusion could be expected. It could therefore be expected that some conversion to ferrite of the austenitic 316L material could take place. This would be due to the simultaneous influx of Cr (a ferrite stabiliser) and outflow of Ni (an austenite former). The Ni should not have an effect on the VFA622 particles, since each particle should still contain a high Cr level. This explanation would appear to be feasible from the microstructural examinations of 80% VFA622 + 20% 316L and 50% VFA622 + 50% 316L in which ferrite has been tentatively identified as the predominant phase. The possible "ferrite stabilisation" effect appears most obvious in 50% VFA622 + 50% 316L. In the absence of any diffusion, a microstructure with 50% ferrite and 50% austenite should be apparent. The presence, (in Figure 4.53), of what appears to be over 70% ferrite (dark etched) could be an indication that ferrite stabilisation has occurred. The spot analyses on the dark etched phase (identified as ferrite) and light etched phase (identified as austenite) are informative (Tables 4.7). The dark etching area contained 38%Cr and 4%Ni and should be ferritic. The light etched phase has 28% Cr and 7% Ni and the literature[73] shows that it roughly corresponds to the composition of a duplex stainless steel, which could therefore explain the possible increased presence of ferrite.

5 15. 50% Hastelloy C + 50% Prem V

The scan of 50% Hastelloy C + 50% Prem V across 1005 microns is shown in Figure 4.70. The surface topography was irregular, with a distinctive variation in Fe, Cr, Mo and Ni content. In the Hastelloy C regions Ni and Mo enrichment was apparent, whilst there was a decrease in Fe and Cr content. As the scan progressed towards a 40Cr-Fe particle the Fe and Cr increased to a definite peak whilst the Mo and Ni descend to a definite minimum value. The centre of a 40Cr-Fe region is shown at point A. The elemental concentration changed as the diffusion zone was crossed until the centre of a Hastelloy C particle was reached at B. The pattern of fluctuation was repeated throughout the scan as different Hastelloy and 40Cr-Fe particles were crossed.

The separate 40Cr-Fe and Hastelloy regions are distinctly observable in Figure 4.70. This is due to the vastly different compositions of the two materials. The effects of diffusion are readily apparent as the Fe and Cr values decrease whilst the Ni and Mo simultaneously increase as the scan moves from a 40Cr-Fe particle to a Hastelloy region (between lines A and B). These results provide an indication of the sensitivity of the SEM scan, since the different materials can immediately be identified. The spot analysis (Table 4.11) of the diffusion zone indicates an intermediate alloy which is rich in Cr, Ni and Fe. On a purely compositional basis, this region of the diffusion zone could possibly be fairly corrosion resistant due to the high Cr and Ni content.

The sinusoidal variation in composition when moving from the Hastelloy regions to the Prem V regions indicated that equilibrium in composition had not been reached. Once the rates of interdiffusion between the two alloys have stabilised, then a step function variation in composition would be expected.

5.16. The effect of HIPping on the kinetics of sigma formation

The result obtained by HIPping the cast, solution annealed, sigma-free material is particularly interesting. In this trial, the hardness of the cast VFA622 alloy increased from 238Hv to only 276Hv. This indicates that only relatively small amounts of sigma phase were formed by the end of the HIP cycle. In comparison, the as-HIPped VFA622 steel consisted completely of sigma phase, with a hardness in excess of 800Hv. Both the cast and HIPped alloys come from the same parent melt and therefore should have the same composition. These hardness differences, therefore, cannot be attributed to differences in chemical composition.

The only time sigma phase can form in a 2Ni-2Mo-40Cr alloy is during exposure to the 600-900°C temperature range. During the HIP cycle this occurs during heating up to the maximum temperature of 1120°C, and also during cooling from 1120°C to room temperature. From the trials involving solution annealing it can be seen that a temperature of 1100°C is sufficient to take all the sigma into solution for the majority of the 2Ni-2Mo alloys. Any sigma phase formed during the heating stage of the HIP cycle should be removed during the sustain period at 1120°C. It therefore follows that the sigma apparent after HIPping could only have formed during the cooling stage

Each HIP cycle contains different thermal loads and the cooling rate is not consistent. However, examination of the cooling rates indicates that there is no major difference from cycle to cycle. Therefore, while differences in the HIP cooling rate may play a role in promoting sigma formation, the role is felt to be fairly minor.

Another cause for the promotion of sigma could be the possibility that HIPping might introduce some kind of forging effect on the powder particles. The hot-worked powder particles would then have more high energy sites to allow sigma nucleation and growth. The results of the repeated HIPping of a fully dense specimen made from VFA622 powder reinforces this theory. After the initial powder consolidation cycle, a hardness in excess of 800Hv was measured and the microstructure consisted completely of sigma phase. However, after being HIPped for a second time in the standard HIP cycle, the hardness of the specimen decreased to 282Hv and only 30 percent sigma was found in the microstructure.

The following explanation was initially suggested. During the initial powder consolidation cycle some kind of hot working effect, caused by particle movement and deformation, could have taken place during diffusion bonding and pore closure.

A diagram of the plastic deformation and hot working of powder particles is shown in Figure 5.1.

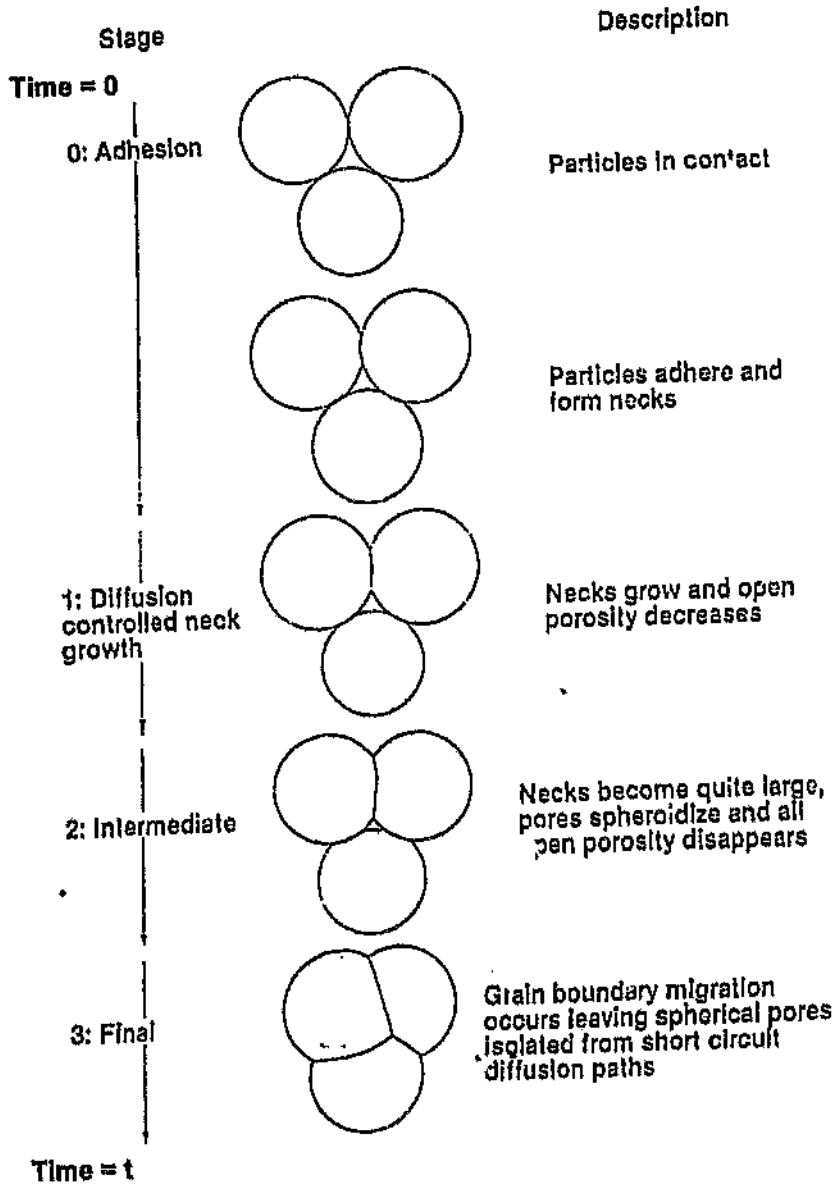

Figure 5.3: Plastic deformation of spherical powders particles during HIPping.[34]

This would cause accelerated sigma formation during cooling, hence the complete conversion to sigma phase. However, during the second HIP cycle, the material is fully dense, so no particle movement or plastic deformation can take place. The four hour exposure at 1120°C (maximum HIP temperature) would therefore act as a stress-relief heat treatment. Thus, an essentially strain-free material would be exposed to the sigma formation temperature during cooling and the amount of sigma phase formed would be reduced.

However, it was noted that the HIP sustain period at 1120°C is generally equivalent to an annealing treatment which reduces the dislocation density and thus the favoured sites for sigma nucleation.

An examination of the consolidation process provides an alternative explanation. As temperature is applied, the sigma particles pack together but do not deform appreciably due to their high hardness. The powder speedily transforms to ferrite once the critical temperature above 1050°C is exceeded. Plastic deformation occurs and the newly-formed ferrite particles weld and form necks at their points of contact. These necks widen by a process driven by atomic diffusion along the free surfaces and grain boundaries. Interconnected porosity is removed. After sufficient time, only isolated, spherical pores exist in a recrystallised equiaxed microstructure. It could be possible that the material produced by the first HIP cycle may not be fully consolidated and may have a profusion of small pores and defects which offers a favourable site for sigma nucleation. The defects would not be observed during metallographic examination since the sigma phase is gouged and cracked during sample preparation, effectively inhibiting detailed examination. The ferrite formed during the second HIP cycle will have a further four hours to achieve full density and will be more resistant to sigma nucleation

This theory applies to the cast material since the material is also fully dense and explains why similar hardness values of 276Hv (cast+HIP) and 282Hv (HIPped twice) are obtained. These results are highly interesting, as no mention is made in the HIP literature regarding similar effects during powder consolidation which have such a profound effect on the final microstructure.

5.17. Corrosion behaviour (Fe-39Cr-2Ni-2Mo alloys)

Figures 4.71-4.72 show the corrosion scans for Prem V in 10 weight percent sulphuric acid. The alloy passivated spontaneously in the solution with the transpassive region starting at approximately 900mV. The passive range was not static and current density increased gradually over an order of magnitude with increasing potential. The main effect of heat treatment was to shift the E_{corr} values to more noble (positive) potentials. VFA487, in Figures 4.73-4.74, underwent spontaneous passivation in both the HIPped and heat treated forms. The second scan in Figure 4.73 was due to an error in experimental procedure and should be discounted. A shift to more negative E_{corr} values was observed after solution annealing. The first scan in Figure 4.74 exhibited uncharacteristic behaviour in the cathodic region which was also most likely due to experimental procedure. Figures 4.75 - 6 show the corrosion scans for VFA622 in 10 weight percent sulphuric acid. The scans in Figure 4.75 indicated irregular behaviour in the passive region, with a fluctuation in the stability of the passive layer. This behaviour was also observed in the heat treated state. However, the second scan in Figure 4.76 did not exhibit this fluctuation. Table 4.15 summarises the corrosion data in 10 percent sulphuric acid.

All of the alloys tested in 70 percent sulphuric acid at 70°C (Figures 4.85-4.92) exhibited an unusual "Z"-shaped corrosion profile. This was characterised by current density increasing with increasing overpotential until E_{crit} was reached. The alloys then underwent a sharp decline in current density corresponding to formation of a passive layer. As the overpotential was raised further the current density again increased gradually. However, the deviation from classical corrosion behaviour became apparent in that a second E_{crit} value was reached in which a decline in current density was again observed. Further increases in overpotential beyond this point resulted in the alloys undergoing active dissolution.

The critical values of E_{corr}, i_{crit} and i_{pass} in 70% sulphuric acid are shown in Table 4.16. The values for i_{corr} could not be readily derived, due to the steep gradient of the anodic slope which prevented the satisfactory use of Tafel extrapolation. The value of i_{crit} was thus used instead to provide an estimate of the corrosion rate.

Prem V, VFA487 and VFA622 passivated spontaneously in the 10 weight percent sulphuric acid solution. The corrosion rates were therefore very low and the alloys did not undergo significant attack in the test solution. This behaviour was expected since these materials contain a very high alloying content. Solution annealing produced mixed effects on the E_{corr} values. Prem V moved to more positive (noble) values, whilst VFA487 and VFA622 shifted to a more negative potential. This result is contradictory, since Prem V, VFA487 and VFA622 have the same nominal composition and similar behaviour would be expected.

Potgieter[53] found that decreasing the proportion of sigma phase in a duplex stainless steel resulted in more positive corrosion potentials. This trend was not observed in VFA487 and VFA622. However, excessive emphasis should not be placed on the equilibrium corrosion potential . These potentials should only be used as a guideline. Although a higher corrosion potential is considered beneficial, the values must be evaluated in conjunction with other factors such as the critical current density, passive range and passivation potential. It is these combined indicators which provide a more informed judgement of a material's corrosion resistance.

The 0.15%Ru addition in VFA622 did not appear to produce a high improvement in corrosion resistance compared to Prem V and VFA487. There are a number of reasons as to why this could be so. Initial reports[37] highlighting the dramatic effect of Ru additions examined only the binary Fe-40Cr alloy. The beneficial effects of 2%Ni and 2%Mo additions were not taken into account in those studies. The addition of these elements could thus overshadow the effects of the Ru in certain test solutions. Additionally, all of these alloys passivated spontaneously in the 10 percent sulphuric acid medium. The corrosion rates were therefore all low, without any major differences between the various alloys. The effect of the Ru additions might therefore only become prominent in more aggressive acid solutions, for which the Ni and Mo content do not provide sufficient resistance.

In the 70% sulphuric solution, the shape of the corrosion curves is unusual since there are two minima in the current density. This could be interpreted as a semi-stable passive layer which is broken down and then reforms as the overpotential is increased, although further experimental data is needed for confirmation.

A second aspect of the curves which bears mention, is the fact that the anodic region does not have a sufficiently large gradient to allow for the determination of i_{corr} by means of the Tafel extrapolation. This may be due to the natural behaviour of these alloys in the test solution. Since a satisfactory value for i_{corr} cannot be obtained, the current density at i_{crit} may be utilised to provide an approximate estimate of the behaviour in the acidic media. The approach provides a conservative estimate of corrosion resistance in a "worst-case" scenario.

The 70% H_2SO_4 solution at 50°C is an extremely aggressive environment and provides a better indication of the corrosion resistance of the various alloys. The most marked example of this may be seen in comparing the corrosion behaviour of Prem V, VFA 487 and VFA622: all in the heat treated condition. These are nominally 39Cr-2Ni-2Mo-Fe alloys, with only VFA622 containing 0.2%Ru. Prem V and VFA487 have corrosion rates ranging between 8-30mm per year which is unacceptable in most engineering applications. Alternatively VFA622 has a maximum corrosion rate of only 0.2mm per year. This result is important since it highlights the fact that the benefits of Ru additions only become noticeable in highly corrosive environments, for which the addition of 2%Ni and 2%Mo alone do not provide sufficient resistance. A comparison with the results in 10% H_2SO_4 indicates that all alloys passivated spontaneously in that test environment, and very little differences in corrosion rate could be discerned. The commercial implication of this data is that Ru additions should only be made when an alloy is to be utilised in the most aggressive situations, since the cost of the additions may be unwarranted in certain environments. VFA622 should also be suitable for highly concentrated H_2SO_4 applications.

5.18. Corrosion behaviour (alloys with Fe additions)

5.18.1 (SP001008 and VFA622+Fe)

Figures 4.77-4.78 show the corrosion results for SP001008 in 10 weight percent sulphuric acid. Spontaneous passivation was observed in both the as-HIPped and heat-treated states. The passive range appeared to be fairly stable in the test medium and remained within the same order of magnitude with increasing potential. The inconsistent behaviour of first scan in Figure 4.78 was due to an intermittent electrical contact in the corrosion testing equipment. Heat treatment appeared to result in a shift to a lower corrosion potential. However, with only one reliable scan it could not be determined if the decrease in E_{corr} was truly representative of the behaviour of the material.

VFA622+Fe, in Figures 4.89-4.90, exhibited similar corrosion behaviour in the 70 weight percent sulphuric acid solution, in both the as-HIPped and solution annealed state. The scans followed the classic pattern of a material which underwent passivation. However, a deviation occurred in the transpassive region. The alloy appeared to corrode actively but then experienced a decrease in current density corresponding to the possible formation of a second passive layer. Solution annealing did not appear to produce a significant difference in corrosion behaviour.

The central aim of Fe additions to VFA622 is to eliminate sigma formation during HIPping, whilst still maintaining corrosion resistance. In terms of sigma removal the technique is successful. The results of corrosion testing indicate spontaneous passivation in both the as-HIPped and heat treated states. The following mechanism could provide a plausible explanation for this behaviour.

Fe was introduced into alloy VFA622 by ball milling (alloy SP001008). The main aim is of milling to produce thorough mixing of the individual Fe and VFA622 particles and communition of the particles. The reduction in particle size should increase homogeneity during HIPping, since there would be a shorter inter-particular diffusion distance. In effect, each Cr-rich VFA622 particle should be surrounded by a number of pure Fe particles (Cr-deficient). During HIPping the simultaneous application of high temperatures and pressures could result in sufficient diffusion of the Cr from the VFA622 to the surrounding Fe particles. This Cr would then provide the bulk of the corrosion resistance in the Fe particles. Although Ni and Mo diffusion could also occur, these elements are present in far smaller amounts (2%Ni and 2%Mo) compared to the far higher 40% Cr content. There would therefore tend to be a smaller Ni and Mo diffusion gradient between the VFA622 and Fe particles and consequently less of a driving force for large scale diffusion.

In the limiting case, in which minimal diffusion occurs, complete dissolution of the Fe particles in the sulphuric acid would be expected. A "sieve" consisting of VFA622 particles surrounded by open regions formerly occupied by Fe particles should be the result after immersion in the acid solution. This should produce some signs of active corrosion in the potentiodynamic scans. However, the results which were obtained indicate passive behaviour. This result (combined with the data from Section 5.13.1) provides evidence that sufficient interparticular diffusion took place to ensure overall passivation of the alloy. These results are observed in the as-HIPped alloy. The subsequent solution annealing treatment would provide energy for further homogenisation. Heat treatment results in a slightly lower corrosion rate with a drop in corrosion potential compared to the as-HIPped state. The decreased corrosion rate could be due to further homogenisation in heat treatment. This alloy contains a high C content (0.176%C) and is correspondingly rich in carbides. However, despite the evidence that these carbides are possibly enriched in Cr and Mo, the alloy still exhibits a low corrosion rate in the test media.

In the as-HIPped state some unusual behaviour was noticed in VFA622+Fe (hand mixed). In the first scan of Figure 4.79 the passive layer initially appeared stable. At higher potentials the passive layer had a tendency to break down and reform. This was not observed in the second scan, possibly due to not allowing a sufficiently high potential to be achieved. Unusual loops were also present in the cathodic region of the second scan. There was a large difference in the E_{corr} values of the two scans. In the heat treated state (Figure 4.80), the passive layer appeared to be more stable and occurred over a more closely defined current density. The cathodic regions in both scans (Figure 4.80) do not exhibit any obvious irregularities.

Alloy VFA622+Fe was manufactured utilising the same principle of adding Fe prior to HIPping. However, simple, low energy hand mixing was used instead of ball milling. The results in Figure 4.79 for the as-HIPped material indicate unusual behaviour. Although both scans show spontaneous passivation, the anodic curve in scan one fluctuates with increasing potential. In the second scan fluctuations are observed in the cathodic region. Although it might be suggested that the fluctuations in the first scan are due to the continuous formation and breakdown of the passive layer, indicating borderline passivity in the acid media, there is no further evidence to reinforce this claim. The fluctuations could be due to experimental difficulties, most likely intermittent connections in the corrosion rig external circuitry, and further trials on the as-HIPped material are suggested before any firm conclusions may be drawn.

In short, there are three factors which suggest bulk diffusion between the VFA622 and Fe particles. In the first instance, no sigma phase is formed after HIPping. Since sigma formation is highly dependent on a high Cr content, this implies that the Cr percent of the VFA 622 particles must have been sufficiently lowered below some critical value. The corrosion scans do not indicate any signs of active dissolution. This could only be possible if some Cr had diffused to the Fe particles. The elemental dispersion scans (Section 5.13.1) did not indicate any regions which are greatly Cr or Fe enriched relative to their surrounding areas. It may therefore be feasible to assume that the addition of Fe by means of ball milling or hand mixing can be used to produce an alloy which is sufficiently homogeneous to resist corrosive attack in certain acid media.

5.19. Corrosion of alloys from duplex powders in 10 wt% H_2SO_4

The central aim of producing alloys from duplex powders is to determine if 316L can be used as a partial substitute for the 40Cr-Fe, steel or if the 40Cr-Fe steel can likewise be used as a filler for Hastelloy C. Austenitic 316L is less costly than 40Cr-Fe, whilst 40Cr-Fe is in turn cheaper than the nickel- ased Hastelloy C. Changing the percentages of the different materials should also allow the proportions of ferrite and austenite phases to be varied as required. The trials were to examine if such substitutions can be performed without compromising corrosion resistance.

The corrosion scans for 20% 316L + 80% VFA 622 are shown in Figure 4.81. This composite alloy underwent spontaneous passivation in the 10 weight percent sulphuric acid solution. There was a fairly large difference in the E_{corr} values of the two scans, in the heat treated state. The 20%316L+80%VFA622 alloy passivated spontaneously in the test solution, and therefore displays a low corrosion rate which is similar to plain VFA622. This perhaps be an indication that the addition of 20% 316L is not detrimental to the corrosion resistance of the VFA622 alloy in this specific test environment.

Alloy 50% 316L + 50% VFA622, in Figure 4.82, exhibits a small active loop, followed by passivation in the first scan whilst only spontaneous passivation is observed in the second scan. Without further experimentation, it cannot be determined if the first scan is indicative of borderline passivation characteristics, or is simply due to experimental procedure. A direct method would be to examine the behaviour of conventional 316L under the same test conditions. The corrosion rate of 50% 316L + 50 % VFA622 at E_{corr} is of a low magnitude.

The corrosion data (Figure 4.83) obtained on alloy 80% 316L + 20% VFA622 was highly irregular. The material would not stabilise, and the potentiodynamic scan indicates a general trend of increasing current density with increasing potential. This is possibly due to the widespread porosity present in the test piece. Porosity is deleterious since it allows for localised regions within the pore to experience a far higher acid concentration relative to the bulk solution. Porosity arises most frequently due to leaks in the mild steel capsule during HIPping. Leaks occur most commonly in the welded areas of the capsule. This allows argon gas to enter the capsule and further bonding is inhibited. The degree of porosity is dependent on the stage at which the leak occurs. If the leak occurs early in the cycle (before maximum temperature and pressure) then no bonding takes place. Alternatively, if a leak occurs after some bonding takes place, then residual porosity will be present. In the most desired scenario, no leaks occur and full density is achieved.

In general, porosity should be minimised since it is detrimental to mechanical properties and decreases corrosion resistance.

Alloy 50% Hastelloy C + 50% Prem V, shown in Figure 4.84, was found to undergo anomalous behaviour during potentiodynamic testing. The composite alloy took over 2500 minutes to stabilise in the 10 weight percent sulphuric acid medium. However, it did passivate spontaneously. In the second scan the alloy was not allowed to stabilise and fluctuations are noticed in the anodic and cathodic regions. This unusual characteristic is not due to porosity since microstructural examination (Figure 4.59) reveals the test piece to be pore-free. Alloys which require long periods to stabilise often exhibit borderline passivity in the test media. It has been shown that Prem V has a stable passive layer in 10 weight percent sulphuric acid. The literature[74] indicates a corrosion rate of less than 0.0508mm per year for Hastelloy C under similar corrosive conditions. This low corrosion rate is consistent with a stable passive layer in the solution. A possible explanation could be the existence of a galvanic effect within the inhomogeneous regions of the composite alloy. Prem V is Fe- and Cr- rich whilst the Hastelloy is Ni, Cr and Mo rich. From Figure 4.62, it can be seen that the Prem V and Hastelloy regions are in intimate contact with each other, with a widespread diffusion zone between the particles. The diffusion zone is rich in Ni,Cr, and Fe. It could therefore be possible that a galvanic effect between the three regions could prevent the alloy from establishing a stable equilibrium corrosion potential. However, at present there is very little evidence to substantiate this suggestion, and no feasible explanation can be made at this time. Despite the fluctuations in the scans the composite alloy has a low corrosion resistance in 10 weight percent sulphuric acid.

5.20. Summary of corrosion resistance of duplex powders

It initially appears that the simple mixing technique can be used to manufacture composite alloys. However, discrete particles from each alloy are still observed in alloys 80% 316 + 20% VFA622 and 50% Hastelloy C + 50% Prem V. The composites passivated spontaneously in 10 weight percent sulphuric acid at room temperature. This indicated that partial substitutions of 316L and 40Cr-Fe could be a possible method of manufacturing future corrosion resistant alloys.

The results of the alloys with the Fe additions (SP001008, VFA622+Fe) are informative. These alloys demonstrate satisfactory resistance to the 70% H_2SO_4 solution. This is an important test of the homogeneity of the mixed powders. No preferential corrosion of possible low Cr regions was therefore detected in either the 10 percent or 70 percent H_2SO_4 environment. It thus indicates that HIPped composite powders could be a viable method in producing corrosion-resistant high Cr stainless steels which have a low tendency to form sigma phase.

The corrosion scan of 80% 316 + 20% VFA622 (heat-treated), in 70 percent sulphuric acid at 50°C is shown in Figure 4.83. The alloy passivated but exhibited a second minimum in current density in the transpassive region. The critical current density was fairly high at 0.6 mA/cm^2. The 80% 316L + 20% VFA622 composite had an unacceptable corrosion rate of 6mm per year at i_{crit}. In addition, the corrosion rate at i_{pass} is the highest out of all the alloys evaluated. This is expected, since 316L is a far less alloyed material than 40Cr-Fe, and since it makes up the bulk of the composite powder, lower corrosion resistance would naturally be expected. It is reported[74] that 316L typically corrodes at over 1.3mm per year in the test environment. The lowest measured corrosion rate (i_{pass}) for the composite is an order of magnitude larger than the other alloys, and agree with the expected corrosion behaviour of plain 316L steel. No improvement is thus observed due to the VFA622 additions and thus further work on this particular composite is not justifiable.

The 50% Hastelloy C alloy + 50% Prem V (Figure 4.84) had a distinct anodic loop in the 70 weight percent sulphuric acid medium. The passive layer appeared fairly stable and no transpassive region was observed even at an overpotential of 1000mV. The 50% Hastelloy C + 50% Prem V composite has a fairly high i_{crit}, However, the i_{pass} value indicates acceptable corrosion behaviour in the passive state. Both Hastelloy C and Prem V are highly alloyed, so that even in the diffusion zones between the different materials high Cr and Mo levels are obtained. It might therefore be possible that a composite of this nature could be the basis of further study.

5.21. Springlock field trials

The present results are from an intermediate stage of the field trial. Nevertheless, they do provide a rough idea as to the initial behaviour of VFA622 in this particular industrial application. VFA622 and 904L, so far, appear to exhibit equivalent resistance to the acid leaching process. This is important since 904L is a highly alloyed austenitic stainless steel grade (Table 5.1) which is only used in the most demanding corrosion applications. It could therefore be possible that the 40Cr-2Ni-2Mo-0.15Ru-Fe alloys might be viable as an alternative material in certain applications in which 904L is currently used.

The initial results are encouraging in that there are no overt signs of corrosive attack. It must be mentioned that the equipment used to measure mass loss is only sensitive to the nearest 0.2g, so any mass loss between 0 and 0.2g was undetected. A more detailed view of the behaviour of VFA622 and 904L will only become available after further prolonged exposure to the industrial environment. It is reported that the service life of a 904L spring lock is 1-2 years.

Table 5.1: Nominal composition of grade 904L (weight %)[7]

C	Mn	Si	Cr	Ni	P	S	Mo	Cu	Fe
0.02	2	1	19-23	23-28	0.045	0.035	4-5	1-2	Balance

The satisfactory behaviour of the test components in field trials may be explained in part by the good results obtained in the laboratory electrochemical tests. It is now known that VFA622 is fairly resistant to concentrated H_2SO_4 at 50°C, and H_2SO_4 exposure is a substantial part of the industrial field trial. Some resistance to the H_2SO_4 in the field trial would therefore be expected. The continued survival of VFA622 compared to 904L provides an indication of future possible commercial applications for the 40Cr-2Ni-2Mo-0.2Ru alloys.

5.22. Composition and manufacturing guidelines

While it initially appears beneficial to utilise the highest alloying contents possible, in practice this is not always feasible. Excessive levels of Ni, Mo and Cr result in materials which are extremely brittle after HIPping. Conversely, compositions with relatively lower alloying additions, do not embrittle easily and cannot be transformed into an usable powder. The requirement for maximum corrosion resistance must therefore be balanced by two other factors: the ease of powder manufacture, and the toughness characteristics directly after HIPping.

The various trials which have been undertaken provide approximate guidelines. An alloy should contain a maximum of two percent Ni, two percent Mo and 38 percent Cr. The HIPped material must be solution annealed prior to exposure to a corrosive environment, or before any working, shaping or machining operation is performed. Solution annealing may be performed at a temperature of 1100°C for a period of 2 hours, followed by a room temperature water quench.

In terms of minimum alloying levels, these are 36 percent Cr in plain alloys, whilst 30 percent Cr is acceptable in a duplex powder. Earlier trials experimented with combined Ni and Mo contents of less than 4 percent. These alloys could not be embrittled sufficiently to form powder. In order to maintain pitting corrosion resistance, Mo levels should not be dropped significantly below the two percent range. Ni should also not be decreased very far below two percent, since it is required to provide resistance in reducing environments and improve impact toughness. The effect of composition is shown in Figure 5.4.

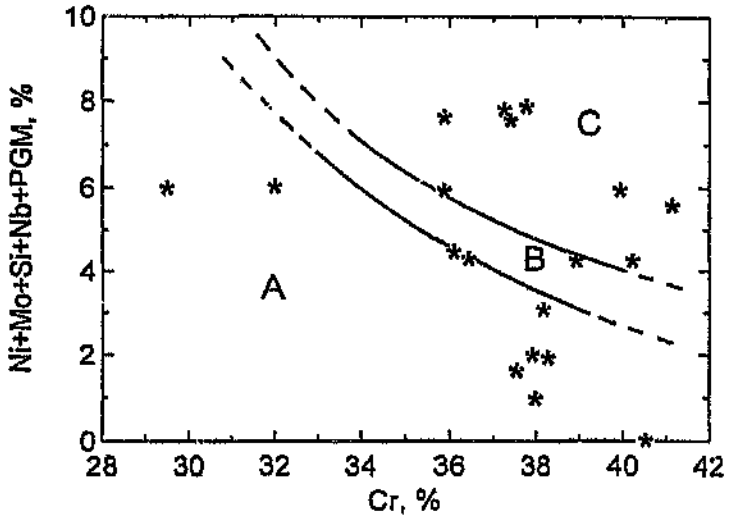

Figure 5.4: Diagram illustrating the effect of composition on the properties of the alloys. A - takes too long to convert to powder, B - Comes out of HIP as ferrite, C - comes out of HIP as sigma phase.[78]

The relatively high level of non-metallic inclusions in the majority of the powders is a cause for concern. Inclusions are detrimental since they can affect mechanical properties, corrosion resistance and surface finish. Commercial grade atomised powders typically have far lower inclusion concentrations than the milled 40Cr-Fe powders, and steps will have to be taken to improve the cleanliness of the powders. The inclusions could have entered the powder during any of the manufacturing stages such as melting, milling or encapsulation. It is considered most likely that the vibratory milling stage is the main source of contamination. Silica sand is used as a cleaning agent in the vibratory mill, and it is difficult to remove completely from the mill chamber. The fine silica particles would therefore enter the 40Cr-Fe powder and be assimilated. Scale from heat treatment is also a factor, and should also be removed. Contamination could be lessened by milling an initial batch of 40Cr-Fe powder and then scrapping this material, since most of the residual silica would be removed with the powder.

5.23. Mathematical model comparison

The addition of pure powder Fe to VFA622 produced a compact which was shown to be reasonably homogeneous by elemental scans and by corrosion tests. This mixture also had the advantage of being free of sigma phase after HIPping. The above characteristics could only have been possible if sufficient diffusion had occurred between the Fe and VFA622 particles. The process is therefore suitable for examination by the mathematical models proposed by Arunsingh, Heckel and Larsson. The experimental data have shown that isothermal annealing at 1120°C for a period of four hours (during HIPping) or less was sufficient for homogenisation. This may be seen by comparing the elemental scans of alloy VFA622+Fe after a further two hours solution annealing at 1100°C (Figures 4.68-4.69). There was very little change in elemental distribution after the extended exposure, implying that homogenisation had been achieved. The results of VFA622+Fe may also be extended to SP001008. This alloy also exhibited homogeneous elemental scans. However it was felt that since the particle size was much finer after milling, the diffusion distance between the VFA622 and pure Fe particles would be less and homogenisation would occur in a shorter time than in the VFA622+Fe.

Some assumptions have to be made in order to apply the models. The first assumption is that the VFA622 particles contain only Fe and Cr. Although Ni and Mo are present in proportions of 2 weight percent each in VFA622 it is felt that they may be excluded since they are relatively minor alloying elements. The second assumption is that a spherical powder particle geometry is applicable. This assumption is reasonable as a first order approximation since Heckel indicated that the effect of particle shape on interdiffusional coefficients was minor compared to the effects of other variables which could be accounted for mathematically.

The spherical geometry and diffusion distances used for examination of the mathematical models are shown in Figure 5.5. Since the Fe particles are the minor alloying constituent they are assumed to be surrounded by a continuous matrix or shell comprised of a binary 60% Fe - 40%Cr alloy. The particle sizes were obtained from the average sizes in the relevant Malvern analyses (Figure 4.6 and Table 3.3).

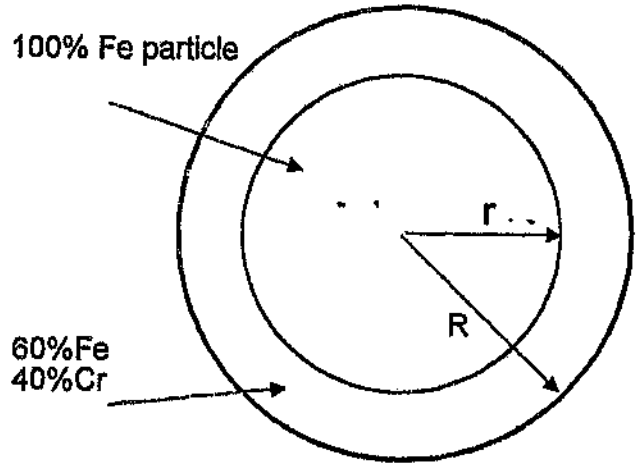

Figure 5.5: Parameters utilised in the examination of Arunsingh's and Heckel's homogenisation models.

The average particle size of the Fe powder was 12 μm. Therefore
$r = a = 0.5l_o = 6\mu m = 6 \times 10^{-4}$cm.
The average particle size of the VFA622 powder was 128μm, therefore
$R = 0.5L = 64\mu m = 64 \times 10^{-4}$ cm.

The diffusion data in Table 5.2 are required by the models:

Principal metal	Alloying additive (Weight %)	Tracer	Temperature range (°C)	Activation energy Q ($kJ.mol^{-1}$)	Frequency factor D_o ($cm^2.s^{-1}$)	Calculated diffusion coefficient D at1393K using $D = D_o e^{-Q/RT}$ ($cm^2.s^{-1}$)
Fe	41.5 Cr	^{59}Fe	1000-1200	265	5	5.86×10^{-10}
Cr	48.3 Fe	^{59}Fe	1000-1200	288.1	27	4.34×10^{-10}
Cr	49 Fe	^{51}Cr	1000-1275	293.1	40	4.14×10^{-10}
Cr	<<1 Fe	^{55}Fe	930-1240	232.4	0.2	3.90×10^{-10}
Fe	2 Cr	^{51}Cr	800-1400	244.5	3.21	2.18×10^{-9}

Table 5.2: Diffusion data and calculated diffusion coefficients at 1120°C (1393K).[57]

A diffusion coefficient of D (Fe in Fe-41.5Cr, at 1393K) = 5.86×10^{-10} $cm^2.s^{-1}$ is used in all diffusion calculations.

5.23.1. The infinite diffusion couple

The equation describing the concentration profile in an infinite diffusion couple is:

$$C(x,t) = 0.5C_o[1 + \text{erf}(\frac{x}{2\sqrt{Dt}})]$$

For homogenisation $C(x,t)=0.5C_o$,

i.e.

$$0.5C_o = 0.5C_o[1 + \text{erf}(\frac{x}{2\sqrt{Dt}})]$$

which simplifies to:

$$0 = \text{erf}(\frac{x}{2\sqrt{Dt}})$$

A property of the error function is that erf(0) = 0.

Thus

$$0 = \frac{x}{2\sqrt{Dt}} \qquad (25)$$

Equation 25 can only be satisfied if $x = 0$.

Equation 25 indicates that for all t and D the homogenised composition $0.5C_o$ can only occur at the position $x = 0$ ($x = 0$ is the interface between two infinite bars of composition C=0 and C=C_o). In reality, a finite homogenised bar would have a concentration of $0.5C_o$ for all x. This result is not surprising since the infinite diffusion couple model was never formulated to provide information about homogenisation times. The calculation with C=$0.5C_o$ is informative in that it indicates that the model (commonly employed in other diffusion systems) cannot be used even as a first order approximation to the homogenisation problem, since the graph (Figure 2.50) never reaches uniformity.

5.23.2. Arunsingh's model

Arunsingh's expression for homogenisation time is:

$$t_{Arunsingh,\ homogenisation} = \frac{a^2}{D\pi^2} \log \frac{2C_o}{C}$$

Substituting the relevant values:

$$t_{Arunsingh,\ homogenisation} = \frac{(6 \times 10^{-4} cm)^2}{5.86 \times 10^{-4} cm^2.s^{-1}\pi^2} \log \frac{2(100)}{70}$$

$$= 28.4s$$

5.23.3. Heckel's model

Heckel's model for homogenisation is described by:

$$F = 1.10 + 0.44\log_{10}[(\frac{Dt}{l_o^2})n^2Y]$$

For complete homogenisation F = 1, i.e. matter transport across the interface reaches its limiting value. Thus:

$$1 = 1.10 + 0.44\log_{10}[(\frac{Dt}{l_o^2})n^2Y]$$

Which can be simplified to arrive at an expression for homogenisation time:

$$t_{Heckel,\ homogenisation} = \frac{0.593l_o^2}{Dn^2Y}$$

For spherical geometry $n = 3$.

For Y:

$$\overline{C} = (\frac{l_o}{L})^3 = (\frac{12um}{128um})^3 = 8.8 \times 10^{-3}$$

Which is close to zero, thus from Figure 2.54, Y = 0.2.

Now:

$$t_{Heckel,\ homogenisation} = \frac{0.593(12 \times 10^{-4} cm)^2}{5.86 \times 10^{-10} cm^2 s^{-1}(3)^2(0.2)}$$

$$= 8.1 \times 10^2 s$$
$$= 13.4 \text{ minutes}$$
$$= 0.22 \text{ hours}$$

5.23.4. Larsson's model

Larsson's model allows the visualisation of the homogenisation problem as shown in Figure 5.6. The pure Fe particle is surrounded by numerous Fe-Cr particles. The thickness of the enclosing spherical shell is thus the distance (R-r) from the centre of the Fe-Cr particles to the circumference of the pure Fe particle. The total homogenisation distance is therefore the total distance R between the centres of the Fe-Cr and Fe particles.

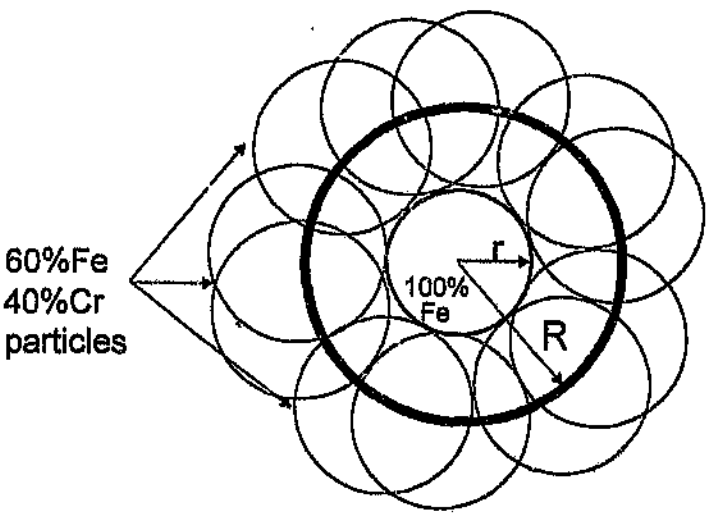

r = radius of Fe particle
= 6 microns
R = distance between centres of Fe and Fe-Cr particles
= 70 microns.

Figure 5.6: Application of Larsson's model to the homogenisation of spherical Fe-Cr and pure Fe particles. The overlapping circles indicate the different 60Fe-40Cr layers in contact with the Fe particle in three dimensions.

Larsson's expression for homogenisation time is:

$$t_{\text{Larsson, homogenisation}} = \frac{0.3A^2}{D}$$

Substituting the relevant values yields:

$$t_{\text{Larsson, homogenisation}} = \frac{0.3(70 \times 10^{-4} cm)^2}{5.86 \times 10^{-10} cm^2 s^{-1}}$$

$$= 2.5 \times 10^4 \text{ s}$$
$$= 418{,}1 \text{ minutes}$$
$$= \underline{7 \text{ hours.}}$$

The models of Arunsingh and Heckel produce values for homogenisation time which are far too short and deviate unreasonably, by one to two orders of magnitude, from the experimental values. The results are not due to any inconsistencies in the choice of an appropriate diffusion constant. An examination of the various calculated diffusion constants for the Fe-Cr system at 1393K (Table 5.2) indicates that the constants are all of the order of 10^{-10} cm^2s^{-1}. Interchanging the constants or using a calculated chemical diffusion coefficient value (Equation 9) does not change the order of magnitude of the results.

Alternatively, Larsson's model produces a value which is in relatively good agreement with the experimental data. The calculated value of 7 hours is less than a factor of 2 greater than the observed value of 4 hours. This agreement is acceptable when considering that the model does not take into account the effect of applied isostatic pressure and makes simplifying assumptions regarding particle geometry and ideality of mixing. In addition the effects of other species such as Mo and Ni have been ignored in the calculation. It appears the model may therefore be used to provide an order-of-magnitude approximation to the homogenisation problem in HIPped compacts with powders of binary composition.

However, the question remains as to how three models of essentially the same homogenisation problem can produce such widely differing results from the same starting data. The answer may be found be examining the basic assumptions made by each model. Arunsingh's model views each solvent particle as being surrounded by an infinite matrix which provides the material for homogenisation within that particle. The system is thus "semi-infinite". The time equation is therefore dependent on the radius (a) of the solvent particle only and ignores the effect of the solute particle size. Heckel's model differs in that both the solute and solvent particles have a defined radius in a finite system. The influence of the solute particles are taken into account by the inclusion of the Y factor in the homogenisation equation, where $Y=f(\overline{C})$ and $\overline{C}=f(l_o,L)$. However, the influence of the solvent particle radius (a) is dominant in equation (19) since a is raised to the second power, whereas Y is only raised to the first power. Larsson's model attempts a more comprehensive approach to homogenisation in a finite system. The influence of both the solvent and solute particle size is taken into account by the inclusion of the starting condition ($\frac{b}{a}<X\leq 1$, $C=C_s$ at $T=0$) in the solution of Fick's equation. Thus although Larsson's model provides the simplest expression for t, the result is more accurate since the entire diffusion distance, and not just the distance involving the solvent particle, is taken into account. This is obviously a more general interpretation of the homogenisation problem which should intuitively yield more realistic results.

It is interesting to note that Larsson's solution corresponds to an early proposal by Rhines and Colton[59] that the attainment of a given degree of homogeneity could be expressed by:

$$\frac{X^2}{Dt} = k \quad (26)$$

where:
X is the distance between adjacent centres of maximum and minimum concentration.
t is the time of homogenisation.
D is the diffusion coefficient.
k is a constant which describes the degree of homogenisation.

6. CONCLUSIONS

1. The 2Ni-4Mo-40Cr-Fe family of alloys are easily embrittled for powder manufacture, but form excessive amounts of sigma phase after HIPping.

2. The 2Ni-2Mo-40Cr-Fe alloys possess the most suitable composition for commercial applications due to a slower rate of sigma formation during HIPping.

3. There is a difference in the kinetics of sigma formation under conditions of continuous cooling as compared to isothermal annealing. Sigma phase formed more speedily during continuous cooling.

4. Cast-only material and HIPped-only material of alloy VFA622 exhibit different rates of sigma formation when subjected to similar HIPping conditions. The HIPped material formed sigma far more quickly than the cast material.

5. Hot forging promotes sigma phase formation.

6. Slight differences in composition and prior hot working have a significant effect on the kinetics of sigma formation.

7. A reduction in starting particle size of a readily sigmatised alloy does not improve the toughness characteristics and appears to increase the rate of sigma formation in the alloy.

8. Very little carbon or oxygen pickup occurred during Seib milling, whilst ball milling with steel media introduces significant carbon and oxygen contamination.

9. HIPped alloys of the type Fe-39Cr-2Ni-2Mo, both with and without Ru additions, passivated spontaneously in ten weight percent sulphuric acid at room temperature.

10. The beneficial effects of Ru on corrosion resistance only became apparent in highly corrosive environments such as 70 weight percent sulphuric acid

11. An alloy of the type 2Ni-2Mo-39Cr-0.2Ru-Fe (VFA622) exhibits a low corrosion rate in 70 weight percent sulphuric acid at 50°C.

12. The performance of VFA622 was equivalent to the commercial super-austenitic alloy 904L in the industrial field trial in the results so far, although the test has not reached completion.

13. Simple mixing techniques are effective in producing a uniform dispersion of different particles. Some of these duplex alloys exhibit distinct and widespread diffusion zones between individual particles e.g. 50% Hastelloy + 50% Prem V.

14. The simple mixing of Hastelloy C and Prem V does not decrease sigma formation.

15. The addition of pure Fe particles to the VFA622 powder is successful in inhibiting sigma phase formation.

16. Simple mixing techniques are preferable over ball milling since similar effects are achieved in a shorter period of time, and contamination of the powder is minimised.

17. Elemental scans coupled with corrosion data indicate that some homogeneity is achieved after HIPping in duplex powder VFA622+Fe.

18. The combination of 316L and VFA622 appeared to enhance the conversion of austenite to ferrite in the 316L material and duplex microstructures are obtained.

19. The combination of dissimilar powders produced modifications in microstructure which was attributable to enhanced interactive diffusion during HIPping.

20. The addition of VFA622 as a filler material did not enhance the corrosion resistance of 316L in 70 weight percent sulphuric acid at 50°C.

21. VFA622+Fe exhibited satisfactory resistance to 70 weight percent sulphuric acid at 50°C.

22. The combination of VFA622 and Hastelloy C did not result in any marked improvement or degradation in corrosion resistance over conventional Hastelloy C, or plain VFA622.

23. The infinite diffusion couple and the homogenisation models of Arunsingh and Heckel do not provide realistic results when applied to the problem of HIPped, mixed powders of binary composition.

24. Larsson's model allows for an order-of-magnitude approximation of the homogenisation problem.

7. COMMERCIAL PROSPECTS AND FUTURE WORK

The 40Cr-Ni-Mo-Fe series of alloys with Ru additions have been available in South Africa on a commercial basis since 1996. The alloy is sold in the cast form under the trade-name "Ruthalloy" (a trademark of Steloy Precision Castings). This family of alloys therefore has achieved representation and exposure in both the local and overseas market. It is understood that the alloy has already gained acceptance in certain applications. The introduction of a commercial powder metallurgy method should therefore have the benefit of the advance marketing which has already taken place.

Future work should involve pitting and localised corrosion tests, particularly of the compacts formed from duplex powders. The optimisation of heat treatment temperatures and times and the effect on mechanical and corrosion properties would be informative. This would help characterise the alloys for any further potential commercial applications.

The accuracy of Larsson's homogenisation model in other HIPped alloy systems should be examined to determine if it could be utilised as an appropriate tool in other development work. The shortcomings of Larsson's solution could possibly be overcome by the development of a model which examines the behaviour of a dispersed heterogeneous phase in a continuum. Crank[56] provides some suggestions as to how the model may be derived.

8. REFERENCES

1. Fontana, M., Greene, N.,"Corrosion Engineering", pub.McGraw-Hill, 1978.

2. Cortie, M.B., "History and development of ferritic stainless steels", J.-S. Afr. Inst. Min. Metall, vol 93, no.7, Jul.1993, p.165-176.

3. Tullmin, M.A., "The development of experimental ferritic stainless steels containing 40 percent chromium", Ph.D. thesis, Faculty of Engineering, University of the Witwatersrand, 1992.

4. Hermanus, M.A., "The development of a tough, high chromium ferritic stainless steel", MSc dissertation, Faculty of Engineering, University of the Witwatersrand, 1986.

5. DeMarsh, E.A., "A study of the embrittlement and toughening of Fe-40Cr alloys" M.Sc. dissertation, Faculty of Engineering, University of the Witwatersrand, Johannesburg, South Africa, 1986.

6. Van Zwieten, "The effect of interstitials on the dynamic toughness properties of Fe-40Cr", M.Sc. dissertation, Faculty of Engineering, University of the Witwatersrand, Johannesburg, South Africa, 1987.

7.Wolff, I.M., "Investigation of the fracture mechanisms of high chromium alloys" , Ph.D thesis, Dept. of Metallurgy, University of Cape Town, 1989.

8. "Chemical Processing SA", pub. Primedia Publishing, p.4, April 1996.

9. Shubat, G., "Metals Handbook-Eighth Edition-1973, Volume 8" pub. The American Society for Metals, 1973.

10. Spendelow, H.R., "The influence of Cr on the mechanical properties of plain chromium steels", Transactions of the American Society for Metals, Vol.43 , p.211, 1951.

11. Demo, J.J., "Corrosion", vol.27, no.12, Dec., p.531, 1971.

12. Nichol, T.J., "Embrittlement of ferritic stainless steels", Metallurgical Transactions A, April, Vol.11A, p.573, 1980.

13. Heger, J.J., "Metals progress", August, p.55, 1955.

14. Houdremont, E., "Hanbuch der Sondertstahlkunde", Springer Verlag, Berlin, Germany, 1943.

15. Grobner, P.J., "Metallurgical Transactions", Vol.4, January, p.251, 1973.

16. Davis, J., "ASM Handbook - Volume 4: Heat treatment", pub. The American Society for Metals, p. 895-897, 1991.

17. Jacobsson, P., "Metallurgical Transactions", Vol.6A, August, p.1577, 1975.

18. Cortie, M.B., Pollack H., "Embrittlement and aging at 475°C in an experimental ferritic stainless steel containing 38 wt.% chromium", Materials Science and Engineering, Vol.A199, p. 153-163, 1995.

19. Wright, R.N., "Toughness of ferritic stainless steels", ASTM STP 706, ASTM, p.145, 1980.

20. Otaguchi, M., "Influence of high hydrostatic pressure on the sigma transformation of an Fe-Cr alloy", J. Japan Inst. Metals, Vol.45, No.6, p.620-623, 1981.

21. Premachandra, K., "Sigma phase formation in high chromium ferritic stainless steels" , MSc dissetation, Faculty of Engineering, University of the Witwatersrand, 1993.

22. Chernova, G.P., "Corrosion", Vol.343, No.12, p.445, 1978.

23. Tomashov, G.P.,"Zashchita Metallov", vol.17, No.1, p.16, 1981.

24. Iorio, L.E., Witcomb, M.J., Cornish, L.A., "A transmission electron microscopy study of a nominal Fe-40%Cr alloy", Proceedings of the Electron Microscopy Society of Southern Africa, p.27, 1994.

25. Cortie, M., Wolff, I., Premachandra, K., Tullmin, M., DeMarsh. E., "Superferritic stainless steels containing 40 percent chromium", Proceedings of International Conference on stainless steels, Chiba, ISIJ, p.555, 1991.

26. Premachandra, K., Cortie, M.B., Eric, R.H., "Effect of stabilising elements on formation of sigma phase in experimental stainless steels containing 39%Cr", pub. Materials Science and Technology May, vol. 8, p.437-442, 1992.

27. Higginson A, "Passivation of cathodically modified alloys" , pub. British Corrosion Journal, Vol.24, No.4, p.297-301, 1989.

28. Wolff, I., Iorio, L.E., Scheers, P.V.T., "Oxidations and corrosion behaviour of FeCr and FeCrAl alloys with minor alloying additions", Materials Science and Engineering A., Vol.A241, p.264-276, 1998.

29. Mintek information pamphlet pub. Mintek, South Africa, Second Quarter issue, 1995.

30. Wong-Kian, M., Cornish, L.A., Van Bennekom, A."Comparison of erosion-corrosion behaviour of hot isostatically pressed and welded Stellite coatings", Journal of the South African Institute of Mining and Metallurgy, Vol.95, December, p.319 1995.

31. "Introduction to Powder Metallurgy", pub. European Powder Metallurgy Association, 1994.

32. Cortie, M.B., Nana,S., Wolff. I.M.,"Stainless steel material and the production of stainless steel artifacts therefrom", South African Provisional Patent Application No. 94/0410, 1994.

33. Klar, E., "ASM Handbook - Volume 7: Powder Metallurgy", pub. The American Society for Metals, 1984.

34. Atkinson, H.V., "Hot Isostatic Pressing", pub. Adam Hilger, 1991.

35. Jarvenpaa M., "Consolidation and diffusion bonding of stellite and stainless steel by Hot Isostatic Pressing", Proceedings of the International Conference on the Hot Isostatic Pressing of Materials, p.3.1, pub. the Royal Flemish Society of Engineers, 1988.

36. Dunford, D.V., Partridge P.G., " Diffusion bonding of Al-Li alloys", pub. Materials Science and Technology May, Vol 8, p. 385, 1992.

37. Li,W.B., Easterling, K.E., " Cause and effect of non-uniform densification during hot isostatic pressing" , pub. Powder Metallurgy, Vol.35, No. 1, p. 47-52, 1992.

38. Eisen, W-B., "Mathematical modelling of hot isostatic pressing", pub. Reviews in Particulate Materials, Vol.4, p.1-42, 1996.

39. Erhard, K., "Metals handbook, Ninth edition-volume 7", pub. American Society for Metals, 1984.

40. Janousek M., Greiner H., Kautz S., Kock W., Singer R.F.,"Ductile brittle transition and high temperature creep behaviour of recently developed ODS Cr-based alloys", Proceedings of the 1995 European Conference on Advanced PM Materials, Vol.1, p.324, 1995.

41. Bolton J., Grant A.J., "Heat treatment of PM high speed steel metal matrix composites", proceedings of the 1995 European Conference on Advanced PM Materials, Volume 1, p. 388, 1995.

42. Velasco F., Torralba J.M., Anton N., Garcia-Cambronero L.E., Ruiz-Prieto J.M.,"Stainless steel matrix composites: mechanical properties and wear behaviour", Proceedings of the 1995 European Conference on Advanced PM Materials, Vol. 1, p.65, 1995.

43. Pierronnet M., Raisson G., "Manufacture of corrosion and wear resistant composite materials", International Conference on Hot Isostatic Pressing 1993 p.185, pub. Elsevier Science, 1994.

44. Zeedijk H.B., van der Eerden R.M., "Some preliminary experiments on HIP diffusion bonding", Proceedings of the International Conference on the Hot Isostatic Pressing of Materials p. 3.23, pub. the Royal Flemish Society of Engineers, 1988.

45. Raisson G., Rouby M., Buekenhout L., "Diffusion bonding of low-alloyed steel and nickel base superalloy", Proceedings of the International Conference on the Hot Isostatic Pressing of Materials p.3.33, pub. the Royal Flemish Society of Engineers, 1988.

46. Ashworth M.A., Greenwood R.M., Jacobs M.H. King S., Armstrong G.R., "The microstructure and properties of HIP diffusion bonds", International Conference on Hot Isostatic Pressing 1993 p.333, pub. Elsevier Science, (1994).

47. Jones, D.A., "Principles and prevention of corrosion", pub. Macmillan Publishing, 1992.

48. Tomashov, N.D., Chernova, G.P.: Prot.Met Vol.9, p.379, 1975.

49. Streicher, M.A.: Corrosion, Vol.30, p.77, 1974.

50. Higginson, A., Newman, R.C., Procter, R.P.M.:Corros.Sci., Vol 29, p. 1293, 1989.

51. Potgieter, J.H., Van Benekom, A., "The effect of varying Ru content on the corrosion behaviour of two cathodically modified superferritic stainless steels", pub. Canadian Metallurgical Quarterly, Vol.34, No. 2, 1995 p.143-146, 1995.

52. Wilms, M.E., Gadgil, V.J., Krougman J.M., Ijsseling, F.P., "The effect of sigma phase precipitation at 800°C on the corrosion resistance in sea-water of a highly alloyed duplex stainless steel.", pub. Corrosion Science, Vol.36, p.871. 1994.

53. Potgieter, J.H., "Influence of sigma phase on general and pitting corrosion resistance of SAF 2205 duplex stainless steel", pub. British Corrosion Journal, Vol. 27, No. 3, p. 219-223, 1992.

54. Wallis, E.: Werkst.Korros., Vol.90, p.155, 1990.

55. Gaskell, D.R., " An introduction to transport phenomena in materials engineering", pub. Macmillan Publishing Company, 1992.

56. Crank, J., "The mathematics of diffusion", pub. Clarendon Press, 1979.

57. Mrowec, S., "Defects and diffusion in solids: An introduction", pub. Elsevier Scientific Publishing Company, 1980.

58. Shewmon, P.G., "Diffusion in solids", pub. McGraw-Hill Book Company, 1963.

59. Rhines, F.N., Colton, R.A., Trans. ASM, Vol.30, p.166, 1942.

60. Karlsson,B., Larsson, L.E., "Homogenisation by two-phase diffusion", Materials Science and Engineering, Vol. 20, p. 161-170, 1975.

61. Aaron, H.B., Kotler, G.R., "Second phase dissolution", Metallurgical Transactions, p. 393-408, 1971.

62. Arunsingh, Dayal, D., "On estimation on homogenisation time in powder metallurgy", Zeitschrift Metallukunde, Vol. 61, p. 298, 1970.

63. Purdy, G.R., Kirkaldy, J.S., "Homogenisation by diffusion", Metallurgical Transactions, Vol. 2, p. 371-378, February 1971.

64. Heckel, R.W., Balasubramaniam, M., "The effects of heat treatment and deformation on the homogenisation of compacts of blended powders", Metallurgical Transactions, Vol. 2, p. 379-391, February 1971.

65. Pabi, S.L., "On the dissolution kinetics of silicon in an aluminium-rich matrix", Materials Science and Engineering, Vol. 43, p. 151-158, 1980.

66. Larsson, L.E., Karlsson,B., "Homogenisation by one phase diffusion", Materials Science and Engineering, Vol. 20, p. 155-160, 1975.

67. Fisher, B., Rudman, P.S., J.appl. Phys., Vol. 32, p. 1604, 1961.

68. Lavender, J.D., Jones, F.W., "An investigation on banding", J. Iron Steel Inst. (London), Vol. 163, p. 14, 1949.

69. Jackson, E.M.L.E.M., "Kinetics of sigma formation and dissolution in duplex stainless steels", Ph.D. thesis, Faculty of Engineering, University of the Witwatersrand, South Africa, 1997.

70. Lampman, S.R., "ASM Handbook - Volume 2: Properties and selection: Non-ferrous and special alloys", pub. The American Society for Metals, 1991.

71. Mills, K.,"Metallography and Microstructure", ASM Handbook, Vol.9, 1985.

72. Rickinson I A., Thompson, J.C., "Applications of hot isostatic pressing to ferrous and non-ferrous metal castings", Proceedings of the Second International Conference on Isostatic Pressing , Vol. 1, p. 16, 1982.

73. Davis J., "ASM Handbook - Volume 1: Properties and selection: Irons, steels and high performance alloys", pub. The American Society for Metals, 1991.

74. Schweitzer. P.A., "Corrosion Resistance Tables-Third Edition", pub. Marcel Dekker Inc., 1991.

75. Peckner, D. "Handbook of stainless steels" , pub. McGraw-Hill, 1977.

76. Lula, R.A,. "Source book on the ferritic stainless steels", American Society for Metals, 1982.

77. Nana,S., Cortie, M.B.,"Retardation of intermetallic phase formation in experimental superferritic stainless steels", Mintek paper no.8318., 1995.

78. Wong-Kian, M., Cortie, M.B., Cornish, L.A., "Hot isostatic consolidation and transformation of sigma phase powders", pending publication, Materials Science and Technology, United Kingdom, 1998.

9. APPENDIX

The following technical papers, based on the current investigation, have been accepted for overseas and local oublication in 1998.

Wong-Kian, M., Cortie, M.B., Cornish, L.A., "Hot isostatic consolidation and transformation of sigma phase powders", Materials Science and Technology, United Kingdom.

Wong-Kian, M., Cortie, M.B., Cornish, L.A., "A microstructural study of mixed hot isostatically pressed stainless steel powders", Proceedings of the Microscopy Society of Southern Africa, 1998.

(i) title page

to be submitted to *Materials Science & Technology*

Hot isostatic consolidation and transformation of sigma phase powders

M. Wong-Kian[1], M.B. Cortie[2] and L.A. Cornish[3]

1. Ultra High Pressure Units, P.O. Box 561, Springs 1560, South Africa

2. Mintek, Private Bag X3015, Randburg 2125, South Africa

3. School of Process and Materials Engineering, University of the Witwatersrand, Private Bag 3, Wits 2050, South Africa

(ii) abstract

Super-ferritic stainless steel compositions containing 38% chromium and at least 2% each of nickel and molybdenum can be converted to sigma phase by a heat treatment and, thereafter, to powder by mechanical attrition. This powdered sigma phase has been experimentally processed by powder metallurgical techniques to produce green compacts which were consolidated in a hot isostatic press. Depending on composition, several of the powdered alloys were converted back to ferrite during HIPping. The mechanism of the consolidation process, the nature of the microstructures produced, and the prognosis for its industrial exploitation are examined.

Introduction

It is well known that the corrosion resistance of stainless steels is dependent to a large degree on their content of chromium. Howev , the chromium contained in the common austenitic and ferritic stainless steels is almost inevitably in the range 12 to 20%, for a variety of practical reasons, not least of which is that alloys with this amount of chromium have adequate corrosion resistance for most common applications. In those cases where these common alloys do have insufficient corrosion resistance, recou se is sometimes made to super-austenitic, super-ferritic or duplex compositions. These contain between 20 and 30% chromium. Of course, chromium is a strong stabiliser of the ferrite phase, and super-austenitic or duplex alloys with such high contents of chromium must contain correspondingly high contents of nickel to promote the formation of the desired amount of austenite. Since nickel is a relatively expensive alloying element, this generally raises the cost of such materials significantly.

The super-ferritic alloys in contrast, do not necessarily contain nickel and would be, in principle, relatively cheap to produce were it not for the fact that they normally require either very pure starting materials or specialised production processes. In addition, they generally also have very poor toughness in the cast or welded conditions. These factors currently militate strongly against the large scale production of super-ferritic materials containing more than 30% chromium. Nevertheless, it has been previously shown that properly processed super-ferritic compositions containing up to 38% chromium possess excellent corrosion resistance in a variety of extremely aggressive environments while

maintaining adequate mechanical properties.[1] The key requirements are to ensure that the alloys have very low contents of impurities, especially of the interstitial elements carbon, nitrogen and, to a lesser degree, oxygen,[2,3] and that they contain at least two percent each of nickel and molybdenum.[4] The corrosion resistance can be further considerably enhanced in reducing environments such as sulphuric acid solutions by the incorporation of small amounts (about 0.2%) of the elements ruthenium, palladium, platinum or iridium, which induce electrochemical passivity by the phenomenon of cathodic modification.[5,6]

One, relatively unusual way to produce components from super-ferritic alloys containing between 30 and 40% chromium was developed in 1994 by Cortie *et al.*[7] The required alloy composition is selected for an ability to transform completely into sigma phase, and is induction melted and cast into an ingot. Next, it is heat-treated in a manner designed to bring about its complete transformation into sigma phase. Sigma is a hard, and exceedingly brittle intermetallic compound between iron and chromium, nominally with the stoichiometry FeCr. The 'sigmatized' ingots are then crushed and milled to produce fine powder, and the powder can be further processed by the known techniques of powder metallurgy to produce green components of sigma phase. Finally, the consolidated items are transformed back to ferrite phase by an appropriate sintering heat treatment.

The present paper describes the production and properties of prototype components manufactured from such sigma powders with the aid of a hot isostatic press.

Experimental

The rates of formation of sigma phase in a variety of super-ferritic alloys containing between 29% Cr and 41% Cr have previously been measured by Premachandra *et al.*[8,9] Interestingly, it was found that sigma phase formed exceedingly slowly in as-cast binary Fe-39%Cr alloys, and even heat treatments of 200 hours at 750°C failed to induce transformation in such material. However, the addition of alloying elements such as nickel and molybdenum caused a marked acceleration in the kinetics of the transformation in the as-cast alloys (Fig.1). It was considered in the present work that an alloy that could be heat-treated to transform substantially to sigma phase in not less than two hours and not more than twenty four hours would be the most suitable for the present work. The two hour criterion was to ensure that the material should not transform back to sigma too readily during the cooling cycle of the HIP. It is evident from Fig.1 that an alloy with the desired transformation characteristics can be selected in principle by control of the Cr, Mo and Ni contents. Preliminary experimentation by the authors revealed that an alloy with at least 36% Cr, and at least 2% each of nickel and molybdenum was required in order to obtain a conveniently rapid conversion to sigma phase.

Production of sigma powder

Four kilogram ingots of the stainless steel compositions were prepared from the elements by melting in a sealed induction furnace. The compositions of those mentioned in the present paper are listed in Table 1. Where not specified in Table 1, the residual and minor elements were present at the levels shown in Table 2. The purpose of the niobium, where

added, was to tie up interstitial carbon and nitrogen, whereas the ruthenium was added as a cathodic modifier. The ingots were then reheated to 1050°C and hot rolled to approximately 50% of their starting thickness. This process is known to accelerate the subsequent conversion to sigma phase, ostensibly because it introduces a multiplicity of nucleation sites into the microstructure.[1,9,10] Complete transformation to sigma phase was thereby achieved by annealing for 4½ hours at 750°C. Thereafter, the material was passed through a jaw crusher and then milled for 30 seconds in a Sieb mill.

Chemical analysis of the ingots and their corresponding powders indicated that about 150 ppm each of oxygen and carbon were picked up during milling. The powders were in all cases relatively angular in morphology (Fig. 2). A typical particle size distribution produced by a single operation in the Sieb mill followed by screening through a 170 μm sieve is shown in Fig. 3, and unless otherwise noted, the HIPping experiments to be described were conducted with powders with this approximate size distribution. However, even finer particles sizes could be readily prepared by 24 hours of milling in a ball mill with a 9 :1 ratio of steel balls to charge. Acetone was used as a lubricant. The resulting particle size distribution is given in Fig.4.

Hot isostatic pressing

Sigma powders were poured into mild steel canisters of 20 mm diameter which were evacuated and then sealed by welding. HIPping was carried out at UHPU by a proprietary process, in which the samples were raised to a temperature of 1120°C for 4 hours under an ambient pressure of 1000 bars. Thereafter the furnace was switched off,

and the components cooled. After HIPping, the mild steel can was removed and the samples were sectioned for examination. Solution-annealing heat treatments were carried out on selected samples at 1100°C for two hours, followed by a quench into water.

Metallography

Samples were prepared for metallography by the usual grinding and polishing techniques. Potentiostatic etching in 5 wt% KOH solution at 8 volts was carried out to reveal any sigma phase in the samples. The general microstructure was conveniently revealed by a reagent consisting of 5 g $FeCl_3.6H_2O$, 50 ml of conc. HCL and 100 ml H_2O, while the distribution of carbides was made visible with Murakami's reagent.

All Vickers hardness test results cited were obtained with a 30 kg load and are the average of several determinations.

Corrosion testing

Potentiodynamic scans were carried out in a 10% (by mass) aerated H_2SO_4 solution at room temperature and in 70% (by mass) H_2SO_4 solution at 50°C. Specimens were allowed to stabilise to the equilibrium corrosion potential before being scanned at 12 mV/minute. Each test was repeated after regrinding the specimen's surface with 1200 grit paper. Potentials were measured against a standard calomel electrode (SCE). The standard hydrogen potential is -236 mV on the SCE scale. Corrosion rates for the tests conducted at room temperature were determined by plotting the intersection of the linear region of the anodic curve with E_{corr}. This provides a value for i_{corr}. An i_{corr} value of 1

$\mu A/cm^2$ is approximately equal to a corrosion rate of 0.01 mm/y in the present materials The slopes of the cathodic and anodic reactions were considered to be too steep and limited in extent in the case of the tests in 70% H_2SO_4 for this extrapolation technique to have any validity, and in those cases an upper ceiling for the rate of corrosion was derived directly from the value of the critical current, i_{crit}.

Results

Initial transformation to sigma phase

It was observed that the tendency to transform to sigma phase was acutely sensitive to the alloy composition and thermo-mechanical condition, and was significantly accelerated in material that had been hot rolled. However, hot-working of the ingots could arguably be considered to be a potentially expensive processing step. On the other hand, small changes in the alloy composition, such as over-stabilizing with niobium, were also found to induce a marked acceleration in the kinetics of transformation. The two alloys whose transformation kinetics are compared in Fig. 5, for example, differed for the most part only in niobium content. Therefore it is apparent that further control of the transformation kinetics, even at a constant content of Cr, Ni and Mo in as-cast material, can be achieved by small changes to parameters such as niobium content, and that there would be in principle no need to use mechanical deformation in the production process for the powder.

Microstructural observations

A single HIP cycle was found to have the effect of consolidating the angular particles into a jigsaw-like aggregate, apparently free of gross porosity (Fig. 6). The deleterious effect of a lack of isostatic pressurisation is dramatically evident in Fig. 7, which shows the microstructure of a HIPped compact in which the weld seam of the mild steel perforated. This sample had therefore been sintered but not pressed.

It was observed that the hardness of the samples provided a convenient indication of their microstructure. A hardness value of below 250 HV can be interpreted as indicating that the materials contained a negligible amount of sigma, whereas one of in excess of 800 HV would be correlated in these materials with a substantially sigmatized condition. Such materials were exceedingly prone to cracking. Materials whose hardnesses were in the range 250 to 300 HV generally contained up to 20% sigma by volume but were not prone to cracking and could therefore be considered for engineering applications. A summary of the hardness values obtained after HIPping and solution annealing the samples is given in Table 3.

While the powders with 38% Cr, 2% Ni, and 2% Mo (samples VF552 and VFA487) were found to contain at most 20% sigma phase after HIPping, and had a hardness of about 275 to 290 HV, those with an additional 2% Cr or Mo, such as VFA622, emerged from the HIP in a nearly fully sigmatized condition. Such samples were extensively cracked and very brittle, with as-HIPped hardnesses of between 700 and 900 HV. However, they could generally be converted back to the ferrite phase with a hardness of

between 240 and 255 HV by solution annealing followed by quenching. Unfortunately, the solution-annealing heat-treatment did not eliminate any of the pre-existing cracks.

Also present in the microstructures of the consolidated materials were carbide precipitates and oxide inclusions (Fig. 8), of the same type as had been found in previous work on these alloys.[11] These were especially prevalent along the boundaries of the prior particles. However, the new grains of ferrite formed somewhat independently of these pre-existing networks of inclusions and they evidently did not significantly impede ferrite grain growth.

The microstructure of the material produced by HIPping the very finely milled powder whose size distribution is shown in Fig. 4, was microduplex, and consisted of an exceedingly fine-scale mixture of ferrite and sigma phases (Fig. 9).

Factors effecting sigma formation

The sigmatized microstructure of many of the as-HIPed samples was an unwelcome development, and was not expected from the sigma formation curves previously obtained by Premachandra.[8]

A sample of the VFA622 ingot, in the solution-annealed state, was then subjected to the same HIP cycle as had been applied to the powdered alloys. This sample was free of sigma at the start of the cycle, with a hardness of 238 HV and, after the cycle, had a hardness of 276 HV. However, no sigma was evident in the microstructure and the

increase in hardness appeared to be correlated with an extensive intragranular precipitation of fine carbides and nitrides. In contrast, when a HIP-consolidated sample of powdered VFA622 in the fully sigmatized condition was HIPped for a second time, it was found to have a hardness of 282 HV and a sigma content of 30% (Fig. 10). Evidently, the susceptibility to form sigma had been somehow imparted to the material by some characteristic of the powder-manufacturing process, and it was very much diminished when solid samples were HIPped for a second time.

The sigma present in the various microstructures (whether HIPped twice or not) could generally be removed by the solution annealing treatment previously described. For example, the sample whose microstructure is shown in Fig. 10 was solution annealed. The resulting microstructure is shown in Fig 11 and can be seen to be comprised of ferrite grains in which an abundance of carbo-nitride precipitates are distributed However, some of the alloys with a 4% Mo content (specifically VFA418 and VFA420) were not completely free of sigma after this treatment. Molybdenum is a potent stabilizer of the sigma phase and sufficiently large additions of it are known to raise the temperature at which sigma is stable to in excess of 1100°C.[10]

Corrosion

Samples of three of the materials based loosely on the composition Fe-38%Cr-2%Ni-2%Mo were corrosion tested in 10% sulphuric acid as described previously. The VFA622 sample was tested in the double-HIPped condition, and again after a subsequent solution-anneal. The alloys VFA487 and VF552 samples were tested as-HIPped, and

again after the solution-annealing heat treatment. Since these latter materials were comparatively similar in composition, their corrosion behaviour should have been similar too.

It was found that all three alloys spontaneously passivated in this solution. The corrosion potentials obtained are listed in Table 4. A more positive corrosion potential should normally be correlated with the passivation of the alloy. However excessive emphasis should not be placed on the equilibrium corrosion potentials alone, since the values must be evaluated in conjunction with other factors such as the critical current density, passive range, passivation potential and corrosion current, i_{corr}. The combination of these indicators provide a more reliable indication of a material's corrosion resistance. In this case, the i_{corr} value was calculated as described in the Experimental section and converted to an estimated corrosion rate using Faraday' law. However, it is evident that the materials are already effectively passive in this solution and the Ru and Nb additions made to the VFA622 alloy do not appear to produce any further improvement in corrosion resistance compared to that of the other two alloys. This is no doubt due to the beneficial effect in these alloys of Ni and Mo additions on the corrosion resistance in sulphuric acid.[4]

However, when the same alloys were tested in 70% H_2SO_4 at 50°C it was found that the two alloys without the ruthenium corroded at up to 8 to 30 mm/yr, whereas the alloy containing the small addition of ruthenium corroded at less than 0.12 mm/yr. Three representative potentiodynamic scans are shown in Figure 12. In addition, the passive

current density of the ruthenium containing alloy was significantly lower than that for the other two alloys. The various electrochemical parameters are listed in Table 5. The corrosion rate of the ruthenium containing alloy is similar to or better than that which would be experienced by many super-austenitic or nickel-base alloys in this environment.

It is evident that the effect of the Ru additions only becomes prominent in more aggressive acid solutions in which the Ni and Mo content do not provide sufficient resistance.

Discussion

Sigma formation in the HIP

The product generated from any of the powders was particularly susceptible to sigma reformation during cooling after the first HIP cycle. An alternative explanation, that the temperature during HIPping was not high enough to secure an initial transformation of the powder to ferrite, is not tenable because those samples which went into the HIP in the monolithic condition, whether as-cast or HIPped once already, emerged in the ferritic condition. This begs the question as to what the essential metallurgical differences are between material in the powdered and monolithic states are.

Since the sigma phase forms in the present alloys by the process of nucleation and growth,[8] it is clear that powders that have been HIPped for the first time contain either more sites upon which sigma can re-nucleate or the growth rates of the sigma regions are,

for some reason, far faster than in the other material conditions.

As mentioned, the kinetics of sigma formation are certainly faster in material that has been deformed or which for some other reason contains a high density of dislocations. However, ferritic stainless steels are rapidly recrystallised or polygonised in a few minutes by the application of temperatures above 800°C. Therefore, the dislocation density in material produced during HIPping should be similar to that normally obtained by annealing at 1120°C and, in these materials, is likely to be very low indeed.[12] It is unlikely therefore that the increased susceptibility to sigma formation during the first of the HIP cycles was caused by an anomalously high dislocation density. Another possibility is that the two types of sample differ significantly in composition. However, not only is it unlikely that the difference in behaviour of the powder could have been induced by the relatively small pick-up of interstitial impurity elements induced during milling, but also the substantial reduction in amount of sigma re-formed when a powdered sample was HIPped for a second time proved that the problem of sigma re-formation was not caused by the minor difference in chemical composition. Therefore this possibility can also be discarded.

Evidently, therefore, the explanation must be that the powdered material, HIPped for the first time, contained an abundance of suitable sites upon which sigma could nucleate during the cooling cycle. One possibility is that the sigma in the particles had not been completely converted to ferrite during the 4 hours at 1120°C. Such hypothetical residual sigma might then serve as convenient sites on which to grow further sigma during the

cooling part of the HIP cycle. This may have been the case for those alloys containing 4% molybdenum, since both the relevant phase diagrams and the various solution-annealing heat-treatments conducted, show that molybdenum is a potent stabiliser of the sigma phase, and that not even a solution anneal at 1100°C was sufficient to dissolve all the sigma in those alloys. However, this is less likely in those alloys containing only 2% molybdenum, which could be expected to transform very rapidly to ferrite if held at temperatures above about 1050°C.[13] In the case of these alloys, the explanation must lie in some other property of the product produced at 1120°C during the first HIP cycle.

The consolidation process very likely consists of the following steps:

- the sigma particles pack together as temperature is applied but being both hard and ordered do not initially weld or deform appreciably.
- the powder transforms speedily to ferrite once the temperature exceeds a particular value, which is as high as 1050 to 1100°C in the alloys containing 2% nickel and 2% molybdenum.
- the ferrite particles are at first merely touching one another at their asperities, however as time progresses they weld and form necks at these points of contact (as shown in Fig. 7).
- the necks widen by a process driven by the diffusion of atoms along both the free surfaces and the grain boundaries until the interconnectivity of the porosity is destroyed. Some plastic deformation of the particles also occurs as the can enclosing the sample is displaced inwards.
- given sufficient time, grain boundary migration and further densification occurs leaving

only isolated, spherical pores in a recrystallized equiaxed microstructure.

However, it is feasible that the material produced by the first HIP cycle is not fully consolidated and may have a profusion of very small pores and defects, each of which offers a free surface on which sigma can subsequently nucleate. As the samples cool down through the sigma-forming temperature range, new sigma phase nucleates on the remaining heterogeneity's. The result is a material containing a substantial amount of sigma phase. The ferrite formed in the second HIP cycle will have a further 4 hours in which to become dense, and will therefore be appreciably freer of nucleation sites. Therefore, it would be more resistant to the reformation of sigma during cooling. Presumably, the problem could be solved by a longer or hotter HIP cycle. However, this would have been incompatible with the normal commercial usage of the particular HIP used and was not attempted.

Finally, it should be noted that the presence of a little sigma phase in the microstructure is not necessarily undesirable. Sigma is very hard and has been found to improve the wear resistance of ferritic alloys considerably if present in an intragranular fashion in the microstructure.[14] It is however essential to avoid the formation of intergranular sigma phase, which will always be detrimental.

Prognosis

The key to the successful implementation of the process on an industrial scale is the selection of an alloy composition that can be conveniently converted to sigma phase by

heat treatment, but which is sufficiently resistant to sigma-reformation, so that it ideally emerges in a fully ferritic condition from a HIP-cycle. If it does not emerge from the HIP in a fully ferritic condition, then it should at least be possible to solution heat treat and quench the item to obtain a substantially ferritic and crack free component.

The various alloy compositions investigated in the course of the present work are compared in Figure 13, which plots content of chromium against the sum of the contents of nickel, molybdenum, silicon and platinum group metals. There are three regions of interest. In region A the alloys form sigma very slowly and it is not convenient to convert them to sigma powder. In region B the alloys can be conveniently converted to sigma powder and can furthermore be HIPped to produce a substantially ferritic component. In region C the alloys form sigma phase very readily but convert substantially to sigma phase during cooling in the HIP. However, they can be converted back to ferrite by a solution anneal followed by a quench. Unfortunately, if any cracks developed while the components were in the sigma condition they would not be removed by solution heat treatment alone. In this case a double HIP cycle would be necessary.

An example of a prototype component that has been manufactured out of the VFA622 alloy (which contained 2%Ni and 2% Mo) is shown in Figure 14. It is a 'springlock' for use in an industrial leaching process. The items are subjected in service to a mixture of hot, concentrated sulphuric and nitric acids and a super-austenitic stainless steel is currently the preferred material. The components shown were produced by HIPping to produce a cylindrical workpiece, which was then solution annealed and quenched, and

finally machined to final dimensions. No unusual difficulty was encountered during the machining process. The springlocks were placed into service on 1 May 1997 and had not shown any visible corrosive attack by November of that year.

It is interesting to note that there are other potential applications of the sigma powder. Knight and Cortie,[15] for example, have investigated its use as a consumable in thermal spraying devices, and found that layers of superferritic stainless steel could be readily deposited onto a substrate by use of HVOF (high velocity oxygen-fuel) technology. In addition, it has been demonstrated that the brittle nature of the sigma powder can also be exploited to produce powders that are significantly finer than those normally obtained in stainless steels. These powders may be of use in technologies such as metal injection moulding or rapid prototyping using laser aided direct metal deposition (LADMD).

Conclusions

It is possible to produce corrosion-resistant super-ferritic stainless steel compositions that can be converted to powdered sigma phase, processed using the techniques of powder metallurgy, and converted back into ferritic items by hot isostatic pressing. The Fe-38%Cr-2%Ni-2%Mo alloy is an example of such a composition. However, it may be necessary to use a double HIPping practice to obtain the best results. It was observed that material HIPped once was susceptible to sigma phase formation, ostensibly because it still contained a significant amount of internal porosity. Therefore, it should be possible to improve the situation by conducting longer and hotter HIP cycles than was possible in the present work. Nevertheless, the process has already been shown to be capable of producing corrosion resisting components and might find application in industry.

Acknowledgements

This paper is published by permission of Mintek, Ultra High Pressure Units and the University of the Witwatersrand. The authors also wish to acknowledge the significant contributions of Messrs J. Maskrey (ingot manufacture), K. Premachandra (phase transformation studies), D. Knight (powder preparation) and L. Langenhoven (corrosion testing).

References

1. M. CORTIE, I. WOLFF, K. PREMACHANDRA, M.TULLMIN and E. DE MARSH: in Proc Conf. 'Stainless Steels '91', Chiba, Japan, June 1991, The Iron and Steel Institute of Japan, Tokyo, 555-564
2. J. HOCHMANN : *Mem. Sci. Rev. Met.*, 1951. **48**, 734-758.
3. W. BINDER and H. SPENDELOW : *Trans. ASM*, 1951. **43**, 759-777.
4. M.A.A. TULLMIN : 'Development of experimental ferritic stainless steels containing 40% chromium', PhD thesis, University of the Witwatersrand, Johannesburg, 1992.
5. I.R. GILL : *Platinum Metals Rev.*, 1990, **34**, 85-97.
6. A. HIGGINSON, R. NEWMAN and R. PROCTER : *Corros. Sci*, 1989. **29**, 1293-1318.
7. M.B. CORTIE, S. NANA, and I.M. WOLFF : 'Stainless steel material and the production of stainless steel artifacts therefrom', S. Afr. Patent Application 95/2676, 1994.
8. K. PREMACHANDRA : 'Sigma phase formation in high chromium ferritic stainless steels', MSc thesis, University of the Witwatersrand, Johannesburg, 1993.
9. K. PREMACHANDRA, M.B. CORTIE and R.H. ERIC : *Mat. Sci. Technol.*, **8**, 1992, 437-442
10. J.J. DEMO: in 'Handbook of Stainless Steel', E. Peckner and I.M. Bernstein (eds.), McGraw Hill, New York, 1977. Chapter 5.
11. I.M. WOLFF, K. PREMACHANDRA and M.B. CORTIE : *Mater. Charact.*, 1992, **28**, 139-148.

12 I.M. WOLFF and A. BALL : *Acta Metall. Mater.*, 1991, 11, 2771-2781.

13. E.M.L.E.M. JACKSON : 'Kinetics of sigma formation and dissolution in duplex stainless steels', PhD thesis, University of the Witwatersrand, Johannesburg, 1997.

14. M.B. CORTIE and F. PREMACHANDRA : *Scripta Met*, 1992, 27, 1847-1852.

15. D.S. KNIGHT and M.B. CORTIE : in prep.

(vi) tables (no section (v))

Table 1. As-cast compositions of experimental materials that were converted to powder, percent by mass. The nominal levels of the elements not listed are shown in Table 2. (Note: n.d. = not determined.)

Alloy	Cr	Ni	Mo	C	N	Others
VFA390	37.9	2.3	<0.1	0.003	n.d.	
VFA391	38.0	0.6	0.5	0.005	n.d.	
VFA392	38.2	1.0	1.0	0.005	n.d.	
VFA393	38.2	1.7	1.3	0.004	n.d.	
VFA395	37.6	<0.1	1.8	0.002	n.d.	
DS-1-air	35.7	2.6	4.4	0.070	?	0.6Si
VFA417	37.0	2.4	4.2	0.004	0.001	0.2Al, 0.6Si
VFA418	37.0	2.4	4.2	0.008	0.001	0.2Al, 0.6Si, 0.1Ru
VFA419	37.1	2.4	4.3	0.009	0.002	0.2Al, 0.5Si, 0.2Ru
VFA420	37.1	2.4	4.4	0.011	0.001	0.35Al, 0.6Si, 0.1Ru, 0.1Ir
VFA423	37.1	2.4	4.4	0.008	0.001	0.2Al 0.6 Si, 0.2 Ir
VFA487	36.4	2.3	2.0	0.010	n.d.	
VFA543	39.7	2.4	3.8	0.015	0.004	0.2Ru
VF552	38.8	2.2	2.0	0.022	0.002	
VFAo22	38.5	2.3	2.0	0.015	0.003	0.15Ru, 0.4Nb
VFA647	36.0	2.5	1.9	0.012	0.002	
VFA654	36.6	2.2	1.9	0.010	0.003	0.34Nb
VF238	40.5	-	-	0.014	0.002	
VF245	40.7	5.8	-	0.016	0.003	

Table 2. Nominal content of minor and residual elements, percent by mass.

C	Si	Mn	P	S	Al	Cr	Ti	O
0.004	0.05	0.05	0.006	0.004	0.10	38.0	0.05	0.02-0.05

Table 3. Vickers hardnesses and microstructure of specimens after HIPing and solution heat treatment

Alloy	Vickers hardness	
	HIPped	HIP followed by solution anneal
DS-1	836	276
VF552	289	252
VFA417	876	263
VFA418	890	862
VFA419	890	277
VFA420	817	736
VFA423	>800	277
VFA487	274	321
VFA543	-	277
VFA543 fine	876	318
VFA622	>800	253

Table 4. Corrosion potentials and rates in 10% H_2SO_4 solution at 25°C.

Alloy	Corrosion potential vs SCE, mV		Corrosion rate, mm/y	
	as-HIPped	as-HIPped plus solution anneal	as-HIPped	as-HIPped plus solution anneal
VFA487	+16	+209	0.011	<0.001
VF552	-14	-223	0.001	0.001
VFA622	+14	0	0.001	0.002

Table 5. Corrosion potentials and rates in 70% H_2SO_4 solution at 50°C.

Alloy	Corrosion potential vs SCE, mV	Critical current mA/cm^2	Passive current mA/cm^2	Corrosion rate, mm/y
VFA622	-172	1.2×10^{-2}	2.7×10^{-3}	~0.1
VF552	-403	3.0	9.1×10^{-3}	~30
VFA487	-378	0.83	1.2×10^{-2}	~8

Figures

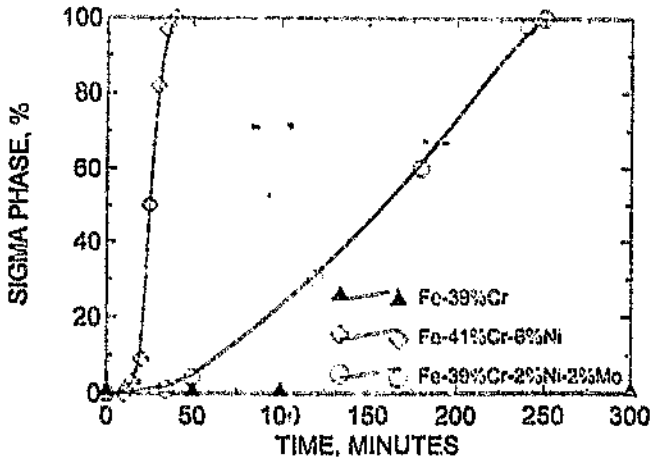

Figure 1. Effect of nickel and molybdenum on the transformation of as-cast ingots to sigma phase at 750°C (data courtesy of K. Premachandra,[8] alloy compositions listed in Table 1 under designations VF238, VF245 and VF552).



Figure 2. Angular morphology of powder particles (SEM)

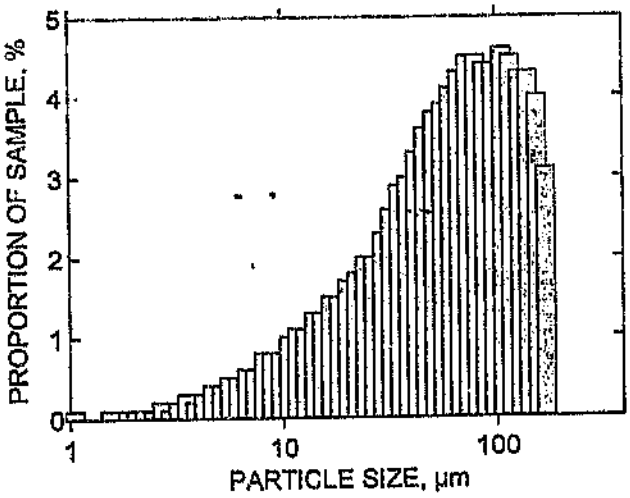

Figure 3. Particle size distribution of minus 170 µm fraction of powder produced by 30 seconds of milling in a Sieb mill (VF543).

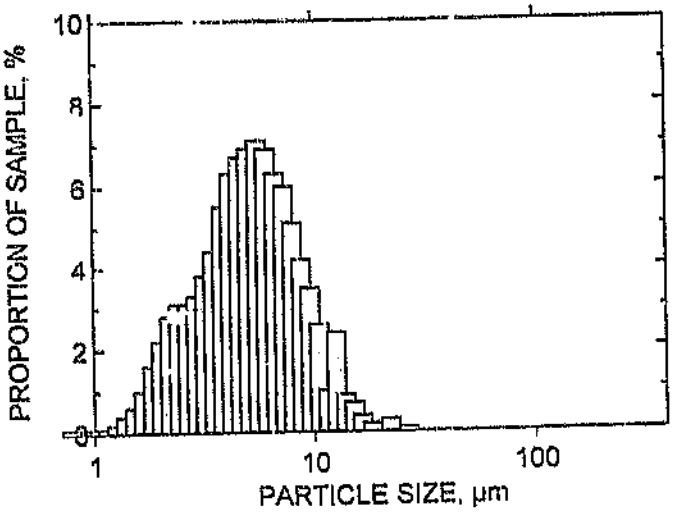

Figure 4. Particle size distribution of powder produced from Sieb mill product by a further 24 hours of milling in a ball mill (VFA 543).

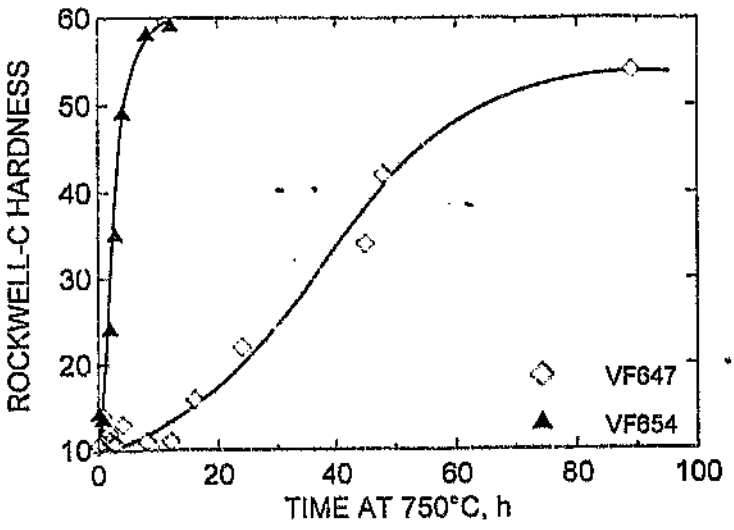

Figure 5. Effect of a 0.35% Nb addition on the kinetics of sigma phase formation of as-cast ingots of materials 36%Cr, 2% Ni and 2% Mo.

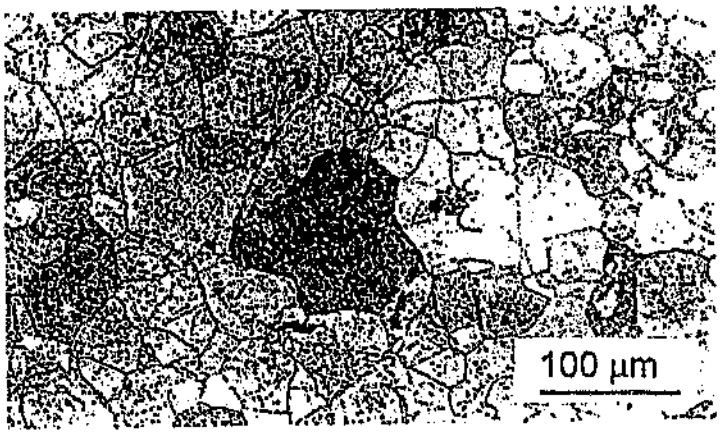

Figure 6. Typical angular microstructure of sigma phase produced by a single HIP cycle conducted on highly alloyed material (VF417).

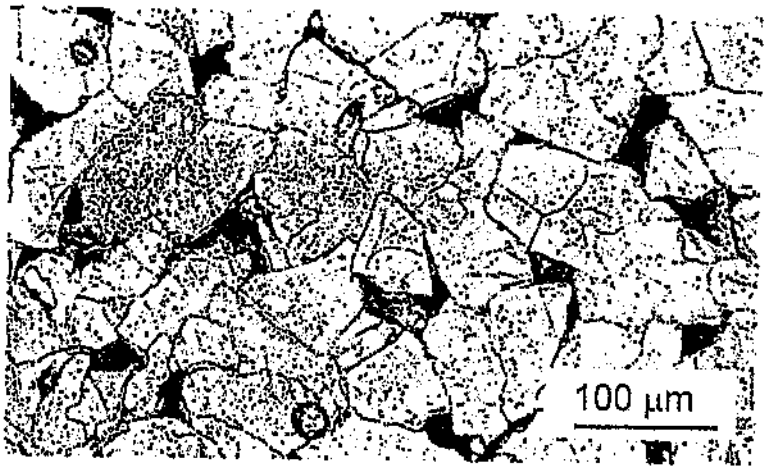

Figure 7. Porous microstructure of material produced during the HIP cycle in the absence of effective pressurization (VF420)

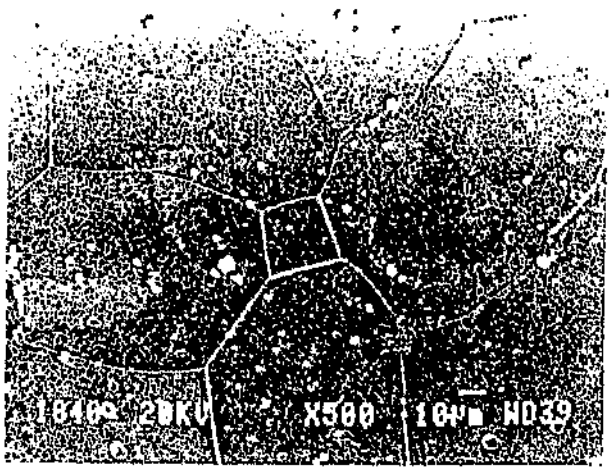

Figure 8. Microstructure of alloy VF552 in the HIPped and solution-annealed condition, showing a recrystallized ferritic matrix, and a network of oxide and carbo-nitride precipitates that outlines the original particle boundaries.

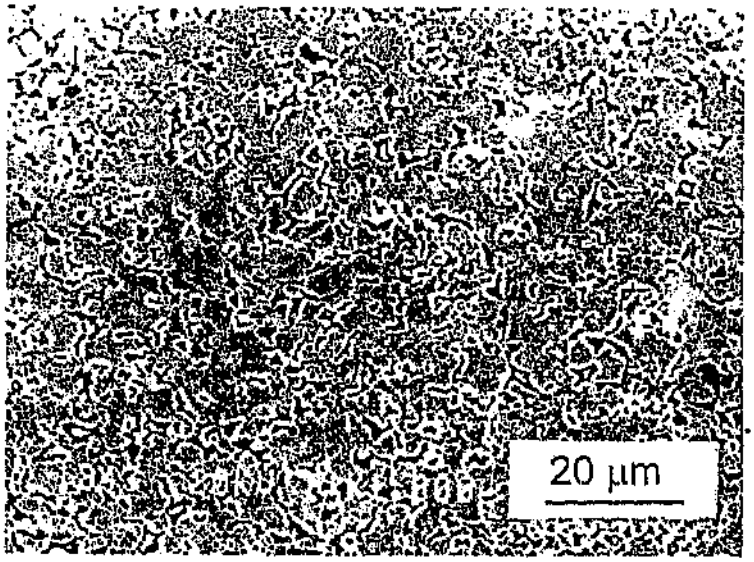

Figure 9. Microduplex mixture of ferrite and sigma phase produced by HIPping ultra-fine sigma powder (much of the sigma has been etched out in this micrograph).

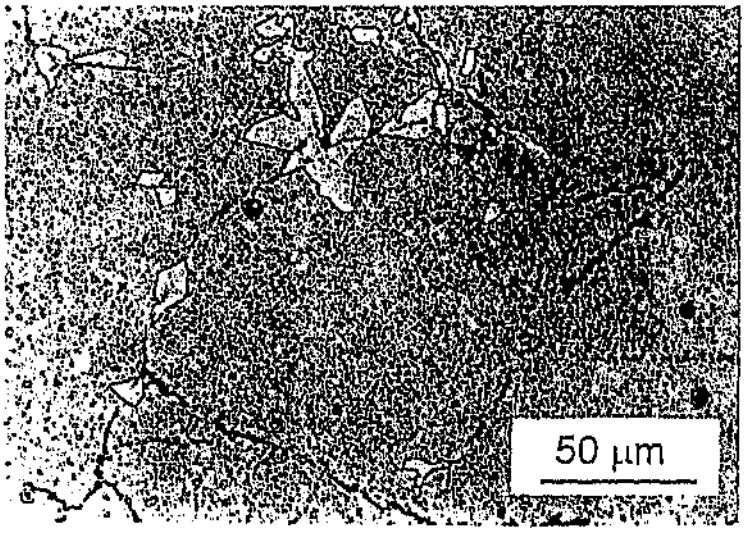

Figure 10. Microstructure of material VFA622 HIPped a second time showing intergranular sigma phase and carbo-nitride precipitates.

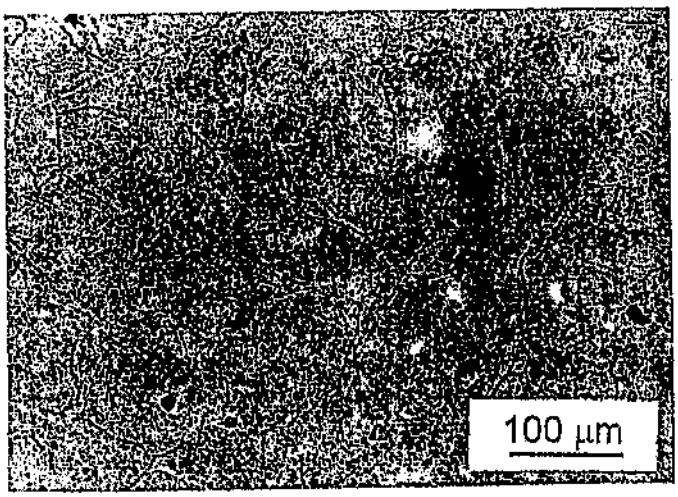

Figure 11. Microstructure of alloy VFA622, after a solution anneal and quench showing ferrite grains with intergranular precipitation of carbide and nitride precipitates.

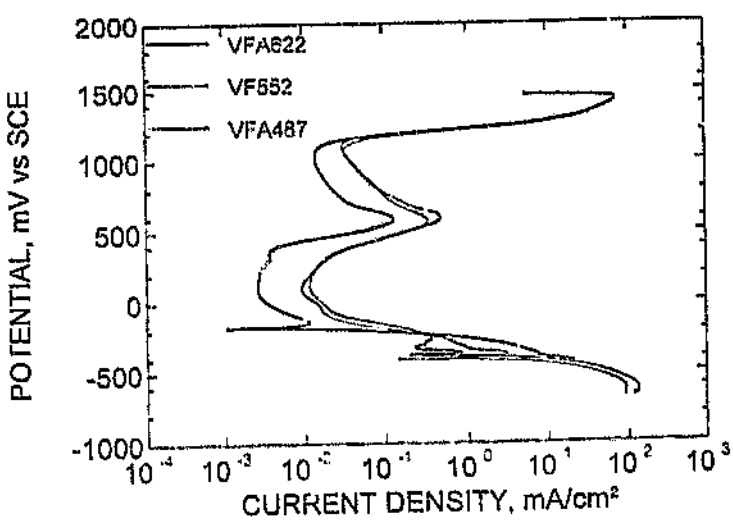

Figure 12. Potentiodynamic behaviour of three alloys in 70% H_2SO_4 at 50°C. The alloy with ruthenium (VFA622) shows considerably greater resistance to corrosion.

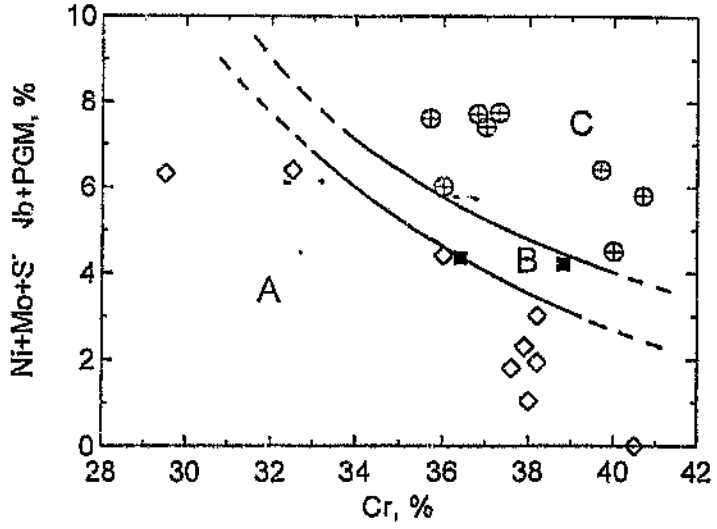

Figure 13. Diagram illustrating the effect of composition on the properties of the alloys, A - takes too long to convert to powder, B - comes out HIP as ferrite, C - comes out of HIP as sigma phase.



Figure 14. Experimental springlocks manufactured from sigma powder. Components shown have a diameter of 20 mm.

A MICROSTRUCTURAL STUDY OF MIXED HOT ISOSTATICALLY PRESSED STAINLESS STEEL POWDERS

M. Wong-Kian[1], M.B. Cortie[2] and L.A. Cornish[1]

[1] School of Process and Materials Engineering, University of the Witwatersrand
[2] Physical Metallurgy Division, Mintek, Private Bag X3105, Randburg

A novel preparation route for stainless steel powders has been developed, in which the sigma-forming ability of the alloys is utilised to facilitate the milling of the powder[1]. Stainless steels of high chromium content can be heat treated to produce the sigma phase, which being brittle, is very easily crushed. The advantage of this method is that fine powder can be easily and cheaply manufactured. The powder is then shaped by hot isostatically pressing (HIPping) in a proprietary method[2]. HIPped components are well known for their homogeneous microstructures and resulting excellent properties. However, there are two disadvantages: firstly, that some sigma forms on cooling from the HIPping process, and secondly the danger that sigma could reform during use of the item, if high enough temperatures (~750°C) were experienced. In either case, sigma could be detrimental to the mechanical properties.

A safer approach is to mix powders, so that the cheapness of the sigma-comminution is still retained, but the resulting powder's sigma-forming capability is avoided by the addition of lower Cr-content, commercially available powders.

A master alloy of composition Fe-2Ni-2Mo-40Cr-0.4Nb was "sigmatised" by annealing at 750°C for 4.5 h. New alloys were made up by mixing the milled master alloy in different weight ratios with commercial 316L stainless steel. These samples were then HIPped, and the resulting microstructures were studied using optical microscopy, and SEM with EDS. Annealing was also carried out subsequently, at 1100°C for 2 hours.

In the as HIPped 80:20 master alloy:316L sample, it was easy to see the prior particle boundaries, and the smaller rounded particles were identified as 316L, whereas those from experimental alloy additions were larger and irregular. Approximately 10% by volume of lamellar sigma was observed in the microstructure. After annealing, no sigma was observed, and the microstructure was predominantly ferrite with some grain boundary oxide particles.

A second alloy, with the proportions [illegible] alloy:316L [illegible] had roughly equal amounts of ferrite and austenite [illegible] irregular [illegible]. After annealing, [illegible] boundaries [illegible].

Another alloy [illegible] and in the as HIPped [illegible] particles within an austenite [illegible]. At high [illegible] morphologies were resolved within the ferrite particles. These were bulk and lamellar sigma. It is highly likely that the bulk sigma is the pro-eutectoid phase, and formed before the eutectoid sigma and secondary austenite[3] (Fig. 4). After annealing, there was less sigma, although the ferrite colonies were still easily observed. There were also regions between the ferrite and austenite where interdiffusion had occurred.

The investigation has illustrated that "synthetic" duplex alloys comprising differing ratios of the master alloy and 316L have potential for HIP manufacture. Corrosion experiments are now being undertaken, with a view to establishing the applicability of these novel materials.

The financial support of Mintek and the FRD is gratefully acknowledged.

References

1. Cortie, M.B., Nana, S., & Wolff, I.M., RSA Patent 95/2676, 1995.
2. Wong-Kian, M.W., Cortie, M.B. & Cornish, L.A., Mat. Sci. and Tech., in press.
3. Bareik, J., Met. Trans. A, 18A, 1171, 1987.

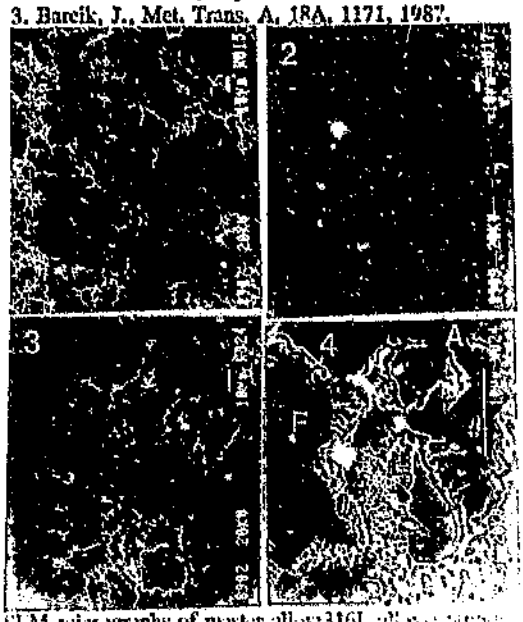

SEM micrographs of master alloy:316L alloys [illegible] Fig. 1. BSE image: As-HIP: ferrite (dark) and austenite (light). Fig. 2. BSE image: Annealed alloy: ferrite (dark) and austenite (light). 20:80 alloy: Fig. 3. SE image: Ferrite particles (dark) in as-HIP. Fig. 4. SE image: Ferrite (F), bulk sigma (B), eutectoid sigma (E) and austenite (A).

Author: Kian, Michael Christopher Wong.

Name of thesis: The consolidation and transformation of an ultra-ferritic stainless steel by hot isostatic pressing / Michael Christopher Wong Kian.

PUBLISHER:

University of the Witwatersrand, Johannesburg
©2015

LEGALNOTICES:

Copyright Notice: All materials on the University of the Witwatersrand, Johannesburg Library website are protected by South African copyright law and may not be distributed, transmitted, displayed or otherwise published in any format, without the prior written permission of the copyright owner.

Disclaimer and Terms of Use: Provided that you maintain all copyright and other notices contained therein, you may download material (one machine readable copy and one print copy per page)for your personal and/or educational non-commercial use only.

The University of the Witwatersrand, Johannesburg, is not responsible for any errors or omissions and excludes any and all liability for any errors in or omissions from the information on the Library website.